ELECTROSPUN NANOFIBRE-BASED STRATEGIES FOR REMOVAL AND DETECTION OF WATER CONTAMINANTS

Report to the

WATER RESEARCH COMMISSION

by

B. Pletschke [a], C. Frost [b], Z. Tshentu[c], N. Torto[c]

[a]Department of Biochemistry, Microbiology and Biotechnology, Rhodes University

[b]Department of Biochemistry and Microbiology, Nelson Mandela Metropolitan University

[c]Department of Chemistry, Rhodes University

WRC Report No. 1991/1/13

ISBN No. 978-1-4312-0395-6

APRIL 2013

Obtainable from

Water Research Commission
Private Bag X03
Gezina, 0031

orders@wrc.org.za or download from www.wrc.org.za

EXECUTIVE SUMMARY

BACKGROUND

The work focused on nanotechnology-based solutions for drinking water in which electrospun nanofibres were used either for removal or detection of contaminants in water. The project was inspired by the need to contribute towards addressing the current global challenge to ensure the availability of clean drinking water. Potential impact areas for nanotechnology in water applications are divided into three categories, namely treatment and remediation, sensing and detection, and pollution prevention. Therefore, the project was part of a global drive towards nanotechnology-based strategies for addressing water challenges.

RATIONALE

To develop low cost and highly efficient electrospun nanofibre-based devices and/or systems for water purification as well as instant and continuous monitoring of water quality suitable for resource poor communities.

AIMS AND OBJECTIVES

The aim of the project was to develop nanomaterial-based contaminant removal or detection systems for water applications relying on a versatile nanofabrication technique.

Electrospinning is a versatile technique that finds application in the area of nanotechnology as it allows the fabrication of nanofibres from a wide range of materials with controlled functionalities and morphology. The fact that electrospinning is a simple and low cost technique in addition to the large surface area to volume ratio of nanofibres, makes electrospun nanofibres the optimal material for use as a low cost platform for the development of contaminant removal or detection systems for water purification and/or quality control.

The objectives for the project were as follows:

1. To develop electrospun nanofibre-based sorbents for uptake of metals in water;
2. To develop electrospun nanofibres with antimicrobial properties for control of pathogens in water;
3. To develop electrospun nanofibre-based optical detection probes for the detection of heavy metals and organic contaminants in water; and
4. To develop enzyme/substrate immobilised electrospun nanofibres for removal and monitoring of contaminants in water.

METHODOLOGY

Nanofibres were fabricated using the electrospinning facilities in the Chemistry Department at Rhodes University. The experimental approach consisted of two stages; firstly, evaluating the recognition principle (compounds or metallic nanoparticles) responsible for selectivity in solution phase before incorporating them in or on a nanofibre platform. The methodologies of the major tasks conducted in the development of nanofibre-based platforms are summarised below;

- 2-amino-4,6-dihydroxylpyrimidine functionalized polyvinylmethylketone nanofibres were employed as a sorbent for the selective uptake of arsenate from water.
- Nylon 6 nanofibres functionalized either with 2-substituted *N*-alkylimidazole derivatives or silver complexes containing *N*-alkylimidazole-2-methanol ligands were employed as antibacterials against gram-positive (*Staphylococcus aureus* and *Bacillus subtilis* subsp*. spizizenii)*, gram-negative (*Escherichia coli*) bacteria and fungi (*Candida albicans)*.
- Glutathione capped silver/copper alloy nanoparticles embedded in nylon 6 nanofibres were employed for the colorimetric detection of nickel(II) ions.
- Pyridylazo-2-naphthol functionalized polyacrylic acid nanofibres were employed as a florescence quencher for the detection of nickel(II) ions.
- 2-(2′-Pyridyl)imidazole functionalised poly(vinylbenzyl chloride) nanofibres were employed for the colorimetric detection of iron(II) ions.
- Gold nanoparticles embedded in either nylon 6 or polystyrene nanofibres were employed for the colorimetric detection of 17β-estradiol in water.
- Acetylcholinesterase immobilised blend of nylon 6/chitosan nanofibres was employed for the detection of carbofuran in water.

- A glyphosate detection system in the solution phase was scaled down by reducing the volume of reagents for complexation.

RESULTS AND DISCUSSION

The most important results and their implications towards the development of nanofibre-based strategies for contaminant removal or detection are summarised;

Development of electrospun nanofibre-based sorbents for uptake of metals

The selective uptake of arsenate species from aqueous solution by 2-amino-4,6-dihydroxylpyrimidine functionalized polyvinylmethylketone nanofibres was found to be highly pH dependent. The material displayed rapid sorption capacity between 98 and 100% within 20 min at the pH range of 3-5. In the presence of a 100-fold molar excess of chloride, nitrate and nitrite anions, the removal of arsenate by 2-amino-4,6-dihydroxylpyrimidine functionalized polyvinylmethylketone nanofibres was not affected by the competing anions. The interaction between arsenate and the electrospun nanofibres is suspected to be via hydrogen bonding of the anion with the hydroxyl groups on the primidine ring.

Development of electrospun nanofibres with antibacterial properties

The antimicrobial activity of the 2-substituted *N*-alkylimidazole was tested against a Gram-negative (*Escherichia coli)*, Gram-positive (*Staphylococcus aureus* and *Bacillus subtilis* subsp*. spizizenii*) bacteria and fungi (*Candida albicans*) using the disk diffusion method. *Escherichia coli* proved to be the most resistant of the bacterial strains. All the compounds tested were not active against *Candida albicans*. *N*-decylimidazole-2-carboxylic acid proved to have excellent activity across the entire range of tested bacterial strains. Several compounds, including *N*-decylimidazole-2-carboxylic acid and the commercial imidazole-based anti-biotic metronidazole, were identified for the incorporation into nanofibres. The 2-substituted vinylimidazoles were also immobilized onto the surface of electrospun fibres using UV initiated graft polymerization. The imidazole derivatives that were screened performed better than metronidazole across the entire range of tested bacterial strains. Silver complexes containing *N*-alkylimidazole-2-methanol ligands with shorter alkyl chain length were predominantly active against *Escherichia coli.* The complexes containing ligands with longer alkyl chain length displayed predominant activity against *Bacillus subtilis* subsp*. spizizenii*.

The electrospun nanofibres incorporated with 2-substituted *N*-alkylimidazoles showed excellent antimicrobial activity against Gram-positive bacterial strains (*Staphylococcus aureus and Bacillus subtilis* subsp*. spizizenii*) and the latter was more susceptible. However, the antimicrobial activity against *Escherichia coli* was poor. Electrospun nanofibres incorporated with silver(I) complexes showed a broad spectrum antimicrobial activity. The antimicrobial activity against *Escherichia coli* and *Candida albicans* was solely attributed to the silver(I) ions. For *Staphylococcus aureus* and *Bacillus subtilis* subsp*. spizizenii*, the antimicrobial activity was attributed to both the silver(I) ions and the 2-hydroxymethyl-*N*-alkylimidazoles. The electrospun nanofibres on which 2-substituted vinylimidazoles were grafted onto the surface displayed excellent percentage growth reduction against *Staphylococcus aureus*. The grafted nanofibres also exhibited lower cytotoxic effects against Chang liver cell lines.

Development of electrospun nanofibre-based optical detection probes

In the first approach, 1-pyridylazo-2-napthol functionalised poly(acrylic acid) nanofibres were employed as a fluorescent probe for selective detection of Ni^{2+} ions. A decrease in fluorescence intensity of the fluorophore was observed and it was attributed to a photoinduced electron transfer mechanism. Selective complexation of the ligand with Ni^{2+} ions played a major role in inducing selectivity of the fluorophore towards Ni^{2+} ions.

The second approach involved the synthesis of glutathione-stabilized silver/copper alloy nanoparticles in nylon 6 nanofibres with subsequent colorimetric detection of Ni^{2+} ions. The silver/copper alloy nanoparticles were dark green in colour due to their intense surface plasmon absorption band. In the presence of Ni^{2+}, the green silver/copper alloy nanoparticles were discoloured. However, there was a negligible colour change in the presence of other transition, alkali and alkali earth metal ions. The selectivity towards Ni^{2+} ions was attributed to the preferential complex formation of the capping agent glutathione with the Ni^{2+} ions.

In the third approach, 2-(2′-pyridyl)imidazole functionalised poly(vinylbenzylchloride) fibres were employed for the colorimetric detection of Fe^{2+} ions. A change in colour from colourless to red-orange was easily observed by the naked eye in the presence of Fe^{2+}. However, alkali metal and alkaline earth metal cations

did not induce such a change. The response time upon exposure to Fe^{2+} was instantaneous. This observation was attributed to the formation of a spin-paired six-coordinate iron(II) complex in the presence of 2-(2'-pyridyl)imidazole. Systems of this nature tend to form an orange-red complex.

The fourth approach involved the incorporation of gold nanoparticles into electrospun nylon 6 and polystyrene polymer nanofibres for the colorimetric detection of 17β-estradiol. It was observed that when nylon 6 was employed as the supporting matrix, the colour changes were not very distinct at the different concentrations of analyte. On the contrary, when polystyrene was employed as the supporting matrix, distinct colour changes were observed at different analyte concentrations. In the presence of 17β-estradiol colour changes observed were white to pink at higher concentrations and white to blue at medium concentrations. The probe was further evaluated for selectivity where cholesterol was employed as the competing analyte. At the same conditions, the probe showed a very deep pink colour within a few min of adding 17β-estradiol while cholesterol resulted in a faint pink colour after 5 h. The selectivity was attributed to the difference in polarity of the analytes as it had a direct influence on mass transfer.

Development of enzyme/substrate immobilised nanofibres

The first task involved the scaling down of the conventional glyphosate detection under predetermined optimal conditions. The system was successfully scaled down to a total assay volume of 1 mL. Experiments utilizing micellar media containing hexadecyl trimethylammonium bromide (CTAB), sodium dodecyl sulphate (SDS), Triton X and Tween 20 were carried out in an attempt to improve on system sensitivity. Despite the fact that Triton X and Tween 20 provided no improvement in detection, other surfactants improved detection. The detection system showed specificity for glyphosate, when tested on its structural analogues, namely, glycine and aminomethylphosphonic acid (AMPA, a primary metabolite of glyphosate).

The second task involved the immobilisation of acetylcholinesterase onto a blend of electrospun nylon 6/chitosan nanofibres and the detection of carbofuran. Immobilisation of acetylcholinesterase onto nanofibres was achieved with glutaraldehyde crosslinking. Relative to free acetylcholinesterase, the immobilised enzyme showed considerable storage stability retaining ~50% of its activity when stored for 49 days at 4°C. Immobilised acetylcholinesterase also retained > 20% of its initial activity after nine consecutive reuse cycles. When exposed to fixed concentrations of carbofuran immobilised acetylcholinesterase showed similar inhibition characteristics to that of the free enzyme.

CONCLUSIONS

The research detailed in this report has enhanced the understanding of the use of electrospun nanofibres as a platform for water purification and contaminant detection strategies. All four objectives set out at the initiation of the project were achieved with great success as all the respective electrospun nanofibre-based devices and/or systems showed positive results.

RECOMMENDATIONS FOR FUTURE RESEARCH

The experimental design at this stage of the work was biased towards proof of using electrospun nanofibre-based platforms for detection and removal of contaminants in water. Therefore, the next stage of the work will focus on developing prototypes as a step towards scaling up and/or commercial use of electrospun nanofibre-based systems or devices for water applications.

ACKNOWLEDGEMENTS

The authors would like to thank the Reference Group of the WRC Project for the assistance and the constructive discussions during the duration of the project:

Prof L Chimuka	University of the Witwatersrand
Dr M de Kwaadsteniet	Stellenbosch University
Prof R Krause	Rhodes University
Dr N Musee	Council for Scientific and Industrial Research
Prof L F Petrik	University of the Western Cape
Dr J E Burgess	Water Research Commission

TABLE OF CONTENTS

LIST OF FIGURES

LIST OF TABLES

LIST OF SCHEMES

LIST OF ABBREVIATIONS

AA	Acetic acid
AChE	Acetylcholinesterase
AMPA	Aminomethylphosphonic acid
ANOVA	Analysis of variance
ATChI	Acetylcholineiodide
AuNPs	Gold nanoparticles
CP	Carbamate pesticide
CT	ChargeTransfer
CTAB	Hexadecyl trimethylammonium bromide
DMF	Dimethyl formamide
DMSO	Dimethyl sulphoxide
DNA	Dioxyribonucleic acid
DTNB	Beta dystrobrevin
DTT	Dithiothreitol
E2	17-β-estradiol
ELISA	Enzyme Linked Immunosorbent Assay
EPSP	5-enolpyruvylshikimate-3-phosphate synthase
FA	Formic acid
FDFA	Federal Department of Foreign Affairs
FID	Flame Ionisation Detector
FTIR	Fourier Transform Infrared Spectroscopy
GA	Glutaraldehyde
GC	Gas chromatography
GSH	Glutathione
IARC	International Agency for Research on Cancer
ICP	Inductively Coupled Plasma
ICT	Internal Charge Transfer
IPA	Isopropylamine
LC	Liquid chromatography
LOD	Limit of detection
LOQ	Limit of quantification
LPS	Lipopolysaccharide
MeCN	Acetonitrile
MIC	Minimum inhibitory concentration
MS	Mass Spectrometric Detection
MTT	(3-(4,5-Dimethylthiazol-2-yl)-2,5-diphenyltetrazolium bromide
N6	Nylon 6
NMR	Nuclear Magnetic Resonance Spectroscopy
NP	Nanoparticle
OP	Organophosphate
PAN	Polyacrylonitrile
PET	Photoinduced electron transfer
PIMH	2-(2′-Pyridyl)imidazole
POEA	Polyoxyethyleneamine
PS	Polystyrene
PVBC	Poly(vinylbenzyl chloride)
RPMI	Rose Park Memorial Institute
RSD	Relative Standard Deviation
SDS	Sodium dodecyl sulphate
SEM	Scanning Electron Microscopy
SPR	Surface Plasmon Resonance
TEM	Transmission Electron Microscopy
TMB	3.3’,5,5’-Tetramethylbenzimidine
TNFα	Tumour necrosis factor
TOABr	Tetraoctylammonium bromide
UNEP	United Nations Environment Programme
UV	Ultraviolet region
VBC	Vinylbenzylchloride
Vis	Visible region

1 INTRODUCTION

Clean drinking water is a resource that is rapidly depleting and it is estimated that 1.2 billion people do not have access to safe drinking water worldwide. In addition, millions of people die from various waterborne diseases, including almost 5000 children a day. These numbers are increasing as the world population keeps growing (Montgomery and Elimelech, 2007). Therefore, providing access to clean water is a priority worldwide. In South Africa, an estimated 5.7 million people lack access to basic water services and about 17 - 18 million lack basic sanitation services (Kasrils, 2003). Most of these people are the marginalised poor; and these figures are likely to increase due to industrial expansion, rising population, and impacts of climate change. Access to safe drinking water free of disease causing bacteria and viruses is a basic human right and essential to maintaining healthy people. It also impacts on economic growth and development especially in developing countries such as South Africa.

In principle, water is a renewable resource as a result of the water cycle, that is, it simply gets shuffled around through the processes of evaporation, condensation and precipitation. Therefore, the global challenges of water are classified into three as;

1. The demand for water is increasing at a rapid pace such that it has been predicted that it could exceed water supply in just two decades.
2. Water is not always distributed to where it is needed in an efficient manner (see Fig.1.1). Canada, for example, has ample supplies of clean water; but the Middle East and North Africa are constantly in need. Re-routing large volumes of water from regions with an excess of water to regions of water scarcity is possible but difficult, and requires large scale changes in infrastructure.
3. Pollution of water is increasing due to the expansion of various agricultural and industrial processes that introduce pathogens, pesticides and heavy metals into water sources. Various contaminant inputs effectively lower the supply of fresh water as natural water cycles are not fast enough to efficiently clean the contaminated water.

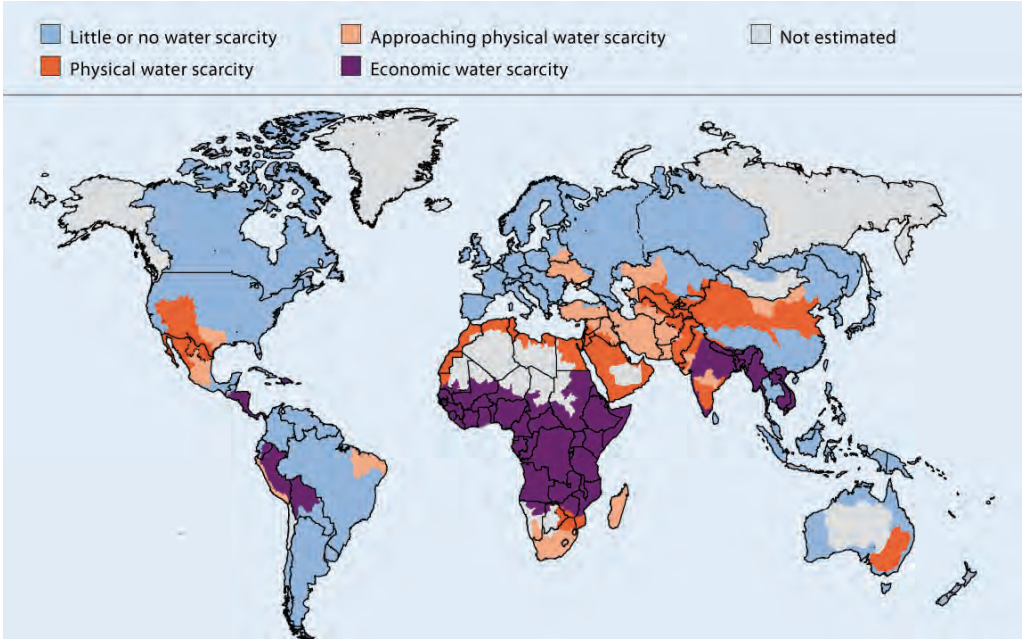

Figure 1.1: World map showing areas of physical and economic water scarcity (UNEP/GRID-Arendal, 2008)

Currently, many countries rely on centralized water treatment plants for providing safe drinking water. However, it is difficult to provide clean water where such infrastructure is not available due to financial limitations as is the case with most developing countries. What is critically needed is to develop small to medium scale methods for purifying water in a cost effective way. Instead of cleaning water in a centralized location and distributing it, the more practical option is to clean water right where it is needed. Consequently, nanotechnology makes it possible to purify water on a much smaller scale. The water sector could apply

nanotechnology to develop more cost effective and high performance water treatment systems as well as instant and continuous ways to monitor water quality (FDFA, 2006).

Some innovative products are now emerging to remedy the situation in developing countries, and these are highly relevant to the needs of South Africa (see Table.1.1).

Table 1.1: Nanobased products relevant to developing countries seeking to improve water supplies (Abraham, 2006, Brown, 2006, Institute, 2006, Nanowerk, 2007, Yavuz et al., 2006)

Product	**How it works**	**Importance**	**Developer**
Nanosponge for rainwater harvesting	A combination of polymers and glass nanoparticles that can be printed onto surfaces like fabrics to soak up water	Rainwater harvesting is increasingly important to countries like China, Nepal and Thailand. The nanosponge is much more efficient than traditional catching nets.	Massachusetts Institute of Technology, United States
Nanorust to remove arsenic	Magnetic nanoparticles of iron oxide suspended in water bind arsenic, which is then removed with a magnet	India, Bangladesh and other developing countries suffer thousands of cases of arsenic poisoning each year, linked to poisoned wells.	Rice University, United States
Desalination membrane	A combination of polymers and nanoparticles that draws in water ions and repels dissolved salts	Already on the market, this membrane enables desalination with lower energy costs than reverse osmosis	University of California, Los Angeles and NanoH_2O
Nanofiltration membrane	Membrane made up of polymers with a pore size ranging from 0.1 to 10 nm	Field tested to treat drinking water in China and desalinate water in Iran, using this membrane requires less energy than reverse osmosis	Saehan Industries, Korea
Nanomesh waterstick	A straw-like filtration device that uses carbon nanotubes placed on a flexible, porous material	The waterstick cleans as you drink. Doctors in Africa are using a prototype and the final product will be made available at an affordable cost in developing countries	Seldon Laboratories, United States
World filter	Filter using a nanofibre layer, made up of polymers, resins, ceramic and other materials that removes contaminants	Designed specifically for household or community level use in developing countries. The filters are effective, easy to use and require no maintenance	KX Industries, United States
Pesticide	Filter using nanosilver to adsorb and then degrade three pesticides commonly found in Indian water supplies	Pesticides are often found in developing country water supplies. This pesticide filter could provide a typical Indian household with 6000 L of clean water over one year	Indian Institute of Technology in Chennai, India and Eureka Forbes Limited, India

Current efforts have already resulted in new water purification devices that are smaller in scale and cheaper to operate than traditional centralized treatment plants. Nanotechnology thus holds great promise to tackle the global water challenge. Therefore, the research direction that should be taken could focus on the search for new materials with respect to chemical composition as well as alternative material fabrication techniques at the nanoscale. From our research team's perspective, a plausible approach would be to use electrospun nanofibres as alternative materials for water applications. This is based on the fact that through electrospinning, the benefits of nanoparticles could be derived in nanofibrous form at the same time addressing some (if not all) of their limitations. Further, as a result of their fibrous and continuous nature, electrospun nanofibres may expand possibilities for device fabrication. Therefore, the report presents our efforts towards taking advantage of the properties of electrospun nanofibres for the benefit of ensuring a supply of safe drinking water.

2 LITERATURE REVIEW

Electrospinning is a term used to describe a fibre forming process by which repulsive electrostatic forces are employed to draw a solution or melt of optimal viscoelasticity into nanofibres (Teo and Ramakrishna, 2006). Spinning in this context is a textile term that derives from the early use of spinning wheels to form yarns from natural fibre staples like cotton and is commonly used to identify fibre forming processes for synthetic fibres as well (Doshi and Reneker, 1995, Zeleny, 1914).

The process of electrospinning was discovered by Lord Rayleigh (Rayleigh, 1882), patented by Cooley and Morton (Cooley, 1902, Morton, 1902), studied in more detail by Zeleny in 1914 (Zeleny, 1914), and further developments towards commercialization of the process were reported by Formals in 1934 (Formhals, 1934). However, a large industrial use was not seen until the advent of nanotechnology around 1990. Since then, electrospinning has found increasing use as studies have shown that a large variety of materials can be electrospun (Reneker and Chun, 1996).

2.1 Basic electrospinning set-up

In its simplest incarnation, the process of electrospinning is relatively easy to implement. The set-up is made up of three basic components (see Figure 2.1);

1) a high voltage power supply
2) a way to deliver a viscoelastic solution; and,
3) a means of collecting the fibres

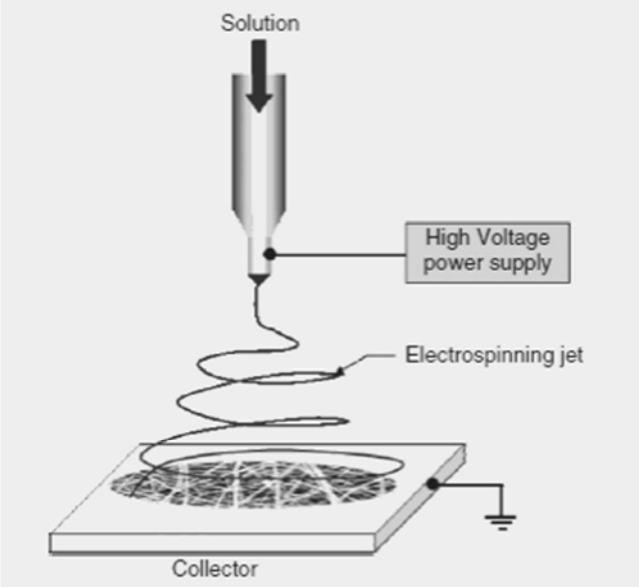

Figure 2.1: Basic components of an electrospinning set-up (Teo and Ramakrishna, 2006)

Modifications of electrospinning designs to achieve the desired nanofibre assemblies are centred on these three components (Teo and Ramakrishna, 2006). In addition, there are many factors which affect the electrospinning process and the resultant fibre properties, including polymer materials (e.g. polymer structure, molecular weight, solubility), solvent (e.g. boiling point, dielectric properties), solution properties (e.g. viscosity, concentration, conductivity, surface tension), operating conditions (e.g. applied voltage, collecting distance, flow rate) and ambient environment (e.g. temperature, gas environment, humidity).

2.2 Mechanism of electrospinning

On application of a voltage that exceeds the critical point (typically above 5 kV); the induced electric field causes the repulsive interactions between like charges in the viscoelastic solution and the attractive forces with the oppositely charged collector to exert tensile forces. This leads to elongation of the pendant drop at the needle tip. As the electric field strength is increased further, a point will be reached at which the

electrostatic forces balance out the surface tension of the viscoelastic solution leading to the development of the Taylor cone. Figure 2.2 shows a schematic representation of Taylor cone formation at the needle tip due to accumulated surface charges. If the applied voltage is increased beyond this point, a jet will be ejected from the apex of the cone and accelerated towards the collector (Doshi and Reneker, 1995, Sill and von, 2008, Taylor, 1964, Taylor, 1969). As the jet travels through the electric field, charges accumulate on the surface of the jet. The uneven distribution of charges results in a whipping or bending motion of the jet. As a result, solvent evaporation rapidly occurs, while the polymer chains within the jet tend to stretch and orient. The thin jet containing the polymer molecules (Doshi and Reneker, 1995) is then deposited on the collector plate as a fibre.

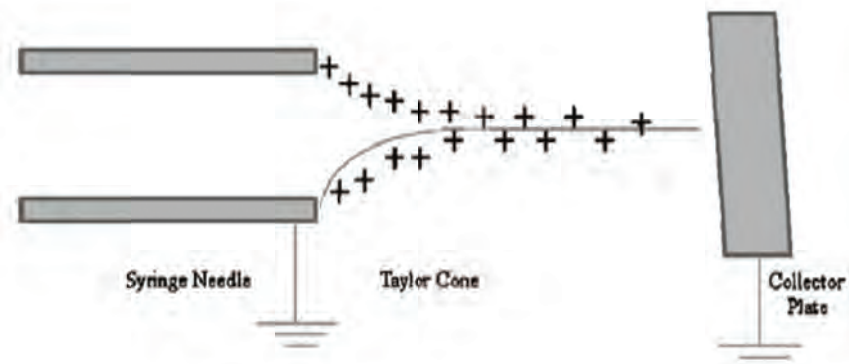

Figure 2.2: Schematic representation of Taylor cone formation (Taylor, 1969)

The process of electrospinning is still not fully understood, a major challenge being the confusion around the exact details of charge motion of the polymer solution jet as it travels towards the collector. Nevertheless, it is believed that charges accumulate at the surface of the polymer jet such that they are essentially static with respect to the moving coordinate systems of the jet (Reneker *et al*., 2000). On that basis, the electrospinning jet can be thought of as a string of charge elements connected by a viscoelastic medium with one end fixed at the point of origin and the other end free. The free end initially follows a stable trajectory until a point where the electrostatic interactions between the charge elements begin to dominate the ensuing motion, initiating and perpetuating chaotic motion. Figure 2.3 shows a simulation of an electrospinning jet based on numerical modelling as proposed by Kowalewski and co-workers (Kowalewski *et al*., 2005).

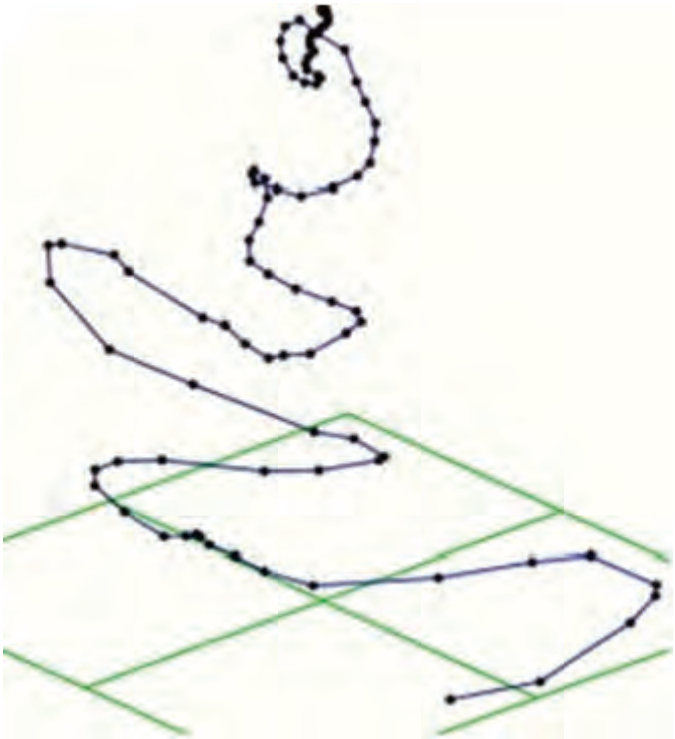

Figure 2.3: Numerical model simulation of an electrospinning jet (Kowalewski et al., 2005)

If the electrospinning jet is thought to be a moving charged object, then it follows that electric, magnetic and mechanical forces could be employed to control the deposition patterns of electrospun nanofibres.

2.3 Electrospinning designs

Controlled deposition of nanofibres

To achieve various fibre assemblies, there are generally two main methods, one is to control the flight of the electrospinning jets through ,manipulation of the electric field and the other is to use a dynamic collection device. It has been reported that the average velocity of the electrospinning jet ranges from 2 m/s (Kowalewski *et al*., 2005, Sundaray *et al*., 2004) to 186 m/s (Smit *et al*., 2005). Therefore, rotating collectors have been used to match the velocity of the electrospinning jet and thus induce electrospun fibre alignment. Figure 2.4 (a) shows an electrospinning set-up in which a rotating drum collector was used to match the rotation speed of the electrospinning jet and thus induce uniaxial fibre alignment (Figure 2.4 (b)).

(a) 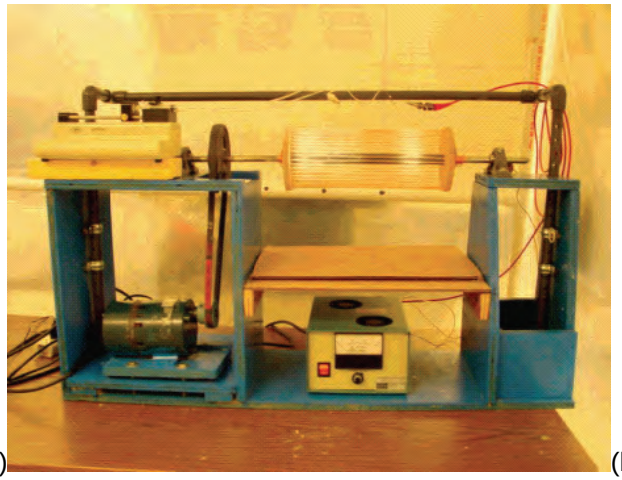 (b) 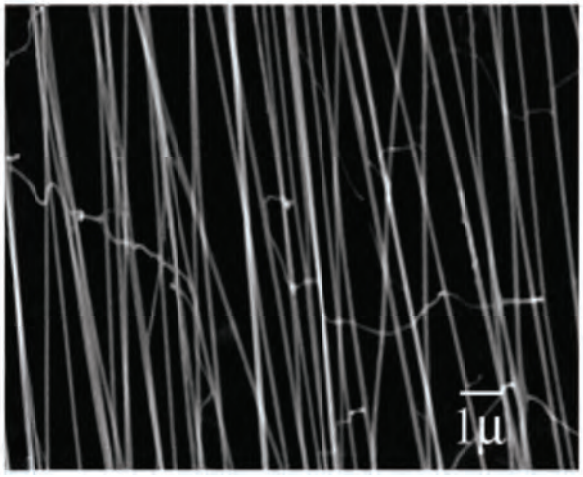

Figure 2.4: (a) Apparatus for rotating the copper wire drum during electrospinning (b) SEM image of axially aligned polymer nanofibres on the copper wire drum (Katta et al., 2004)

Although matching the rotation speed has been shown to induce uniaxial alignment of fibres, there are some instances where this is not achieved. Consequently, electric field alignment is preferable in some instances. Electric field alignment is based on the fact that an electrospinning jet is charged thus deposition of fibres will follow electric field lines. In 2004, Sundaray and co-workers (Sundaray *et al*., 2004) combined a rotating collector and electric field manipulation to achieve deposition of fibres in a controlled area. Figure 2.5(a) shows a schematic diagram of an electrospinning set-up in which a sharp pin was used to control the deposition of the fibres. Controlled deposition was based on the fact that the sharp edge of the pin is a centre of strong electric field such that the electric field lines converge towards the tip (see Figure 2.5(b)) to induce alignment of fibres.

(a) 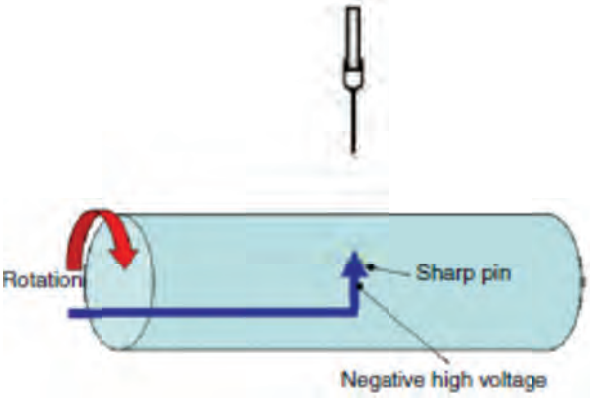

(b) 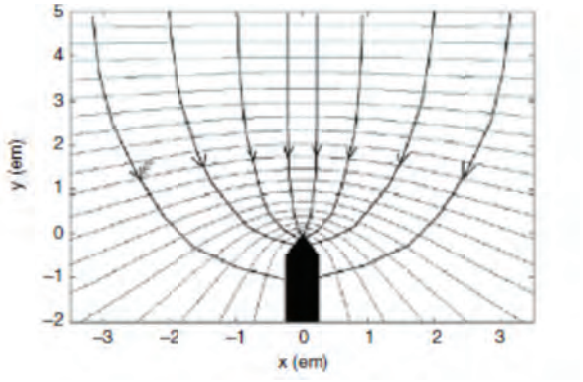

Figure 2.5: (a) Schematic diagram of an electrospinning set-up in which a rotating drum collector with a sharp pin inside to induce fibre alignment (b) convergence of electric field lines towards a sharp edge (Sundaray et al., 2004)

Scaling up electrospinning

Although production rate of fibres through electrospinning is relatively low in comparison to conventional textile processes, various strategies have been implemented towards scaling up the electrospinning set-up (Zhou *et al*., 2009), the predominant strategy being the multiple nozzle electrospinning set-up. The efforts to

scale up the electrospinning technology to an industrial production level used to be based on the manipulation of the jets using multi-nozzle constructions (Kirichenko, 2007). In Figure 2.6, the multi-nozzle spinning head developed by Nanostatics Company is shown. The principle is based on an idea to feed multiple nozzles from a single source of the polymer solution.

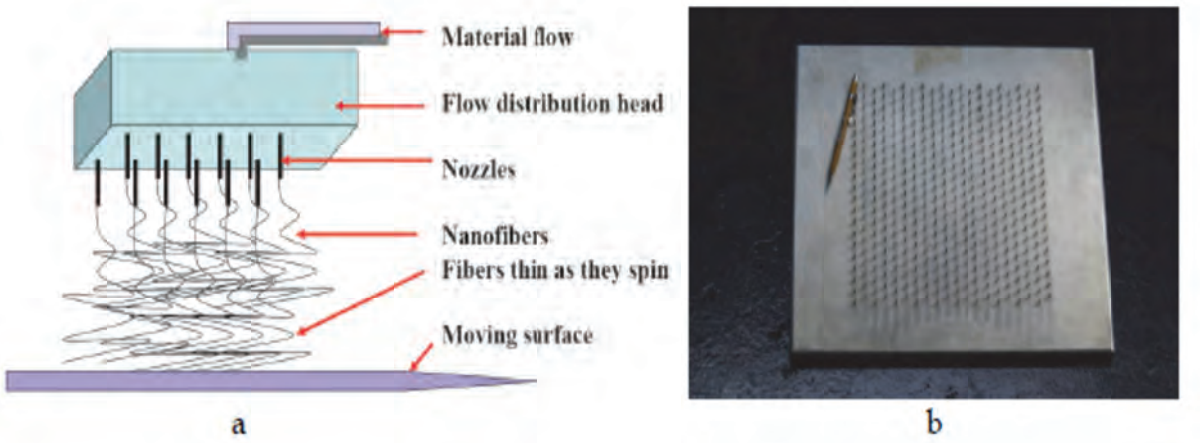

Figure 2.6: (a) Schematic (b) and photograph of a multi-nozzle spinning head by Nanostatics (NanoStatics, 2007)

Figure 2.7 shows the multi-nozzle spinning part of the machine being commercialised by TOPTEC Company. The device uses upwards direction of electrospinning in order to eliminate polymer droplets eventually falling from conventional down-oriented electrospinning elements.

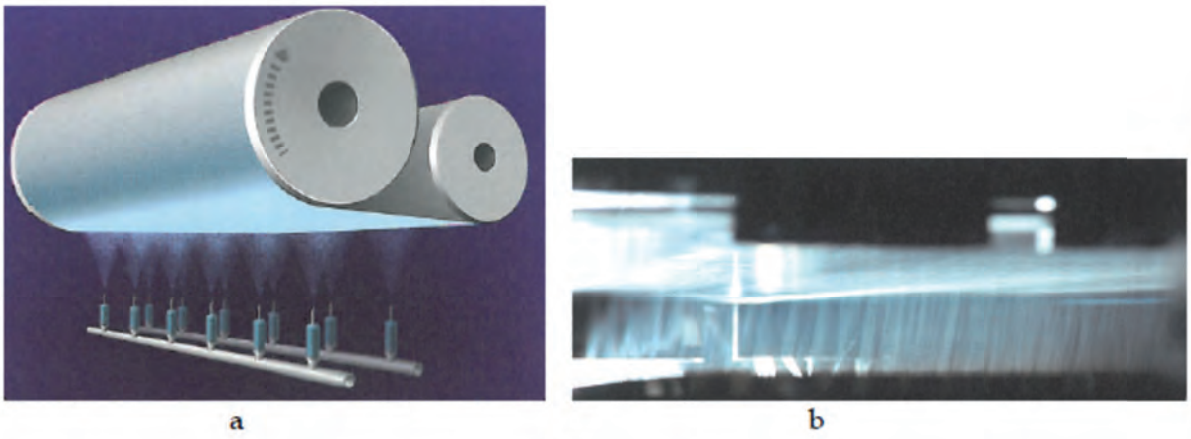

Figure 2.7: (a) Schematic and photograph (b) of a multi-nozzle spinning head by TOPTEC (TOPTEC, 2011)

Initially, the thinking regarding efforts to scale up the electrospinning set-up to an industrial production level was biased towards multiplication of the jets using multi-nozzle constructions (Zhou *et al*., 2009). However, this approach posed a challenge associated with the number of jets needed to reach economically acceptable productivity, typically thousands. Furthermore, challenges associated with reliability, quality consistency, and machine maintenance (especially cleaning) also surfaced.

A welcome development to electrospinning technology was nozzle-less electrospinning reported in 2004 by Jirsak and co-workers (Jirsak *et al*., 2004). The nozzle-less electrospinning set-up solves most of the limitations associated with multiple needle electrospinning due to its mechanical simplicity. However, the process itself is more complex because of its spontaneous multi-jet nature.

The main difference between nozzle-less electrospinning and conventional electrospinning is that multiple jets are ejected from a free liquid surface where the voltage is applied. This means that the number of electrospinning jets is solely dependent on the available liquid surface area unlike conventional electrospinning which is dependent on the number of needles.

The simplest realization of the nozzle-less electrospinning head is in Figure 2.8. A rotating drum is dipped into a bath of liquid polymer. The thin layer of polymer is carried on the drum surface and exposed to a high voltage electric field. If the voltage exceeds the critical value, a number of electrospinning jets are generated. The jets are distributed over the electrode surface with periodicity. This is one of the main advantages of nozzle-less electrospinning: the number and location of the jets is set up naturally in their optimal positions. When the roller was partially immersed into a polymer solution and slowly rotates, the polymer solution was loaded onto the upper roller surface. Upon applying a high voltage to the electrospinning system, an enormous number of solution jets can be generated from the roller surface upward (see Figure 2.8). Several types of rotating electrodes for free liquid surface electrospinning for industrial machines have been developed (Figure 2.8 b). However, the drum type is still one of the most productive.

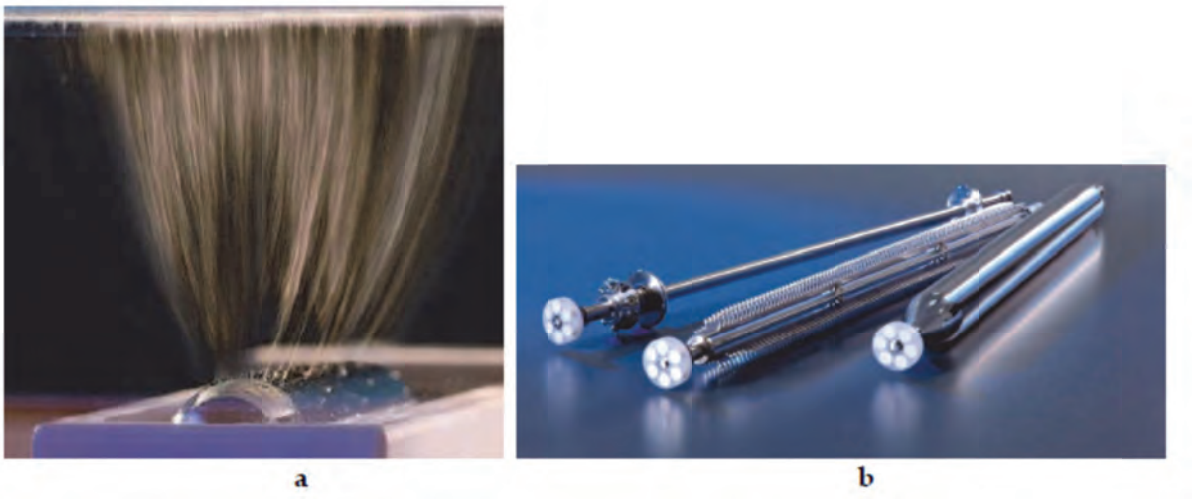

Figure 2.8: Free liquid surface electrospinning from a rotating electrode (a) and various types of spinning electrodes (Petrik and Maly, 2010)

The nozzle-less principle using rotating electrodes has been developed into a commercially available industrial scale by Elmarco Co with the brand name “Nanospider™” (see Figure 2.9).

Figure 2.9: Nozzle-less production electrospinning line (Nanospider™) (Petrik and Maly, 2010)

With the increase in the number of electrospinning companies (see Table 2.1) over the last decade, electrospinning is expected to progressively move from a laboratory bench process to an industrial scale process. On the basis of the electrospinning companies, it may be said that in the near future, large scale production of electrospun nanofibres will be possible thus paving way for industrial scale production of nanofibre-based devices for water treatment or detection of contaminants.

Table 2.1: Some electrospinning companies established in the last decade (Chigome and Torto, 2011)

Company name	**Country**
Applied Sciences, Inc. (ASI)	United States of America
Elmarco	Czech Republic
eSpin Technologies, Inc.	United States of America
Fibertex Nonwovens	Denmark
Finetex Technology	United States of America
IME Technologies	Netherlands
NanoFMG	Turkey
Neotherix	United Kingdom
Nicast	Israel
SNS Nanofiber Technology, LLC	United States of America
Zeus	United States of America
Electrospinz nanofibre engineering	New Zealand
Fluence	Japan
KES Kato Tech, Co., Ltd.	Japan
Mechanics Electronics Computer Corporation	Japan
NanoNC	Korea
Yflow Technology	Spain
The Electrospinning Company	United Kingdom
PolyNanotech	Germany
Fanavaran Nano-Meghyas	Tehran
ANSTCO	Turkey
Fiber Materials Electrospinning Laboratory	Russia

2.4 Range of materials that can be electrospun

The primary requirement for fibre formation through electrospinning is the viscoelasticity of the spinning solution. Solutions based on high molecular weight polymers possess the requisite viscoelasticity due to their long chains, hence making them the most popular electrospun material (Frenot and Chronakis, 2003). However, there is a wide range of pre and post electrospinning modification processes that have made it possible to broaden the range of materials that can be electrospun (Ramakrishna *et al*., 2006, Greiner and Wendorff, 2007).

Generally, materials are classified into five groups according to their chemical composition; metals, semiconductors, polymers, ceramics and composites (Smith, 2003). This means that it should be possible through electrospinning to fabricate all the materials from the five classes into nanofibrous form (Frenot and Chronakis, 2003, Ramakrishna *et al*., 2006, Greiner and Wendorff, 2007). Therefore, as long as a melt or solution can be formed, the material composition cannot limit the applicability of electrospun nanofibres for water purification or detection of water contaminants. Numerous examples exist of the pre and post electrospinning modification strategies that have made it possible to broaden the application areas of electrospun fibres (Chigome and Torto, 2012, Chigome and Torto, 2011, Ramakrishna *et al*., 2006). However, a few examples will be mentioned related to functionalisation strategies that can afford fibres with; (a) Colorimetric properties either by immobilising dyes or metallic nanoparticles, (b) Analyte selectivity either by intermolecular forces or molecular recognition, (c) Antimicrobial properties by immobilising biocides (organic molecules, metal complexes and metallic nanoparticles) and lastly (d) Specific detection properties by immobilising enzymes.

A simple fabrication approach of materials that combine two properties; a large specific surface area and a reversible visual colour change, is the basis of our research team's perspective towards the development of

electrospun nanofibre-based colorimetric analytical devices. The fact that chromism is based on a change in the electronic states of molecules (Bamfield, 2001), electrospun nanofibres functionalised with the appropriate chromogenic materials (either organic dyes or metallic nanoparticles) are expected to have fast response times in the order of seconds. Furthermore, the large specific surface area of electrospun nanofibres is expected to facilitate the development of highly sensitive colorimetric devices due to the large number of active sites. Assuming the absence of matrix effects that can suppress the chromic transition, the only two parameters that would affect the limit of analyte detection are the sharpness of the eye sight of the observer and the relationship between colour intensity and the chromogenic material interaction.

Copolymerisation is a method that has been used to introduce requisite functionalities onto electrospun nanofibres. Wan and co-workers reported the fabrication of porphyrinated nanofibres by copolymerisation and electrospinning (Wan *et al*., 2006). Figure 2.10 shows a synthetic pathway for porphyrin functionalised copolymer fibres and the insert showing red luminescent fluorescence microscope image.

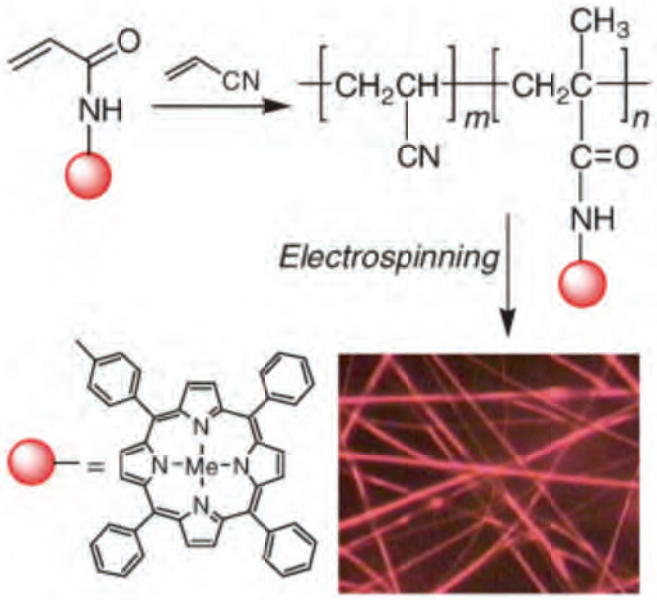

Figure 2.10: The formation of luminescent nanofibres from porphyrinated polymers (Wan et al., 2006)

A whole range of other dye molecules that possess a vinylic functionality can be introduced onto the surface of electrospun nanofibres using a similar approach.

Graft polymerisation is an alternative surface functionalisation approach that can be adopted to introduce dye ligands of interest. In a report by Ma and co-workers, Cibacron blue F3GA (CB) was attached onto the surface electrospun polysulphone (PSU) nanofibres by graft polymerisation (Ma *et al*., 2006). Figure 2.11 shows the steps involved in graft polymerisation onto polysulphone nanofibres.

Polydiacetylene (PDA) polymers are an interesting class of dyes that can be used as chromogenic material. A major advantage of using conjugated polymers as the sensing interface in comparison to small dye molecules lies in the potential for signal amplification. Among the conjugated polymers, functionalized PDAs have the advantage of easy preparation as they are generally synthesized using photopolymerisation of self-assembled monomers (Hoeben *et al*., 2005, Yoon *et al*., 2009). One unique property of nanostructured PDAs that has fostered their application in sensing systems for analytical chemistry purposes is the occurrence of a blue to red colour change that takes place in response to the presence of ions (ionochromism) (Kolusheva *et al*., 2000) and ligand-receptor interaction (affinochromism or biochromism) (Reichert *et al*., 1995). Figure 2.12 shows the polymerisation of PDA within electrospun nanofibres.

Figure 2.13 shows a schematic representation of PDAs functionalised with ligands for selective detection of biomolecules and carbohydrates.

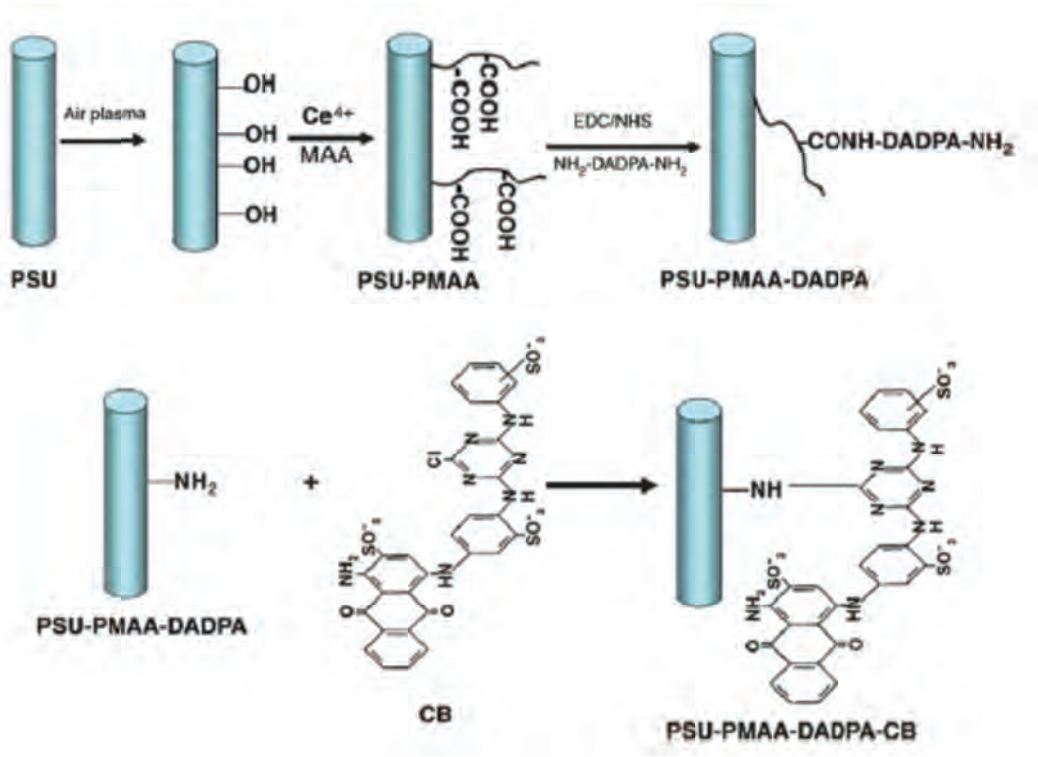

Figure 2.11: Schematic representation of the preparation of PDA embedded electrospun fibres , where NH_2-DADPA-NH_2 equals to $NH_2CH_2CH_2CH_2NHCH_2CH_2CH_2NH_2$ (Ma et al., 2006)

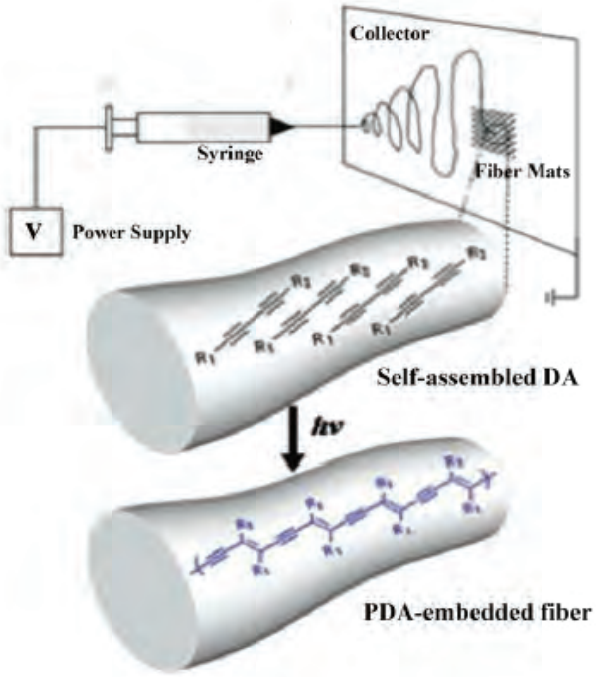

Figure 2.12: Schematic representation of the preparation of PDA embedded electrospun fibres (Yoon et al., 2007)

Noble metallic nanoparticles are currently regarded as emerging building blocks for construction of optical sensors due to their localised surface plasmon resonance enhanced properties (Jain *et al*., 2007). Of all the metal nanoparticles, AuNPs have attracted the most attention due to the fact that they have an extremely high extinction coefficient higher than those of traditional dye chromophores (Zhao *et al*., 2008a, Ghosh and Pal, 2007). The physics responsible for the colour of AuNPs differs from the molecular electronic excitation underpinning the colour of organic dyes (Bamfield, 2001). Fundamentally, the concept of surface plasmon resonance (SPR) has been widely accepted as the plausible explanation for the occurrence of colour on AuNPs. The chromic transitions observed for AuNPs-based colorimetric sensors are red to purple and blue

typically due to aggregation of AuNPs upon perturbation (Zhao *et al*., 2008b). Hence, it is plausible to explore the possibility of incorporating AuNPs into electrospun nanofibres to develop colorimetric probes.

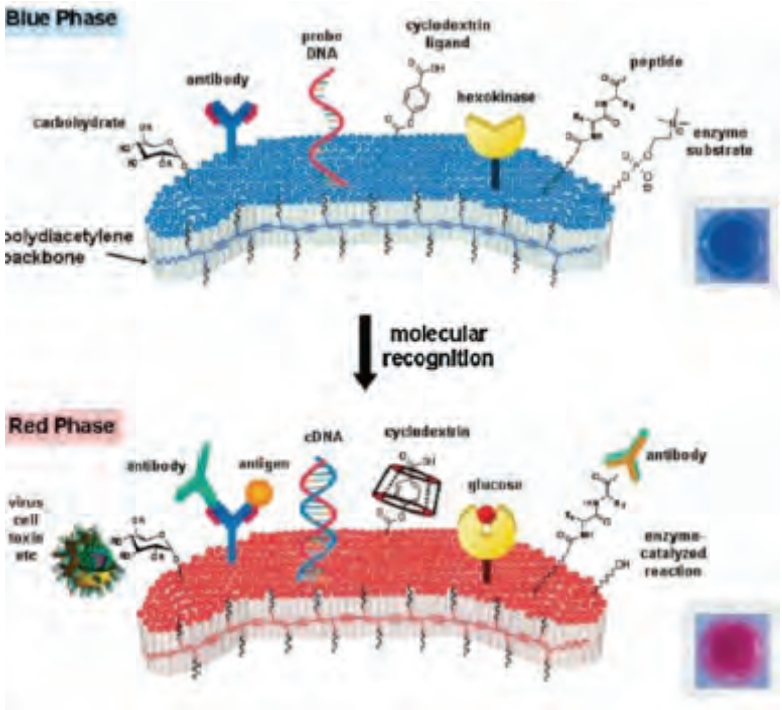

Figure 2.13: A schematic representation of selected affinochromism type interactions in colorimetric PDA sensors (Ahn and Kim, 2008)

Although there are no reports on the use of AuNPs embedded electrospun nanofibre colorimetric sensors, the fact that, incorporation of AuNPs into electrospun nanofibres has been reported (Figure 2.14) brings confidence that it could be possible to use electrospun fibres as the matrix to facilitate sensing mechanisms that rely on variable proximity phenomena of AuNPs. In addition, the large surface area of an electrospun nanofibre matrix may play an important role in facilitating faster detector response due to its nanoscale as compared to the bulk materials.

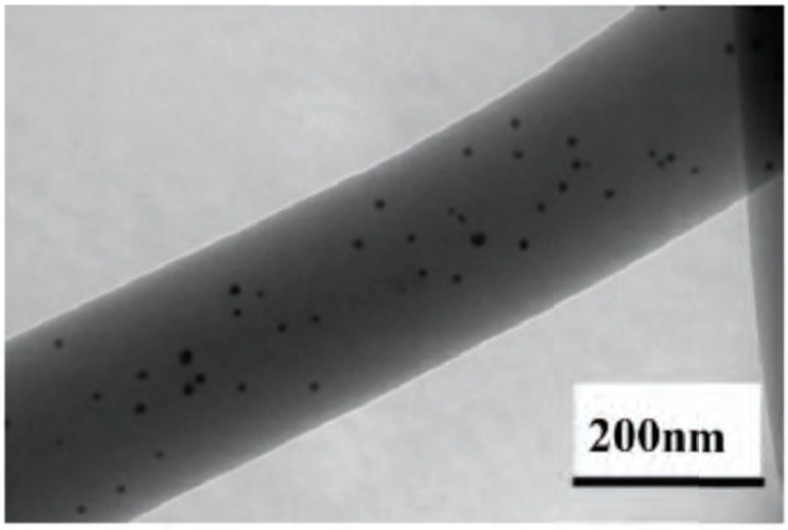

Figure 2.14: TEM image of AuNPs embedded electrospun PVP nanofibres (Wang et al., 2007)

Besides incorporating AuNPs within electrospun nanofibres, the ability to immobilise them on the surface offers a possibility of reducing analyte response time. Figure 2.15 shows a photograph of AuNPs immobilized on the surface of polyethylineimine (PEI)/polyvinyl alcohol (PVA) nanofibres.

Similar to functionalisation strategies that are useful for immobilising dyes, ligands or metallic nanoparticles, enzymes can also be immobilised by surface immobilisation or encapsulation (Wang *et al*., 2009).

Stoilova and co-workers reported the surface immobilisation of acetylcholine esterase (AChE) onto polyacrylonitrile (PAN). Figure 2.16 shows the steps involved in the immobilisation of AChE onto PAN nanofibres.

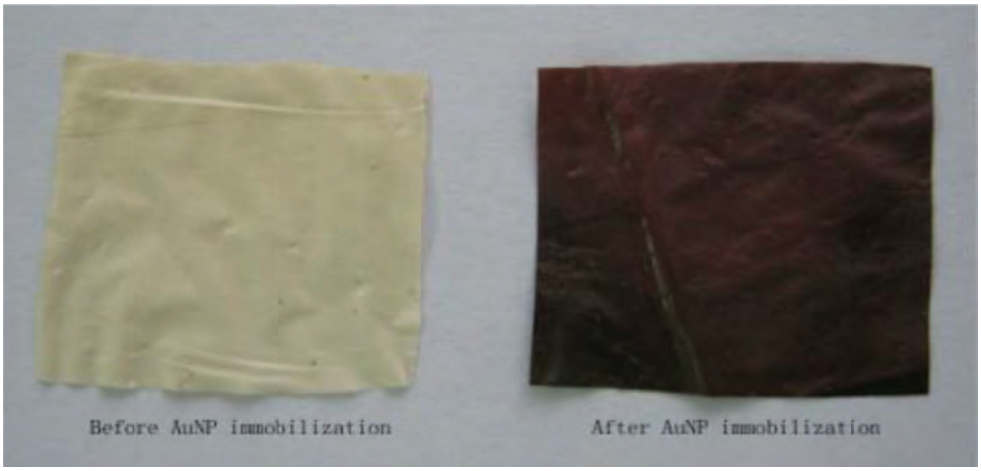

Figure 2.15: Digital photograph of free standing crosslinked PEI/PVA nanofibrous mat before (left panel) and after (right panel) AuNP immobilisation (Fang et al., 2011)

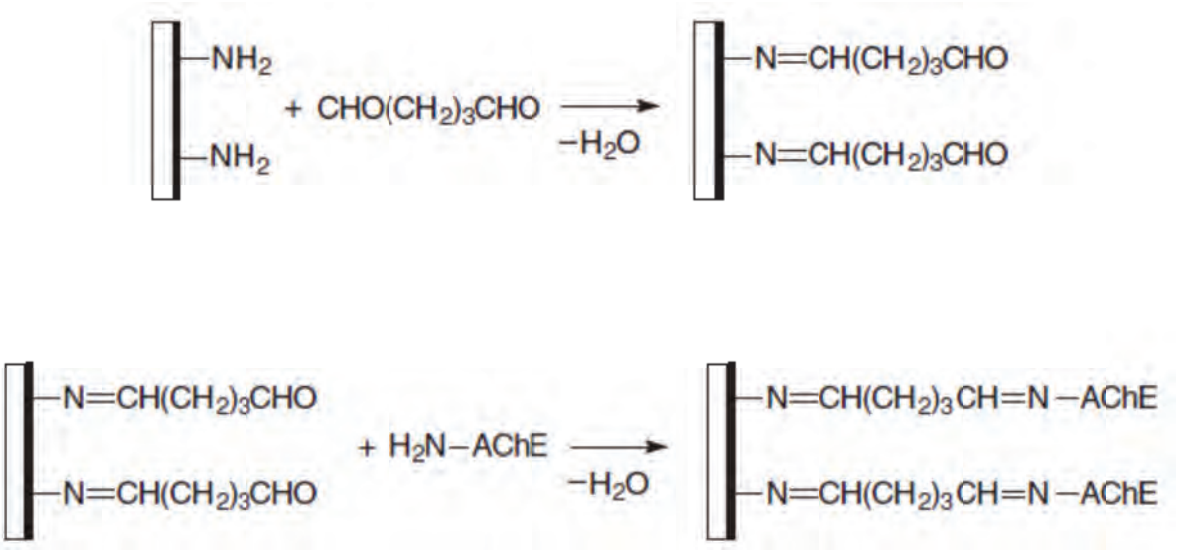

Figure 2.16: Steps for immobilization of AChE to PANNF/CHI fibres (Stoilova et al., 2010)

More examples of the application of electrospun nanofibres in the respective areas will appear under each section. It is based on this background that the experiments were designed to achieve the four objectives of the overall project.

3 DEVELOPMENT OF ELECTROSPUN NANOFIBRES FOR UPTAKE OF ARSENATE FROM AQUEOUS MEDIUM

3.1 Introduction

The objective of the study was to fabricate 2-amino-4,6-dihydroxylpyrimidine electrospun nanofibre-based solid phase extraction sorbent for the selective uptake of arsenate from wastewater.

Arsenic is a worldwide pollutant in ground and surface waters with serious health effects upon long term intake of even low concentrations through portable water consumption (Berg *et al*., 2006). Arsenic contamination in drinking water has become a major concern in many regions around the world, and has affected more than 100 million people worldwide (Quaff and Ashhar, 2005). Recently, the acceptable level of arsenic in drinking water was limited to 10 µg/L according to the U.S. Environmental Protection Agency and World Health Organization, but many developing countries still comply with a limit of 50 µg/L (Zhang *et al*., 2009).

Some water treatment technologies including coagulation, co-precipitation with ferric sulphate, precipitation as the sulphide using sodium sulphide or hydrogen sulphide, ion-exchange, adsorption, reverse osmosis, and electrodialysis are available for removing arsenic from water, but still suffer from a post treatment challenge regarding the alkaline sludge produced after the treatment (Hering *et al*., 1997, Singh and Pant, 2004, Salame *et al*., 2011). The sludge, which contains a mixture of gypsum, heavy-metal hydroxides and carbonate in addition to a large amount of water, leak back arsenic to the environment after exposure to water and air. Adsorption is one of the commonly used mechanisms for the removal of arsenic from water, especially for individual homes and small community systems in low income regions because the system is simple to operate and is cost effective (Dixit and Hering, 2003).

Many sorbents including mixed metal oxides, resins, activated alumina and modified materials were reported to be effective for arsenic removal (Ofomaja *et al*., 2005, Lin and Wu, 2001). Although activated alumina has been the most often used sorbent for arsenic removal, its disadvantages include relatively low sorption capacity which leads to leakage and the need for pH adjustment due to low working pH range (Armienta and Segovia, 2008, Pokrovski *et al*., 2002). Recently, more effective Fe(lll) bearing material such as goethite, ferrihydrite, granular ferric hydroxide (GFO), iron oxide coated activated carbon and Fe(lll) loaded cellulose have been developed for arsenic and consequent selectivity of adsorption process (Mohan and Pittman, 2007, Driehaus *et al*., 1995, Meng *et al*., 2001, Da and Masotti, 2010, Huang *et al*., 2011, Sun *et al*., 2011). Fibrous sorbents can be used directly and are easily separated from aqueous solution after adsorption due to their long size (Kuenstl *et al*., 2009).

Some researchers have prepared modified fibres to remove toxic anions, such as humic acid, fluoride and phosphate (Pokrovski *et al*., 2002, Kuenstl *et al*., 2009) but few studies have been conducted to remove arsenate from wastewater (Endo *et al*., 2012, Ren *et al*., 2009, Toda *et al*., 2005). Sorbents prepared from electrospun nanofibres have come to the forefront of analyte uptake due to their characteristics such as specific surface area, porosity, flexibility to surface functionalisation and ability to conform to a wide variety of physical and chemical conditions. The large surface area offers the nanofibres enhanced sorption capacity (Wu and Clark, 2008, Chigome *et al*., 2011). The concentrations of arsenic in water samples are very low, therefore sensitive analytical methods are required in order to achieve accurate and reliable results. Thus, an uptake of arsenate was quantified using inductively coupled plasma optical emission spectrometer (ICP–OES) US-EPA (2001).

3.2 Experimental

Reagents and materials

The sodium salts of nitrate and nitrite, arsenic(lll) oxide (all of purity more than 99%), 2-amino-4,6-dihydroxylpyrimidine and polyvinylmethylketone were purchased from Sigma Aldrich (St. Louis, USA and South Africa). *N*,*N*–Dimethylformamide, diethylether and tetrahydrofuran were purchased from Merck Chemicals (Wadeville, South Africa). All other chemicals were of analytical grade and were used without any further purification. Standard solutions were freshly prepared using ultrapure water generated from milliQ system (Massachusetts, USA). All glassware were washed, rinsed and soaked overnight in concentrated HNO_3 and then before use.

Instrumentation

Infrared spectra of the product as well as the polyvinylmethylketone and 2-amino-4,6-hydroxylpyrimidine were recorded on a Perkin-Elmer 100 FT-IR spectrophotometer (Massachusetts, USA). The morphology of the nanofibres was studied by a Tescan (TS5 136ML) field emission scanning Electron Microscope (Brno, Czech Republic) operating at an accelerated voltage of 20 kV after gold sputter coating. The diameters of the fibres were evaluated through the distance transform approach using Scandium Software (Ziabari *et al*., 2009). The concentrations of the anions in solution were measured using a Thermo Electron (iCAP 6000 series) inductively coupled plasma–optical emission spectrometer (ICP OES). Emission line of 193.76 nm for As was selected based on the EPA method of determining arsenic (V) (Ma *et al*., 1992). The pH of the solution was determined using Jenway (3510) pH meter (Essex, UK).

Synthesis of 2-amino-4,6-dihydroxylpyrimidine functionalised polyvinylmethylketone* (*APPMK)

2-Amino-4,6-dihydroxylpyrimidine was prepared by dissolving 0.330 g (0.0026 mmol) in 15 mL of aqueous 0.02 N NaOH solutions and was refluxed for 2 h at 70°C after complete dissolution. 0.035 g (0.0026 mmol) of the polyvinylmethylketone was dissolved in 10 mL of DMSO in a beaker and was added to the solution drop wise with continuous stirring for 12 h. On cooling, the solution was slowly poured while stirred vigorously into ethanol to precipitate the polymer, which was filtered under vacuum suction, washed extensively with diethyl ether and dried in a desiccator for 24 h.

Fabrication of 2-amino-4,6-dihydroxylpyrimidine functionalised polyvinylmethylketone nanofibres* (*APPMKNFs)

The electrospun nanofibres (20%) w/v were prepared by dissolving 2.0 g of the functionalized polymer in 10 mL of DMF:THF (3:7 v/v). The solution was stirred overnight to obtain a homogeneous solution. The polymer solution was loaded into a 10 mL syringe which was mounted onto a programmable syringe pump (New Era, NE- 1000). The solution was pumped at a flow rate of 0.50 mL/h through a stainless steel needle of 0.584 mm internal diameter. The applied voltage at the tip and the collector was maintained at +15 kV and -5 kV respectively.

Adsorption/desorption studies

To vials containing 20 mL aliquots of standard solutions, 10 mg of the functionalized nanofibre (sorbent) was added and stirred for 2 h. The concentration of the arsenate anion left in the solution was determined using ICP–OES after filtering the sorbent. 10 mg of the sorbent dose was used for the uptake of anion. They were placed in 20 mL aliquots of standard solutions and stirred for 2 h. The sorbent was then filtered off, washed with ultrapure water and was dried on the filter using vacuum suction (Chigome *et al*., 2011). To investigate the pH range of arsenate in the solution, adsorption studies were carried out in a standard solution of (50 µg/L) arsenic (V) within the pH range of 3 – 12. The extent to which arsenate anion was enriched was determined using ICP–OES. The effect of contact time on the uptake of arsenate anion was also investigated in (10 µg/L) of arsenate solution in batch experiments. The pH of the solution was adjusted with 0.1 M NaOH or 0.1 M HCl.

The desorption studies were carried out in 0.1 M NaOH and 0.1 M NaCl solutions, in batch experiments, in order to find a suitable solvent system for desorption of arsenate recovery from APPMKNFs. The effect of this was due to the stripping ability of OH^- at the higher concentration and effective in eluting adsorbed arsenate (Schwarzenbach and Schellenberg, 1965).

Desorbability (%) was calculated by the following equation:

$$Desorbability\ (\%) = \frac{C_a}{C_f} \times 100 \quad (1)$$

C_a = Quantity of desorbed to the elution
C_f = Amount of ion adsorbed on the adsorbent

3.3 Results and Discussion

Synthesis and characterization

The Schiff base ligand, 2–amino–4,6-dihydroxylpyrimidine, was synthesized with polyvinylmethylketone through a condensation reaction (Scheme 3.1).

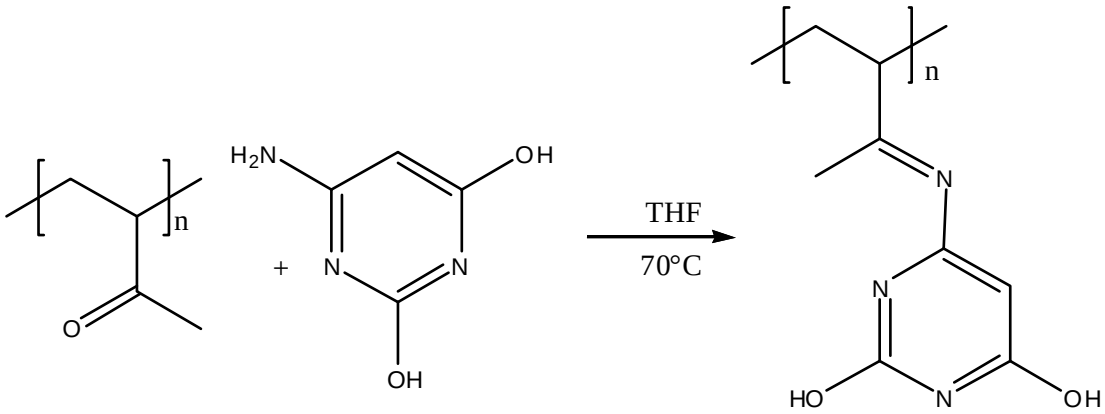

Scheme 3.1: Synthesis of aminodihydroxylpyrimidine functionalized polyvinylmethylketone polymer

The FT-IR spectra for the functionalized polymer and the two starting materials (polyvinylmethylketone and 2–amino-4,6-dihydroxylpyrimidine) are shown in Figure 3.1. The bands at 3139 cm^{-1} and 1696 cm^{-1} were assigned respectively to the amino functional group on the ligand and the carbonyl on the polymer. The peak at 1613 cm^{-1} was assigned to the stretching vibration of the imine functional group of the Schiff base.

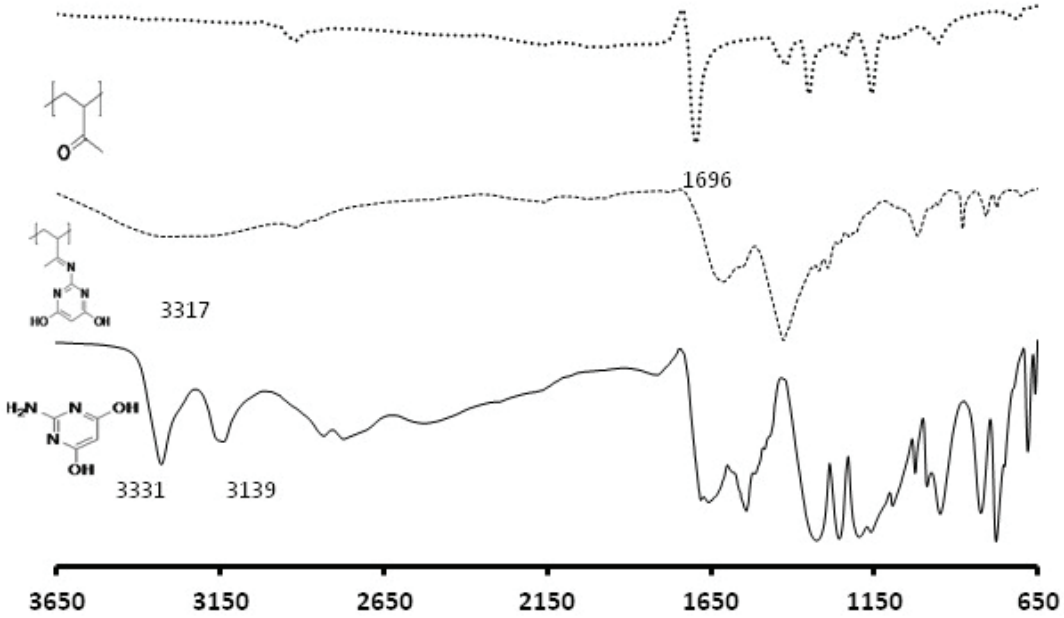

Figure 3.1: The FTIR spectra of polyvinylmethylketone.0, 2-amino 4,6-dihydroxylpyrimidine and APPMKNFs

The diameter of the 20% fibres fell in the range 127 to 200 nm. The specific surface area of the sorbent defines its efficiency for adsorption. However, the determination of fibre BET surface area via carbon dioxide gas adsorption analysis revealed that the sorbent had a good surface area of 57 ± 2 m^2/g.

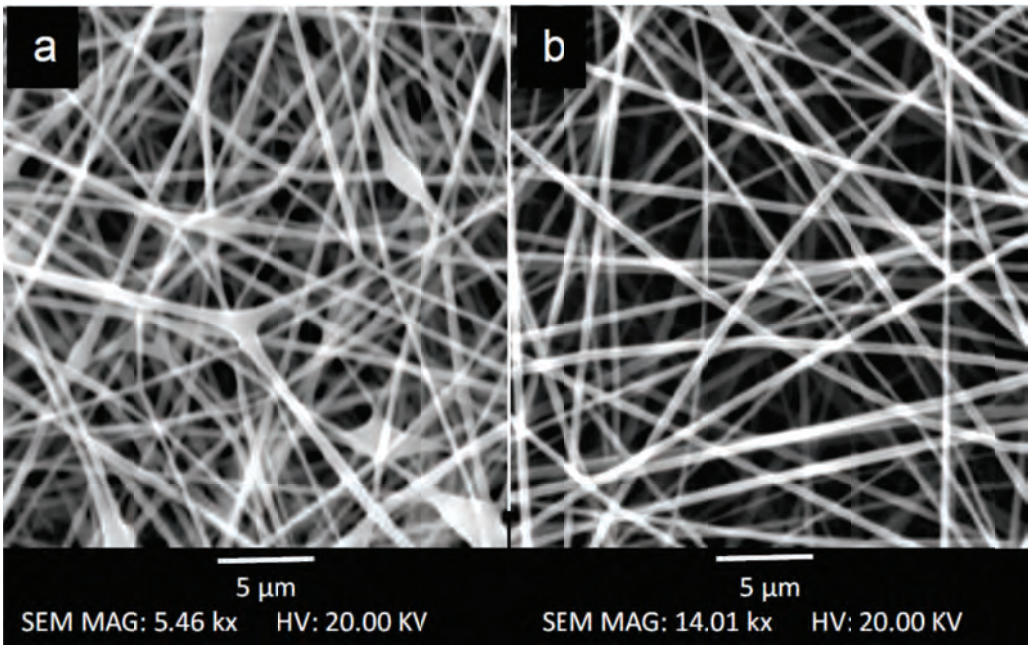

Figure 3.2: The SEM images of APPMKNFs (a) 10% (w/v) and (b) 20% (w/v) of APPMK

Arsenate concentration and adsorbent dosage

The concentration of arsenate and sorbent mass studied for the removal of arsenate were between 10 µg/L and 50 µg/L, 2 mg and 12 mg respectively (Figure 3.3). The optimized concentration of arsenate and sorbent mass used for the study was 50 µg/L and 10 mg.

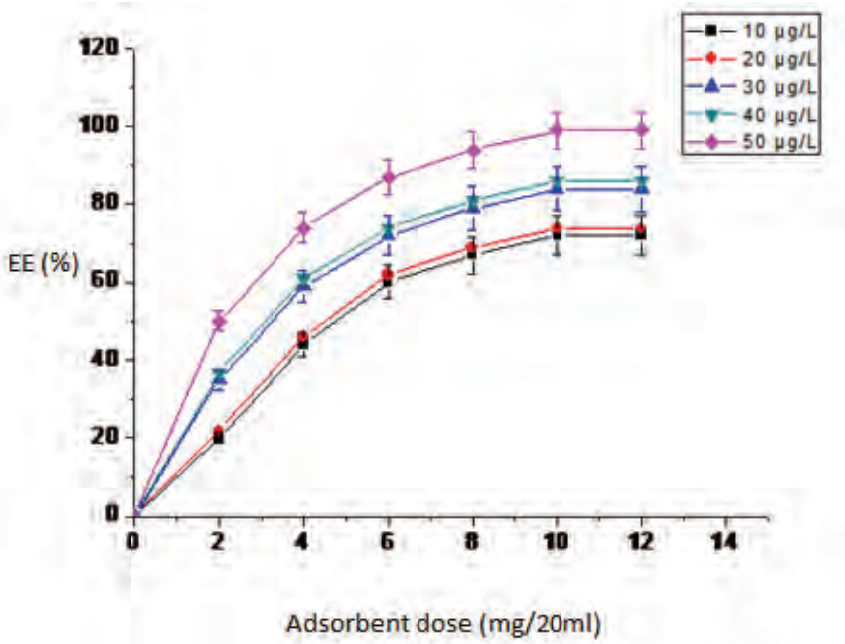

Figure 3.3: Effect of arsenate concentration and adsorbent dosage on arsenate removal onto APPMKNFs

Effect of pH

The pH of solution is generally known to play an important role in adsorption. Adsorption of arsenate on the functionalized sorbent material was highly efficient over a wide pH range as seen in Figure 3.4. The species of arsenate vary with pH as it can be converted from one species to another depending on the pKa value. The equilibrium for the $H_3AsO_4/H_2AsO_4^-$ couple has a pKa = 2.2 and the pKa for $H_2AsO_4^-/HAsO_4^{2-}$ is around 6.9 while the pKa for an equilibrium between $HAsO_4^{2-}$ and AsO_4^{3-} is 11.5 (Smedley and Kinniburgh, 2002). The existence of the species as a function of pH seems to be in line with the observed uptake of arsenate with pH as the oxygens would be available for hydrogen bonding with the hydroxyl groups on the sorbent

material. At the higher pH, the observed decrease could be attributed to the loss of hydrogen on the sorbent material as the pH was increased since the pKa of the hydroxyl groups is around 10-11 (Pagnanelli *et al*., 2000) thus decreasing the attraction of the anion to the sorbent due to partial ionization of hydroxyl groups. Subsequent studies were, therefore, carried out in the pH range of 3-5.

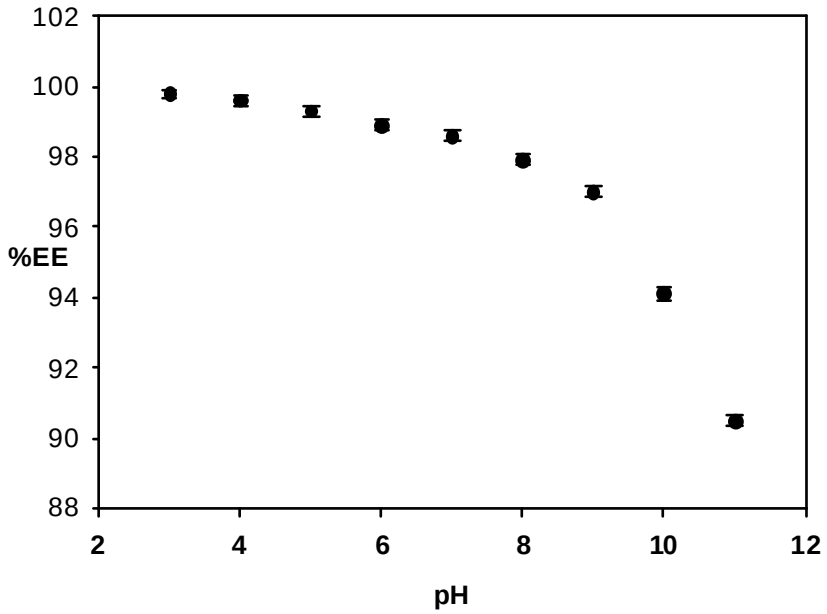

Figure 3.4: The effect of pH on arsenate removal onto APPMKNFs

Adsorption isotherms

The adsorption capacity values were calculated using the Langmuir isotherm [Eq. (2) and Freundlich equation [Eq. (3)].

$$\frac{\mathrm{Ce}}{Qe} = \frac{Ce}{Qm} + \frac{1}{(KaQm)} \quad \text{Langmuir Isotherm} \tag{2}$$

$$\log Q_e = \log K_f + \frac{1}{\mathrm{n}} \log C_e \quad \text{Freundlich Isotherm} \tag{3}$$

where C_e [mg/L] and Q_e [mg/g] are arsenate concentration and adsorption equilibrium, Q_m [mg/g] and K_a [L/mg] are the theoretical maximum adsorption capacity and Langmuir equilibrium constant related to the theoretical maximum adsorption capacity. K_f and n are the Freundlich constants which are indicators of adsorption capacity and adsorption intensity.

The adsorption data best fitted the Langmuir isotherm compared to the Freundlich isotherm (see Figure 3.5). Langmuir equation is used to describe a monolayer adsorption without adsorbate interaction (Scott and O'Reilly, 1991). The correlation coefficient for the Langmuir model was (R^2 = 0.9968) which was higher than that of Freundlich model (R^2 = 0.8313), showing that the adsorption in the experiment better fit the Langmuir model.

Table 3.1: Parameters of Langmuir adsorption equation and Freundlich isotherm equation for adsorption experimental data

Isotherm	**Parameters**	**Values**
Langmuir	Q_m (mg/g) K_a (mg/L) R^2	145.1 1.05 0.9968
Freundlich	K_F n R^2	0.563 2.686 0.8313

Adsorption kinetics

The adsorption kinetics play an important role in the efficiency of arsenate removal from solution (Eblin *et al*., 2006). Figure 3.5 shows that more than 98% of arsenate in the spiked water sample was removed within 20 min of contact time.

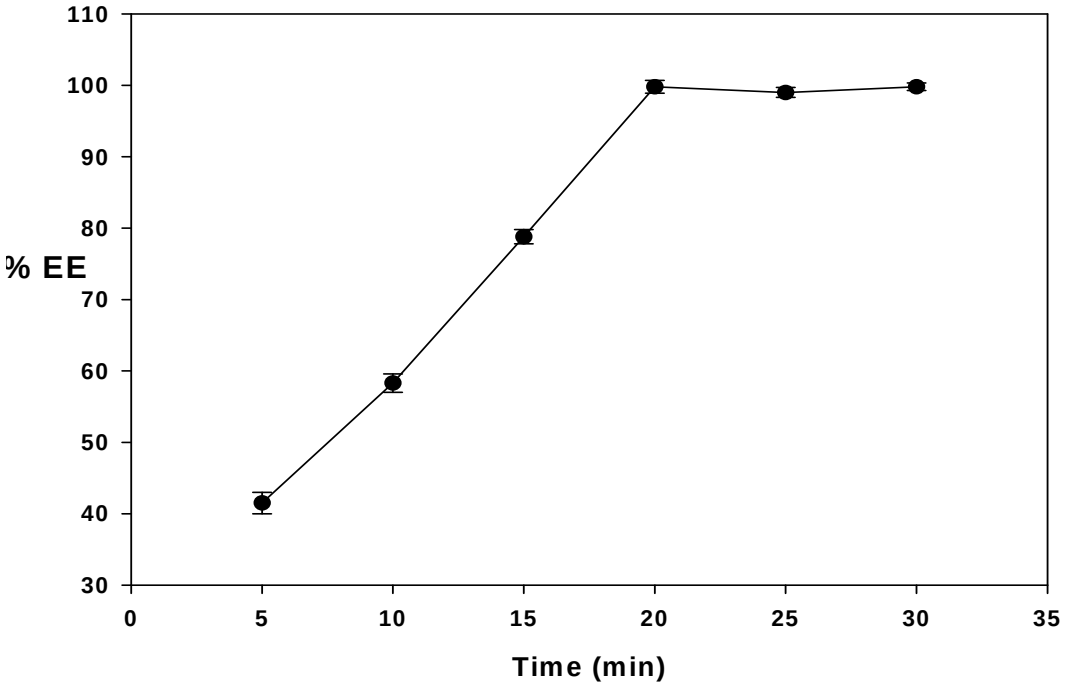

Figure 3.5: Optimization of the time needed to extract maximum arsenate at a pH of 3

Interference studies

The effect of co-existing anions on the removal of arsenate unto APPMKNFs was studied in spiked solutions. Wastewater normally contains coexisting ions which could potentially interfere in the adsorption of arsenate. Thus, the competitive sorption of the coexisting anions including; nitrite, bicarbonate, nitrate and chloride were evaluated in the test solution of arsenate containing 10 µg/L and 50 µg/L of the co-existing anions. There was no significant difference for the adsorption of arsenate in the presence of the co-existing anions. In light of these observations, we can say that the APPMKNFs are well suited for arsenate removal in the presence of the co-existing anion because 98.1 – 99.7% of arsenate was recovered from the solution (Table 3.2).

Table 3.2 Effect of co-existing anions on the removal of arsenate (n = 3)

Anions added	Concentration of anions µg/L	Concentration of arsenate µg/L	Recovery (%)
Chloride	50, 60	50	99.39, 99.78
Nitrate	50, 60	50	99.69, 98.87
Bicarbonate	50, 60	50	99.09, 98.54
Nitrite	50, 60	50	99.79, 98.19

Reusability studies

The adsorbed arsenate was quantitatively recovered by desorption with 0.1 M NaOH and results are shown below in Figure 3.6.

Figure 3.6 shows that the arsenate sorption capacity of the sorbent material was slightly decreased after the fifth cycle and this shows that the sorbent material was good and could be reused several times without loss of binding ability for arsenate.

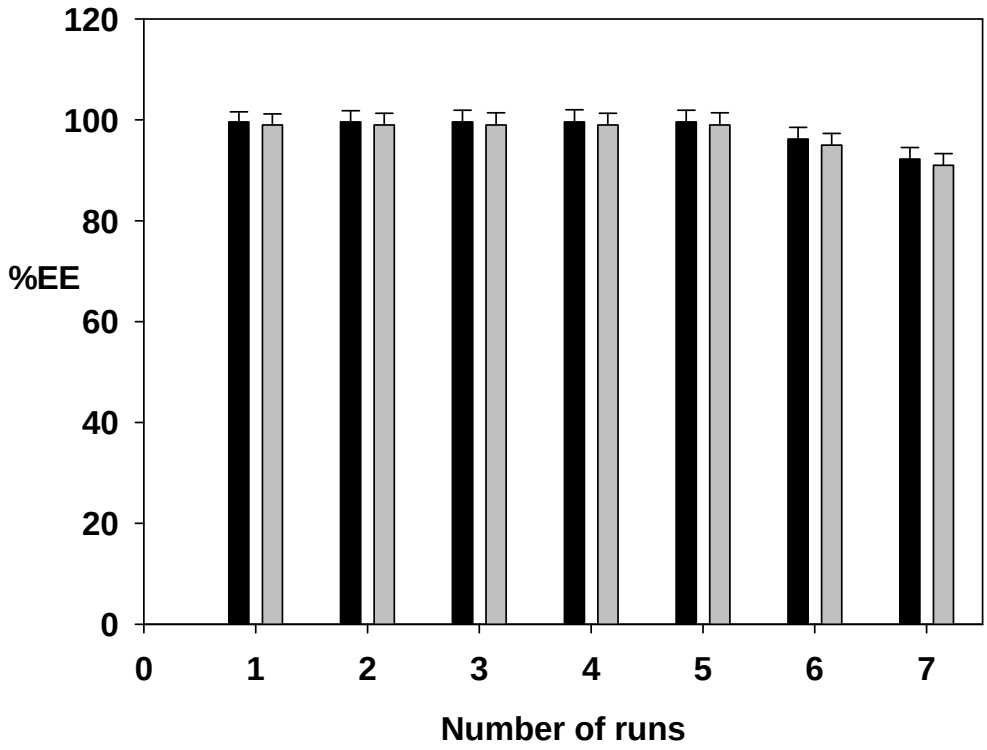

Figure 3.6: The reusability cycles of APPMKNFs

Application of APPMKNFs on environmental water sample

Millipore water and wastewater samples were spiked with arsenic(III) oxide. The measurements were performed three times and the results for the spiked samples are summarized in Table 3.2. It may be concluded from the results presented that APPMKNFs could be effectively used for the specific removal of arsenate from wastewater.

Table 3.3: Analysis of arsenate in Millipore water and wastewater samples (n = 3)

Spiked samples	Quantity spiked (µg/L) of arsenate	% EE using ICP-OES Analysis
Millipore Water	50	99.9
Millipore Water	50	98.3

3.4 Conclusions

The uptake of arsenate using 2–amino-4,6-dihydroxylpyrimidine functionalized polyvinylmethylketone nanofibres was investigated in batch experiments. The maximum adsorption of arsenate was above 98% within the pH range of 2 to 7, and the kinetics of uptake were relatively fast (within 20 min). The sorbent material worked well in the uptake of arsenate in the presence of co-existing anions. Adsorbed arsenate was eluted with 0.1 M sodium hydroxide solution from the sorbent material and this sorbent can be used five times with a slight decrease in performance after the fifth cycle. Therefore, the sorbent material was good and could be reused several times without loss of binding of arsenate.

3.5 Recommendations

Work is currently in progress to establish the column mode for adsorption as a step towards developing pilot scale flow through systems that rely on electrospun nanofibres as the sorbent bed.

4 PREPARATION AND ANTIMICROBIAL ACTIVITY STUDIES OF 2-SUBSTITUTED *N*-ALKYLIMIDAZOLES

4.1 Introduction

The objective of the study was to synthesize 2-substituted *N*-alkylimidazole derivatives and study the effect of the pKa of the 2-substituent [aldehyde (-CHO), alcohol (-CH_2OH), carboxylic acid (-CO_2H)] on the antimicrobial activity against *Escherichia coli*, *Staphylococcus aureus*, *Bacillus subtilis* subsp. *spizizenii* and *Candida albicans*.

Microorganisms occur all around the environment such as in the air, water, skin and food. Due to the adverse health effects of the pathogenic microorganisms, their treatment and control is very important. Some known pathogenic microorganisms include *Escherichia coli*, *Staphylococcus aureus*, *Bacillus subtilis* subsp*. spizizenii* and *Candida albicans*, to name a few. *Escherichia coli*, a Gram-negative bacterium, can cause diarrhoeal disease and usually affects mostly children and adults (Ali *et al*., 2012). Its infectious dose is relatively low (10 microorganisms) compared to other bacterial causes of gastro-enteritis. *Staphylococcus aureus*, a Gram-positive bacterium mainly found on the skin surface and mucous membranes of humans and animals, can cause skin sepsis and wound infections (Muñoz-Bonilla and Fernández-García, 2012). *Bacillus subtilis* subsp*. spizizenii*, another Gram-positive bacterium found in the environment, causes infections such as meningitis. It can also exacerbate previous infections by producing tissue-damaging toxins or metabolites that interfere with treatment. *Candida albicans*, a yeast found in the warm regions of the human skin, causes Candidiasis which is the most common type of yeast infection as well as infections of tissues of the oral cavity, skin and diaper rash and nailbed infections (Pitarch *et al*., 2001).

The use of imidazole compounds is well established in the field of medicinal chemistry, finding applications as anticancer (Congiu *et al*., 2008), antibacterial (Khabnadideh *et al*., 2003), antifungal (Goker *et al*., 1991), antiparasitic (Samant and Sukhthankar, 2011) and antidiabetic (Crane *et al*., 2006) drugs, to name a few. The discovery of azole antibacterial and antifungal agents began with benzimidazole in 1944 (Woolley, 1944). Since then several reports have noted the antifungal activity of imidazoles (Woolley, 1944, Antolini *et al*., 1999, Khan *et al*., 2006), the action of which is suspected to be due to interference with ergosterol synthesis and membrane damage (Sheehan *et al*., 1999). Azoles inhibit lanosterol demethylase, a cytochrome P-450 dependent enzyme which is responsible for the synthesis of ergosterol. Ergosterol is a major sterol of the cytoplasmic membrane and is responsible for a variety of cellular functions. It is responsible for the fluidity and integrity of the cytoplasmic membrane, as well as the proper functioning of chitin synthetase. Chitin synthetase is in turn responsible for cell growth and division (Sheehan *et al*., 1999, White *et al*., 1998). The mechanism of antibacterial action of azoles is believed to be through the inhibition of enoyl acyl carrier protein reductase (FabI), a novel antibacterial target (Rostom *et al*., 2009).

Further development and modification of antimicrobial agents remains crucial, since rapid mutation and subsequent drug resistance of new microbial strains continues (Sharma *et al*., 2009). Derivatizing the imidazole group with long alkyl chains has been demonstrated to dramatically improve the antibacterial activity of simple imidazoles. A few substituents at the 2-position of *N*-alkylimidazole derivatives such as the methyl group and the ether moiety have also been investigated for their effect on the antimicrobial activity (Khabnadideh *et al*., 2003, Samant and Sukhthankar, 2011).

4.2 Experimental

Reagents and Instrumentation

Alkylbromides, n-butyllithium (2.5 M in hexane), imidazole (99.5%) and acetone (laboratory reagent, >99.5%) were obtained from Sigma Aldrich. Hydrogen peroxide (30%), sodium borohydride, silver nitrate, hydrochloric acid (32%), potassium carbonate, sodium sulphate (anhydrous) and potassium hydroxide, diethylether, dimethylformamide and chloroform were obtained from Merck Chemicals (SA) and were used as received. *E. coli* (AATC 8793), *S. aureus* (AATC 6538), *B. subtilis,* subsp*. Spizizenii* (AATC 6633) and *C. albicans* (AATC 2091) were obtained from Microbiologics. Meuller-Hinton, Nutrient (agar/broth) and Potato dextrose agar (Merck), metronidazole discs (50 µg) and blank discs (6.5 mm) were sourced from Davies Diagnostics. Metronidazole (for preparing 100 µg discs) was purchased from Changzhou Longcheng Medicine Raw Material Co., Ltd., Changzhou City, Jiangsu, China, and ketoconazole was purchased from Oman Chemicals and Pharmaceuticals, Al Buraimi, Sultanate of Oman.

The NMR spectra were recorded on a Bruker Avance 400 NMR spectrometer. Infrared spectra were obtained with a Perkin Elmer Spectrum 400 FT-IR spectrometer. Microanalysis was carried using a Vario Elementar Microtube ELIII. The minimum inhibitory concentrations were measured using LEDETECT96 microplate reader, equipped with CAPTURE96 software. For the cytotoxicity experiments, absorbance was measured using a Biotek Powerwave XS Spectrophotometer and the results were analysed using Graphpad Prism 5 software.

Synthesis of N-alkyimidazole-2-substituted derivatives

N-alkylimidazole-2-carboxaldehyde and *N*-alkylimidazole-2-methanol derivatives were prepared as previously reported (see synthesis Scheme 4.1) (Oberhausen *et al*., 1989, Kruse *et al*., 1990, Roe, 1963). Several new *N*-alkylimidazole-2-carboxylic acids were prepared from the corresponding *N*-alkylimidazole-2-carboxaldehydes by hydrogen peroxide facilitated oxidation in aqueous conditions. The reaction required no heating and water was the only by-product of oxidation, making it an environmentally friendly option. The only purification necessary was the removal of residual water *in vacuo*, at room temperature. This afforded the *N*-alkylimidazole-2-carboxylic acid derivatives in quantitative yields.

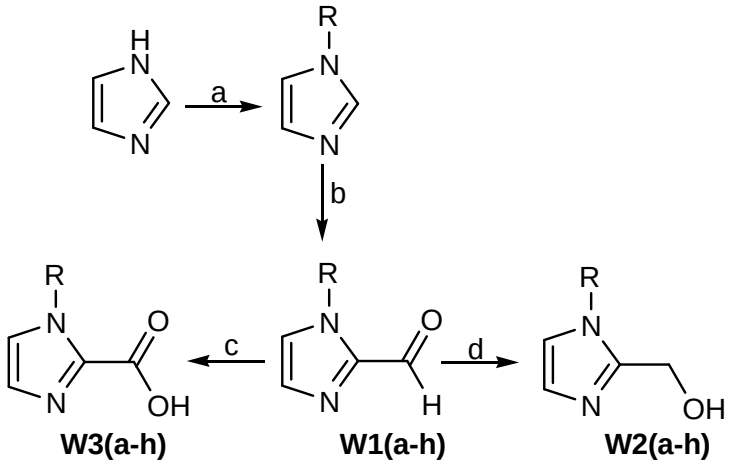

Scheme 4.1: Synthesis of N-alkylimidazole-2-substituted derivatives, 2-substituent = methanol, carboxaldehyde, carboxylic acid. R = benzyl, methyl, ethyl, propyl, butyl, heptyl, octyl, decyl. a. KOH, R-X and acetone. b. Butyllithium, DMF and diethylether. c. H_2O_2

Antimicrobial activity

The antimicrobial activity of the compounds was tested against a Gram-negative (*E. coli)*, Gram- positive (*S. aureus* and *B. subtilis* subsp*. spizizenii*) bacteria and fungi (*C. albicans*) using the disk diffusion method. Blank disks (6.5 mm) were impregnated with 20 µL of a methanolic solution containing the various compounds such that 50 µg and 100 µg of the pure compound remained on the disk. The disks were left overnight at room temperature to allow the methanol to evaporate, and then placed onto Mueller-Hinton agar plates streaked with the various bacteria. The plates were incubated (bacteria at 37°C, fungi at 30°C) for 18 h (fungi for 48 h) after which the zone of clearance was measured and the minimum inhibitory concentrations were determined using the broth microdilution method. Single colonies were suspended in the Mueller-Hinton or Nutrient broth and incubated until an appropriate optical density (OD_{600}) at 600 nm, over a period of 2-6 h. Ethanolic solutions of test compounds (2.5 mg/mL) were serially diluted in 96 well microplates using the broth. The bacterial suspension (5 µL) was added and the plates incubated at 37°C for 18 h. Metronidazole and Ketoconazole were used as positive controls for bacteria and fungi, respectively.

4.3 Results and Discussion

Poor antibacterial activity was observed for compounds with alkyl chain lengths of less than four carbons at the concentrations tested. Therefore, the results were not been included. However, compounds with longer alkyl chain lengths, *N*-alkylimidazole-2-aldehyde (**W1e-g**), *N*-alkylimidazole-2-methanol (**W2e-g**) and *N*-alkylimidazole-2-carboxylic acid (**W3e-g**) derivatives showed excellent concentration dependant antibacterial activity against the Gram-positive bacteria. The activity was also highly dependent on the length of the alkyl chain, a trait previously observed (Khabnadideh *et al*., 2003, Khan *et al*., 2006). At both concentrations (50 and 100 µg), the compounds showed excellent activity against Gram-positive *B. subtilis*

subsp*. spizizenii*, with the exception of **W3e** which showed little activity (Table 4.1). Substitution of the alkyl chain with a benzyl group (**W1h**, **W2h**, **W3h**) eliminated antibacterial activity completely.

Generally, imidazole compounds are more active against gram-positive bacteria (Antolini *et al*., 1999), as was the case in this study. The Gram-negative bacteria, *E. coli* proved to be the most resistant of all the bacteria tested. The resistance of *E. coli* has been attributed to it having an outer cell membrane which regulates the contents that enter or leave the cell (Denyer, 1995).

Table 4.1: Zones of clearance and MICs of N-alkylimidazoles using 50 and 100 µg of compounds

Compound			***E. coli***			***S. aureus***			***B. subtilis* subsp. *spizizenii***			***C. albicans***		
	R	No.	50	100	MIC*	50	100	MIC*	50	100	MIC*	50	100	MIC*
Aldehydes	Heptyl	W1e	-	+	>2.5	+	++	0.04	+++	+++	0.02	-	-	nd
	Octyl	W1f	-	+	>2.5	++	++	0.01	+++	+++	0.005	-	-	nd
	Decyl	W1g	-	+	>2.5	++	++	0.005	+++	+++	0.005	+	+	nd
Alcohols	Heptyl	W2e	-	+	0.15	++	++	0.08	++	+++	0.02	-	-	nd
	Octyl	W2f	-	+	0.04	+	++	0.08	+++	+++	0.01	-	-	nd
	Decyl	W2g	-	+	0.02	++	++	0.01	+++	+++	0.005	-	-	nd
Carboxylic acids	Heptyl	W3e	+	+	0.30	+	+	0.30	+	+	0.02	-	-	nd
	Octyl	W3f	+	+	0.15	++	+++	0.02	+++	+++	0.005	-	-	nd
	Decyl	W3g	+	+	0.04	+++	+++	0.01	+++	+++	0.005	+	+	nd
Metronidazole			-	+	0.65	-	+	0.30	-	++	0.30			
Ketoconazole												+++	+++	nd

- no clearance; **+** < 9 mm; **++** < 15 mm; **+++** > 15 mm
*MIC units are in mg/mL

Only compound **W3g** showed a slight activity at 50 µg, while the rest showed slight activity at 100 µg concentration. *C. albicans* was also highly resistant towards the compounds tested, with only compounds **W1g** and **W3g** showing a slight activity at 100 µg concentration. A similar trend as was observed for the disk diffusion method was observed for broth microdilution method as well. Very low concentrations were required for the inhibition of the growth of Gram-positive *B. subtilis* subsp*. spizizenii*.

4.4 Conclusions

It was clear, from these results that simple modification of the starting imidazole unit could have significant implications for both activity and specificity, and this was a huge advantage considering the ever increasing emergence of resistant strains. Poor antibacterial activity was observed for compounds with alkyl chain lengths of less than four carbons. In fact, *N*-decylimidazole-2-carboxylic acids proved to have excellent activity across the entire range of tested bacterial strains. However, all the compounds tested had poor antifungal properties.

4.5 Recommendations

It is always desirable that antimicrobial agents possess activity over a broad spectrum of pathogenic microorganisms. The 2-substituted *N*-alkylimidazoles prepared in the study demonstrated antimicrobial activity predominantly towards gram positive bacteria. Since chlorine is also known to have antimicrobial activity, investigating the effect of introducing a chloride group at the 2-position of *N*-alkylimidazoles could result in compounds with enhanced potency. The study could focus on the 2-substituted *N*-alkylimidazoles containing shorter alkyl chains since they demonstrated poor antimicrobial activity across the spectrum of microorganisms investigated.

5 PREPARATION AND ANTIMICROBIAL ACTIVITY STUDIES OF SILVER(I) COMPLEXES CONTAINING 2-HYDOXYMETHY-*N*-ALKYLIMIDAZOLES

5.1 Introduction

The objective of the study was to synthesize silver(I) complexes containing antimicrobially active 2-hydroxymethyl-*N*-alkylimidazole ligands and to investigate their antimicrobial activity against *Escherichia coli*, *Staphylococcus aureus*, *Bacillus subtilis* subsp*. spizizenii* and *Candida albicans*.

Silver and its salts have been used as antimicrobial agents for many centuries (Klasen, 2000, Lansdown, 2002). Silver has the most superior properties among all metals with antimicrobial activity because of its higher toxicity to microorganisms and lower toxicity to mammalian cells (Li *et al*., 2010b, Radheshkumar and Münstedt, 2006). Ionic silver is reportedly the active species while metallic silver is inert (Lok *et al*., 2007). The ancient Phoenicians used silver-coated containers to store water so as to prevent spoiling. The storage of water in silver-coated containers is supposed to have aided in the prevention of contamination by microorganisms. It was also reported that aqueous silver nitrate was used as an eye drop to newly born babies for the prevention of *Neisseria gonorrhoeae* transmission from infected mothers (Silvestry-Rodriguez *et al*., 2007, Klueh *et al*., 2000). There are several reported mechanisms by which silver acts on the microorganisms (Guggenbichler *et al*., 1999). For example one mechanism has been described to involve the reversible binding of silver to the nucleotide bases of the bacterial DNA. The reversible binding of silver to the bacterial DNA results in the denaturation by displacement of hydrogen bonds between adjacent purines and pyrimidines. Davis and Etris (Davies and Etris, 1997) proposed that the destruction of bacteria occurs through silver-catalyzed oxidation of sulphydryl (S-H) moieties on the surface of the membrane. Atomic oxygen in the aqueous medium oxidizes Ag(0) to Ag(I) which readily reacts with adjacent S-H groups by replacing the hydrogens. Consequent coupling of these adjacent S-groups results in the formation of S–S bond, thereby blocking respiration and electron transfer.

Silver sulfadiazine was the first silver complex to be used as an antimicrobial agent (Carr *et al*., 1973, Rai *et al*., 2009). It is currently clinically administered for the treatment of burn wounds. Due to the emergence of resistant microorganisms, new broad spectrum antimicrobial agents are necessary. Consequently, many silver complexes have been investigated for their antimicrobial activity (Kazachenko *et al*., 2000, Abu-Youssef *et al*., 2007). Interestingly, silver complexes containing imidazole ligands have exhibited remarkable broad spectrum antimicrobial activity (Nomiya *et al*., 1997, Rowan *et al*., 2006). However, the antimicrobial activity of the silver complexes containing imidazole ligands is often entirely due to the Ag(I) metal ion, since these metal-free imidazole ligands possess no activity. For example, Rowan and his co-workers (Rowan *et al*., 2006) reported a series of imidazole derivatives which displayed no antimicrobial activity when not in a coordination sphere while their corresponding silver complexes displayed better activity. It is desirable, therefore, to synthesize silver complexes containing antimicrobially active imidazole ligands. It is also worth noting that the purpose for the preparation of silver sulfadiazine was to combine an antimicrobially active sulphonamide (sulfadiazine) with the Ag(I) metal centre. The presence of antimicrobially active silver(I) and imidazole ligands in a complex should result in enhanced activity.

5.2 Experimental

Synthesis of silver(I) complexes containing 2-hydroxymethyl-N-alkylimidazoles

To a solution of $AgNO_3$ (1 mol equivalent) in ethanol (15 mL) was added 2-hydroxymethyl-*N*-alkylimidazole (2 mol equivalents). The reaction mixture was stirred at room temperature for 24 h. The reaction mixture was filtered, ethyl acetate (15 mL) was added to the mother liquor and the solvent evaporated slowly at atmospheric pressure to obtain a pure product in good yield (Scheme 5.1).

Antimicrobial activity

The antimicrobial activity experiments for the Ag(I) complexes were carried out in the similar manner as described for the 2-substituted *N*-alkylimidazoles (Section 4).

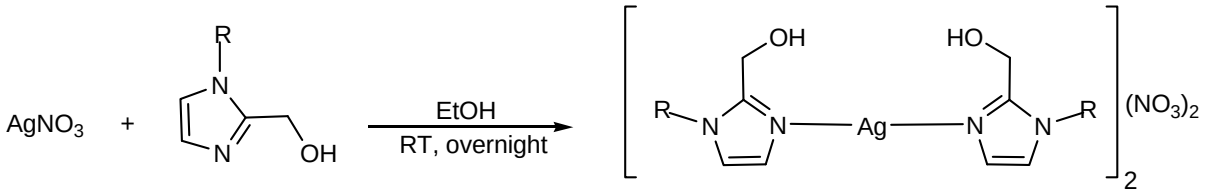

R = Me (Ag-W2a); R = Et (Ag-W2b); R = Pr (Ag-W2c); R = But (Ag-W2d);

R = Hep (Ag-W2e); R = Oct (Ag-W2f); R = Dec (Ag-W2g); R = Bz (Ag-W2h)

Scheme 5.1: Synthesis scheme of silver(I) complexes containing 2-hydromethyl-N-alkylimidazole ligands

5.3 Results and Discussion

The antimicrobial activity of the silver(I) complexes was investigated against *E. coli*, *S. aureus*, *B. subtilis* subsp*. spizizenii* and *C. albicans*. A summary of the results for the *in vitro* antimicrobial activity experiments is presented in Table 5.1. The Ag(I) complexes containing 2-hydroxymethyl-*N*-alkylimidazole ligands display antimicrobial activity against a broad spectrum of microorganisms (Table 5.1). The antimicrobial activity against *E. coli* and *C. albicans* is due entirely to Ag(I) for all the complexes tested. As shown in Table 4.1, the metal-free 2-hydroxymethyl-*N*-alkylimidazoles exhibited poor activity against *E. coli* and *C. albicans* (Kleyi *et al*., 2012). In addition, it was also shown that only metal-free ligands with long alkyl chain length display excellent activity against *S. aureus* and *B. Spizizenii* (Kleyi *et al*., 2012). It was, therefore, anticipated that the Ag(I) complexes containing these ligands (**Ag-W2e** - **Ag-W2g**) would display better activity than $AgNO_3$ (Table 5.1) because the antimicrobial activity of these complexes is imparted by both Ag(I) and the ligands. There have been reports showing that the Ag(I) complexes performed better as antifungal than as antibacterial agents (McCann *et al*., 2003, Ruan *et al*., 2009). Other reports showed that the Ag(I) complexes possess antimicrobial activity predominantly against Gram-negative than Gram-positive bacteria (Kazachenko *et al*., 2000) or vice versa (Nemati Kharat *et al*., 2011). In the study, it was observed that the predominance of activity towards a particular microorganism was dependent on the alkyl chain length of the ligand. For complexes containing ligands with shorter alkyl chain length (**Ag-W2a** - **Ag-W2d**), the activity is in the order *E. coli* (MIC = 0.02 mg/mL), *B. subtilis* subsp*. spizizenii* (MIC = 0.04 mg/mL), *S. aureus* and *C. albicans* (MIC = 0.08 mg/mL). For complexes containing longer alkyl chain length (**Ag-W2e** - **Ag-W2g**), the activity order is *B. subtilis* subsp*., spizizenii* (MIC = 0.005 mg/mL), *E. coli* (MIC = 0.01 mg/mL), *S. aureus* (MIC = 0.02 mg/mL) and *C. albicans* (MIC = 0.04 mg/mL).

Table 5.1: Zones of clearance (50 or 100 µg of compound) and MICs for the silver(I) complexes containing 2-hydroxymethyl-N-alkylimidazoles (Ag-W2a-Ag-W2h)

Complex	**R**	***E. coli***		***S. aureus***		***B. spizizenii***		***C. albicans***	
		Diam (mm)	**MIC (mg/mL)**	**Diam (mm)**	**MIC (mg/mL)**	**Diam (mm)**	**MIC (mg/mL)**	**Diam (mm)**	**MIC (mg/mL)**
Ag-W2a	Methyl	13	0.02	12	0.08	11	0.04	11	0.08
Ag-W2b	Ethyl	12.3	0.02	12	0.08	11.3	0.04	11.3	0.08
Ag-W2c	Propyl	10	0.02	11	0.08	10.5	0.04	10.7	0.08
Ag-W2d	Butyl	10.2	0.02	11.5	0.08	11.3	0.04	11.5	0.08
Ag-W2e	Heptyl	12	0.01	12.2	0.04	17.3	0.02	12	0.04
Ag-W2f	Octyl	13.7	0.005	19.7	0.02	18	0.005	12.3	0.04
Ag-W2g	Decyl	12	0.01	18	0.02	16.3	0.005	12.7	0.04
Ag-W2h	Benzyl	11	0.04	12	0.08	11	0.08	10.3	0.04
$AgNO_3$		12.7	0.01	12	0.02	11	0.01	14	0.02

5.4 Conclusions

Silver(I) complexes containing 2-hydroxymethyl-*N*-alkylimidazole ligands were successfully synthesized and characterized using elemental analysis and IR spectroscopy. X-ray crystal structures of complexes **Ag-W2b** and **Ag-W2h** were also obtained. The Ag(I) complexes displayed a broad spectrum antimicrobial activity. The complexes containing ligands with shorter alkyl chain length displayed predominant activity against *E. coli*, while those containing longer chains had predominant activity against *B. subtilis* subsp*. spizizenii*. The antimicrobial activity of the complexes against *E. coli* and *C. albicans* was entirely due to Ag(I) ions

since the metal-free ligands possess poor activity. The antimicrobial activity of the complexes containing ligands with longer alkyl chain length was due to both Ag(I) and the ligands.

5.5 Recommendations

The Ag(I) complexes demonstrated a broad spectrum antimicrobial activity, however, the activity was entirely due to the silver(I) ion for E. *coli* and C. a*lbicans*. Silver(I) complexes containing *N*-alkylimidazoles with a CI group at the 2-position could be investigated for dual antimicrobial effect against pathogenic microorganisms.

6 INCORPORATION OF 2-SUBSTITUTED *N*-ALKYLIMIDAZOLES AND SILVER(I) COMPLEXES CONTAINING 2-HYDROXYMETHYL-*N*-ALKYLIMIDAZOLES INTO ELECTROSPUN NYLON 6 NANOFIBRES

6.1 Introduction

The objective of this study was to use electrospun nylon 6 nanofibres as solid supports to host selected 2-substituted *N*-alkylimidazoles and Ag(I) complexes containing 2-hydroxymethyl-*N*-alkylimidazoles and to investigate the antimicrobial activity of these nanofibre composites.

Electrospun nanofibres have highly interesting properties such as high surface to area ratio and the ease of surface modification. Research has always been focussing on exploitation of these nanofibre properties to achieve specific outcomes in many fields, including filtration, catalysis, tissue engineering and drug delivery systems.

The use of electrospun nanofibres as solid supports to host bio-active molecules has received much attention especially in drug delivery systems (Kriegel *et al*., 2008, Yoo *et al*., 2009). It is believed that because of their porous structure, electrospun nanofibres are able to release drugs at the targeted site and in a controlled manner although the mechanism is not yet well understood (Zamani *et al*., 2010). Antimicrobial electrospun nanofibres fabricated from natural and synthetic polymers were reported previously. For example, electrospun polyethylene oxide (PEO): chitosan nanofibre filters were fabricated and investigated for their heavy metal binding, antimicrobial and physical filtration efficiencies (Desai *et al*., 2009). Electrospun nylon 6 nanofibres incorporated with three structurally different *N*-halamines were fabricated and their antimicrobial activity evaluated. It was observed that the electrospun nylon 6 nanofibre composites inhibited the growth of *E. Coli* and *S. aureus* within a contact time of 40 min (Tan and Obendorf, 2007).

6.2 Experimental

Reagents and Instrumentation

Nylon 6 (Mw = 11200 Da) was obtained from Sigma Aldrich. Formic acid (85%) and acetic acid (95%) were purchased from Merck. The flow rate of the polymer solution was controlled using a NE 300 digital pump (New Era Pump Systems, Inc. USA). The bacteria colonies were enumerated using an aCOLade colony counter (Synbiosis). Surface characterization of grafted electrospun nylon 6 nanofibres was performed using Environmental Scanning Electron Microscopy (ESEM-EDAX) Quanta 200 operating at an accelerated voltage of 20 kV.

Electrospinning of nylon 6 nanofibres incorporated with 2-substituted N-alkylimidazoles and Ag(I) complexes containing 2-hydroxymethyl-N-alkylimidazoles

The polymer solution for electrospinning was prepared by dissolving nylon 6 (1.6 g, 16% (w/v)) and the compound (0.08 g, 5% (w/w)) in 10 mL of $HCOOH/CH_3COOH$ mixture (1:1). The optimized electrospinning conditions were as follows; flow rate (0.75 mL/h), applied voltage (+22.5 kV, -5 kV), tip-to-collector distance (8 cm), at ambient conditions. The flow rate of the solution was controlled using a digital pump. Figure 6.1 illustrates the electrospinning set-up for the fabrication of electrospun nylon 6 nanofibre composites.

Grafting of vinylimidazole derivatives onto electrospun nylon 6 nanofibres

Electrospun nanofibre mats (cut into 5 cm × 5 cm squares) were immersed into test tubes containing vinylimidazoles (1 g) and benzophenone (0.015 g) in a H_2O/CH_3OH mixture (80/20). The test tubes were purged with N_2 gas and placed in the oven preheated to 70°C. The test tubes were allowed to equilibrate at 70°C prior to UV irradiation of the solutions using a 400W mercury vapour lamp. At the end of the experiment, the grafted nanofibres were Soxhlet extracted with methanol overnight and then dried at 60°C. The percentage grafting was calculated using Eqn.4

$$Grafting\ (\%) = \frac{B-A}{A} \times 100 \quad (4)$$

Where A is the mass of electrospun nylon 6 nanofibres before and B after grafting.

Figure 6.1: Electrospinning setup for fabrication of nylon 6 composite nanofibres

Antimicrobial activity

Antimicrobial activity of electrospun nylon 6 nanofibres was investigated using a modified version of American Association of Textile Chemists and Colorists (AATCC) Test Method 100-2004 (Tan and Obendorf, 2007). *E. coli* and *S. aureus* were used as model challenge microorganisms. A diluted bacterial suspension with about 1×10^8 CFU/mL concentration was used, and (500 µL) of this suspension was loaded onto the electrospun nylon 6 nanofibre swatches (d = ~4.8 cm) surface in the presence of a nonionic wetting agent (Triton X-100). The inoculum on the surface was then carefully covered with another identical nylon 6 nanofibre in a sterilised glass jar. After incubation for 24 h contact time, 0.02 N sodium thiosulphate was added in excess to quench the biological growth. The mixture was then vortexed vigorously for 2 min. An aliquot of the solution was serially diluted, and dilutions were plated onto nutrient agar plates. The same procedure was applied to electrospun nylon 6 nanofibres with no additives as a negative control. Viable bacterial colonies on the agar plates were counted after incubation at 37°C for 48 h. The reduction rate in the number of bacteria was calculated:

$$R\ (\%) = \frac{B-A}{B}\ x\ 100 \tag{5}$$

where *R* is the reduction rate, *A* is the number of bacteria recovered from the inoculated electrospun nylon 6 nanofibres over 24 h of contact time, and *B* is the number of bacteria recovered from the inoculated electrospun nylon 6 nanofibres at zero contact time.

Dynamic shake flask test method (ASTM E2149-10)

The antimicrobial activity of electrospun nylon 6 nanofibres grafted with vinylimidazole derivatives was evaluated using the dynamic shake flask test method (American Society for Testing and Materials (ASTM) E2149) (ASTM, 2010). A working suspension was prepared by diluting with a sterile 3 mM phosphate buffer (pH 7.2±0.1), a 24 h culture to an optical density of 0.28 at 475 nm (1.5-30 × 10^8 CFU/mL). Further appropriate dilution using a sterile phosphate buffer gave a final concentration 1.5-30 × 10^8 CFU/mL. Electrospun nylon 6 nanofibre composites (0.2-0.3 g) were placed into flasks containing 20 mL of the working solution. The flasks were incubated with continuous shaking at 37°C for 1 h. After serial dilutions using the phosphate buffer, the bacterial suspensions (0.1 mL) were plated in nutrient agar. The inoculated plates were incubated at 37°C for 24 h and surviving bacterial cells counted using a colony counter. The percentage reduction of the microorganisms after contact with the test specimen (nanofibre composites) was compared to the number of bacterial cells surviving after contact with the control. Equation 5 was used to calculate the percentage reduction of microbial growth.

6.3 Results and Discussion

Nylon 6 nanofibres incorporated with 2-hydroxymethyl-N-alkylimidazoles

The electrospun nanofibres composites were fabricated by electrospinning a solution containing nylon 6 (16% (w/v)) and the compound (5% (w/w)) in a HCHO/CH_3COOH mixture. The morphology of the

electrospun polymer composites was characterised using scanning electron microscopy (SEM). The SEM micrographs (Figure 6.2) showed smooth, beadless nanofibres with uniform diameters were obtained. Furthermore, the diameters of the electrospun nanofibres were so small such that it was difficult to measure. The electrospun nanofibre composites were also characterized using ATR-FTIR to ascertain the presence of the compounds within the electrospun nanofibres. The two bands observed in the region 1000-1200 cm^{-1} and one band in the region between 650-800 cm^{-1} coincided with those observed in 2-hydroxymethyl-N-octylimidazole (**W3f**) and were present in nylon 6 nanofibres. These bands were a confirmation that the compound had been incorporated in the nanofibres (Figure 6.3).

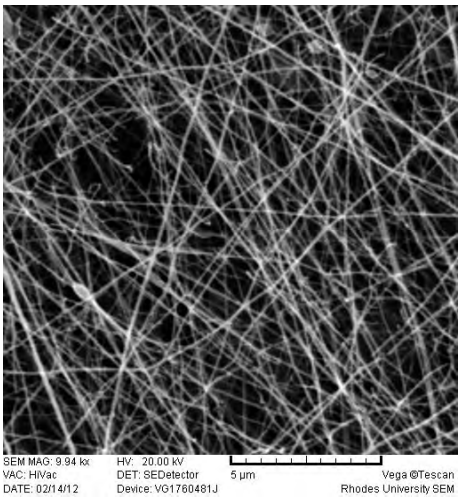

Figure 6.2: SE micrographs of electrospun nylon 6 nanofibre incorporated with W3f

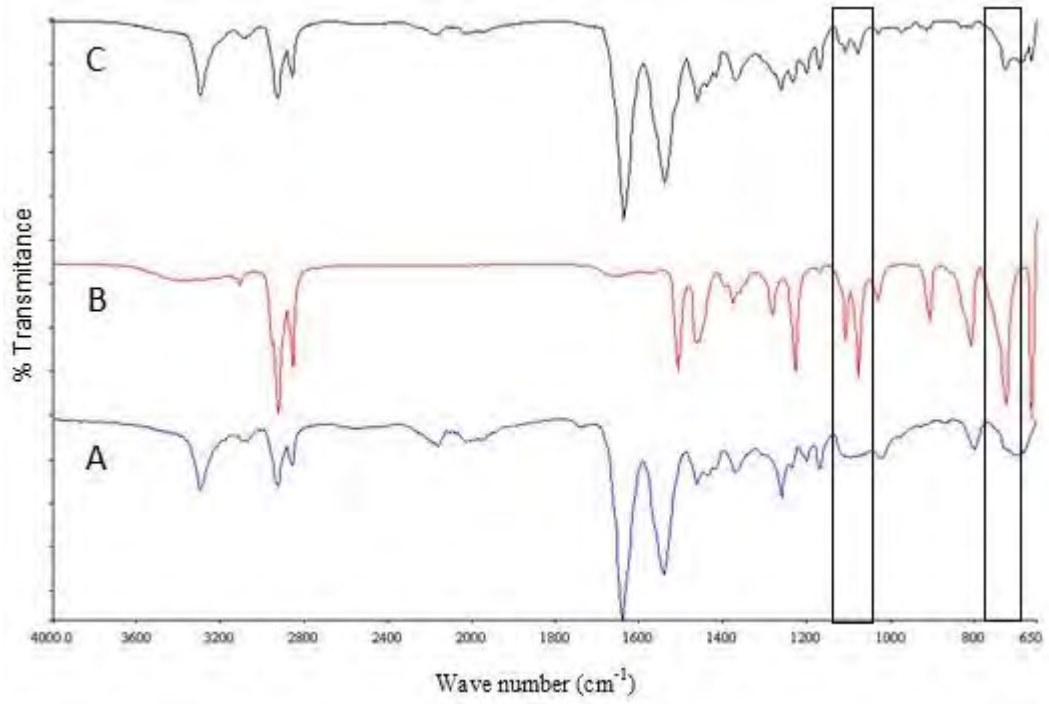

Figure 6.3: ATR-FTIR spectra of (A): nylon 6 nanofibres, (B): 2-hydroxymethyl-N-octylimidazole (W3f) and (C): nanofibre composite

Antimicrobial activity of electrospun nylon 6 nanofibres incorporated with 2-hydroxymethyl-N-alkylimidazoles

The antimicrobial activity of electrospun nylon 6 nanofibres incorporated with selected 2-hydroxymethyl-*N*-alkylimidazoles was investigated using the disk diffusion and AATCC Test 100 methods. The disk diffusion method showed that the 2-substituted *N*-alkylimidazoles maintained the antimicrobial properties even when incorporated into polymer nanofibres as solid support. It was also observed that the antimicrobial activity was

still predominantly against Gram-positive bacteria (*S. aureus* and *B. subtilis* subsp*., spizizenii*) with the latter being the most susceptible (Table 6.1).

The American Association of Textile Chemists and Colorists (AATCC) Test Method 100 was also used to investigate the antimicrobial activity of the electrospun nylon 6 nanofibres incorporated with 2-substituted *N*-alkylimidazoles. The nanofibre composites were first cut into swatches (d = ~4.8 cm) and these swatches were used for conducting the experiments. The results showed that the percentage reduction of bacterial growth against *S. aureus* ranged between 73.2-99.8% for the 2-substituted *N*-alkylimidazoles.

Table 6.1: Diameters of zones of clearance for the electrospun nylon 6 nanofibre containing 2-substituted N-alkylimidazoles

Compound in nanofibres	***E. coli***	***S. aureus***	***B. subtilis* subsp. *spizizenii***	***C. albicans***
	Diameter (mm)	***Diameter (mm)***	***Diameter (mm)***	***Diameter (mm)***
W1f	7.2 (±0.3)	12.7 (±0.3)	29.7 (±0.6)	7.0 (±1.0)
W1g	7.0 (±0.1)	11.8 (±1.0)	22.7 (±0.6)	7.2 (±0.2)
W2f	8.3 (±0.6)	12.8 (±1.2)	22.0 (±1.7)	7.0 (±0.2)
W2g	7.7 (±0.6)	12.2 (±1.0)	24.0 (±1.7)	7.1 (±0.1)
W3f	7.3 (±0.6)	16.7 (±0.6)	23.3 (±2.3)	7.1 (±0.1)
W3g	8.0 (±0.1)	15.7 (±0.8)	28.7 (±0.6)	7.2 (±0.1)

Once more the electrospun nylon 6 nanofibres incorporated with *N*-alkylimidazoles containing carboxylic acid substituents at the 2-position showed the best percentage reduction of all compounds used. Figure 6.4 illustrates the reduction of bacterial growth due to nylon 6 nanofibre composites in comparison to pristine nylon 6 nanofibres.

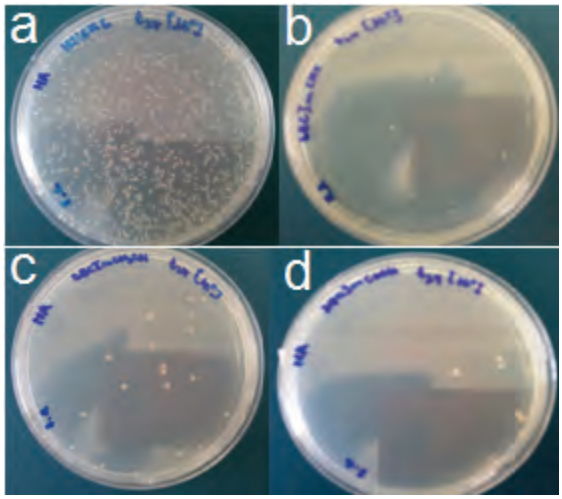

Figure 6.4: Bacterial growth after 24 h contact time with antimicrobial nanofibres (a) nylon 6 nanofibres; (b) nanofibre incorporated with W1g; (c) nanofibres incorporated with W2g and (d) nanofibres incorporated with W3g

Nylon 6 nanofibres incorporated with Ag(I) complexes containing 2-hydroxymethyl-N-alkylimidazoles
Electrospun nylon 6 nanofibres incorporated with Ag(I) complexes containing 2-hydroxymethyl-*N*-alkylimidazole were fabricated using the same optimized conditions as described for the electrospun nylon 6 nanofibres, except for slight changes in applied voltages. The morphology of the nanofibres was characterized using scanning electron microscopy (Figure 6.5) while the presence of the Ag(I) complexes after electrospinning was confirmed using ATR-FTIR spectroscopy (Figure 6.6).

The SE micrograph revealed that the nanofibres obtained had uniform and very thin diameters. As expected, it was very difficult to identify bands belonging to the compounds used for fabrication of the antimicrobial nylon 6 nanofibres. This challenge was attributed to the quantity (5% w/w) of the compounds that was incorporated into the nanofibres. Nonetheless, a low intensity band was observed in the region 1000 - 1200 cm^{-1} which corresponded to a band from the spectrum of the compound used (Figure 6.6).

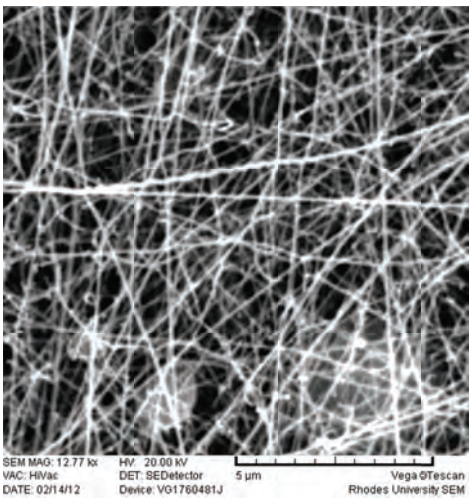

Figure 6.5: SE micrograph of electrospun nylon 6 nanofibres incorporated with Ag-W2g

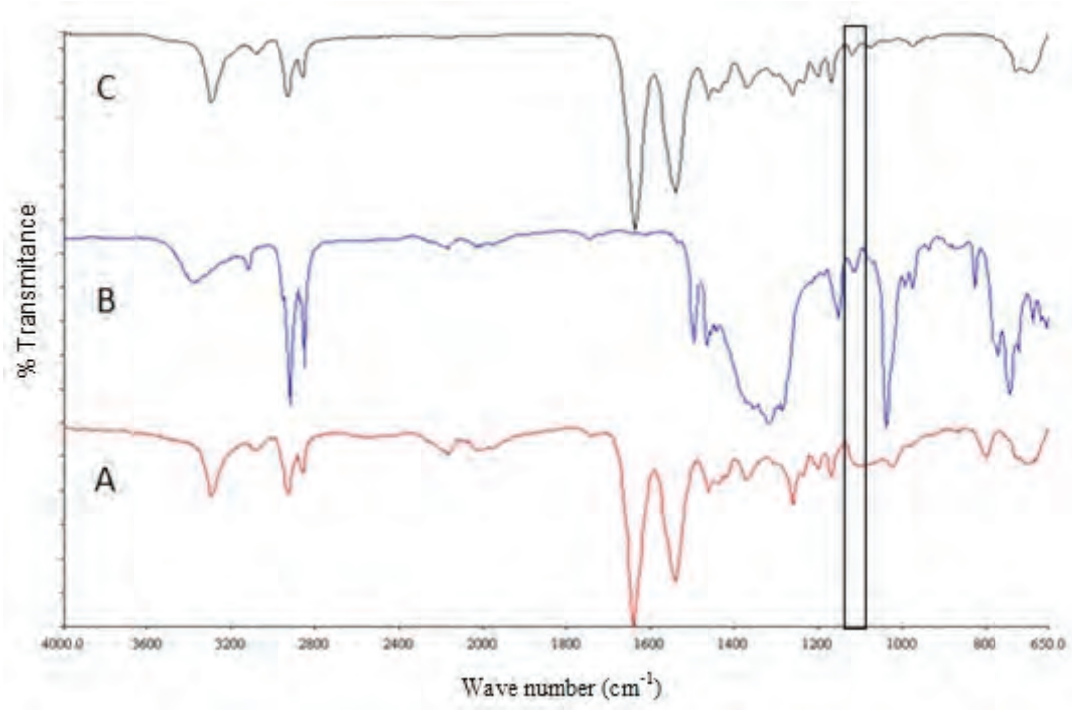

Figure 6.6: ATR-FTIR spectra of (A) nylon 6; (B) 2-hydroxymethyl-N-decylimidazole (W2g) and (C) nanofibre composite

Antimicrobial activity of electrospun nylon 6 nanofibres incorporated with Ag(I) complexes

The antimicrobial activity of electrospun nylon 6 nanofibres incorporated with selected Ag(I) complexes containing 2-hydroxymethyl-*N*-alkylimidazoles (**W2f & W2g**) with long chains was investigated using the disk diffusion and AATCC Test 100 methods. The disk diffusion method showed that the Ag(I) complexes maintained their broad spectrum antimicrobial properties after being incorporated into polymer nanofibres as solid support (Table 6.2).

Table 6.2: Diameters (in mm) of the zones of clearance for the electrospun nylon 6 nanofibres incorporated with Ag(I) complexes (Ag-W2f & Ag-W2g)

Compound no. in nanofibre	***E. coli***	***S. aureus***	***B. subtilis* subsp., *spizizenii***	***C. albicans***
Ag-W2f	13.3 (±0.6)	22.3 (±0.6)	24.3 (±1.5)	13.3 (±0.6)
Ag-W2g	10.7 (±0.6)	15.7 (±0.6)	16.7 (±0.6)	12.7 (±0.6)

The American Association of Textile Chemists and Colorists (AATCC) Test Method 100 was also used to investigate the antimicrobial activity of the electrospun nylon 6 nanofibres incorporated with 2-substituted *N*-alkylimidazoles. The nanofibre composites were first cut into swatches (d = ~4.8 cm) and these swatches

were used for conducting the experiments (Figure 6.7). The results showed that the percentage reduction of bacterial growth against *E. coli* and *S. aureus* was significantly low. The low percentage reduction of bacterial growth for the nanofibre composites was attributed to poor contact of the bacteria with the Ag(I) complexes. The effect could probably be due to lack of moisture on the nanofibres resulting to low diffusibility of the Ag(I) complexes. It has been reported previously that moisture is necessary for the release of Ag(I) ions from the electrospun nanofibres (Melaiye *et al*., 2005). Even the presence of a surfactant (Triton X100) seemed not to have assisted probably due to lack of solubility of the Ag(I) complexes in it.

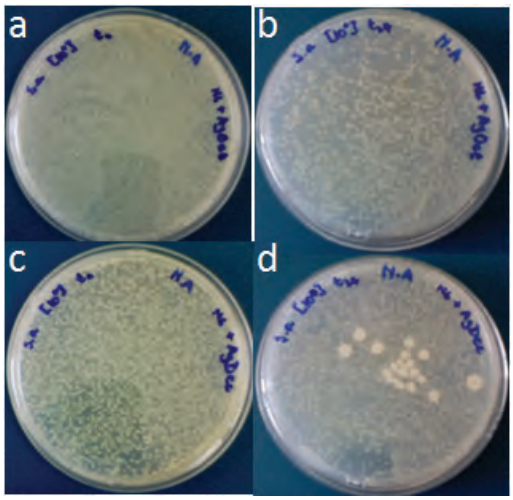

Figure 6.7: Bacterial growth after 0 and 24 h contact times with antimicrobial nanofibres. (a) nanofibres incorporated with Ag-W2f (contact time = 0 h); (b) nanofibre incorporated with Ag-W2f (contact time = 24 h); (c) nanofibres incorporated with Ag-W2g (contact time = 24 h)

6.4 Antimicrobial activity evaluation of grafted nanofibres

The antimicrobial activity of the grafted electrospun nylon 6 nanofibres was evaluated using the dynamic shake flask test method (ASTM E2149-10). In Chapter 4, it was demonstrated that the free 2-substituted *N*-alkylimidazoles were predominantly active against Gram-positive bacterial strains (*S. aureus* and *B. subtilis,* subsp*. spizizenii*). The antimicrobial activity of was evaluated against *S. aureus* because it was the easier of the two strains to work with. Table 6.3 presents the data of the percentage reduction of the growth of *S. aureus* after treatment with grafted electrospun nanofibres.

Table 6.3: Percentage reduction data for grafted electrospun nylon 6 nanofibres

Material tested	**Reduction (%)**
Poly(nylon6-g-1-Vim)	99.94
Poly(nylon6-g-1-VImCH_2OH)	99.95
Poly(nylon6-g-1-VImCOOH)	99.98
Poly(nylon6-g-4(5)-VIm)	99.95

From the results that were obtained, it was observed that all the grafted electrospun nanofibres demonstrated excellent antimicrobial activity. The percentage reduction of the growth of *S. aureus* in water was in the range 99.55-99.98%. However, it was surprising to see that the electrospun nylon 6 nanofibres that were grafted with 1-VImCH_2OH displayed the lowest percentage reduction. The discrepancy could be attributed to some experimental errors. Consequently, the displayed reduction in growth of *S. aureus* by electrospun nylon 6 nanofibres grafted with 1-Vim and 4(5)-Vim was not surprising. For instance, the antimicrobial activity of *N*-vinylimidazole grafted polymers was reported by other researchers (Caner *et al*., 2007,Chung *et al*., 2012, Sabaa *et al*., 2010).

6.5 Cytotoxicity studies

The cytotoxicity effects of free 2-substituted *N*-alkylimidazoles, electrospun nylon 6 nanofibres incorporated with 2-substituted *N*-alkylimidazoles and electrospun nylon 6 nanofibres grafted with 2-substituted vinylimidazoles were evaluated on the Chang liver cells. The IC_{50} values were obtained from dose response curves (percentage inhibition versus log concentration).

Table 6.4: IC50 values for the tested compounds and nanofibres

Test compound or material	Concentration (µg/mL)
N-Decylimidazole-2-carboxaldehyde (W1g)	13.80
Complex Ag-W2g	10.91
Poly(nylon6-g-1-VIm)	25.12*
Poly(nylon6-g-1-VImCH_2OH)	26.81*
Poly(nylon6-g-4(5)-VIm)	23.48*
Nylon 6	33.20*

(*) represents the mass of nanofibres per mL of cell culture medium

The cytotoxicity effect of a compound is indicated by the IC50 values, the concentration required to inhibit the growth of cells by 50%. A smaller IC50 value indicates that the test compound has a stronger affinity for the cell receptors and thus possesses more cytotoxicity (Thomas, 2007). *N*-Decylimidazole-2-carboxaldehyde **(W1g)** and the silver(I) complex **(Ag-W2g)** exhibited the lowest IC50 values (Table 6.4) indicating that they could have more cytotoxic effects to human cells. The grafted electrospun nylon 6 nanofibres [poly(nylon6-g-1-VIm), poly(nylon6-g-1-VImCH_2OH) and poly(nylon6-g-4(5)-VIm) exhibited higher IC50 values which indicated that they could be less toxic than the free imidazoles and silver(I) complexes. Electrospun nylon 6 nanofibres displayed the least IC50 values which implied the lowest cytotoxic effect.

The cytotoxicity results implied that application of biocides incorporated electrospun nanofibres in drinking water treatment could have side effects to human health because of leaching. On the other hand, grafted electrospun nanofibres would have less adverse effects to human health. Thus, immobilization of biocides for antimicrobial applications in drinking water should be the method of choice for the functionalisation of nanofibres. Another added advantage is the possibility of reusability of the electrospun nanofibres. However, experiments to evaluate the reusability of grafted electrospun nylon 6 nanofibres could not be conducted due to time limitations.

6.6 Conclusions

The electrospun nylon 6 nanofibres incorporated with 2-substituted *N*-alkylimidazoles were successfully fabricated and their antimicrobial activity also investigated. Results showed that the incorporation of these antimicrobially active compounds into electrospun nylon 6 nanofibres did not affect the antimicrobial activity. The electrospun nylon 6 nanofibre composites maintained the antimicrobial activity against Gram-positive bacteria (*S. aureus* and *B. subtilis* subsp*., spizizenii*) while the activity remained poor against Gram-negative bacteria (*E. coli*) and the fungus (*C. albicans*). The AATCC Test Method 100 showed that the antimicrobial activity of electrospun nylon 6 nanofibres incorporated with Ag(I) complexes containing 2-hydroxymethyl-*N*-alkylimidazoles appeared to decrease because of the lack of moisture and subsequently the poor diffusibility of the Ag(I) complexes. However, the disk diffusion method showed that the nanofibres maintained the antimicrobial activity of the Ag(I) complexes because of the presence of moisture throughout the experiment. Grafted electrospun nylon 6 nanofibres showed excellent antimicrobial activity, as exhibited by a very high percentage reduction of bacterial growth. Cytotoxicity studies also showed that grafted electrospun nylon 6 nanofibres had lower cytotoxic effects compared to the biocide-incorporated electrospun nanofibres.

6.7 Recommendations

Immobilization of biocides onto electrospun nanofibres brings about the prospects of reusability of the nanofibres since they remain intact for a very long period. Therefore, we recommend the evaluation of the reusability of the developed grafted electrospun nanofibres in water applications. The effect that the grafting process has on the morphology of the electrospun nanofibres could also be investigated. The investigation could be useful in deciding the mode of application (filtration or immersion) of the grafted nanofibres for drinking water.

7 A HIGHLY SELECTIVE AND SENSITIVE PYRIDYLAZO-2-NAPTHOL-POLY (ACRYLIC ACID) FUNCTIONALIZED ELECTROSPUN NANOFIBRE FLUORESCENCE "TURN-OFF" CHEMOSENSORY SYSTEM FOR NICKEL (II) IONS

7.1 Introduction

The objective of the study was to develop a 1-(2-pyridylazo)-2-naphthol (PAN) functionalized poly(acrylic acid) (PAA) nanofibre fluorescent probe for the determination of Ni^{2+} in water samples.

In recent years a great deal of research has been devoted to the detection of metal ions in environmental or biological systems (Rurack, 2001). Nickel is an essential metal for supporting life, as loss of nickel homeostasis is harmful to prokaryotic and eukaryotic organisms alike (Sigel *et al*., 2007). Although the contributions of nickel homeostasis to mammalian health and diseases remain largely unexplored (Goodman *et al*., 2009), excess nickel accumulation can aberrantly affect respiratory and immune systems (Costa *et al*., 2005, Nemec *et al*., 2009). Therefore, it is very important to detect nickel ions. Advances in both electronics and mechanics have yielded high-tech facilities that are widely available for the detection of nickel metal ions at low concentration level (0.1 ng/mL) (Kokkinos *et al*., 2008). For example, inductively coupled plasma-optical emission spectrometry (ICPOES) (Bezerra *et al*., 2007, Takara *et al*., 2005), microwave-induced plasma (MIP) (Jankowski *et al*., 2005), electrothermal atomic absorption spectrometry (ETAAS) (Shiowatana *et al*., 2000, Stafilov, 2000, Zendelovska *et al*., 2001), flame atomic absorption spectrometry (FAAS) (Elci *et al*., 2003, Karatepe *et al*., 2003), spectrophotometry (Kiriyama and Kuroda, 1988, Li *et al*., 2007), voltammetry and inductively coupled plasma-mass spectrometry (ICP-MS) (Tonello *et al*., 2007). However, some of these techniques are complicated and not suitable for quick and on-line monitoring. To this regard, the fluorescence detection techniques remain the most favourable options due to their advantages over other techniques, which include ease of detection, sensitivity and instantaneous response (Cheng *et al*., 2008, Chmielewska *et al*., 2006, Dodani *et al*., 2009, Fan and Jones, 2006, Ogawa *et al*., 2009, Wang *et al*., 2010, Yao *et al*., 2009).

In fluorescence techniques, suitable indicators which are sensitive to analyte concentrations and exhibit changes in fluorescence intensity are used as molecular recognition materials (Lee *et al*., 2000). Recently, derivatives of 8-hydroxyquinoline were used as sensitive and reliable tools to measure concentrations and fluctuations of cellular Mg^{2+} by comparing enhancement of the fluorescence with analyte concentrations (Farruggia *et al*., 2006). Also, boradiazaindacene as the fluorophore with 4-(bis(pyridin-2-ylmethyl)amino)-benzaldehyde was employed for an intracellular emission fluorescent Cd^{2+} sensor based on the internal charge transfer (ICT) mechanism (Peng *et al*., 2007, Qi *et al*., 2006). Other examples involve a fluorescence response system with poly[(*p*-phenyleneethynylene)-*alt*-(thienyleneethynylene)]. It showed varying fluorescence "turn-on" behaviour in the presence of cations including Li^{+}, Na^{+}, K^{+}, Mg^{2+}, Ca^{2+}, H^{+}, Mn^{2+}, Fe^{2+}, Co^{2+}, Ni^{2+}, Zn^{2+}, Cd^{2+} and Hg^{2+} (Fan and Jones, 2006). Most of these literature reports involve the use of fluorescent sensors in liquid rather than in solid state.

Successively, exploration of well-defined fluorescence "turn-off" indicator with large Stoke shift, high quantum yield, strong absorbance, excellent photostability and non-toxicity will be of high interest to research. Fluorophores for heavy metals take advantage of the high affinity of oxygen and nitrogen donor atoms towards these ions according to the principles of hard or soft bases and acids (HSAB) by Pearson (Pearson, 1963). An example of such an indicator with complexing preference for border line acid like Ni^{2+} is 1-(2-pyridylazo)-2-naphthol (PAN), more so it is one of the most sensitive reagents among heterocyclic azo compounds for determining heavy metals (Gavrilenko and Saranchina, 2009). In order to confer some special properties, organic and inorganic polymers have been used as solid supports for the fluorescence indicator. It is known that the choice of solid supports and the immobilization of indicator into the supports have significant effects on the performance of the sensors in terms of selectivity, sensitivity, response time, and stability (Brook and Narayanaswamy, 1998, Xavier *et al*., 1998). Most importantly, it should afford electrospinnable material for transformation into nanofibre mat for solid phase measurement.

Electrospinning of polymeric materials into well-defined fibre mat has received significant interest due to their potential for a variety of applications. Specifically, the technique has been found to be a unique and cost-effective approach for fabricating large surface area membranes for a variety of sensor applications (Balaji *et*

al., 2006, Gao *et al*., 2007, He *et al*., 2009, Reneker and Chun, 1996, Shin and Jang, 2007, Wang *et al*., 2002). Previously, Wang *et al.* had shown that the sensitivities of electrospun nanofibre to detect Fe^{3+} and Hg^{2+} are 2 to 3 orders of magnitude higher than those obtained from thin film sensors (Balaji *et al*., 2006). Since new methods are emerging to develop highly sensitive solid-state detectors of heavy and transition metal ions by fluorescence (Gao *et al*., 2006, Kledzik *et al*., 2007, Lee *et al*., 2008b, Ruedas-Rama and Hall, 2008, Sarkar *et al*., 2009), it is expected that electrospun polymers featuring fluorescence indicators could exhibit amplified fluorescence "turn-off" effects when the complexing units bind to metal ions.

The indicators are immobilized by physical or chemical procedures onto the polymeric materials (Brook and Narayanaswamy, 1998). The physical procedures used for immobilization include adsorption (Carraway *et al*., 1991, Demas *et al*., 1995, Xu *et al*., 1996b), dissolution (Klimant and Wolfbeis, 1995, Mills *et al*., 1997), entrapment in a porous network (Di *et al*., 1995, McDonagh *et al*., 1998), and ion exchange (Zhang and Seitz, 1984). These methods are simple but suffer from the limitation of insolubility of indicator in the polymeric support, which results in leaching-out of the indicator. The chemical procedure involves the formation of covalent bonds between the indicator and support materials. Sensors with covalently immobilized indicators have the advantage of not suffering from indicator leaching-out (Lobnik *et al*., 1998, Zhang *et al*., 1989).

Therefore, considering the importance of detecting Ni^{2+} in the environment, this contribution focused on functionalisation of PAN into poly(acrylic acid) (PAA) by a simple esterification procedure (Scheme 7.1) to yield a fluorescence polymer PAN−PAA. The functionalized polymer was further electrospun into nanofibre mat to obtain the fluorescence "turn-off" chemosensory system as a highly selective and sensitive detector of Ni^{2+} in an aqueous solution.

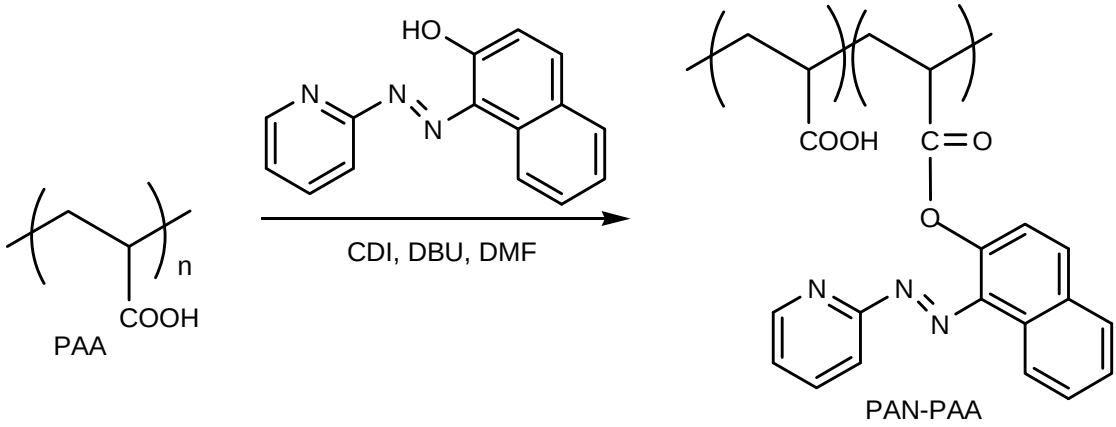

Scheme 7.1: Synthetic pathway for the functionalisation of poly(acrylic acid) (PAN-PAA) with 1-(2-pyridylazo)-2-naphthol

7.2 Experimental

Materials and reagents

All experimental manipulations and data collections were performed at room temperature, unless otherwise stated. PAA (Mw = 50000 g/mol), PAN, 1,1'carbonyldiimidazole (CDI), 1,8-diazabicyclo[5.4.0]undec-7-ene (DBU) and all inorganic salts ($NiCl_2.6H_2O$, $CoCl_2.6H_2O$, $CrCl_3.6H_2O$, $CuCl_2.6H_2O$, $FeSO_4.7H_2O$, $Cd(NO_3)_2.4H_2O$, $Zn(NO_3)_2.H_2O$, $Pb(NO_3)_2$ and $Al_2(SO_4)_3.15H_2O$) were of analytical grade and used as obtained from Sigma Aldrich (St. Louis, USA). N,N-dimethylformamide (DMF) was purchased from Merck Chemicals (Wadesville, South Africa) and distilled over nitrogen at reduced pressure. Standard solutions were freshly prepared by dissolving known quantities of metal salts in deionised ultrapure water obtained from a Millipore system.

Synthesis of fluorescence polymer (PAN−PAA)

A solution of CDI, (0.34 g, 2.1 mmol) and a catalytic amount of DBU in 10 mL of DMF were added to a solution of PAA (1.5 g, 20.8 mmol) in 40 mL of DMF. After stirring the solution at 70°C until the evolution of carbon dioxide subsided (15 min), a solution of PAN (0.52 g, 2.08 mmol) in 15 mL DMF was added and the solution was stirred at 70°C for 18 h. The solution was slowly transferred with vigorous stirring into diethyl ether to precipitate the polymer. After filtration, the obtained solid was washed extensively with ether and acetone and dried in a vacuum oven for 24 h at 25°C.

Fabrication of fluorescence electrospun nanofibre

A solution for electrospinning was prepared by dissolving 6.6 wt% PAN−PAA in 1:4 (v/v) water/ethanol solvent system and stirred overnight to obtain a homogenous solution. After loading the polymer solution into a 10 mL glass syringe, the syringe was mounted on a programmable syringe pump (New Era, NE-1000). The solution was pumped at a flow rate of 1 mL/h through a steel needle of 0.584 mm internal diameter. Nanofibres were collected on glass slides which were covered with masking tape and only the targeted area (0.5 x 2.5 cm) exposed for deposition to occur. This system was mounted on aluminium foil and collection was carried out in 8 min. The distance between the needle tip and the collector was 15 cm and the applied voltage at the needle tip was 8.75 kV. In order to improve the insolubility of the fibre mat in an aqueous medium, the electrospinning solution with cross-linker was prepared with the addition of β-cyclodextrin at 20 wt% of the product. After the deposition process, fibres were heat treated at 120°C for 20 min to cross-link the films.

Characterization

Infrared spectra were recorded on a Perkin-Elmer 100 FT-IR spectrophotometer. Electronic absorption spectra were recorded on a Perkin Elmer Lambda 25 UV/VIS spectrophotometer in a quartz cell (1 cm). Emission spectra were recorded on Varian Cary Eclipse spectrofluorometer in a 1 cm quartz cell. The spectrofluorometer was equipped with xenon discharge lamp (75 kV), Czerny-Turner monochromators and an R-928 photomultiplier tube with manual or automatic voltage that was controlled using the Cary-Eclipse software. All samples were illuminated at an excitation wavelength of 500 nm and the emission was scanned from 510 to 640 nm, while the detector voltage was maintained between 600 and 650 V. The morphology of the nanofibre mat was studied by the Tescan (TS5136ML) Scanning Electron Microscope (SEM) operating at an accelerated voltage of 20 kV after a gold sputter coating. The fluorescence images were taken with a DMLS fluorescence microscope. The excitation source was a high-voltage mercury lamp and light with a wavelength of around 470**-**570 nm was emitted with the help of an optical filter. The exposure time was the same for all images.

Fluorescence measurements

In order to perform fluorescence measurements, the glass slides containing sensor layers (Figure 7.1) were placed in a 1 cm quartz cuvette which was filled with various metal salt solutions. The cuvette was placed in the sample holder of the spectrofluorometer, and samples were illuminated at an excitation wavelength of 500 nm and the emission was scanned from 510 to 640 nm, while the detector voltage was maintained between 600 and 650 V.

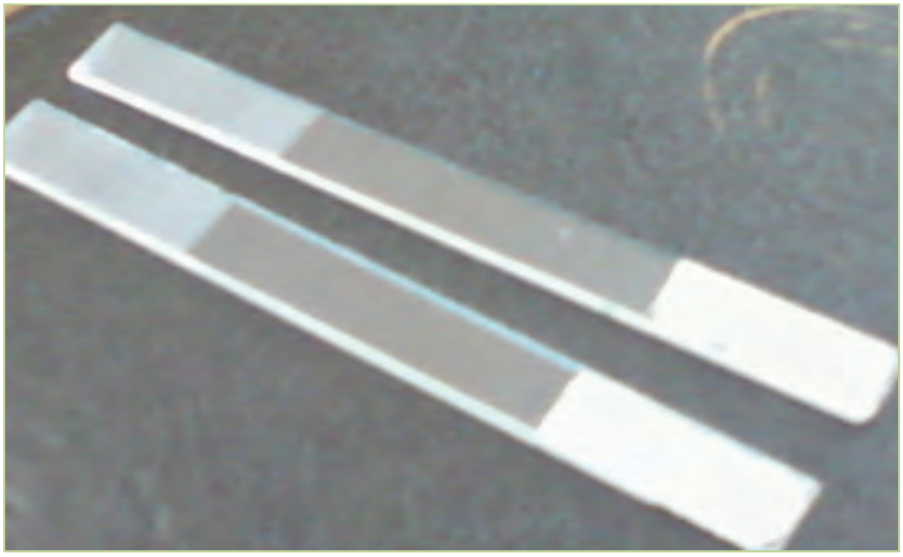

Figure 7.1: Photograph of glass slides coated with fluorescent nanofibres

Fluorescence quenching detection of Ni^{2+} by electrospun nanofibre

In fluorescence data collection, the 5 mL aliquots of nickel ion stock solutions (ranged 0.1**-**1.0 µg/mL) were added into an optical cell containing a glass slide coated with the sensing nanofibre. Upon introducing series of the nickel ion solutions, fluorescence quenching of the sensing nanofibre was observed. The data, corresponding to the average of three determinations, were fitted by a standard least-squares treatment and

the Stern-Volmer equations were evaluated. The procedure for examining the influence of other metal ions on the fluorescence quenching of Ni^{2+} was essentially the same. For this instance, the sensing nanofibre was exposed to several metal cations at higher equivalence with or without a fixed concentration of nickel ion. A custom-made certified reference material for groundwater (SEP-3) purchased from Inorganic Ventures (Christiansburg, USA) was used to validate the analytical procedure. Repeatability of the method was evaluated by comparing the signals obtained from three determinations of the reference material.

7.3 Results and Discussion

Fabrication and characterization of fluorescence PAN−PAA nanofibres

FTIR spectra shown in Figure 7.2 indicate a new ester bond formation (υ = 1737.07 cm^{-1}) between the hydroxyl groups of PAN and carboxylate groups of PAA. The formation of the new covalent bonds between the indicator and support materials prevents the indicator from leaching-out and afforded electrospinnable material for transformation into nanofibre mat for direct solid phase measurement of nickel ion in water without further sample preparation. To obtain the optimal electrospinning conditions, several operational parameters were investigated including voltage, working distance and flow rate. Within the tested range (5 - 15 kV voltage, 10 - 20 cm working distance and 0.5 - 1.5 mL/ h flow rate), the optimal spinning parameters which gave bead-free nanofibres prepared from 6.6 wt% solution are 8.75 kV voltage, 15 cm working distance and 1 mL/h flow rate (Figure 7.3).

The fibres obtained were very soluble in water and even heating the fibre mat at 120°C for 30 min did not affect solubility. Since their application was intended to be carried out in water samples, water solubility posed a challenge. Therefore there was need to render these fibres water insoluble. In this regard, we employed the use of a cross-linker with the aim to form a covalent bond. Cross-linking can be performed by chemical reactions that are initiated by heat, pressure, and change in pH or radiation. In this case, thermally cross-linkable β-cyclodextrin was chosen since it has free hydroxyl ends that are reactive and are capable of further esterification with the carboxylic acid groups on the product to form new ester bonds (Li and Hsieh, 2005). The cross-linked PAN-PAA electrospun fibres retained their fibrous structure after a long immersion in water.

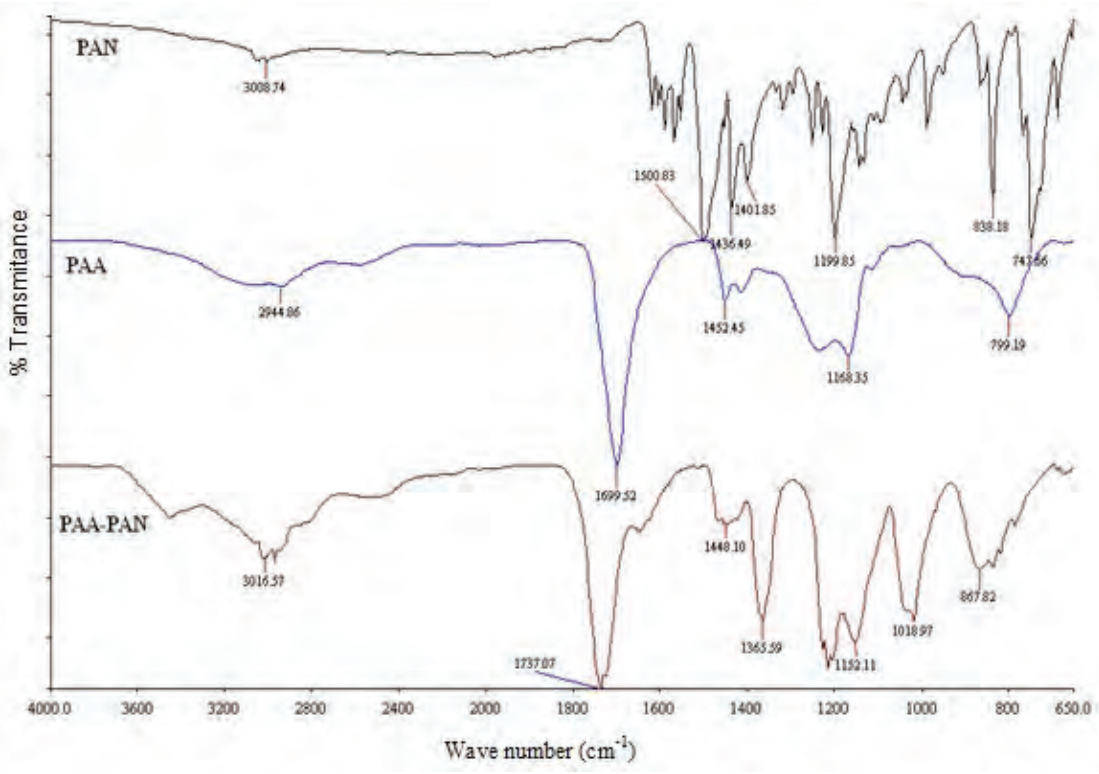

Figure 7.2: FTIR spectra of new fluorescence polymer PAN−PAA, PAN and PAA

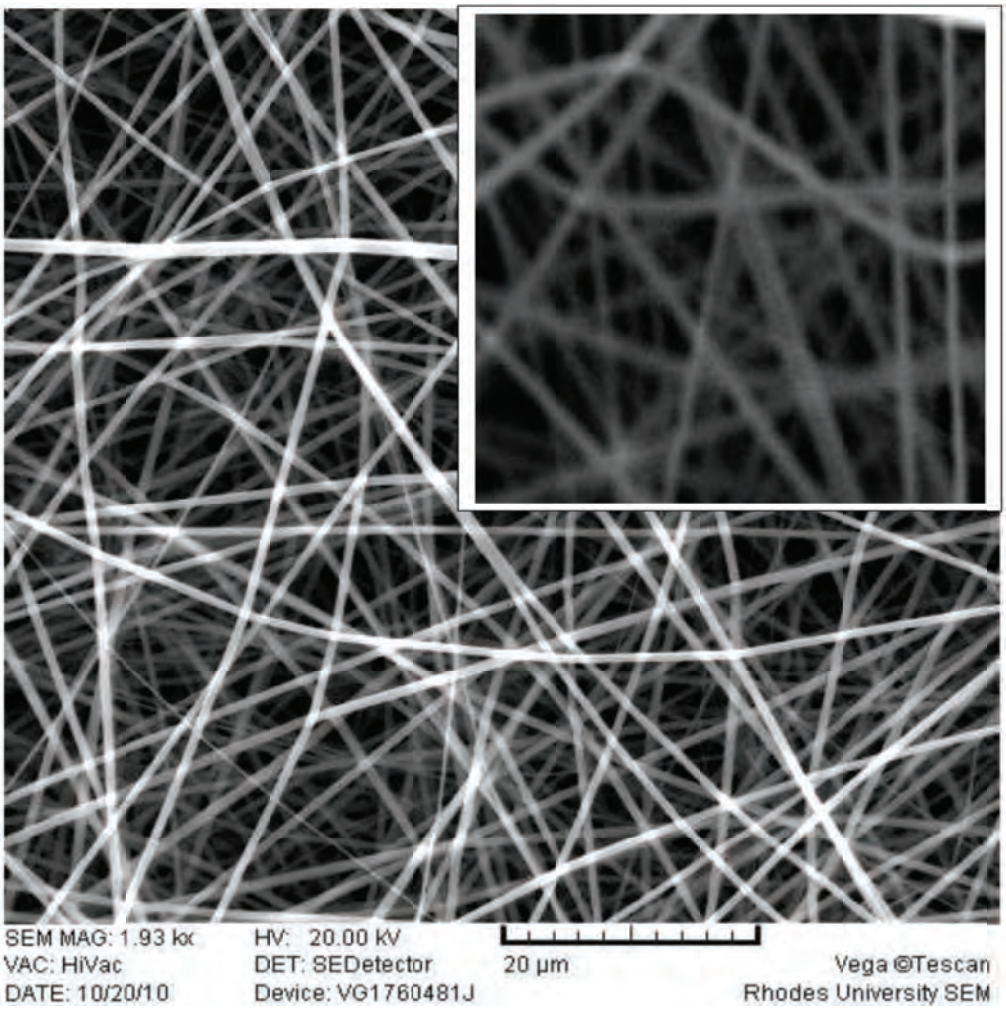

Figure 7.3: Scanning electron micrograph of fluorescence functionalized electrospun PAA-PAN nanofibres (Inset shows image of cross linked fibres, average fibre diameter range is 230 - 800 nm)

The electrospun nanofibre PAN-PAA exhibited distinct and well-defined emission peak as shown in Figure 7.4. Previously, the intrinsic absorbance of PAN has been determined to be 470 nm (Gavrilenko and Saranchina, 2009). However, the absorbance maximum of the new PAN-functionalized molecule was slightly red shifted to 479 nm. Emission maximum of the nanofibre mat was at 557 nm which is indicative of a good Stokes' shift. With the functionalisation, the rate of self-quenching of PAN as a result of site isolation was greatly reduced. Consequently, the fluorescence efficiency and sensitivity of the nanofibre mat were remarkably improved.

Ni^{2+} response and selectivity of fluorescence PAN−PAA nanofibre

In order to get a clearer insight into the florescence of the nanofibre, the fluorescence behaviour was evaluated after addition of various concentrations of Ni^{2+}. Figure 7.5 shows the fluorescence "turn-off" effects of the nanofibre upon addition of Ni^{2+}. It was observed that addition of Ni^{2+} at low concentration of 0.1 µg/mL significantly decreased the emission intensity. When 1.0 µg/mL of Ni^{2+} was added, the fluorescence intensity decreased to less than 2%.

The sensitivity of the nanofibre was further visualized by fluorescence microscopy. After treating the nanofibre mat with a 1.0 µg/mL Ni^{2+} solution, remarkable quenching effects were observed from the fluorescence images (Figure 7.6). Prior to the quenching processes, the fluorescence images evidently revealed fluorescence emission of the nanofibre and uniform dispersion of fluorophores. The sensitivity of the nanofibre could be restored by destabilizing the complex formed by rinsing with an acidic solution and this showed satisfactory reversibility and reproducibility of this system.

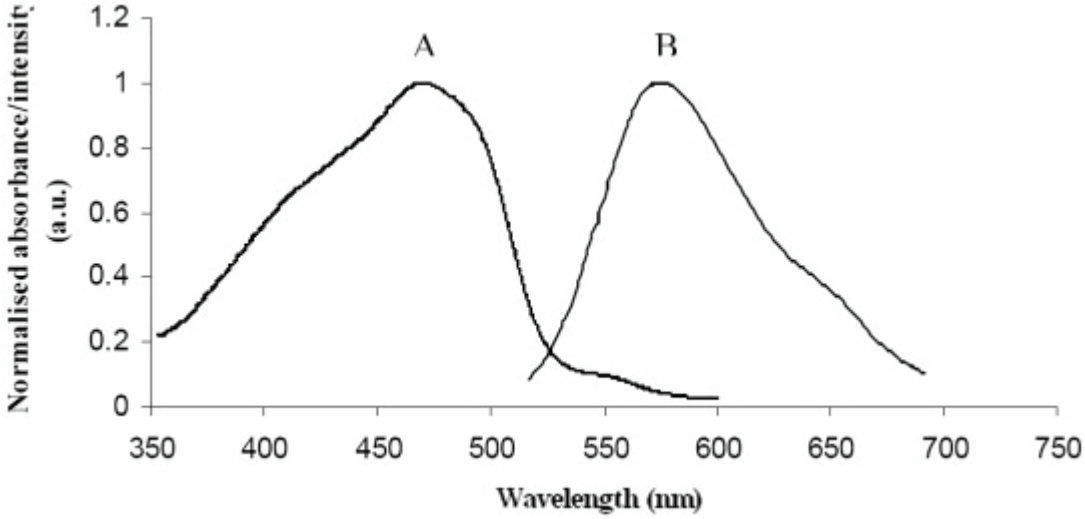

Figure 7.4: UV absorption (A) and fluorescence emission (B) spectra of PAN-PAA nanofibre

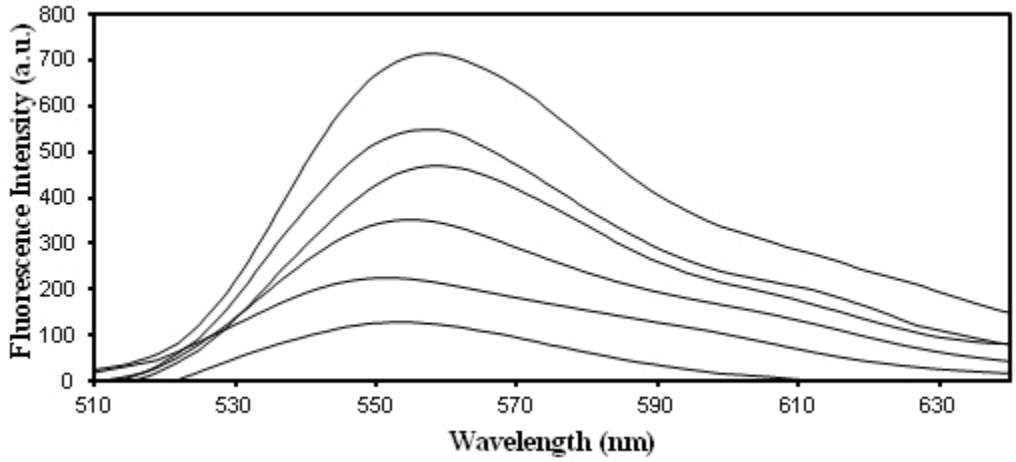

Figure 7.5: Fluorescence emission spectra of PAN-PAA nanofibre as a function of Ni^{2+} concentration. The insert shows relative fluorescence intensities (I/Io) at 557 nm with Ni^{2+} concentration

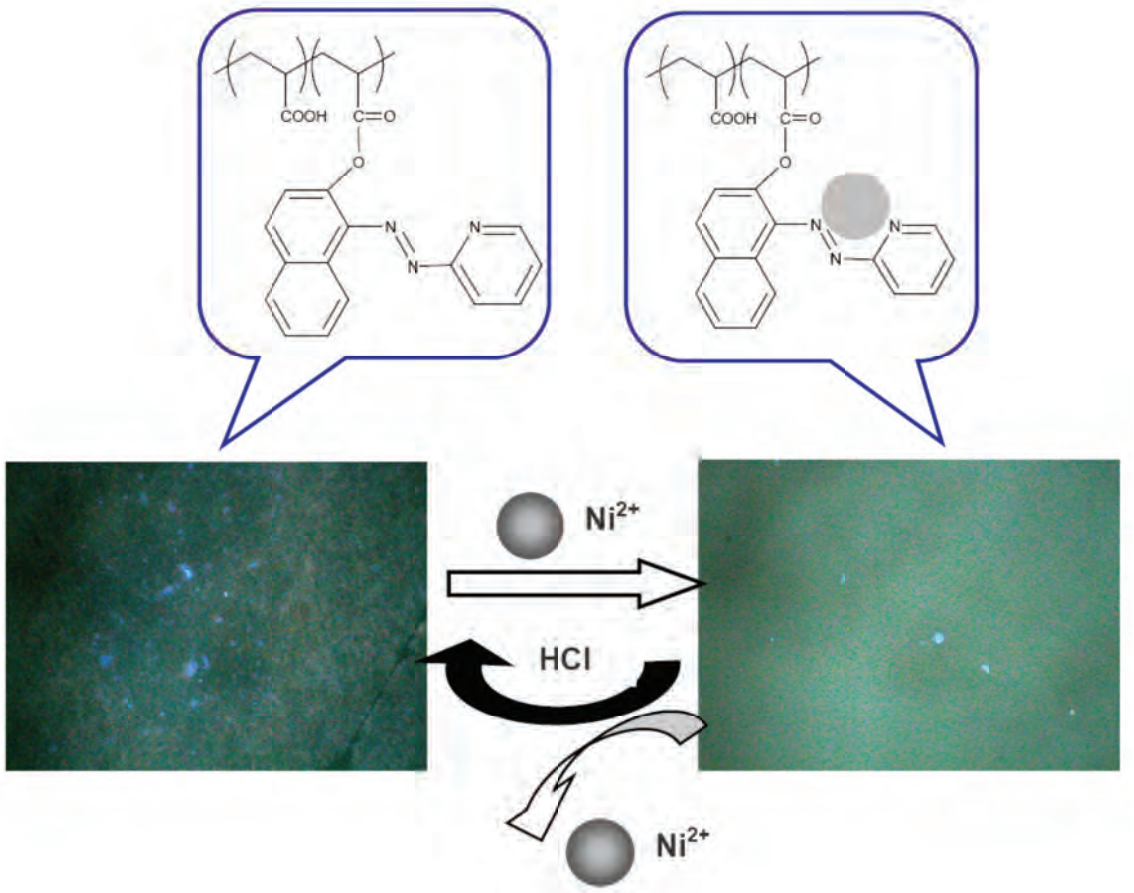

Figure 7.6: Fluorescence images of sensing PAN-PAA nanofibres before and after immersion in a 1.0 µg/mL Ni^{2+} solution

Fluorescence quenching by transition metal ions has been predominantly attributed to electron as well as energy transfer and paramagnetic interactions of the fluorophores and the metal ion (Formosinho, 1976, Kemlo and Shepherd, 1977, Varnes *et al*., 1972). Utilizing the Stern-Volmer mechanism (Figure 7.7), the quenching of fluorescence by a metal ion may occur by at least two different mechanisms (Lakowicz, 1983). In the static quenching, on complexing of the ground state molecule with paramagnetic ion, fluorescence intensity decreases as a function of concentration of the metal ion introduced. However, a second mechanism must involve the excited state, rather than the ground state of the fluorescent molecule. The paramagnetic metal ion causes a reduction of fluorescence intensity by inducing intersystem crossing. In an equilibrium situation, both of these effects may be operating and can be represented for Ni-PAN-PAA system as shown (Scheme 7.2).

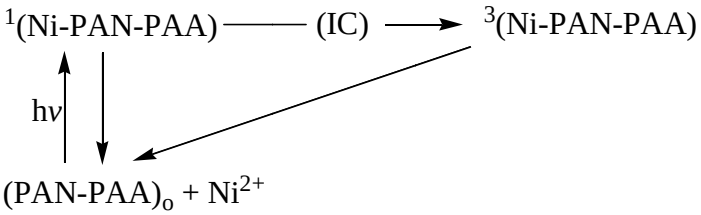

Scheme 7.2: Quenching mechanism of PAN-PAA by Ni^{2+}

(PAN−PAA)o, ^{1}(Ni-PAN−PAA) and ^{3}(Ni-PAN−PAA) are ground state fluorescence molecules, first excited singlet and triplet state respectively. The rationalization is that the rate of intersystem crossing (IC) in the first excited singlet complex is enhanced by the influence of the unpaired electrons of the nickel metal ion. The first excited singlet crosses over to the triplet state, which may then undergo some efficient type of quenching to return to the ground state.

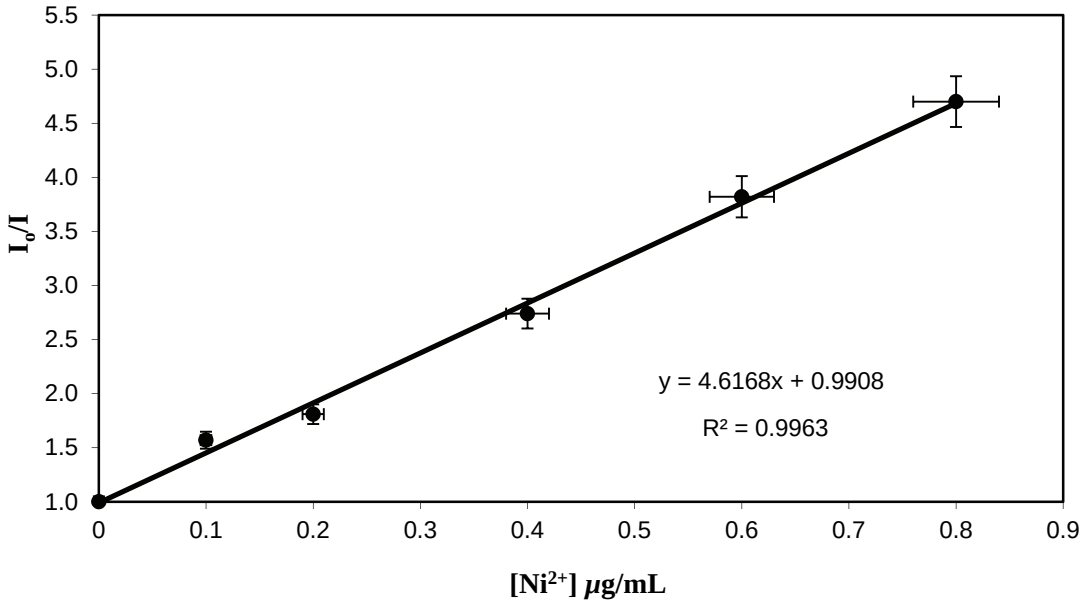

Figure 7.7: Stern-Volmer plots of fluorescence PAN-PAA nanofibre as a function of Ni^{2+} concentration (errors calculated as 5% of the average values)

The relationship between the emission at 557 nm and Ni^{2+} concentrations can be deduced from the Stern-Volmer equation:

$$I_0/I = 1 + K\text{sv}[Q] \quad (6)$$

Where, I_0 is the fluorescence intensity with the absence of quencher (Ni^{2+}), I is the intensity when the quencher is present, K_{sv} is the Stern-Volmer constant and [Q] is the concentration of quencher. The K_{sv} of the nanofibre, calculated from the slope of the plot was found to be 3.69×10^3 mL/µg indicative of enhanced sensitivity of the nanofibre probe that which can be attributed to the higher surface area of the electrospun fibre. The linear range of the method lies between 0.1-1.0 µg/mL Ni^{2+}.

Table 7.1 gives the quality control parameters regarding the detection of nickel metal ion in aqueous solution. Accuracy of the determinations, expressed as relative error between the certified and the observed values of the reference material were ≤ 0.1%. The precision of these measurements expressed as relative standard deviation for eight repeated measurements of 1.0 µg/mL Ni^{2+} was also satisfactory, being lower than 4%. The limit of detection, based on the definition by IUPAC (LOD = (3δ/S) (Irving H. M. N. H, 1981), was found to be 0.07 ng/mL. This LOD achieved with the PAN-PAA nanofibres was lower than 4.5 ng/mL achieved with fluorescence-based sensor from *Escherichia coli* nickel binding protein labelled with N-[2-(1-maleimidyl)ethyl]-7-(diethylamino)coumarin-3- carboxamide (Salins *et al*., 2002). In addition, the LOD was significantly lower than 0.04 µg/mL nickel concentrations above which it is toxic in drinking water as established by EPA (Fay Mike, 2005).

Table 7.1: Analytical quality control

I_0/I	***Certified concentration (µg/mL)***	***Concentration found (µg/mL)***	***Relative error (%)***	***Relative standard deviation (%)***	***LOD (ng/mL)***	***LOD[a] (ng/mL)***	***LOD[b] (ng/mL)***
5.29	0.8980(0.007)	0.8986(0.004)	+0.0668	3.9203	0.0710	0.1	4.5

[a]Square-Wave anodic stripping voltammetry bismuth-film electrode sensing method (Kokkinos *et al*., 2008).
[b]Fluorescence-based sensing system using nickel binding protein from *Escherichia coli* (Salins *et al*., 2002).

The selective binding ability of PAN−PAA nanofibre was determined as shown in Figure 7.8. Given the quenching percentages of fluorescence intensity of PAN−PAA nanofibre, upon addition of 1.0 equivalent of

various metal ions (Al^{3+}, Cr^{3+}, Fe^{2+}, Co^{2+}, Cu^{2+}, Zn^{2+}, Cd^{2+} and Pb^{2+}), PAN-PAA had a large chelation-enhanced quenching (CHEQ) effect only with Ni^{2+} among the metal ions examined with percentage quenching near 100%. In contrast, addition of other metal ions (Al^{3+}, Cu^{2+}, Zn^{2+}, Cd^{2+} and Pb^{2+}) scarcely showed fluorescence quenching. However, Cr^{3+}, Fe^{2+} and Co^{2+} ions showed weak quenching probably due to their paramagnetic nature. Above all, this phenomenon indicated a high selectivity of PAN-PAA in its fluorescence quenching response toward Ni^{2+} against other metal ions.

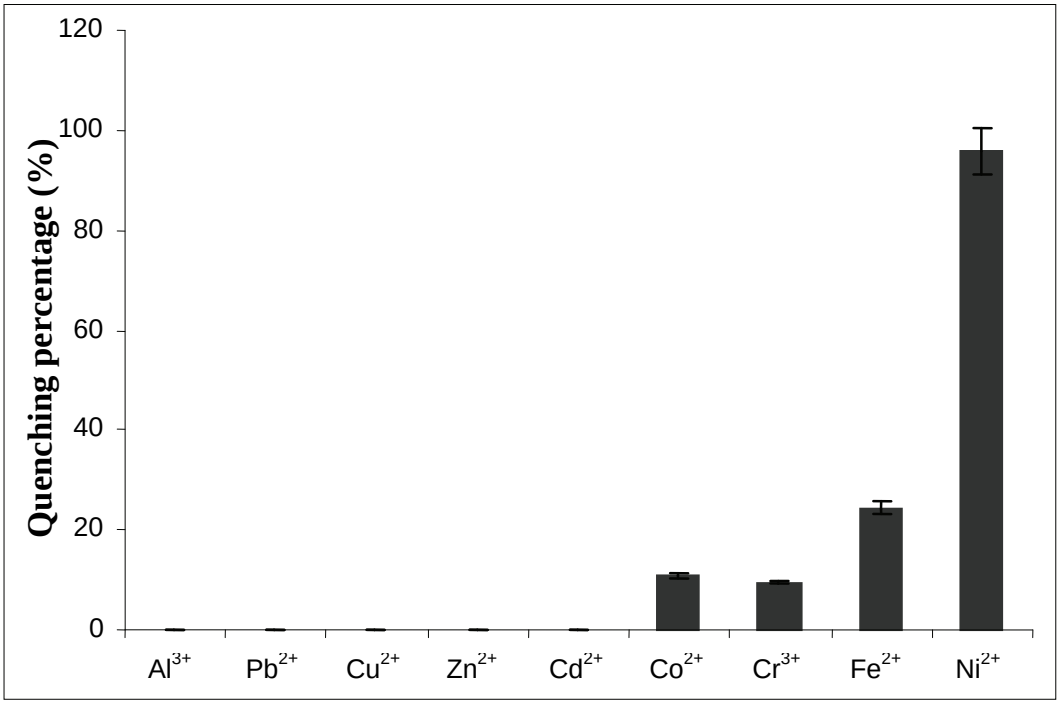

Figure 7.8: Quenching percentage ([Io-I/Io] x 100%) of fluorescence intensity of PAN-PAA nanofibre upon addition of 1.0 equivalent metal ions

The selectivity and tolerance of PAN-PAA for Ni^{2+} over other metal ions was examined by competition experiments. When 1 equivalent of Ni^{2+} in the presence of 10 equivalent of respective metal ions was introduced on the fibre, the emission spectra displayed a similar quenching at near 557 nm to that of Ni^{2+} only. The results indicated that the fluorescence quenching by Ni^{2+} was hardly affected by the co-existence of other metal ions. When analyte solutions containing mixtures of competing species are used, the consideration of sensitivity and selectivity becomes more important. This result afforded a solid sensor for selective detection of nickel ions in water without laborious sample handling steps.

Another requirement for the solid detection sensors is its reusability. To investigate this ability, the nanofibre was used to complex Ni^{2+} through complex-stripping cycles. The stripping agent used was 0.1 M HCl. Figure 7.9 shows a profile of the fluorescence response during five sequential cycles. The whole process included washing the fibre with HCl followed by modulating the pH value to the neutral using 0.1 M NaOH and the sensing of Ni^{2+}. The nanofibre was found to be able to re-combine with Ni^{2+} for at least four times (I_4/I_1 = 94.8%) and the decrease of the fluorescence intensity may be attributed to the effect of stripping agents on the sensing performance and little loss of the fibre during multiple regeneration experiments.

The effect of the pH of the solution on the binding ability of PAN-PAA nanofibre with Ni^{2+} demonstrates that the functionalized polymer was disturbed by proton in the detection of metal ions. HCl was chosen as a simple stripping agent for the regeneration of nickel-free PAN-PAA nanofibre, because at pH below 5.0, the protonation of receptors' nitrogen atoms of the PAN-PAA fibre decreases its electron donating abilities. However, at higher pH (>8.0) value, the precipitation of metal hydroxide which decomposes to the oxide is promoted.

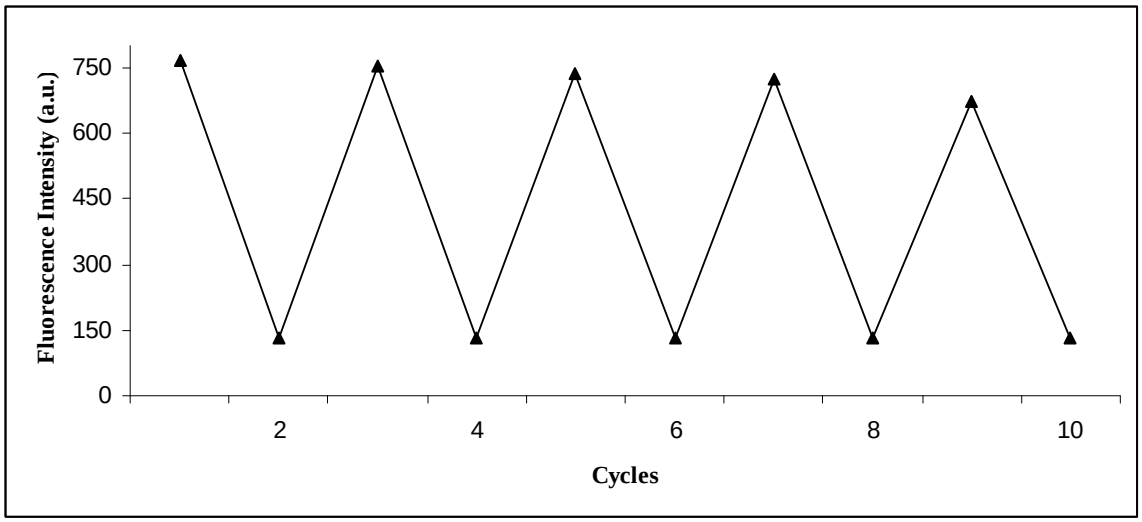

Figure 7.9: Repeated switching of fluorescence emission of the PAN−PAA nanofibre against the number of Ni^{2+} solution/eluent cycles

7.4 Conclusions

A novel heterogeneous PAN-PAA nanofibre for selective detection of Ni^{2+} in water was developed successfully. The fabrication technique involved covalent functionalisation of PAN on PAA polymer followed by electrospinning to produce smooth and beadless fluorescence nanofibre. A Stern-Volmer bimolecular quenching relationship was found to hold when I_0/I was used to determine analyte concentration. Importantly, the system showed high sensitivity in the range of concentration studied and also high selectivity in its fluorescence "turn-off" response toward Ni^{2+} against other metal ions. Further, a reversible process can be realized by breaking of indicator/quencher complexation and fluorescence "turn-on", allowing reusability at least four cycles. The approach may serve as a foundation for the preparation of practical fluorescent detector for potential practical applications. Further work in this regard is in progress in our laboratory. We hope that this work will contribute to the development of the versatile technique of electrospinning for fabrication of fluorescence nanofibre with application in both environmental and biological systems.

7.5 Recommendations

The application of the fluorescent probe can be extended for determination of Ni^{2+} ions in other aqueous samples like in sewage water

8 COLORIMETRIC PROBE FOR NICKEL(II) IONS IN WATER BASED ON SILVER-COPPER ALLOY NANOPARTICLES

8.1 Introduction

The objective of the project was to develop and characterize a colorimetric probe for the detection of Ni^{2+} ions in water based on silver/copper alloy nanoparticles hosted in electrospun nanofibres.

Nickel is an essential trace element for plants and animals where it participates in a variety of cellular processes. It plays important roles in various enzyme activities such as hydrogenases, superoxide dismutases, acetyl-coenzyme, carbon monoxide dehydrogenases, and in catalytic processes (Mulrooney and Hausinger, 2003). However, overexposure to nickel ion can cause acute pneumonitis, dermatitis, asthma, disorders of central nervous system and cancer of the nasal cavity and lungs (Kasprzak *et al*., 2003). The International Agency for Research on Cancer (IARC) classified nickel compounds as group 1 carcinogenic to humans in 1990 (Denkhaus and Salnikow, 2002). Therefore detection of Ni^{2+} ions in industrial, environmental, and food samples has become very important.

Like many transition metals, determination of nickel by photometric methods is well established. Many sensitive instrumental methods, such as spectrofluorometry (Ressalan and Iyer, 2004), X-ray fluorescence spectrometry (Leyden *et al*., 1975), atomic absorption spectrometry (Chen and Teo, 2001) and chemiluminescence (Li *et al*., 2006), have widely been applied for the determination of nickel. While these techniques do an excellent job in accurately detecting low levels of transition metals, they require high cost analytical instruments or at least electricity. This renders these techniques insufficient for online and field monitoring or for resource-poor settings. Hence, there is a need to develop simple, reliable methods that are sensitive and selective as well as capable of use by technicians, preferably in the field. Recently, colorimetric sensing of metal ions has been shown to be a less labour-intensive alternative to techniques based on fluorescence (Nazeeruddin *et al*., 2006). It is well known that solid materials that change their colour upon recognition of macromolecules are widely accepted for fingerprinting and conducting pregnancy tests at home (Prabhakaran *et al*., 2007). The throughput of the testing was profoundly advanced by the elimination of instrumental requirements and organic solvents. This idea can be extended towards developing simple visual detection methods for trace environmental toxins such as heavy metal ions.

Metal nanoparticles with well controlled size have recently been the focus of great interest because of the colour changes associated with their surface plasmon absorption. Their surface plasmon absorption is dependent on a number of parameters such as the size and shape of the particle, the adsorbed species and the distance between particles (Aslan *et al*., 2004). Among the metals, gold, silver and copper are known to display plasmon resonances in the visible spectrum (Kreibig and Vollmer, 1995). These nanoparticles have been used with great success for the detection of a range of analytes such as metal ions (Reynolds *et al*., 2006). For colour signal generation, metal nanoparticles are particularly attractive; as they possess much higher extinction coefficients compared to organic dyes, allowing sensitive colorimetric detections with minimal material consumption (He *et al*., 2005, Rosi and Mirkin, 2005). Metal alloy nanoparticles, on the other hand, have mainly been studied because of their catalytic effects (Dutta *et al*., 2011, Li *et al*., 2010a). They have been reported to offer additional degrees of freedom for tuning their optical properties by altering atomic composition and atomic arrangement (Chowdhury *et al*., 2009). This motivated us to study alloy nanostructure platforms to diagnose the presence of Ni^{2+} ions in aqueous media.

In order to confer some special properties, organic and inorganic polymers have been used as solid supports for nanoparticles. The choice of solid support and immobilization of the indicator onto the support have significant impact on the performance of the probes in terms of selectivity (Brook and Narayanaswamy, 1998), sensitivity, response time and stability (Xavier *et al*., 1998). Furthermore, these polymers can afford electrospinnable material for transformation into nanofibre mat for solid phase measurement. Electrospinning of polymeric materials into well-defined fibre mat has received significant interest in the recent past. Specifically, the technique has been found to be a unique and cost-effective approach for fabricating large surface area mats for a variety of sensor applications (Balaji *et al*., 2006, Gao *et al*., 2007, He *et al*., 2009, Reneker and Chun, 1996, Shin and Jang, 2007, Wang *et al*., 2002).

Herein, we report the development and characterization of a simple, sensitive and selective colorimetric probe for the detection of Ni^{2+} ions in water based on silver/copper alloy nanoparticles hosted in electrospun nanofibres.

8.2 Experimental

Materials and reagents

All chemicals used were of analytical grade. All solutions were prepared with double-distilled deionised water obtained from a Millipore system. Nylon 6 (Mw = 10 000), $AgNO_3$ (ACS reagent ≥ 99%), $NaBH_4$, glutathione and salts of different cations studied ($CuSO_4.5H_2O$, $NiCl_2.6H_2O$, $CrCl_3.6H_2O$, $FeSO_4.7H_2O$, $MnSO_4.H_2O$, $CaCl_2$, NaCl, $Pb(NO_3)_2$ and $CoCl_2.6H_2O$) were obtained from Sigma Aldrich (St. Louis MO, USA). Formic acid (90%) and glacial acetic acid (100%) were purchased from Merck Chemicals (Wadeville, South Africa) and used as received. All glassware were cleaned with 3:1 HCl/HNO_3 and rinsed with double-distilled deionised water before use.

Instrumentation

Surface plasmon absorption spectra were recorded on a Perkin Elmer Lambda 25 UV/VIS double beam spectrophotometer in a quartz cell (1 cm) at room temperature. Transmission electron micrograph (TEM) was recorded on a JEOL JEM 2100 LaB6 working in STEM and HAADF (High Angle Annular Dark Field Mode). The morphology of the nanofibre mat was studied by a JEOL JSM-7001F Field Emission Scanning Electron Microscope operating at 2 kV after gold sputter coating.

In situ synthesis of glutathione-stabilized silver/copper alloy nanoparticles

Nylon-6, silver nitrate, copper sulphate, $NaBH_4$ and glutathione were used as electrospinnable polymer, silver precursor, copper precursor, reducing agent and stabilizer respectively. Nylon 6 pellets were dissolved in a mixture of acetic acid and formic acid in the ratio of 1:1 to make a solution with a concentration of 15 wt/wt%. The mixture was stirred with a magnetic stirrer for 1 h until the lumps of the nylon 6 pellets were broken and well dispersed. 10.5% of $AgNO_3$ and $CuSO_4$ in the mole ratio of 1:1.96 were then added to the nylon 6 solution. The mixture was allowed to stir for further 1 h after which 1.5×10^{-3} moles of $NaBH_4$ was added to this mixture. The colour of the solution changed to black (Scheme 8.1). After stirring for about 5 min 22.8% of GSH was added. The percentage weight of the salts and the capping agent were calculated based on the weight of nylon 6.

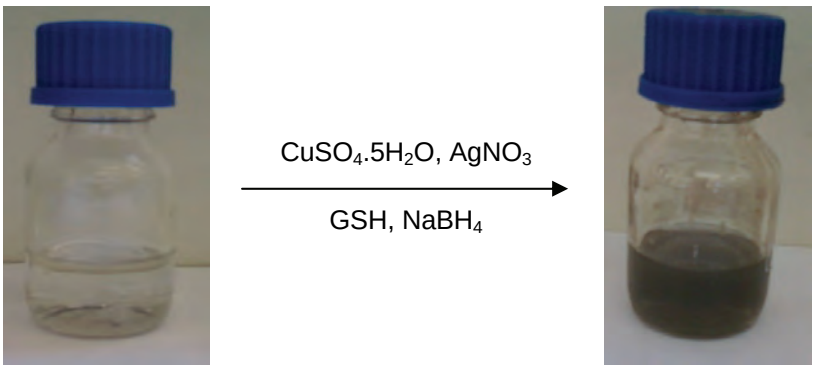

Scheme 8.1: In-situ synthesis of Ag-Cu alloy NPs

Fabrication of electrospun nanocomposite fibres

The homogenous nanocomposite solution was loaded into a 10 mL plastic syringe. The syringe was then mounted on a programmable syringe pump (New Era, NE-1000). The solution was pumped at a flow rate of 0.3 mL/h through a steel needle of 0.584 mm internal diameter. Nanofibres were collected on an aluminium foil collector with the distance between the needle tip and the collector of 12 cm and the applied voltage at the needle tip was 22.5 kV. The electrospun fibre mats were cut into uniform strips and without any further treatment these strips were placed in the various test solutions.

Performance testing of the probe

Standard solutions of various metal salts were prepared by appropriate dilution of their stock solutions with double-distilled deionised water. Aliquots (5 mL) of the standard solutions were measured out in a sample vial and the strips of electrospun fibre mats were placed in these solutions.

8.3 Results and Discussion

Optical properties of synthesized Ag-Cu alloy nanoparticles

UV-Vis spectroscopy is one of the widely used techniques for structural characterization of nanoparticles. The absorption spectrum (see Figure 8.1) of the black silver-copper alloy colloids prepared showed a surface plasmon absorption band with a maximum at 424 nm. If silver and copper ions are reduced simultaneously in the same solution, silver-copper alloy nanoparticles are formed. The alloy formation is concluded from the fact that the optical absorption spectrum shows only one plasmon band and this is in agreement with what has been reported in literature (Mulvaney, 1996, Papavassiliou, 1976, Torigoe *et al*., 1993). Two bands would be expected for the case of a mixture of silver and copper nanoparticles. Also, the appearance of a narrow SPR absorption band at 424 nm confirms the narrow size distribution and the well dispersed state of the alloy nanoparticles.

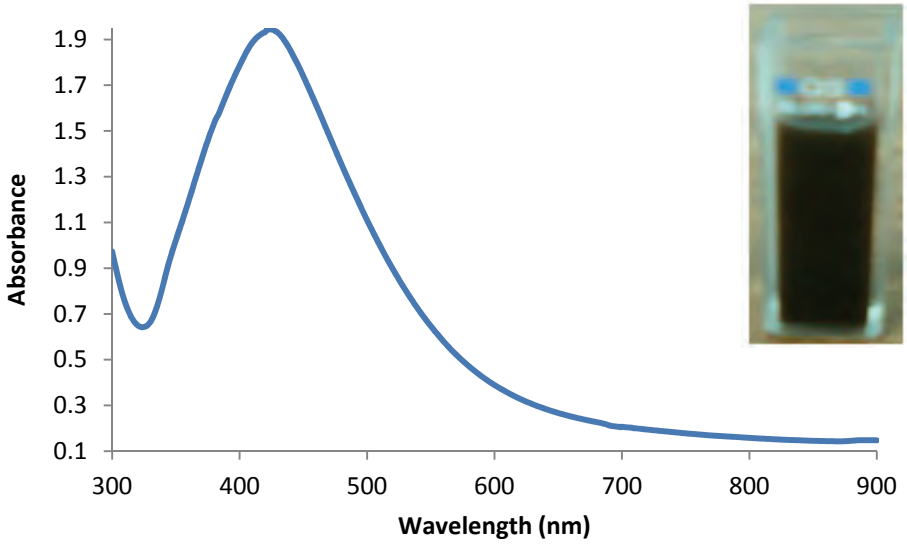

Figure 8.1: UV-Vis spectrum of Ag-Cu/Nylon 6 nanocomposite solution before electrospinning

The appearance of a single absorption band indicates that the synthesized Ag-Cu bimetallic particles were in alloy form rather than being a mixture of individual metal nanoparticles, whereas the physical mixture of synthesized Ag and Cu nanoparticles showed two absorption bands corresponding to the individual metal nanoparticles (Figure 8.2 inset). Ag NPs alone in the polymeric solution had a strong surface plasmon resonance peak at 408 nm, while that of the Ag-Cu NPs was red-shifted to 424 nm and broadened which is agreement with what Mulvaney had reported (Mulvaney, 1996). In addition, the plasmon resonance absorption band of Ag NPs is stronger and sharper in comparison with Cu nanoparticles which was at 551 nm, and occurs at longer wavelengths (Figure 8.2). The collective plasmon resonance absorption band of Ag-Cu alloy differs dramatically from that of Ag or Cu, and can easily be tuned in the UV-Vis region by changing the Cu/Ag mole ratio. The notable change in the absorption spectra can be primarily attributed to a change in the dielectric function when different metal atoms are mixed. Silver displays approximately free electron behaviour in the visible range, which gives rise to a sharp absorption band. Other metals, including Cu and Au, have less free-electrons, which gives rise to a broad absorption band (Chimentao *et al*., 2006).

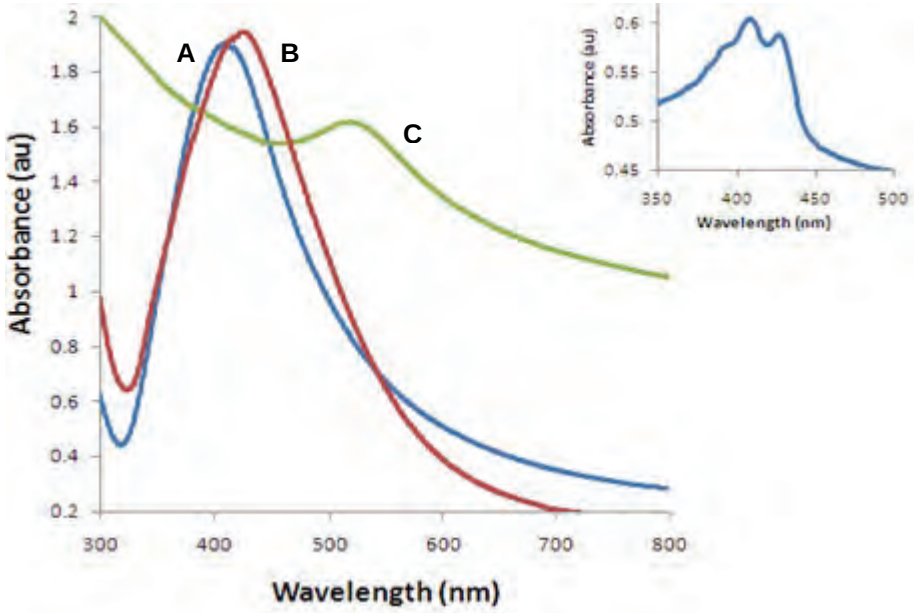

Figure 8.2: Surface plasmon absorption for AgNPs only [A], Ag-Cu alloy NPs [B], and CuNPs only [C]. inset is for the physical mixture of Ag and Cu NPs

Reducing agent

The general chemical reduction reactions involve reducing agents that are reacted with a salt of the metal according to the following chemical equation:

$$mMe^{n+} + nRed \rightarrow mMe^{0} + nOx \quad (7)$$

A study of metal ion reduction by borohydride system shows that BH_4^- ions functions not only as a reducing agent but also as a stabilizer that prevents the nanoparticles from aggregating (Van and Zukoski, 1998). Adsorption of borohydride onto the surface plays a key role in stabilizing growing nanoparticles by providing particle surface charge leading to electrostatic repulsion that keeps them from agglomerating (Scheme 8.2). There must therefore be enough borohydride in solution to stabilize the particles as the reaction proceeds.

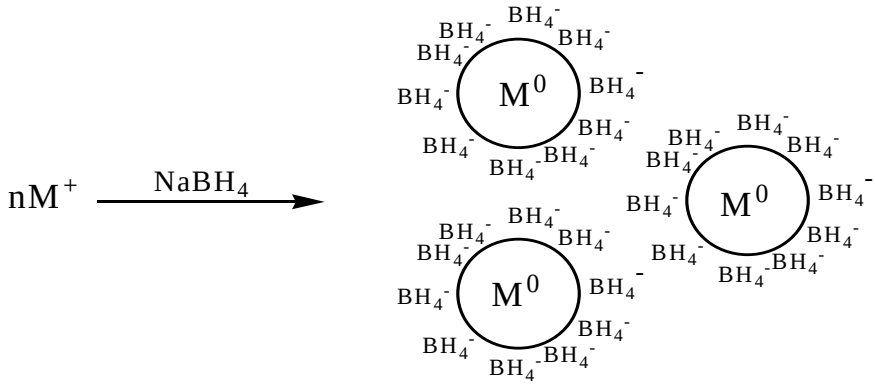

Scheme 8.2: Separation of nanoparticles by repulsive forces induced by adsorbed borohydride

Later in the reaction however, it was observed that too much sodium borohydride increases the overall ionic strength and aggregation occurred. Therefore, the amount of $NaBH_4$ needed must be optimized. The optimized mole ratio of the total salts to sodium borohydride was 1:2.8. Below and above this mole ratio there appeared more than one peak which were also very broad (Figure 8.3). The broad nature of these peaks could be attributed to large size distribution and probably aggregation caused by too much or less reducing agent.

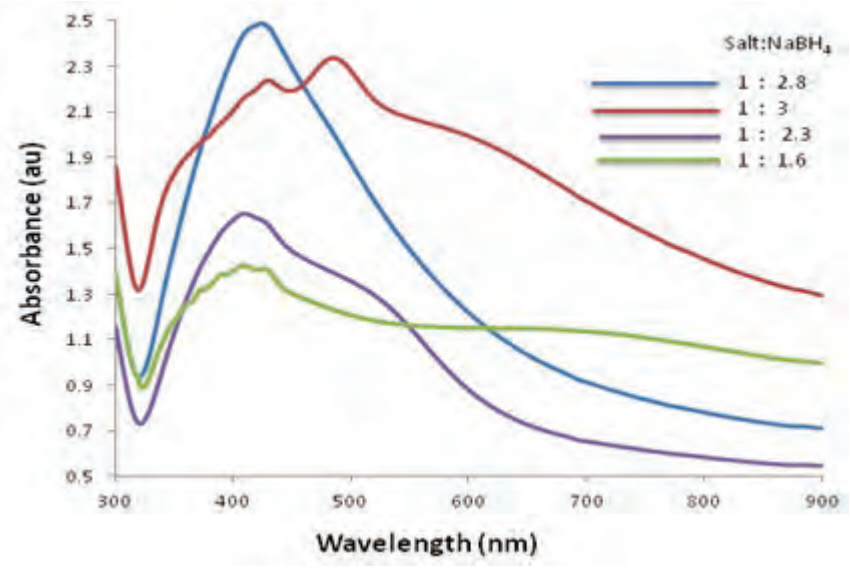

Figure 8.3: UV-Vis spectra of Ag/Cu alloy nanoparticles with varying mole ratios of reducing agent

Upon introduction of GSH, the rather loose shell of borohydride ions on the Ag/Cu NPs surfaces is easily displaced by other desired ligands with valuable functionalities (e.g. N and -SH groups). Molecules with electron-rich nitrogen or sulphur atoms are easily bound onto the surface of metal nanoparticles through the coordinating interactions between sulphur or nitrogen atoms with the electron-deficient surface of metal nanoparticles. In particular, the sulphur atom of GSH exhibits much stronger binding ability/affinity to NPs. A stabilizing agent relies on electrostatic repulsion force caused by either surface charge or steric stabilization, or both to prevent nanoparticles from aggregation.

Characterization of GSH-Ag/Cu alloy nanoparticles nanofibres

The morphology of the GSH-Ag-Cu alloy nanofibres was observed using a transmission electron microscope (TEM). As shown in Figure 8.4, glutathione stabilized Ag-Cu alloy nanoparticles having sizes between 3 and 6 nm were well dispersed in the electrospun nanofibres. Glutathione was used as a stabilizing agent to prevent the nanoparticles from aggregation. For environmental applications, surface functionalisation of nanoparticles is essential to apply them for selective detection of a specific analyte. Therefore, apart from stabilizing nanoparticles formed, GSH also served as a ligand that can selectively bind Ni^{2+} ions in aqueous media.

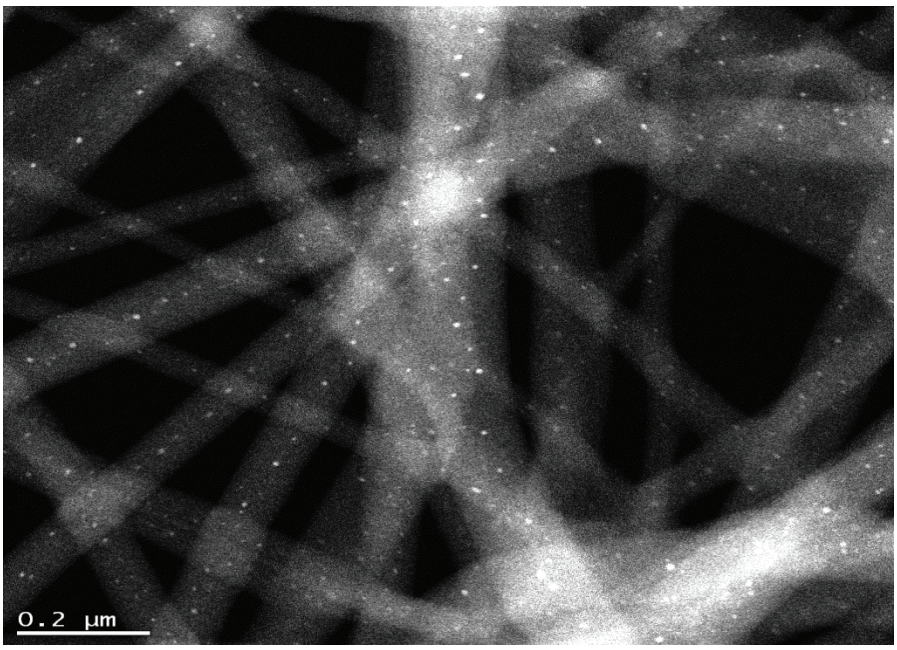

Figure 8.4: Transmission electron micrograph of Ag-Cu alloy nanoparticles in the electrospun nanofibres

Metal ions recognition ability of Ag-Cu alloy nanoparticles

To investigate the metal ions recognition ability of GSH-Ag-Cu NPs, metal ions (Ni^{2+}, Mn^{2+}, Fe^{2+}, Co^{2+}, Cd^{2+} and Pb^{2+}, Na^{+}, Cr^{3+}) of the same concentration (0.1 mol/L) were prepared and the electrospun fibre mats were cut and placed in these solutions. Deionised ultrapure water obtained from a Millipore system was used as control in this experiment. Upon interaction with various metal ions, as can be seen from Figure 8.5, the fibre mat placed in solution containing Ni^{2+} was discoloured, while other metal ions did not discolour the strips.

Figure 8.5: Colorimetric responses of the fibre strips to various solutions from left, H_2O, Pb^{2+}, Ni^{2+}, Fe^{2+}, Na^{+}, Cr^{3+}, Ca^{2+}, Mn^{2+} and Co^{2+} respectively

Glutathione, a tripeptide containing cysteine, contains two carboxylic acid groups. Marco Bieri and Thomas Bürgi (Bieri and Buergi, 2005), recently reported that at least one of these carboxylic acid groups forms an additional anchor to the gold surface, besides the strong gold-sulphur bond when it is used as a stabilizer. Upon interaction with the surface, part of the carboxylic acid groups also deprotonates. Ni^{2+} is known to bind well to groups or ligands containing lone pair electrons such as $-NH_2$, -COOH via the coordination bond (Jones and Vaughn, 1978). Both the terminal carboxylate groups of the glycine moiety and the free $-NH_2$ groups from glutamate moiety were believed to be responsible to bind the Ni(II) centre. The nanoparticles are expected to aggregate upon interaction with Ni^{2+} due to strong coordination bond between Ni^{2+} and $-NH_2$, -COOH of the functionalized glutathione modifier. We therefore believe that the carboxylic acid group that was bound to the surface of the nanoparticles was detached and in the process the nanoparticle surface became exposed and this led to agglomeration and subsequent loss of their surface properties. Agglomeration is mainly caused by excess surface energy and high thermodynamic instability of the nanoparticle surface (Tolaymat *et al*., 2010).

It must be noted that in the presence of Ni^{2+} ions, Ag/Cu alloy nanoparticles were aggregated and precipitated later as silver and copper particles probably because GSH no longer surrounded the alloy nanoparticles. These observations are consistent with the SEM results. The SEM images of alloy nanoparticles before and after the addition of Ni^{2+} ions are shown in Figure 8.6. As can be seen, aggregated nanoparticles are observed in nanofibres treated with Ni^{2+} solution although it was not possible to see these nanoparticles before the fibre was treated with the analyte using SEM microscope maybe because they are encapsulated within the fibres. This discoloration is probably related to the oxidation of the aggregated nanoparticles which are no longer stabilized and the formation of a complex between glutathione and Ni^{2+} ions.

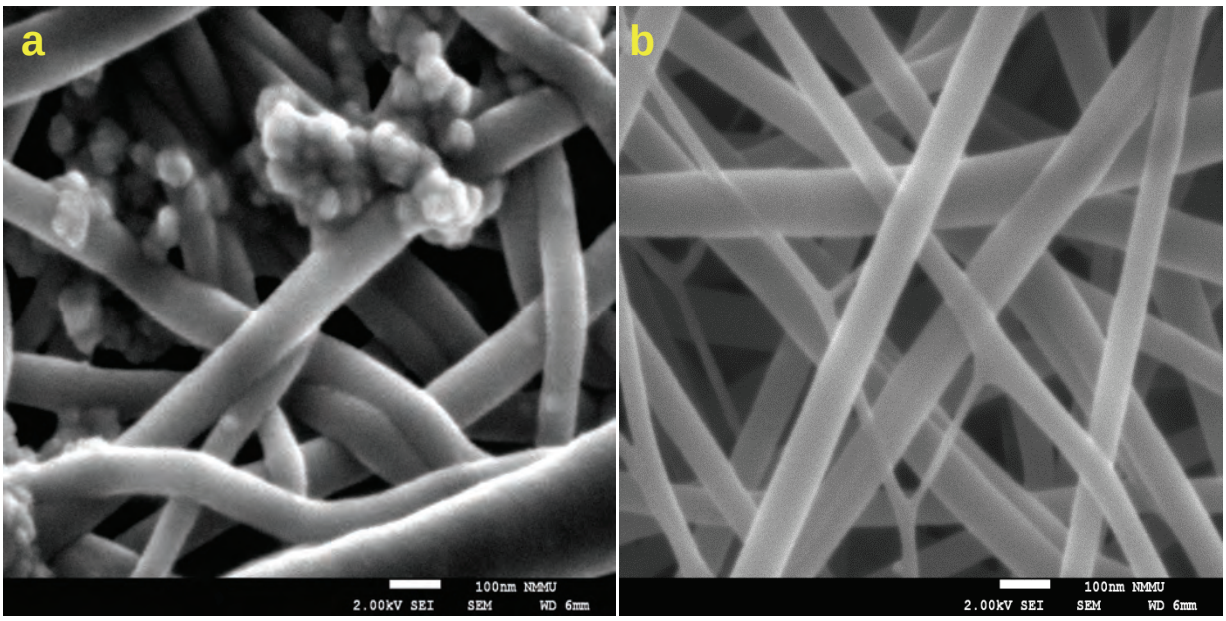

Figure 8.6: Scanning electron micrograph of Ag-Cu alloy-nylon 6 nanocomposite fibres (a) before and (b) after treatment with nickel (II) ions

To further confirm that the nanoparticles had actually been oxidized, some crystals of nickel chloride salt were dissolved in the polymeric mixture before electrospinning and there was a colour change from black to blue (Figure 8.7 inset). The blue colour indicated the presence of Cu^{2+} ions in the mixture while Ag^{+} ions were colourless. This oxidation was further confirmed by UV-Vis spectroscopy (Figure 8.7). It can be seen that the SPR absorbance has been significantly decreased by the presence of nickel in the nanocomposite solution and this indicates a considerable decrease in the concentration of Ag-Cu alloy NPs.

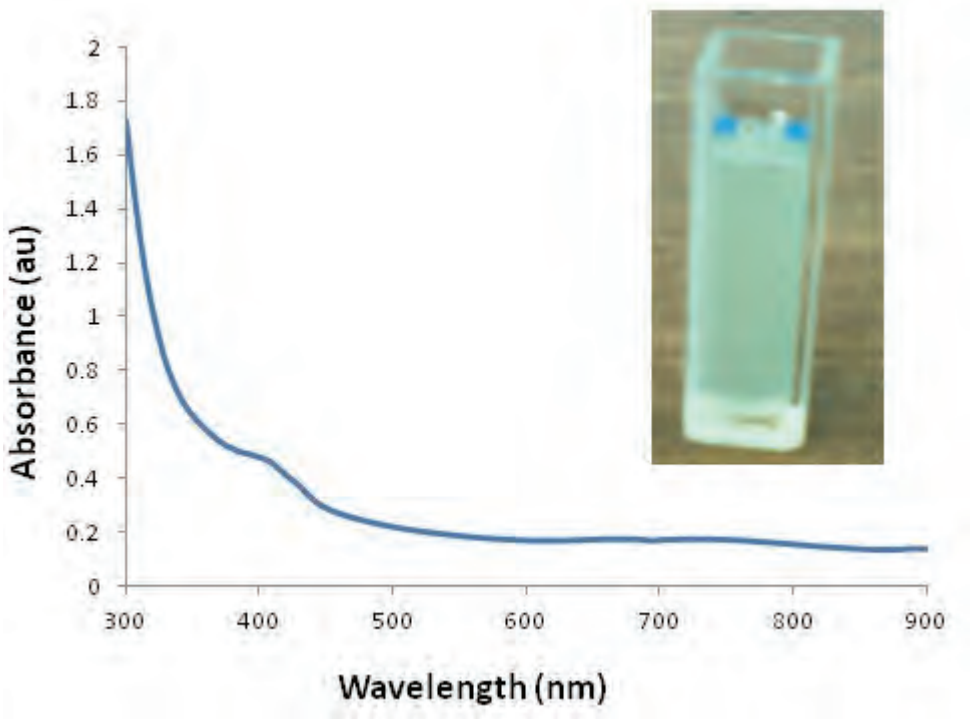

Figure 8.7: UV-Vis spectra of Ag-Cu alloy nanocomposite solution incubated with Ni^{2+} ions and inset Photograph of the mixture

In an attempt to gain insight into the effect of concentration of Ni^{2+} to the colour change of the nanocomposite fibre, a series of solutions of Ni^{2+} with different concentrations ranging from 0.058 µg/mL to 5.8 mg/mL were prepared and the fibre immersed into these solutions. Colour changes were observed on the fibres in solutions having concentrations of 5.8 µg/mL within 30 min, at the rate at which was proportional to the concentration. Below 5.8 µg/mL, the fibres changed after an overnight stay in the nickel ion solutions down to a concentration of 0.058 µg/mL.

Real sample analysis

The proposed method was applied in the determination of the concentration of nickel(II) ions in a water sample; tap water from Prof Torto's research lab at Rhodes University was used. For this purpose, the fibre strip was put in a vial containing 5 mL of tap water sample. No change in the colour of the fibre strip was observed thus showing that the concentration of Ni^{2+} in the sample is less than the limit of detection of the proposed method. The tap water was then spiked with 5.8 µg/mL Ni^{2+} solution and the fibre mats were discoloured. This result demonstrated the application of this probe for detection of Ni^{2+} ion in real water sample.

8.4 Conclusions

Nylon 6 nanofibres containing glutathione stabilized silver-copper alloy nanoparticles were prepared by electrospinning. The nanocomposite was characterized by UV-Vis SEM and TEM. Metal sensing ability of this probe was done and was found to be selective to Ni^{2+} ions. This approach relies on the simple oxidation of the formed nanoparticles in the presence of the analyte. The presence of Ni^{2+} reduces or rather eliminates the SPR band of the nanoparticles at 424 nm at room temperature. In contrast to other nanoparticle-based colorimetric assays, this system does not imply the use of complex nanoparticles modification (i.e., biological material). This method can be related to user-friendly and field-portable detection systems, and it is inexpensive, very simple, rapid, and a reliable alternative in comparison to other techniques. By functionalizing nanoparticles with ligands and other specific heavy-metals receptors, the possibility exist to further improve the sensitivity of the method achieving even efficient throughput screening tests for metal toxicity in general beside single metal detection.

8.5 Recommendations

X-ray diffraction characterization to ascertain the phases of the metal nanoparticles embedded in the fibre could be necessary.

9 ELECTROSPUN NANOFIBRE-BASED COLORIMETRIC PROBE FOR THE RAPID DETECTION OF IRON(II) IONS IN AQUEOUS MEDIA

9.1 Introduction

The objective of the study was to develop a 2-(2′-pyridyl)imidazole (PIMH) functionalized poly(vinylbenzylchloride) (PVBC) nanofibre-based colorimetric probe for the detection of Fe(II).

Iron is an important element in environmental, industrial, medical and biological studies (Lieu *et al*., 2001). It is naturally present in a variety of rocks and soil in oxidation states 2 and 3 (Taylor and McLennan, 1985). Iron is necessary for DNA synthesis and in oxidative processes of living tissues; it exists at the active site of molecules responsible for oxygen transport and mitochondrial electron transfer. Iron also provides fundamental structures of many co-factors involved in enzyme activities (Bothwell, 1979, Cotton, 1976, Hoffbrand and Herbert, 1999, Zhang and Enns, 2009). It plays an essential role in photosynthesis and is a limiting growth nutrient for phytoplankton in some parts of the ocean (Martin and Fitzwater, 1988, Martin *et al*., 1990, Riley and Chester, 1971). For the human body and other high animals, Fe(II) is not only a key element in energy metabolism, but also crucial in the transport and storage of oxygen (Mortatti *et al*., 1982). However, iron deficiency causes anaemia which is one of the world's most common nutritional deficiency diseases (Zeng and Jewsbury, 2000). Normally small concentrations of iron are essential in all mammals but excessive intake of iron has been reported to cause siderosis and damage to organs (Ellis *et al*., 1954), toxicity and even death (Corbett, 1995). Hence, the determination of iron in medicinal, environmental and industrial samples has been an important topic in environmental and biological analysis (Carneiro *et al*., 2002, Qin *et al*., 1998, Safavi *et al*., 2002). All the findings cause great concern regarding public health, demanding accurate determination of this metal ion at trace and ultra-trace levels.

Several methods have been reported for the determination of Fe(II) and these include; anodic stripping voltammetry (Gholivand *et al*., 2011), inverse voltammetry (Stozhko *et al*., 2005), chemiluminescence (Hansard and Landing, 2009), direct potentiometry (Mahmoud, 2001), high-performance liquid chromatography (Tavallali and Nike, 2011), fluorometric analysis (Garcia *et al*., 1983, Zhu *et al*., 2002), capillary electrophoresis (Xu *et al*., 1996a), and spectrophotometric detection (Alula *et al*., 2010, Gupta and Barhate, 2012). Though these methods offer good limits of detection and wide linear ranges, they are not the perfect strategy since they often require complicated sample preparation, advanced instruments and professional operation. Thus, it is highly desirable to design and synthesize novel Fe(II) colorimetric probes in which a signal can easily be visualized by the naked eye without resorting to any instrumentation. In order to provide colorimetric probes with good sensitivity, selectivity and most importantly stability, various support materials for their immobilization have been employed (Mohr and Wolfbeis, 1994).

Polymers have been used as inert supports for ligands and indicator dyes to keep the molecules apart in order to allow for exposure to analytes and to maintain their optical properties (Dini *et al*., 2011). Besides providing a support, polymers can also be transformed into nanofibres by electrospinning.

In order to improve the properties of electrospun nanofibres and extend their applications, researchers have paid attention to their modification. The primary goal of surface modification is to endow specific functionalities to the original polymer with well-defined characteristics. To achieve this, a number of methods have been used which include plasma treatment (Hoecker, 2002), wet chemical method (Nam *et al*., 1999), surface graft polymerization (Mori *et al*., 1994), and co-electrospinning of surface active agents and polymers (Sengonul *et al*., 2007). Surface modification of nanofibres after electrospinning gives a high degree of functionalities that are exposed on the surface for easy accessibility.

In this work, we report the development of a colorimetric probe for detection of Fe(II). Poly(vinylbenzyl chloride) (PVBC) was synthesized by free radical polymerization of 4-vinylbenzylchloride (VBC) and electrospun into nanofibres. The probe was fabricated through post-functionalisation of the nanofibres with 2-(2′-pyridyl)imidazole (PIMH) ligand by wet chemical method. This system is simple and takes advantage of the unique optical properties generated by PIMH-Fe(II) complex. To the best of our knowledge, development of a colorimetric probe for the detection of Fe(II) using 2-(2′-pyridyl)imidazole (PIMH) as a ligand has not been reported.

9.2 Experimental

Materials

All chemicals used were of analytical grade. Pyridine-2-aldehyde 99%, Glyoxal solution (40% weight in water) and 4-vinylbenzyl chloride (90%), Azoisobutyronitrile (AIBN) (recrystallized from THF just before use), certified reference material (Iron, Ferrous 1072) metal salts; ($CoCl_2$, $MnSO_4.H_2O$,$AgNO_3$, $NiSO_4.7H_2O$, $CrCl_3.6H_2O$, $Zn(NO_3)_2$ and $FeSO_4.7H_2O$ $Cd(NO_3)2.4H_2O$, $Pb(NO_2)_2$, $CuSO_4.5H_2O$) were used as obtained from Sigma Aldrich (St. Louis, MO USA). Ethanol, Diethyl ether, Ethyl acetate, N,N-Dimethylformamide (DMF), Tetrahydrofuran (THF), Potassium hydroxide (KOH) and Sodium hydroxide (NaOH), 25% ammonia solution were obtained from Merck Chemicals (Wadeville, South Africa), Sodium dihydrogen phosphate ($NaH_2PO_4.2H_2O$), Potassium hydrogen phthalate ($C_8H_5KO_4$) were obtained from Saarchem Analytic (Krugersdorp, South Africa).

Instrumentation

Infrared spectra were recorded on Perkin-Elmer 100 FT-IR spectrophotometer. ^{1}H and ^{13}C NMR spectra were collected on Bruker Avance 400 MHz spectrometer. Electronic absorption spectra were recorded on a Perkin Elmer Lambda 25 UV/VIS spectrophotometer in a quartz cell (1 cm). The morphology of the nanofibre mat was studied by the Tescan (TS5136ML) Scanning Electron Microscope (SEM) operating at an accelerated voltage of 20 kV after a gold sputter coating. Elemental analyses were performed with Vario Elementar Microtube ELIII (Hanau, Germany) after drying the samples.

Synthesis of 2-(2'-pyridyl)imidazole (PIMH)

2-(2'-pyridyl)imidazole was synthesized following a previously reported literature procedure (Gerber *et al*., 2006). Briefly, a solution of 10.70 g of pyridine-2-aldehyde (0.10 mol) in 10 mL of ethanol was mixed with 20 mL of a 40% aqueous glyoxal solution at 0°C. Immediately, 30 mL of an ice-cold 20% aqueous ammonia solution was added, and the yellow-brown solution was stirred at 0°C for 30 min, and then allowed to stir overnight at room temperature (Scheme 9.1). The ethanol was then boiled off, and the residue was extracted several times with 50 mL aliquots of diethyl ether. The ether was evaporated using a rotary evaporator, and the yellow solid crystals were re-crystallized from ethyl acetate. These were filtered and dried under vacuum.

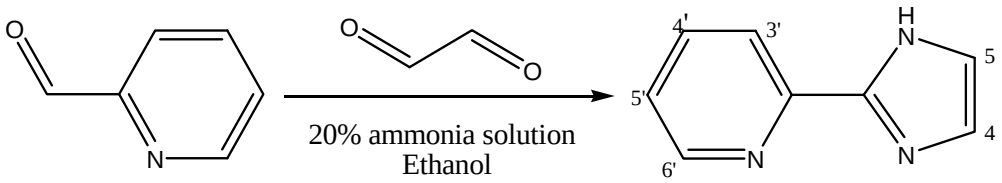

Scheme 9.1: Synthesis of 2-(2'-pyridyl)imidazole (PIMH) ligand

Preparation of standard solutions

Iron(II) stock solution (0.1 M) was prepared by dissolving 2.78 g $FeSO_4.7H_2O$ in 100 mL volumetric flask using 0.2 M of concentrated H_2SO_4 and deionised water. The other metal ion solutions were prepared from their sulphate, nitrate or chloride salts. Ag^{+}, Cu^{2+}, Zn^{2+}, Cd^{2+}, Pb^{2+}, Fe^{3+}, Co^{2+}, Mn^{2+}, Cr^{3+}, Ni^{2+}, Ca^{2+}, Na^{+} and Mg^{2+} salts were dissolved to prepare stock solutions with concentrations of 1.0×10^{-3} M, the synthetic ligand was dissolved in the mixed solution of EtOH: H_2O $(V/V = 10:90)$ to give the stock solution (1 mg/mL). The prepared stock solution of the metal ions and ligand were directly used in the spectroscopic measurement.

Preparation of calibration curve

A series of Fe(II) standard solution having concentrations from 0 to 3.5 µg/mL were prepared. In each case, an appropriate volume of the stock solution of iron(II) standard was mixed with 4.0 mL of the buffer (pH 6.0) followed by the addition of 2 mL of PIMH solution. The pH of the mixtures was brought to 6.0 by using either NaH_2PO_4 or NaOH solutions and the volume was adjusted to 20.0 mL with Millipore water.

Interference evaluation

Evaluation of chemical interferences was conducted by repeating Fe(II) analysis in the presence of each of the interfering species at different concentration levels, and comparing the results with a measurement of a blank solution containing iron with no interfering substance. The interferences were studied by analysing

samples after adding between 2-25 µg/mL of each interfering ion into a fixed concentration (2.0 µg/mL) of Fe(II). All the solutions were prepared according to the standard preparation procedures already described.

Synthesis of poly(vinylbenzylchloride) (PVBC)

PVBC was produced by free-radical polymerization of 4-vinylbenzyl chloride (10 mL, 70.9 mmol) in toluene (2 mL) using azobisisobutyronitrile (AIBN) (0.05 g, 0.3 mmol) as the initiator. The reaction mixture was heated at 70°C under nitrogen gas for 12 h (Scheme 9.2). The polymer obtained was dissolved in THF and precipitated with methanol, filtered and air dried.

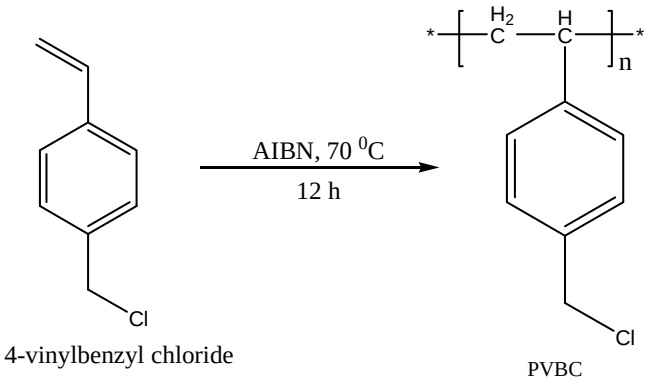

Scheme 9.2: Synthesis scheme of poly(vinylbenzylchloride) (PVBC)

Fabrication of nanofibres by electrospinning PVBC

A solution for electrospinning was prepared by dissolving the polymer to make a 40% (wt/v) in 1:1 (v/v) DMF/THF solvent system and the mixture was stirred for 3 h to obtain a homogenous solution. After loading the polymer solution into 10 mL glass syringe, the syringe was mounted on a programmable syringe pump (New Era, NE-1000). The solution was pumped at a flow rate of 0.8 mL/h through a steel needle of 0.584 mm internal diameter. Nanofibres were collected on a stationary collector covered with aluminium foil. The distance between the needle tip and the collector was 12 cm and the applied voltage was 15 kV.

Fabrication of the colorimetric probe by post-functionalisation of the nanofibres

A strip of approximately 14 cm x 6 cm of the PVBC nanofibre mat measuring 0.65 g was cut out. The strip was placed into a 20 mL methanol solution of PIMH (5.0 g, 0.035 mol) in a 50 mL flask along with KOH (3.93 g, 0.07 mol). The contents were heated at 40°C and stirred gently at 40 rpm for a period of 5 days (Scheme 9.3). Afterwards, the fibres were rinsed in methanol. Finally, the fibres were cleansed with diethyl ether in a Soxhlet extraction system and dried at room temperature, under reduced pressure for 12 h.

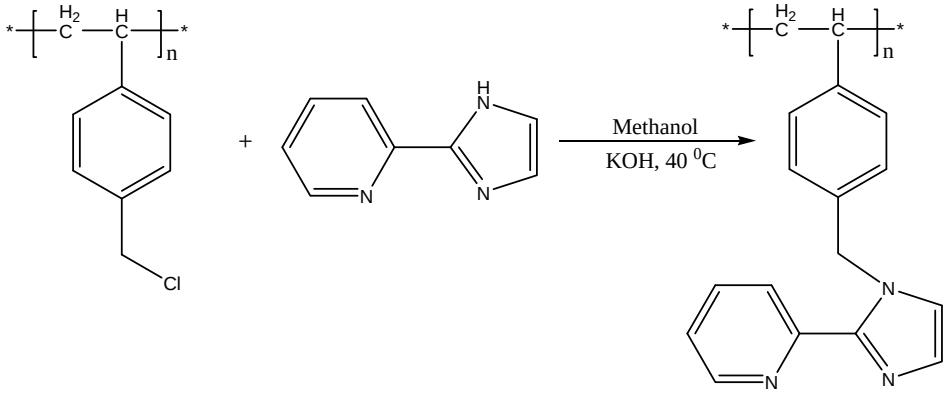

Scheme 9.3: Synthesis scheme of poly(vinylbenzyl-2-(2'-pyridyl)imidazole) nanofibres

9.3 Results and Discussion

Characterization of 2-(2'-pyridyl)imidazole

$mp = 133 - 135$℃. Anal. Calc. for $C_8H_6N_3$ (%): C, 66.65; H, 4.20; N, 29.15. Found: C, 66.29; H, 5.30; N, 29.16. ^{1}H NMR ($CDCl_3$) δ (ppm): 7.19 (s, 1H, H4), 7.22-7.25 (m, 2H, H5, H5'), 7.76 (t, 1H, H4'), 8.25 (d, 1H, H3'), 8.50 (d, 1H, H6'), 12.05 (br s, 1H, NH). ^{13}C NMR ($CDCl_3$) δ (ppm): 149.29 (2C), 77.90 (4C), 77.58 (5C), 148.80 (2'), 123.45 (3'), 137.71 (4'), 120.73 (5'), 146.70 (6'). IR (v_{max}/cm^{-1}): 1592, v(C=N_{im}); 1567, v(C=N_{py}); 3108 v(N-H).

Absorption response of PIMH to different metal ions

The recognition ability of the ligand towards different metal cations was investigated by UV-vis spectroscopy. A 1 mL solution of the ligand was added to 1.0×10^{-3} M of the metal ion solutions. The absorption spectrum of the mixture of Fe(II) and the ligand was red shifted to the visible region. The bathochromic shift could be attributed to spin crossover (SCO) in which the paramagnetic $t_{2g}^4\ e_g^2$ high spin state (HS) of Fe(II) could be switched to the diamagnetic t_{2g}^6 low spin state (LS) through forcing six-coordination on Fe(II) (Guetlich and Goodwin, 2004).

The variation of absorption spectra of ligand upon addition of different metal ions including Ni^{2+}, Mn^{2+}, Cr^{2+}, Co^{2+}, Zn^{2+}, Cd^{2+}, Cu^{2+}, Fe^{2+}, Fe^{3+}, Ag^{+}, Pb^{2+}, alkali and alkaline earth metal ions, were also recorded. As shown in Figure 9.1, there was no significant change observed except with nickel. On addition of Ni^{2+}, the spectrum shifted to 530 nm accompanied by the appearance of a faint purple colour.

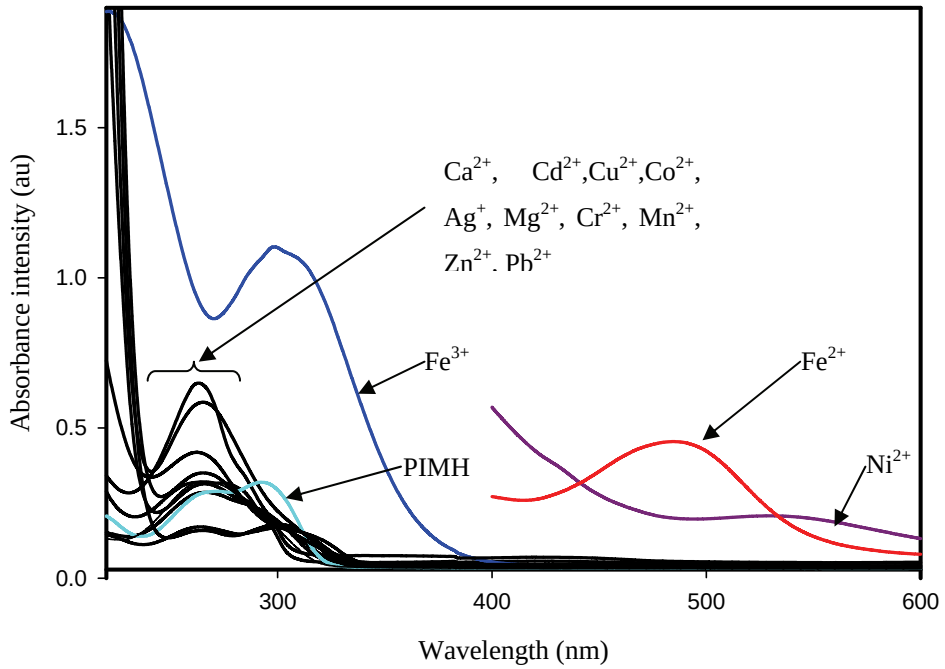

Figure 9.1: UV-vis spectra of PIMH (1 mg/mL) in water-ethanol (90:10 v/v) at pH 6 in the presence of 1 equivalent of Ag^+, Zn^{2+}, Cu^{2+}, Pb^{2+}, Cd^{2+}, Ni^{2+}, Co^{2+}, Fe^{2+}, Fe^{3+}, Mn^{2+}, Mg^{2+}, Ca^{2+}, Cr^{3+}

However, it can be seen that the maximum absorption of the ligand shifted from 292 nm and 271 nm to 484 nm upon addition of Fe(II). The shift was accompanied by a visual colour change from colourless to red-orange after the addition of ligand (see Figure 9.2). These results indicated that PIMH had a high-binding affinity towards Fe(II). The ligand was highly suitable for use in aqueous solutions and showed high selectivity towards Fe(II) over a large number of mono-, bi- and trivalent cations.

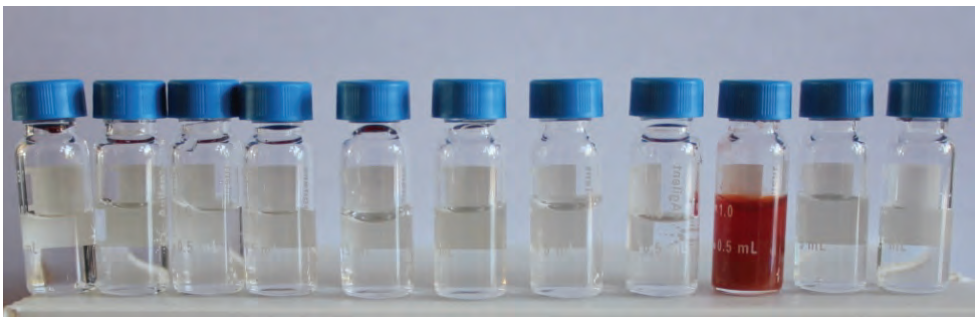

Figure 9.2: Colour changes of PIMH (1 mg/mL) upon addition of PIMH alone, Mn^{2+}, Ag^{+}, Cu^{2+}, Fe^{3+}, Mg^{2+} Pb^{2+}, Cd^{2+}, Fe^{2+}, Ni^{2+} , Zn^{2+} (1.0 equivalent) respectively

Effect of pH on the colour intensity of PIMH-Fe^{2+} complex

In order to select the optimum pH value at which maximum sensitivity occurs, the influence of the pH of the medium on the absorption spectra of Fe(II)-PIMH was studied over the pH range 3.0 to 8.0. The buffer solutions used were potassium hydrogen phthalate-hydrochloric acid (pH 2.2-4.0), potassium hydrogen phthalate-sodium hydroxide (pH 4.5-5.9) and sodium dihydrogen phosphate-sodium hydroxide (pH 6.0-8.0). In each case, a mixture containing 0.34 mg of Fe(II), 5.0 mL of the suitable buffer and 6.0 mL of PIMH solution were taken and the volume was adjusted to 20.0 mL with Millipore water. The experiment was repeated with buffers of different pH values from 3.0-8.0.

It was observed that the absorbance intensity increased as the pH increased from 3.0, reached a maximum at pH 6.0 and started to decrease up to pH 8 (Figure 9.3). Hence, pH 6.0 was taken as the optimum pH value and used for further studies. At lower pH (< 5.0), the absorbance was lower and this could be due to the fact that PIMH could be protonated and hence reduced its chelating ability. It is important to note that at higher pH (> 6.0), there could be a probability of the formation of the hydroxide ions.

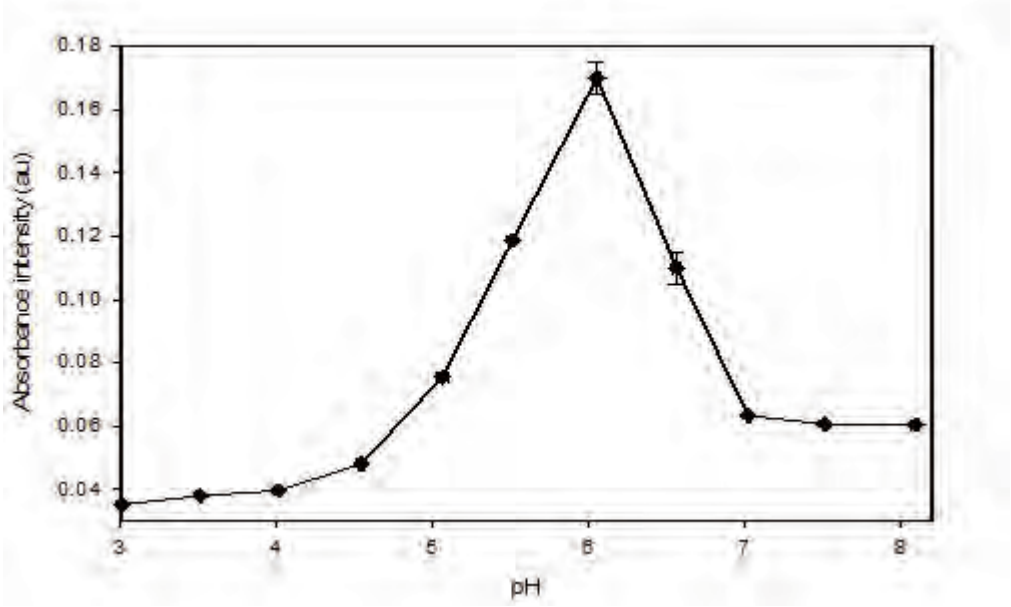

Figure 9.3: The effect of pH on the absorbance of Fe(II)-PIMH complex (error bars from relative standard deviations)

Effect of metal concentration

The change in absorbance intensity as a function of increasing metal ion concentration was monitored. The increasing peak intensity at 484 nm with increasing Fe(II) concentration (Figure 9.4) enabled quantitative determination of test samples by comparison with the calibration curve.

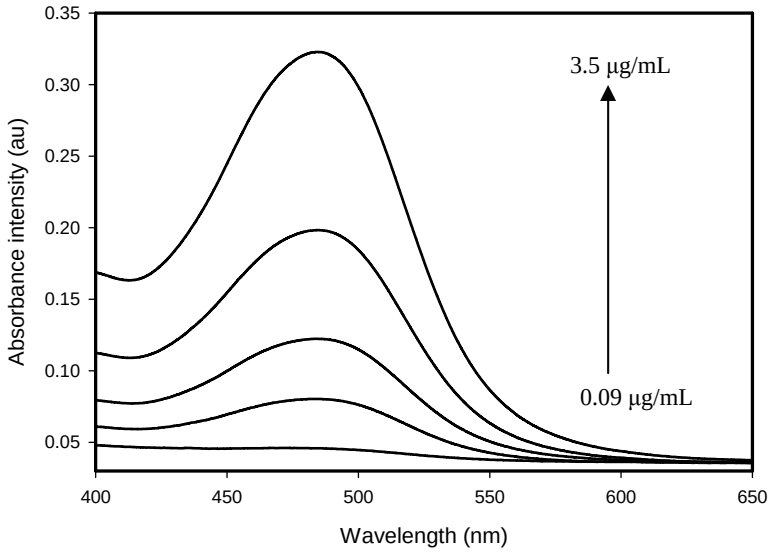

Figure 9.4: Absorption spectral changes of PIMH-Fe(II) complex with increasing concentrations of Fe(II) solution (pH 6.0)

Spectroscopic analysis in very dilute solutions is usually derived from the well-known Beer's law (Equation 8) which gives the relationship between the absorbance at 484 nm and Fe^{2+} concentrations.

$$A = \varepsilon lc \tag{8}$$

where A is the absorbance intensity (arbitrary units), ε is the molar absorptivity (L mol^{-1} cm^{-1}), l is the length of the solution the light passes through (cm) and c is the concentration of the solution ($molL^{-1}$). The $\boldsymbol{\varepsilon}$ of the method calculated from the slope of the plot was found to be 4.353×10^{3} L mol^{-1} cm^{-1}. A linear correlation between the concentration of the metal and absorbance was observed over the range of 0.0988 µg/ mL to 3.5 µg/mL (Figure 9.5).

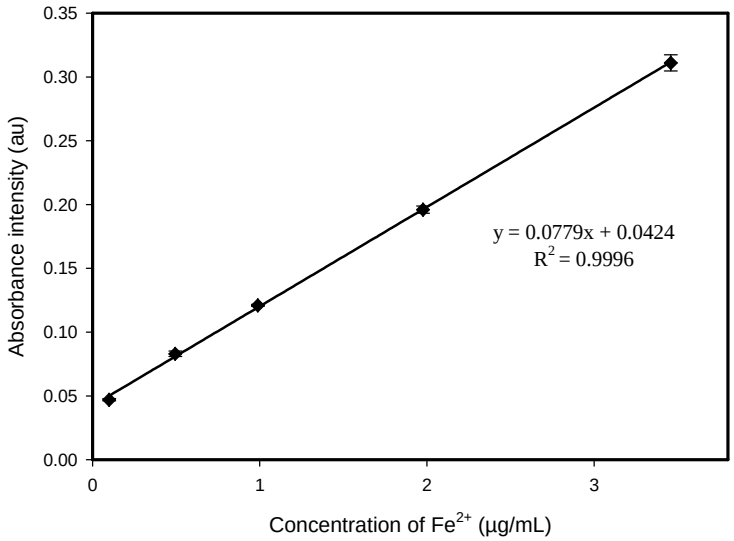

Figure 9.5: Calibration curve for the determination of Fe(II) concentration with PIMH (error bars from relative standard deviations)

Limit of detection (LOD) and limit of quantification (LOQ)

The standard deviation and slope of the calibration curve were used to determine the LOD and LOQ of Fe(II) using the method. Limit of detection is the lowest amount of analyte in a sample which can be detected but not necessarily quantified as an exact value while LOQ is the lowest amount of analyte in a sample which can be quantitatively determined with suitable precision and accuracy. Limit of detection and LOQ were

calculated by Eqs. $LOD = 3.3\delta/s$ (2) and $LOQ = 10\delta/s$ (3) respectively, where δ is the standard deviation and *s* is slope of calibration (Busaranon *et al*., 2006). The limit of detection (LOD) and limit of quantification (LOQ) of the proposed method were found to be 0.102 µg/mL and 0.309 µg/mL respectively.

Composition of the absorbing complex

Most colorimetric analyses particularly for metals depend upon the formation of coloured complex molecules. It is important to ascertain the molar ratio of metal to reagent. The stoichiometry of the absorbing complex can be done from photometric data by different procedures. Continuous variation method attributed to Job and modified by Vosburgh and Cooper (Vosburgh and Cooper, 1941), as well as the mole ratio method (Yoe and Jones, 1944), were applied to ascertain the stoichiometry of the complex. The composition of the complex [Fe(II):PIMH] was determined as 1:3 by both methods (Figures 9.6 & 9.7) which is consistent with six-coordinate diamagnetic Fe(II) species which are usually orange-red in colour (Hagiwara *et al*., 2011).

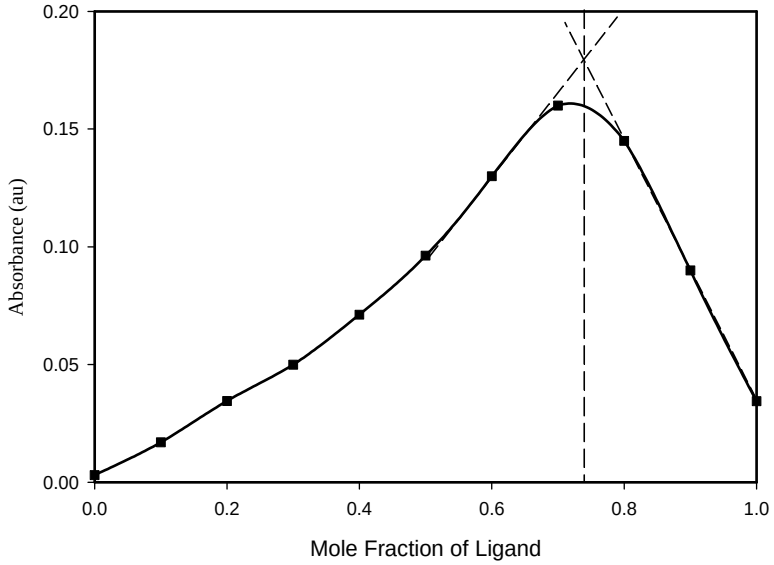

Figure 9.6: Plot of Job's method of continuous variation for determination of the stoichiometry of Fe(II)-PIMH complex at pH 6.0

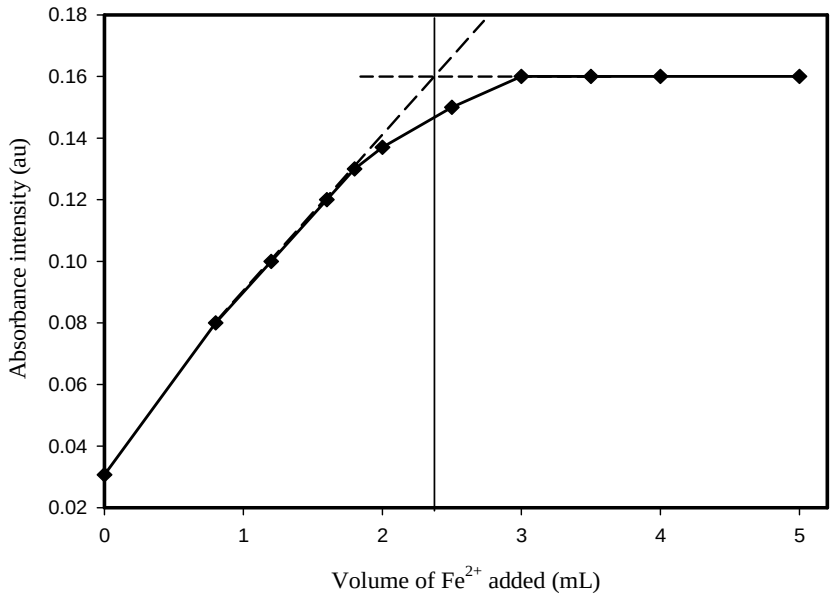

Figure 9.7: Plot of mole ratio method for determination of M:L ratio for Fe(II)-PIMH complex, Fe(II) (1×10-3 M), PIMH (1 mL, 6.9 × 10-3 M) at pH 6.0

Selectivity studies

The ligand showed excellent selectivity for Fe(II) over the alkaline earth and most of the transition metal ions tested. From the results obtained, Ni(II), Cu(II) and Co(II) were found to interfere more with the determination of Fe(II) at higher concentrations. Tolerance limits for the determination of 2.0 μg/mL of Fe(II) in the presence of interfering ions are given in Table 9.1.

Table 9.1: Spectrophotometric determination of Fe (II) in the presence of other metal ions (n =3)

		Proposed method	
Interfering ions with 2.0 μg/mL Fe (II)	**Quantity of the metal added (μg/mL)**	**Fe (II) found method (μg/mL)**	**%RSD**
Ni(II)	2.0	1.78	0.0
	5.0	1.28	0.1
	10.0	0.86	0.1
	20.0	0.70	0.1
	25.0	0.70	0.1
Cu(II)	2.0	1.93	0.0
	5.0	2.01	0.0
	10.0	2.00	0.1
	20.0	1.29	0.1
	25.0	1.13	0.1
Zn(II)	2.0	2.05	0.0
	5.0	2.03	0.0
	10.0	1.99	0.1
	20.0	1.95	0.7
	25.0	1.85	0.1
Mn(II)	2.0	2.01	0.0
	5.0	2.00	0.0
	10.0	1.97	0.9
	20.0	1.92	1.7
	25.0	1.80	0.7
Mg(II)	2.0	2.00	0.1
	5.0	2.00	0.0
	10.0	1.99	0.0
	20.0	1.98	0.9
	25.0	1.99	0.0
Co(II)	2.0	2.01	0.1
	5.0	2.00	0.1
	10.0	1.97	0.0
	20.0	1.92	0.0
	25.0	1.70	1.7

Ferrous ion has an affinity for amine ligands and it has been reported to interact with 1,10-phenanthroline and 2,2-bipyridine resulting in the formation of $[Fe(bipy)_3]^{2+}$ and $[Fe(phen)_3]^{2+}$ coloured complexes (Rajendraprasad and Basavaiah, 2010). The ferric ion does not have the same affinity for amine ligands as the ferrous ion. Colour change was not observed with PIMH even with metal ions that are considered borderline like Fe(II) at tenfold excess. However, Ni(II) showed a faint purple colour in solution. It seems that the level of stabilization of the six-coordinate $Fe(PIMH)_3^{2+}$ complex in relation to the formation of other metal-PIMH species is the main driver for Fe(II) selectivity.

Analytical application

To investigate the potential use of the new probe in complex matrices, an attempt was made to determine Fe(II) ions in certified reference material (Iron, Ferrous 1072), fish farm waste water, dam water and tap water samples. The samples were collected, acidified, stored in polyethylene bottles and analysed within 12 h of collection. The waste water and dam water were filtered with Whatman filter papers before analysis. Each sample was analysed in triplicate using PIMH by standard addition method. The concentration of Fe(II) in spiked samples and the reference material were determined with reference to the calibration curve.

Table 9.2: Determination of Fe(II) in various water samples (n=3)

		Proposed method		
Sample	**Fe (II) added (µg/mL)**	**Fe (II) found (µg/mL)**	**Recovery (%)**	**%RSD**
Waste water[a]	2	1.948	97.4	0.3055
Dam water[b]	2	1.964	98.2	1.0504
Tap water[c]	2	2.08	104	0.465

(a) Collected from fish farm in Port Elizabeth (SA) (b) Collected from Howiesons Poort Dam near Grahamstown (SA) (c) Collected from Rhodes University (SA)

The method was successfully applied for the determination of the environmental samples. The recovery efficiencies for Fe(II) in the real samples were found to be above 97% (Table 9.2). The high recoveries with low RSD values indicated that the method had good accuracy. Table 9.3 gives the quality control parameters regarding the determination of Fe(II) in aqueous certified reference material. The precision of these measurements expressed as relative standard deviation for three repeated measurements was lower than 2% confirming that the method was accurate.

Table 9.3: Analytical quality control (n=3)

Absorbance (au)	**Certified concentration (mg/L)**	**Concentration found (mg/L)**	**% RSD**
0.229	2.44 ± 0.120	2.39	1.15

Solid phase colorimetric experiments

After quantitative analysis of Fe(II) using PIMH in solution, the ligand was used to post-functionalize PVBC nanofibres to obtain a solid state colorimetric probe. The scanning electron microscope (SEM) image of electrospun membrane of PVBC is shown in Figure 9.8a. The fibre mat had 1-dimensional structure with a random fibre orientation that was evenly distributed. The obtained fibres had diameters ranging between 340 nm to 1.08 µm.

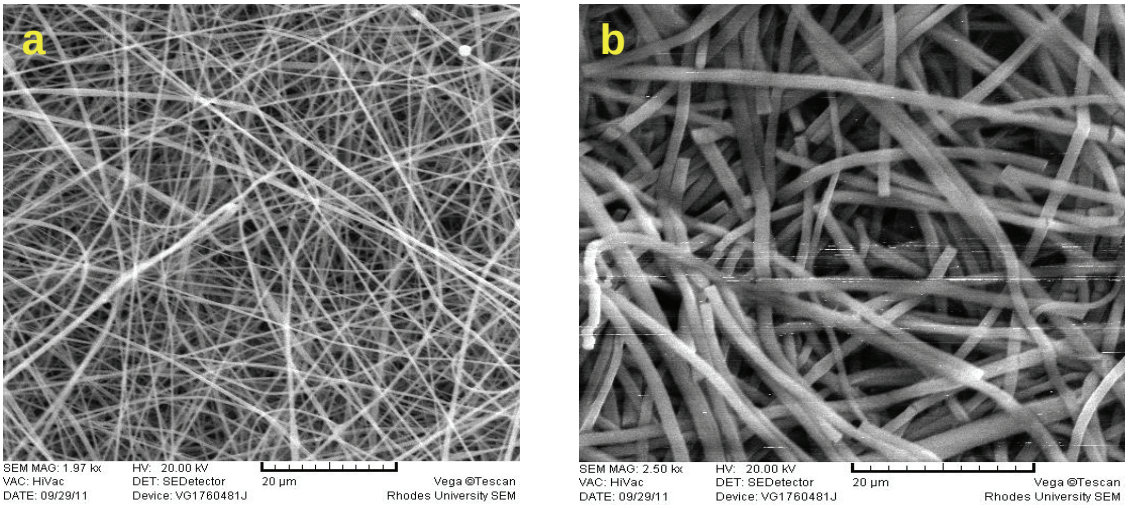

Figure 9.8: Scanning electron micrograph of; (a) PVBC nanofibres, (b) surface-modified PVBC electrospun nanofibre mats

After post-functionalisation of the nanofibres, the SEM image (Figure 9.8b) indicates that the fibrous structure of the nanofibres was not lost but, the diameters of the fibres increased to between 860 nm to 1.9 µm. This increase in fibre diameters could be attributed to swelling which resulted from attachment of the bulky ligand (PIMH) on to the fibre surface. The image also reveals breakage of the nanofibres upon post-functionalisation and this could have been as due to the stirring and heating during the reaction.

The composition of the fibre after functionalisation was verified by elemental analysis. The appearance of nitrogen in the results of the functionalized fibres was an indicator that PIMH had been successfully attached to the polymer back bone (Table 9.4). The successful attachment of the ligand to the polymer was further

confirmed from the FTIR spectra which showed the disappearance of C-Cl band of the polymer at 672 cm^{-1} and N-H band around 3100 cm^{-1} of the ligand (Figure 9.9).

Table 9.4: Elemental analysis results of PVBC and PIMH functionalized PVBC nanofibres

	Elemental composition (%)		
Polymer	**C**	**H**	**N**
PVBC	70.20	6.296	-
PVBC-PIMH	75.65	6.988	10.92

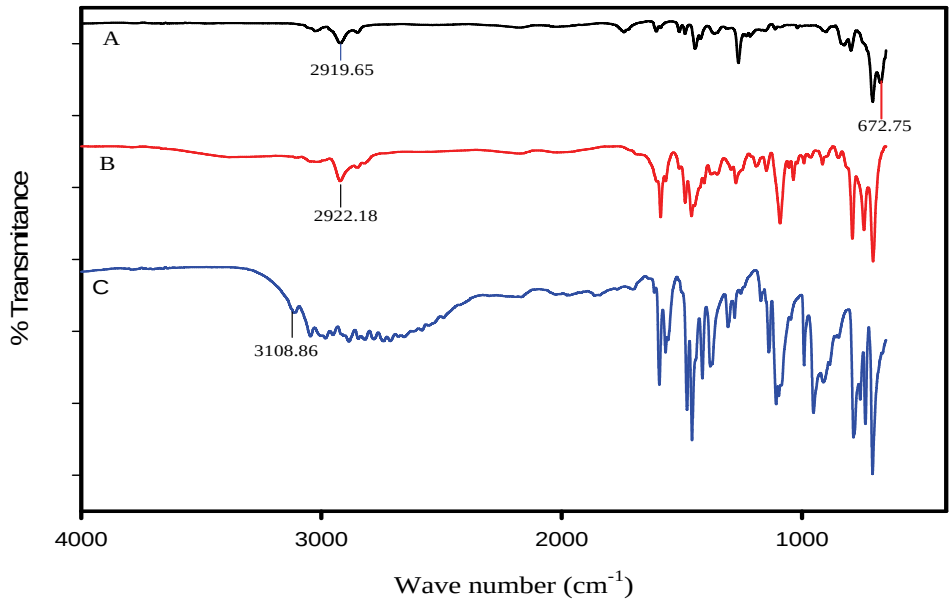

Figure 9.9: FTIR spectra of (A) PVBC nanofibres (B) PVBC-PIMH nanofibres (C) PIMH

The nanofibre mats were cut into circular shapes having diameters of 0.9 cm and 1.4 cm and without any treatment were dipped into the test solutions. While the colour change of the nanofibres from yellow to red-orange associated with the reaction of PIMH with Fe(II) was readily detectable visually, no significant colour changes were promoted by other metal ions (Figure 9.10a).

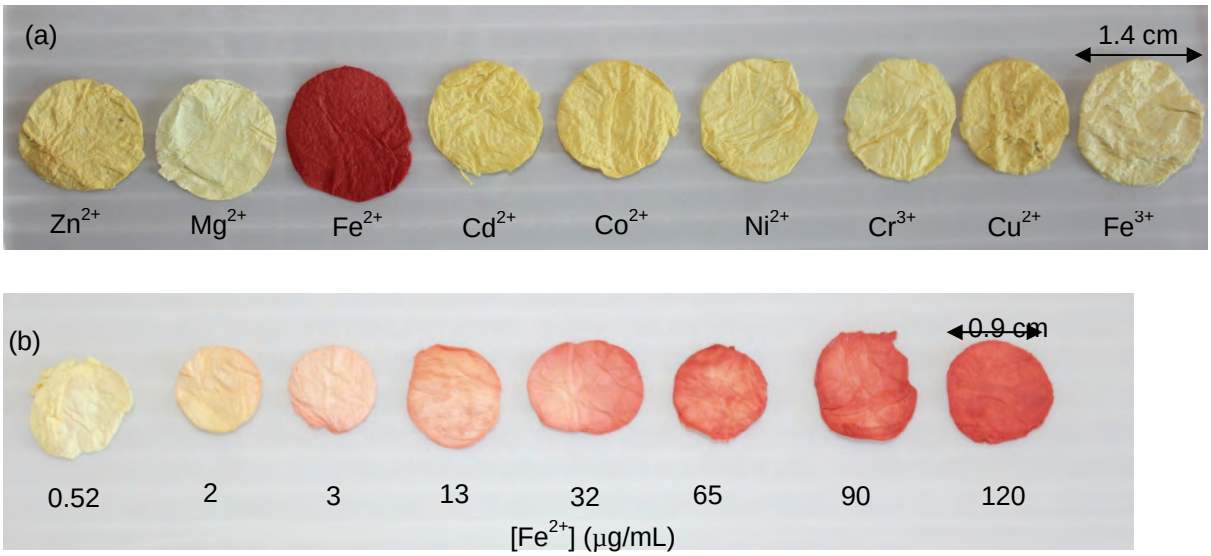

Figure 9.10: (a) Photographs of post-functionalized nanofibres upon treatment with different metal ions (0.01 M) and (b) with different concentrations of Fe(II)

The diagnostic probe showed a marked red-orange colour in the presence of Fe(II) that was detectable down to 3.0 µg/mL (Figure 9.10b). Therefore 3.0 µg/mL was taken as the cut-off for qualitative analysis of Fe(II) in solid state.

9.4 Conclusions

In conclusion, we successfully designed a method to detect and determine Fe(II) in water samples that offered advantages of simplicity, rapidity, high sensitivity, and selectivity. This method could be used to determine Fe(II) in other aqueous environmental samples. It offers a very efficient procedure for speciation analysis. The method has a detection limit of 0.102 µg/mL, which is lower than the WHO limit (2 mg/L) for Fe(II) in drinking water making this assay particularly very sensitive. The sensitivity and precision in terms of relative standard deviation of the present method was very reliable for the determination of iron in real samples down to µg/mL levels in aqueous medium at room temperature (25°C. The ligand was highly selective and doesn't react with Fe(III) or with other metal ions in significant concentrations. Furthermore the developed solid probe allowed for naked-eye detection of Fe(II). The probe was easy to use and showed a fast colour change.

9.5 Recommendations

Satisfactory characterization of the probe has been conducted. The developed diagnostic probe could also be applicable in other fields other than in water quality assurance.

10 DEVELOPMENT OF A GOLD NANOPARTICLES-BASED PROBE FOR THE COLORIMETRIC DETECTION OF ENDOCRINE DISRUPTORS IN WASTEWATER

10.1 Introduction

The objective of the study was to develop a colorimetric probe, which can be used on-site to detect estrogens in wastewater from dairy farming effluents with subsequent quantification based on colour changes induced by interactions of the probe with the analyte (17β-estradiol).

17β-estradiol (E2) belongs to a group of estrogenic endocrine disruptors. These hormones play important roles during the various stages of mammalian development, including prenatal development, growth and reproduction, as well as influence sexual behaviour (Koh *et al*., 2008). Cattle (*Bos taurus*) excrete 90% of estrogens (17β-estradiol, 17α-estradiol and estrone) whereby 17α-estradiol is produced by cattle only (Hanselman, 2003). The 17α-estradiol is however hormonally inactive and hence its β stereoisomer has been selected as a representative of the estrogens for this study. The β and *α* stereo chemical distinction of estradiol could be useful for identifying the livestock species contributing to wastewater (cattle vs. poultry or swine). Estrogens affect reproduction and development in wildlife and fish at ng/L concentration (Hanselman, 2003). Amongst the estrogenic endocrine disruptors 17β-estradiol has increasingly been reported as a potent environmental contaminant. It reaches aquatic environments through domestic effluents, livestock waste and agriculture runoff (Oishi, 2010). Several analytical techniques such as gas chromatography (GC) and liquid chromatography (LC) are given in literature for analysing estrogens in the environment. Due to their high selectivity and sensitivity when GC is coupled with flame ionization (FID) and mass spectrometric (MS) detection have particularly been reported as the main horsepower for the separation and quantification of estrogenic steroid hormones in aqueous samples (Wang, 2011). These techniques are however time consuming as well as been very expensive and sophisticated. Gold nanoparticles (Au NPs)-based colorimetric probes, for the selective and sensitive detection of E2, may be employed to overcome challenges brought about by these hyphenated GC and LC techniques.

Gold nanoparticles have many unique optical, chemical, electrical, catalytic properties and as a result have attracted interest for biological and chemical sensing applications. The ability of Au NPs to absorb and scatter light intensely at Surface Plasmon Resonance (SPR) wavelength region renders Au NPs as some of the most valuable optical probes for sensing applications (Deuk *et al*., 2010). These optical properties of Au NPs are further dependent on the surface chemistry and the inter-particle interactions. To date, techniques involving Au NPs as optical probes are based on the target analyte-induced optical property change of individual Au NPs or Au NP cluster formation (Jain, 2006, Wang, 2009). The strong absorption or scattering of Au NPs at the visible light region makes them easily observable by the naked eye or detectable by inexpensive instruments (Jans and Huo, 2012, Jones *et al*., 2011, Saquing *et al*., 2009). Zhang's group developed a method whereby two types of chemically functionalized Au NPs colorimetric probes were prepared: alkyne-modified Au NPs and azide-modified Au NPs (Zhang *et al*., 2010). These two types of Au NPs exhibited a red colour when dispersed in solution and aggregated as well as turned purple upon addition of the analyte. Additionally, the colour could be observed by the naked eye. We adapted their visual sensing approach for the development of our Au NPs-based colorimetric probe for detection of 17β-estradiol, we however employed a solid support (polymer).

Incorporation of Au NPs into polymers has been widely reported. Some of the approaches included *in situ* preparation of the nanoparticles in the polymer, produced either by the reduction of metal salts dissolved in the polymer matrix (Mayer, 2001) or by evaporation of metals on the heated polymer surface (Sayo *et al*., 1999). While some approaches involved blending of *pre*-made nanoparticles into *pre*-synthesized polymer (Corbierre *et al*., 2001). Our interest lies in nanoparticles incorporated in a polymer that ensures a long term shelf life and high quality production at a low cost, employing a facile technique called electrospinning.

10.2 Experimental

Materials

Polystyrene (M_w = 192 000), Nylon 6 (M_w = 10 000), gold (III) chloride trihydrate ($HAuCl_4.3H_2O$), sodium borohydride ($NaBH_4$) and tetraoctylammonium bromide (TOABr), all of purity more than 99%, were purchased from Sigma-Aldrich, (St. Louis, USA). All reagents were analytical or HPLC grade. Tetrahydrofuran, THF (98%) and N, N-dimethylformamide, DMF (99%) were purchased from Merck Chemicals (Wadeville, South Africa), methanol (MeOH) from Merck KGaA (Darmstadt, Germany) while formic acid and glacial acetic acid (HAc) were from Sigma-Aldrich (St. Louis, MO, USA).

17β-Estradiol and cholesterol were also purchased from Sigma-Aldrich (St. Louis, USA). Primary steroid and cholesterol stock solutions were each prepared at nominal concentrations of 1000 µg/mL in methanol.

Synthesis of Au-N6 composite

Two sets of experiments were carried out to investigate the effects of the capping agent, TOABr within the polymer. Sodium borohydride was employed as a reducing agent in all the experiments. The following optimal conditions were used: 15 wt% N6 and calculated amounts of $HAuCl_4.3H_2O$ (1:4) in 10 mL formic/acetic acid (1:1 v/v). Electrospinning conditions were set at a: positive voltage of 17.5 kV, working distance of 15 cm (the distance between the needle tip and the collecting plate) with 0.300 mL/h feeding rate.

Synthesis of Au-PS composite

In a typical procedure, predetermined amounts (g) of PS and Au salt were dissolved in DMF/THF (8:2 v/v) in a sealed vial. The PS mixture was left to stir for 3 to 4 h to ensure complete dissolution, after which $NaBH_4$ was added to effect the reduction of the metal salt precursor at ambient conditions. After reduction, the solution was left to stir overnight to eliminate the air bubbles and was subsequently electrospun. The electrospinning apparatus included a syringe pump operated at a flow rate of 0.300 mL/ h and a high voltage power supply with a positive polarity. The operating voltage was varied from 15 to 25 kV with an optimum electric field of 22.2 kV.

Characterization of the polymer composites

The N6-Au and PS-Au composites were characterized where size distribution of Au NPs was observed with the solution transmission electron microscope (TEM). Morphology of the fibres was observed with a Vega Tescan (TS5136ML) scanning electron microscope (Brno, Czech Republic) operating at 30 kV in the accelerated voltage of electrons after gold sputter coating. Gold-polystyrene composite fibres were further observed under a high resolution SEM, Jeol JSM – 700 F, Field Emission Scanning Electron Microscope (FESEM) operating at 30 kV in the accelerated voltage of electrons after gold sputter coating. UV-Visible absorption spectra were recorded using a Perkin Elmer Lambda 25 UV/Vis spectrophotometer.

10.3 Results and Discussion

For preliminary studies, two polymers, a polyamide and polystyrene (PS), were investigated based on their different mechanical properties. Polystyrene is an amorphous polymer with a glass-transition temperature (Tg) between 90 to 110°C and has the advantages of being clear, hard, easily processed and its cheaper. Due to these excellent properties, polystyrene has been used in electronic, automotive and industrial films applications. However, polystyrene has a few disadvantages that include its low impact strength and poor chemical resistance at room temperature, especially to ketones and ethers (Samsudin *et al*., 2006). While polyamide, nylon 6 (62.5°C Tg), on the other hand has high mechanical strength and superior resistance to wear and organic chemicals. Nylon 6 is usually used to make bushings, electrical plugs and sockets as well as gears, fibres for textiles, food packaging film, bearings and carpets.

Gold-Nylon 6 composite

The Au ions were reduced *in situ* as confirmed by a Plasmon resonance band at 512 nm. Prior to the addition of the reducing agent the polymer solution was yellow in colour. Upon addition of sodium borohydride, the colour changed from yellow (gold salt) to dark brown for experiments without the capping compound and to a purple colour for those with a capping agent (Figure 10.1).

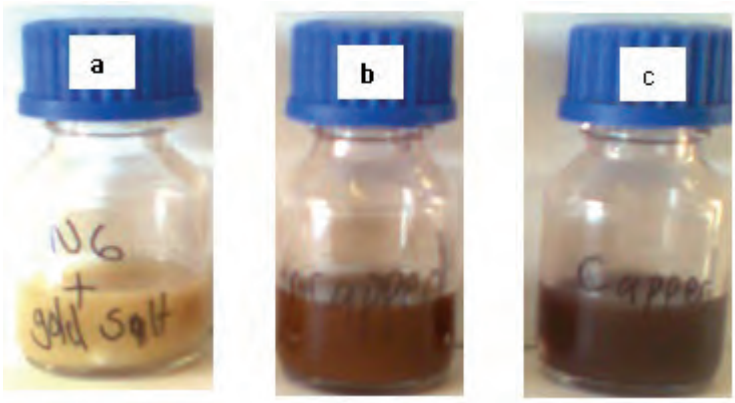

Figure 10.1: Different coloured nylon 6 polymer solutions containing (a) gold salt before (b) after reduction and (c) gold salt and capping after reduction with sodium borohydride

There was, however, no observable difference for the two sets of experiments (capped and uncapped gold nanoparticles) in the TEM images with regards the size and distribution of the nanoparticles (Figure 10.2). This could be attributed to the fact that tetraoctylammonium bromide forms weak bonds with the surface of the Au NPs hence much of the size of the nanoparticles could be due to the interaction between the polymer and the active surface of Au NPs. From the low magnification TEM images it was observed that the nanoparticles were spherical and dispersed prior to electrospinning.

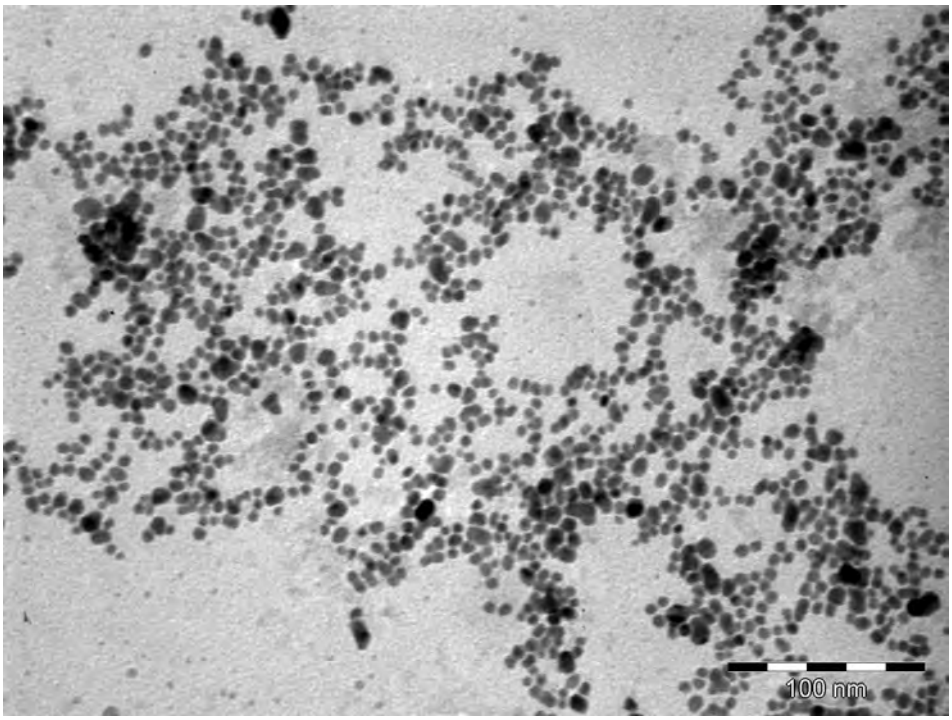

Figure 10.2: A typical TEM image of gold-nylon 6/gold- tetraoctylammonium bromide -nylon 6 in formic acid before electrospinning

The polymer composites were electrospun and gave a white fibre mat. Figure 10.3 is a typical SEM image showing the morphology of N6 polymer composite fibres. From scanning electron microscopy image it can be observed that the fibres were smooth.

The gold-nylon 6 probes were cut into fibre stripes and tested for sensitivity. Based on colour changes for both the capped nanoparticles, AuNPs-TOABr-N6 (Figure 10.4) and uncapped, Au NPs-N6 fibre stripes (Figure 10.5) there was no distinct difference with varying concentration of the analyte. The inference was that the steric hindrance due to the density of the polymer as well as C-N and C=O in N6 prohibited the Au NPs aggregation.

Gold-polystyrene composite

Prior to reduction of Au ions to Au atoms the polymer solution showed a clear yellow colour which turned to dark blue after the $NaBH_4$ reduction (Figure 10.6). Transmission electron microscopy images showed aggregated Au NPs in PS (Figure 10.7A), this is consistent with what has been reported in literature where TEM images of sectioned samples of PS-Au NPs indicated the formation of regular aggregates on the order of several hundreds of nanometres in diameter (Corbierre *et al*., 2001). In this study UV-Vis of the PS-Au in DMF showed a plasmon band at 552 nm (Figure 10.7B).

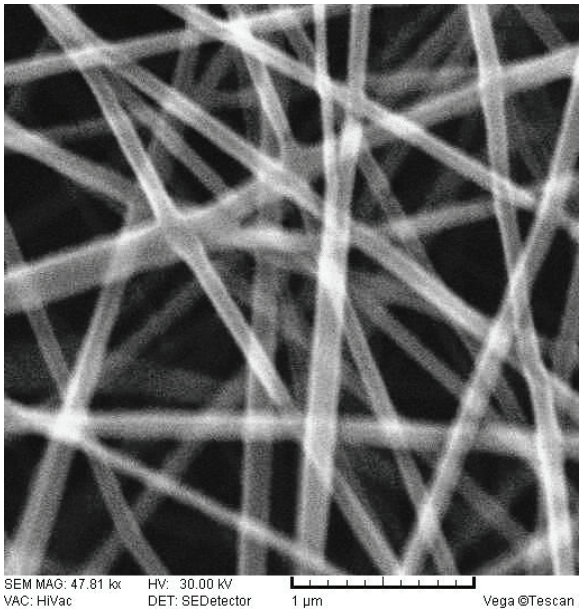

Figure 10.3: SEM image of gold-nylon 6 nanofibres electrospun from 15 wt% nylon 6 with 10: 1 molar ratio

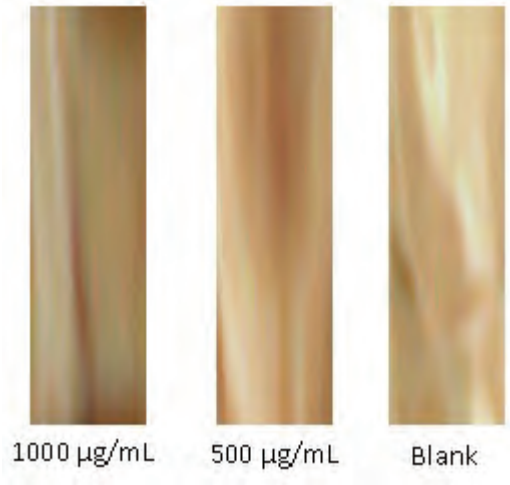

Figure 10.4: Sensitivity studies at different concentrations of 17β-estradiol using fibre with capping agent tetraoctylammonium bromide

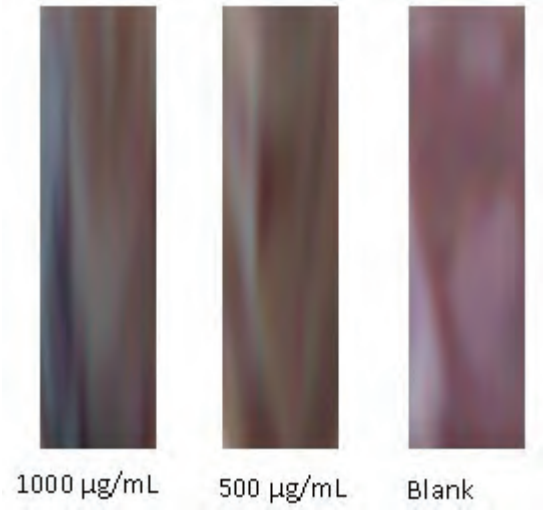

Figure 10.5: Sensitivity studies at different concentrations of 17β-estradiol using fibre without capping agent tetraoctylammonium bromide

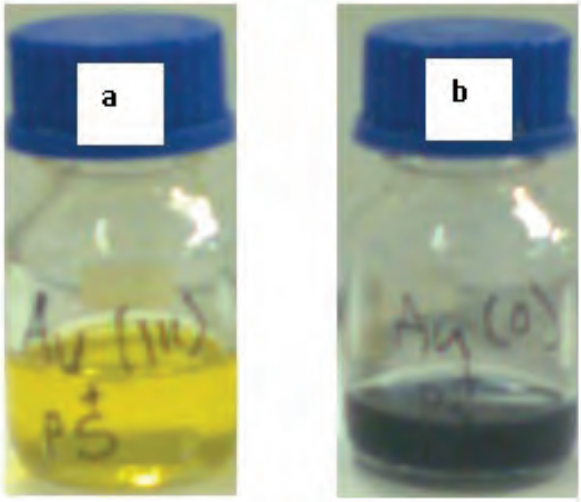

Figure 10.6: Different coloured polystyrene polymer solutions containing (a) gold salt before and (b) after reduction with sodium borohydride

(a) 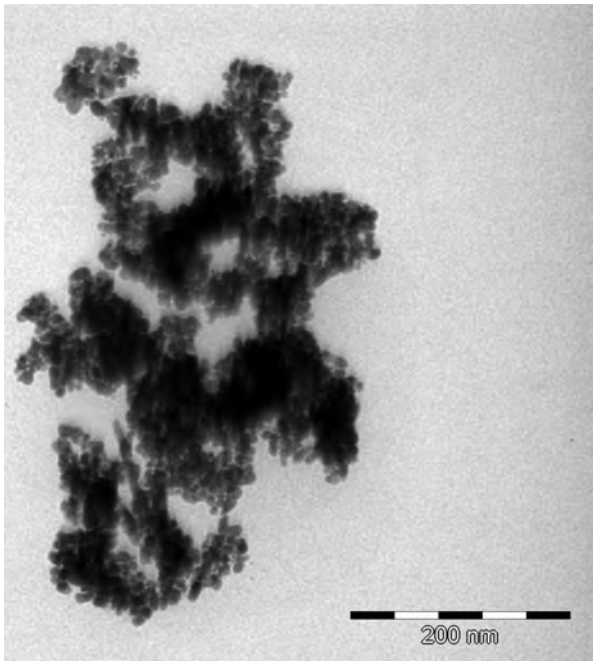

(b) 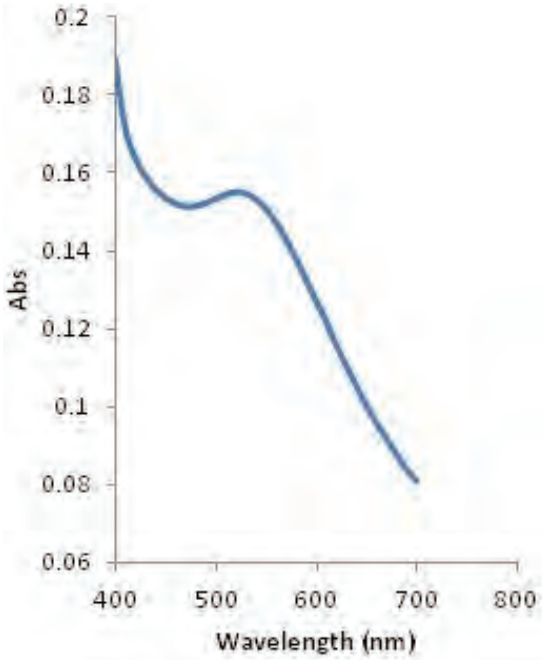

Figure 10.7: (a) TEM image of gold-polystyrene composite prior to electrospinning (b) UV-Vis spectrum for gold-polystyrene in N, N-dimethylformamide

The polymer composite was electrospun to give non beaded fibres (Figure 10.8) which were then employed as a probe. The probe was further tested for sensitivity at different concentrations of 17β-estradiol and at high (1000-800 µg/mL) concentrations colour changed from white to blue and to pink at medium (500 - 350 µg/mL) concentrations.

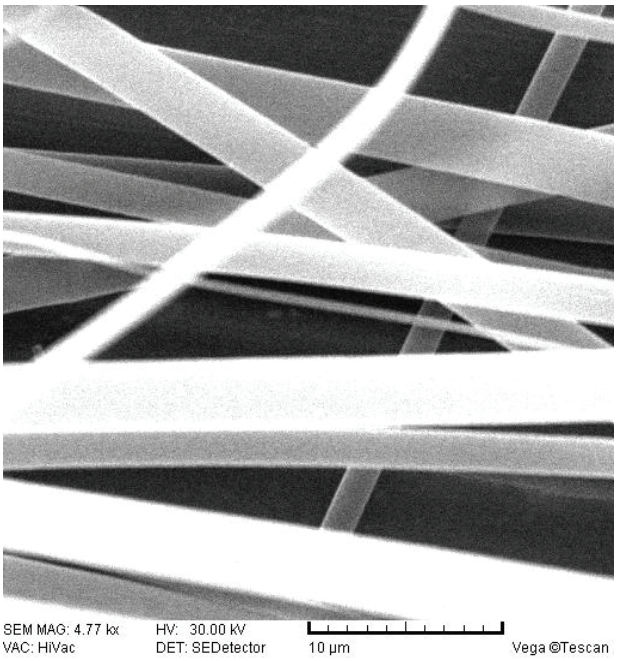

Figure 10.8: SEM image of gold-polystyrene nanofibres electrospun from 15 wt% polystyrene with 4: 1 molar ratio

Similar to the gold-nylon 6 experiments, the gold-polystyrene probe were also investigated as a detection approach in testing water for the presence of 17β-estradiol, where electrospun colorimetric probe was dipped in a sample to be tested. Upon interaction with 17β-estradiol, colour change could be attributed to the binding of gold nanoparticles to 17β-estradiol, thus causing the gold nanoparticles to aggregate and change the light-scattering spectrum for the probe. Figure 10.9 shows very distinct colour changes of the fibre mat with

various concentrations of 17β-estradiol. The concentration 800 and 400 µg/mL where chosen to represent high and lower concentrations of 17β-estradiol respectively.

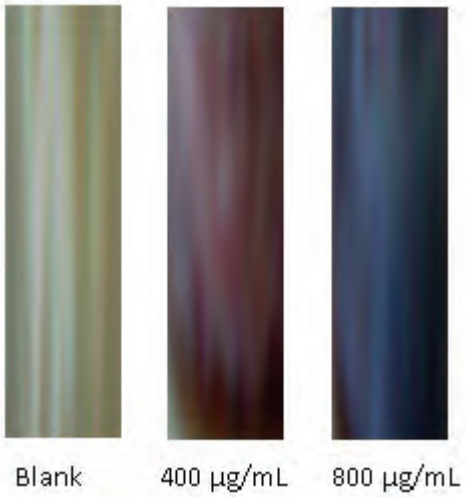

Figure 10.9: Sensitivity studies of the gold-polystyrene probe at varying concentrations of 17β-estradiol

The gold-polystyrene composite, owing to the distinct colour changes given by the probe on interaction with 17β-estradiol, was employed towards developing a colorimetric probe for detecting endocrine disruptors in wastewater from dairy farming effluents. Images of this Au-PS composite probe were further taken by a high resolution scanning electron microscope (Figure 10.10A). Figure 10.10B shows encapsulated and dispersed Au NPs in polystyrene electrospun fibres after electrospinning. Here, the dispersion of the Au NPs could be attributed to the steric hindrance provided by polystyrene which might have been enhanced during electrospinning.

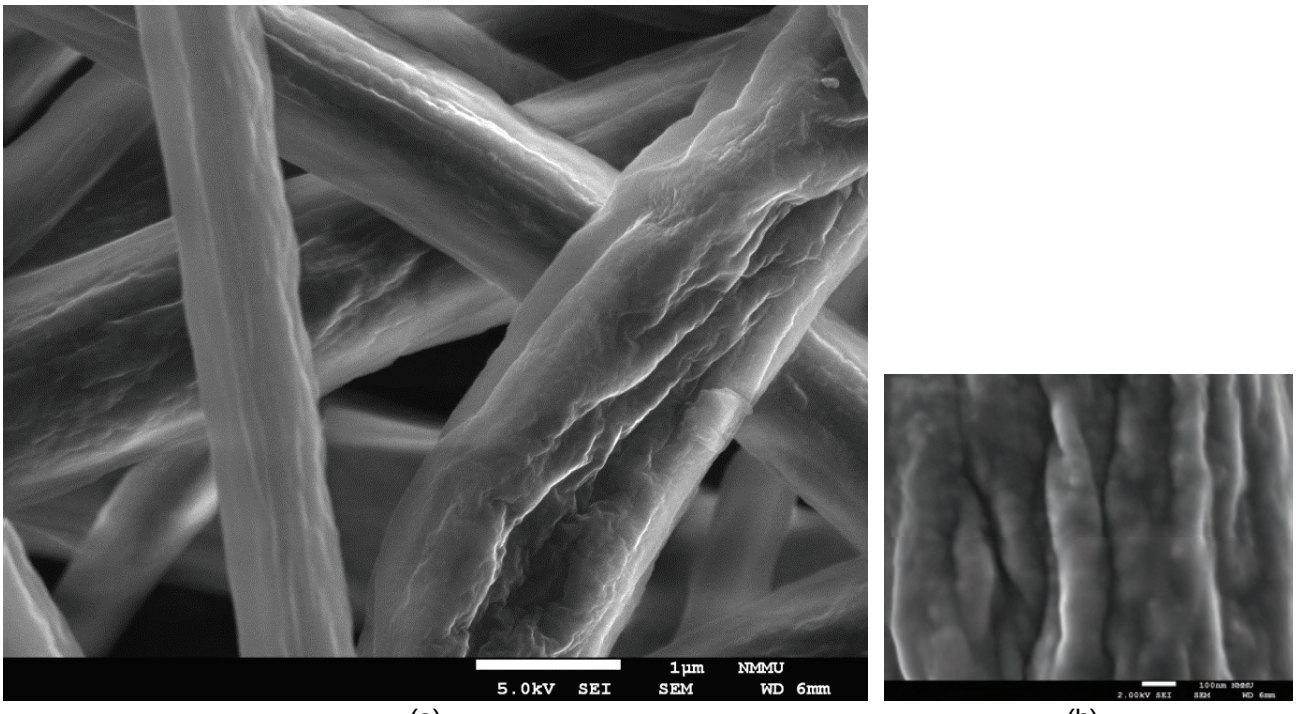

(a) (b)

Figure 10.10: HRSEM image of gold-polystyrene nanofibres electrospun from 15 wt% polystyrene with 4: 1 molar ratio

The intensity of the colour change was demonstrated to depend on the concentration of 17β-estradiol to which the electrospun colorimetric probe was exposed. The electrospun colorimetric probe changed colour immediately upon contact with 17β-estradiol. Figures 10.11 and 10.12 show the gold nanoparticle clusters induced by the interaction of the gold nanoparticles with 17β-estradiol.

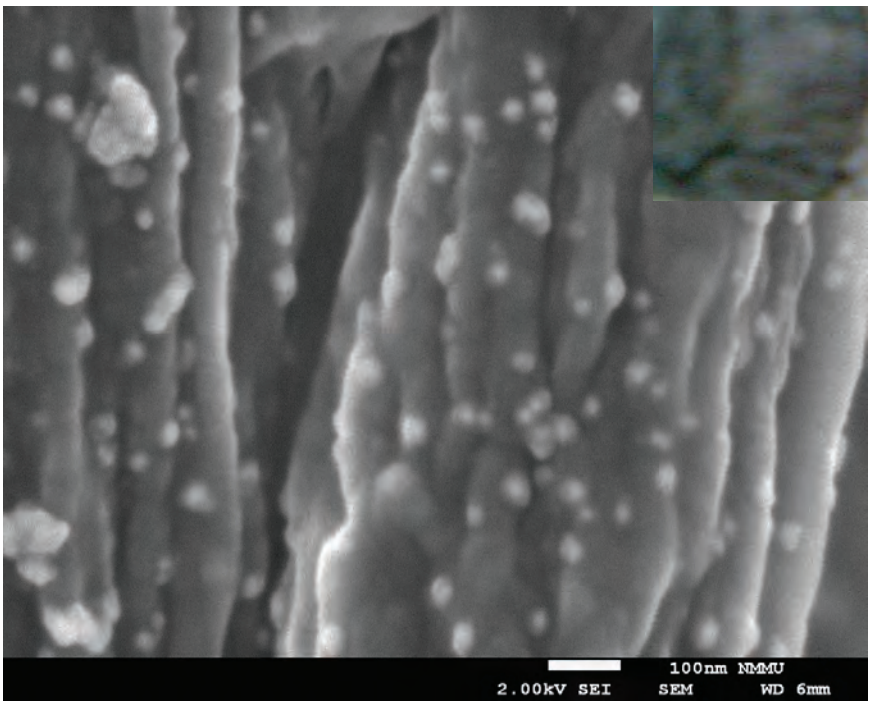

Figure 10.11: A typical HRSEM image showing gold nanoparticles clusters upon interaction with 17β-estradiol at higher concentrations

As mentioned earlier, electrospun colorimetric probe was white in colour. At high concentrations of between 1000-500 μg/mL of 17β-estradiol, the colour of the probe changed from white to a shade of blue. The shade of blue increased with intensity in comparison to the strength of the concentration of 17β-estradiol. At medium concentrations of between 500 – 100 μg/mL of 17β-estradiol and lower concentrations the colour of the colorimetric probe changed from white to a shade of pink (Figure 10.13). The shade of pink intensified in comparison to the strength of 17β-estradiol concentration.

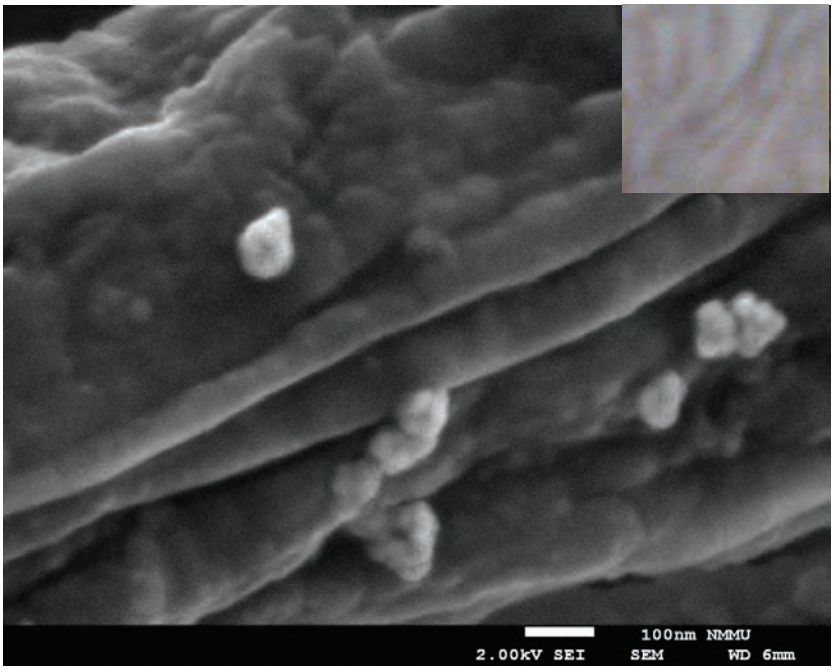

Figure 10.12: A typical HRSEM image showing gold nanoparticles clusters upon interaction with 17β-estradiol at lower concentrations

The probe was further investigated for selectivity. Cholesterol was chosen as it is equally produced in large quantities by cattle. Although when cholesterol comes into contact with the probe a colour change was

produced in the probe, the colour of the probe only changed from white to a very faint pink colour (Figure 10.13). Furthermore, this colour change only occurred at least 4 h after contact. This probe conforms to a fixed-time type of approach. Hence what was detected hours later was not 17β-estradiol, which for the purpose of this study, has been chosen to represent other estrogens.

This selectivity may be attributed to the polarity of the two compounds. Alkaline conditions were employed to focus different classes of steroids, based on their unique physicochemical properties, such as weakly acidic and hydrophobic character (Britz-McKibbin *et al*., 2003). The idea was then adopted and selectivity studies carried out under alkaline conditions (0.1 M NaOH) with the aim of regulating polarity of the two compounds and improve mass transfer into the probe. The results showed that 17β-estradiol was more responsive under these conditions hence the dark pink colour of the probe.

Concentrations of 17β-estradiol below 1×10^{-7} g/mL did not produce any observable colour changes relative to white fibres which served as a blank. 1×10^{-7} g/mL (i.e. 100 ng/mL) was chosen as the cut off concentration (Figure 10.14).

Figure 10.13: Interaction of the probe with cholesterol and 17β-estradiol under the same conditions; 800 µg/mL, after 30 s contact time, alkaline conditions and at ambient temperature

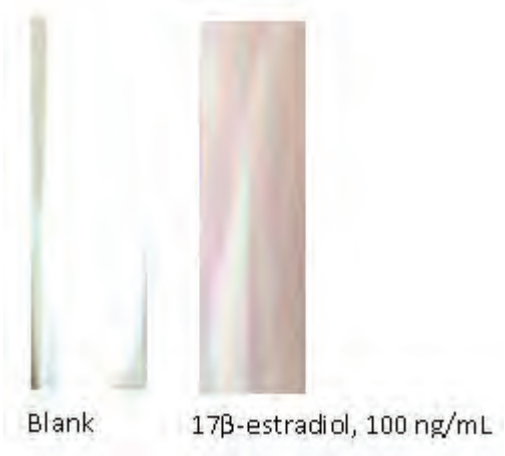

Figure 10.14: Interaction of the probe at lower concentrations of 17β-estradiol, where it was decided that the cut of concentration was 100 ng/mL 17β-estradiol

10.4 Conclusions

It was possible to incorporate gold nanoparticles into a polymeric structure and it was observed that the nanoparticles were randomly distributed in the electrospun fibre mat. For purposes of quantification, different colours were attained with different concentrations of the analyte. The main advantage is that molecular recognition is associated with colour changes, making it easy to observe the result by the naked eye and therefore eliminating the need for sophisticated instruments. Most other detection methods require expensive apparatus and time-consuming sample pre-treatment, while the new indicator is simple to use, produces rapid results and is of low cost.

10.5 Recommendations

Estrogens have been detected with concentrations ranging from 10^{-11} to 10^{-9} mol/L in surface waters and dairy farm effluents. Therefore, in future thiolate polystyrene maybe employed to enable covalent attachment to the gold nanoparticles surface (Au-S 126 kJ mol^{-1}) in order to enhance stability over a wide range of temperature, ionic strength and pH. This attainment hence leads to great opportunities in developing as well as employing the probe at lower concentrations of the analyte not only for dairy farming effluents but also for the probe to find use in a variety of other applications such in determining estrogens in biological samples for the medical health studies.

11 SCALING DOWN OF A GLYPHOSATE DETECTION SYSTEM AND CYTOTOXICITY STUDIES

11.1 Introduction

The first objective of this study was to scale down the glyphosate method and determine the optical characteristics of this system as a first step towards the development of an electrospun nanofibre-based strategy. The second objective of this study was to assess the cytotoxic and proinflammatory effects of glyphosate and its formulations (Wipeout and Roundup) in humans (whole blood assay).

Glyphosate was introduced in 1974 by the Monsanto company as a broad spectrum, post emergence, relatively non-selective herbicide (Al-Rajab and Schiavon, 2010, Anadon *et al*., 2009). This herbicide is one of the most widely used herbicides in agricultural and aquatic weed control applications as well as noxious vegetation control in non crop areas, because of its high water solubility, non-selectivity and its effectiveness especially on broadleaf weeds, sedges and perennial species of grass (Benamu *et al*., 2010, Beuret *et al*., 2005). There is an increasing demand for glyphosate due to its favourable characteristics and it was recorded to be the highest selling active ingredient in South Africa between 1994 and 1999 (Dalvie *et al*., 2009). Glyphosate constitutes 36% of the herbicide formulation Roundup®, glyphosate is formulated with adjuvants, these are the surfactant polyoxyethyleneamine (POEA) and an isopropylamine salt (IPA) in Roundup® as well as other weed killing formulations under the trade names Rodeo®, Glyfonex® and Glycel® (Amoros *et al*., 2007, Cartigny *et al*., 2004). Adjuvants are added to herbicide formulations to increase the stability and solubility of the active agent (Chan *et al*., 2007)

Glyphosate is a low molecular weight organophosphate compound, which contains three chemical groups, an amine, a carboxylate and phosphonate (Anadon *et al*., 2009, Coutinho *et al*., 2007). This compound is characterized by a very stable carbon-phosphorous bond(Kools *et al*., 2005). The herbicidal action of glyphosate (once inside the target plant) involves the competitive inhibition of the shikimate pathway, specifically a vital enzyme of this pathway known as 5-enolpyruvylshikimate-3-phosphate synthase (EPSP) (Gehin *et al*., 2005).

Although some studies have concluded that glyphosate and its formulations are not hazardous to animals and humans, there are studies that challenge this idea and have confirmed that glyphosate and its formulations do have a deleterious effect on human and animal health (Lee *et al*., 2008a, Poletta *et al*., 2009). Glyphosate often uses coupled methods for quantitative determination of this compound; the difficulty in finding simple detection methods is due to the fact that this compound shows complex behaviour, is highly soluble in water and often exists in low concentrations (Zhu *et al*., 2009). This highlights the importance of this research with respect to developing and optimizing a simple spectrophotometric glyphosate detection system (for the detection of glyphosate in environmental water systems) and determining its cytotoxic/pro-inflammatory/genotoxic effect in humans.

11.2 Experimental section

Materials and reagents

Glyphosate, copper nitrate ($Cu(NO_3)_2$) and carbon disulphide (CS_2) solution (1% diluted in chloroform). Aminomethylphosphonic acid (AMPA), glycine, hexadecyltrimethylammonium bromide (CTAB), sodium dodecyl sulphate (SDS), Triton X, Tween 20, Heparin containing tubes (vacutainers), RPMI 1640 media, streptomycin, penicillin, Wipeout, Roundup, lipopolysaccharide, MTT reagent, dithiothreitol (DTT), eBioscience ELISA kits (TNFα, IL-6, IL-1β).

Reassessment of reagent optimization for the glyphosate detection system

The optimized copper II (mM) and carbon disulphide (%) concentrations were previously reported as 5 mM and 2%, respectively. This experiment was repeated to obtain a more accurate assessment of the results reported. The effect of carbon disulphide (0-7%) and copper II (0-8 mM) on glyphosate complex formation was investigated. This procedure was conducted according to (Jan *et al*., 2009).

Scale-down of the glyphosate detection system

The glyphosate detection system was scaled down (from a total reaction volume of 8 mL to 1 mL) for the conservation of reagents, allowing for the ease of preparation as well as the preparation of more sample

reactions. Scale -down experiments were done according to (Jan *et al*., 2009). Modifications to the original protocol involved using smaller reagent and sample volumes. Glyphosate reactions were setup in 1.5 mL microcentrifuge tubes under optimized reagent (2.5% carbon disulphide and 4.5 mM copper II) and pH conditions (pH 12). The volume to volume ratio of glyphosate: carbon disulphide: copper was 2.5:1:5. Briefly, 625 µL of carbon disulphide (2.5% in chloroform) was added to 250 µL of glyphosate (1000 µg/mL in dH_2O). The mixture was shaken for approximately 5 s to allow the formation of the dithiocarbamic acid intermediate. A 125 µL aliquot of ammoniacal copper nitrate (100 µg/mL in a 2 M ammonia solution) was then added to the mixture and shaken for 1 min. The reaction mixture was incubated for 6 h at room temperature for the formation of the yellow coloured complex. Two layers appeared (a yellow coloured chloroform layer and a colourless layer). A spectral scan (200-500 nm) was conducted on the top yellow coloured layer. This experiment was conducted in triplicate with glyphosate, copper and carbon disulphide controls.

Time trial experiment

The effect of incubation time (0-24 h) on the glyphosate detection system was investigated. The experiment was conducted according to the protocol outlined in procedure 2. This study was carried out in triplicate with glyphosate, copper and carbon disulphide controls. Glyphosate complex formation was detected spectrophotometrically at 435 nm.

Jobs method of continuous variation

The stoichiometric ratio between the glyphosate dithiocarbamic acid intermediate and copper II was studied by application of the Jobs Method of Continuous Variation (Bosque-Sendra *et al*., 2003). This method was based on the preparation of a series of solutions in which the total molar concentration was kept constant, while the ratio of the ligand (glyphosate dithiocarbamic acid intermediate) was varied from 0 to 1. Experiments were conducted in triplicate with the appropriate controls and glyphosate complex formation was detected spectrophotometrically at 435 nm. A plot indicating maximum absorbance (corrected for uncomplexed copper II and glyphosate) versus the molar fraction of glyphosate was then plotted. The maximum absorbance observed (from the experimental data) is the absorbance observed containing the actual amount of equilibrated complex. A theoretical maximum (H) absorbance was also derived to validate the experimental data observed by extrapolating two regression lines (from the straightest part of the curve). The point at which these two lines intersect is known as the theoretical maximum (H) and assumes 100% complex formation.

The Jobs plot was used to determine the molar absorptivity (ε, $Lmol^{-1}cm^{-1}$) (molar extinction coefficient) and determine the stability constant (K_f) (strength of interaction between ligand and metal) of the glyphosate detection system.

$$\varepsilon l = H/[C \tag{9}$$

Where ε is the molar absorptivity ($Lmol^{-1}cm^{-1}$), *l* is the path length, *H* is the theoretical maximum and *[C]* is the total concentration of copper II (mM)

$$K_f / K_{glyph} = (A_2/A_1) / (1-A_2/A_1)*(C_{glyph}-C_{copper}*A_2/A_1) \tag{10}$$

Where A_1 is the absorbance at the intersect point, A_2 is the actual absorbance and *C* is the total concentration.

This experiment was carried out in triplicate with the appropriate controls. Results were determined spectrophotometrically at 435 nm.

Glyphosate standard curve

Lower range (0- 90 µg/mL) and higher range (400- 1000 µg/mL) standard curves were prepared for glyphosate. This was done to determine the linearity, range and precision of the glyphosate detection method.

These plots were used to determine the limit of detection (LOD, µg/ml), limit of quantification (LOQ, µg/ml), relative standard deviation (%RSD), correlation coefficient (R^2), intercept and slope.

$$LOD = \left(\frac{SD}{M}\right) * 3 \quad (11)$$

Where *LOD* is the limit of detection, *SD* is the standard error and *M* is the slope.

$$LOQ = \left(\frac{SD}{M}\right) * 10 \quad (12)$$

Where *LOQ* is the limit of quantification, *SD* is the standard error and *M* is the slope

$$RSD \left(\frac{SD}{AVG}\right) * 100 \quad (13)$$

Where *RSD* is the relative standard deviation, *SD* is the standard error and *AVG* is the mean.

This experiment was carried out in triplicate, with appropriate controls. Results were determined spectrophotometrically at 435 nm.

Glyphosate detection system specificity

The specificity of this system was determined by carrying out the glyphosate detection reaction on two glyphosate structural analogues, namely, glycine and its primary metabolite aminomethylphosphonic acid (AMPA). The concentrations of glyphosate, AMPA and glycine were 1000 µg/mL and the reaction was carried out according to the protocol outlined in procedure 2. Spectral scans were carried out (200-500 nm) and results were also detected spectrophotometrically at 435 nm. This experiment was conducted in triplicate with the appropriate controls.

Sensitization of the glyphosate system (micellar media)

Organic micellar media have shown success in improving analyte sensitivity in UV-Vis spectrophotometric methods, because the addition of surfactants improves metal complex stability (Choi and Choi, 2003). The differential effects of cationic (hexadecyl trimethylammonium bromide, CTAB), anionic (sodium dodecyl sulphate, SDS) and non-ionic surfactants (Triton X, Tween 20) on the detection of glyphosate were assessed. Glyphosate (final concentration, 750 µg/mL) was prepared in different micellar media (surfactant and dH_2O) of varying concentrations (final surfactant concentration range: 0.0005-0.01%). The glyphosate reaction was carried out according to the protocol outlined in procedure 2. A control reaction (glyphosate prepared in dH_2O only) was run in parallel. This experiment was conducted in triplicate with the appropriate controls. The results were analysed spectrophotometrically at 435 nm.

White blood cell culture

The effect of glyphosate and its formulations (Roundup™, Wipeout) on cytokine production in whole blood was assessed. Blood was collected from healthy volunteers (n=5; n=3) in heparin containing tubes (vacutainers). Blood samples were then diluted 1:10 in RPMI 1640 media (within 5 h of collection) supplemented with 50 µg/mL streptomycin and 50 U/mL penicillin.

Whole blood exposure and cytokine production sample preparation

Whole blood samples (1 mL) were aliquotted into 24 well plates and incubated for 18 h at 37°C, with different concentrations (0.1, 0.7, 10, 50, 250 500 µg/mL) of pure glyphosate and the above mentioned formulation. All herbicide formulations were made up in RPMI 1640 media supplemented with 50 µg/mL streptomycin and 50 U/mL penicillin. After the incubation period plates were centrifuged at 900 *g* for 5 min and the supernatant was retained and stored at 20°C for cytokine analysis. This experiment was conducted in triplicate with lipopolysaccharide (LPS, 5 µg/mL) as a positive control and RPMI 1640 media as a negative control.

MTT assay

The cytotoxic effect of the different herbicides on whole blood and white blood cells was assessed using the MTT assay. After the exposure period and centrifugation (900 *g* for whole blood and 2000 *g* for white blood cells), MTT reagent (0.5 mg/mL in RPMI 1640) was dispensed into each well and plates were then incubated for 30 min (whole blood) or 24 h (white blood cells). The MTT reagent was then removed and 1 mL DTT was added to each well. Plates were incubated for 15 min at 23°C. After incubation plates were centrifuged for

5 min at 900 *g* (whole blood) or 2000 *g* (white blood cells). The absorbance readings were taken at 560 nm using a microplate reader.

Cytokine production analysis

The production of the cytokines TNFα, IL-1β and IL-6 in cell culture supernatants was determined using quantitative enzyme linked immunosorbent assays (ELISA; eBioscience). This protocol was conducted according to manufacturer's instructions. Briefly microplates were coated with anti-human TNFα, IL-1β and IL-6 in coating buffer overnight at 4°C. After a wash step, wells were blocked at room temperature for 1 h. Test samples (including positive and negative controls) and cytokine standards (data not shown) were then incubated for 2 h at room temperature. Following a wash step, detection antibody was added to the wells and incubated at room temperature for 1 h. The wells were washed and incubated with diluted Avidin-HRP at room temperature for 30 min. Following another wash step, wells were incubated in TMB (substrate) solution for 15 min before the reaction was halted with stop solution (1M H_2SO_4). OD readings were taken at 450 nm (reference wavelength: 570 nm).

Statistical analysis

Results were analysed using ANOVA single factor analysis, to determine variance between sample groups relative to the untreated control. The null hypothesis assumes that all means are equal i.e. H0: $M_1=M_2=M_3$. A p value below or equal to 0.05 (95% confidence) was considered statistically significant, therefore a p value less than the significance level (0.05) means the null hypothesis is rejected and it can be concluded that the test samples are significantly different when compared to the untreated control. Lethal concentration 50 (LC_{50}) values (the concentration of a chemical/agent which is lethal to 50% of the cell population) were determined using probit regression analysis. Probit analysis involves the conversion of a sigmoid-dose response curve to a straight line that can be analysed through least square regression or maximum likelihood. There are several techniques employed when using this analysis tool. The technique chosen for the purpose of this study involved the use of a probit table which allows the estimation of probit values. These probit values are then used to plot a regression curve of probit values versus Log_{10} concentrations (data not shown). LC50 values are then obtained using this type of regression analysis. Probit analysis is a commonly used technique in toxicology studies and is most often used to determine the toxicity of chemicals and pollutants to living organisms.

11.3 Results and Discussion

Scale down of the glyphosate detection system

The results of the scale-down experiment for the glyphosate detection system are shown in Figure 11.1 and Figure 11.2. Scaling-down the glyphosate detection system allows for a reduced cost of reagents and reduced waste generation, considering this assay requires the use of organic solvents.

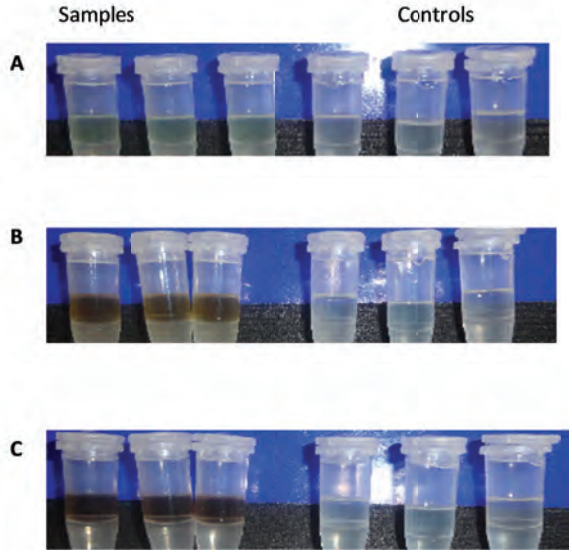

Figure 11.1: Glyphosate (1000 µg/mL) complex formation (scale-down) shown at A: 0 h, B: 1 h and C: 6 h. The total reaction volume was 1 mL and negative controls included no glyphosate, no copper sulphate and no carbon disulphide

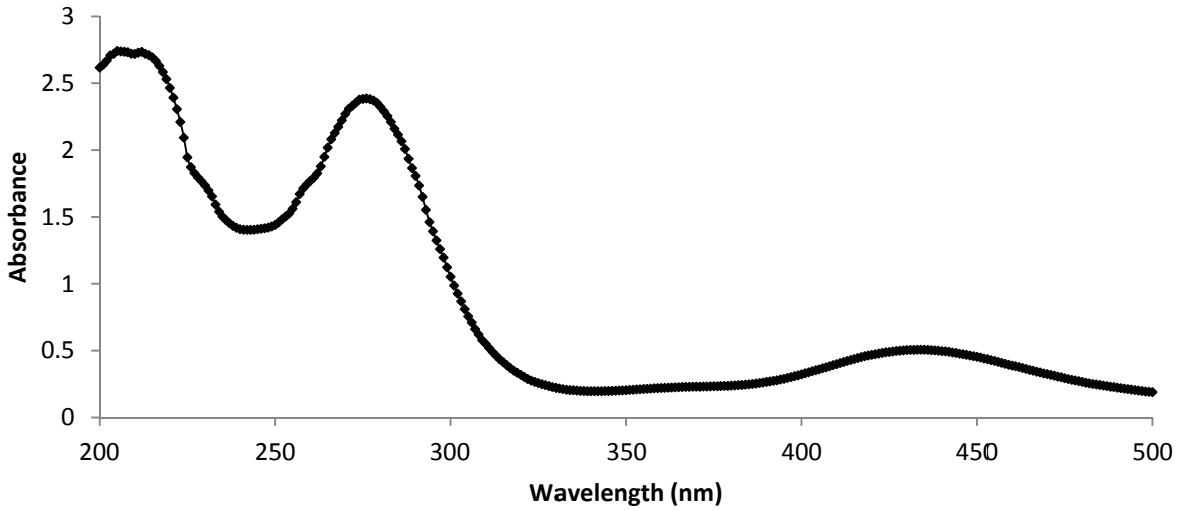

Figure 11.2: A spectral scan (200-500 nm) of the glyphosate complex layer formed (scale-down) after a 6 h incubation period at room temperature

Results observed (Figures 11.1 and 11.2) indicate that the scale-down experiment was successful. These results are also comparable to the results found for the proof of concept experiment, with the formation of a yellow coloured layer (ammonia layer) that intensifies after a 6 h incubation period. The yellow coloured complex was also detectable at 435 nm. Further experiments were carried using the scale-down method, with a total assay volume of 1 mL and a wavelength of 435 nm.

Time trial experiment

The effect of time (t) on glyphosate complex formation (Figure 11.3) was assessed from t= 0 to t = 24 h. Results in Figure 11.3 show an initial increase in absorbance with an increase in time. After 3 h a decrease in absorbance was observed. Although the maximum absorbance (3.31) was seen at 3 h, the absorbance (3.23) observed at 2 h was significantly similar, therefore a shorter incubation time of 2 h was chosen as the optimum time. Future glyphosate reactions were incubated for 2 h for complex formation.

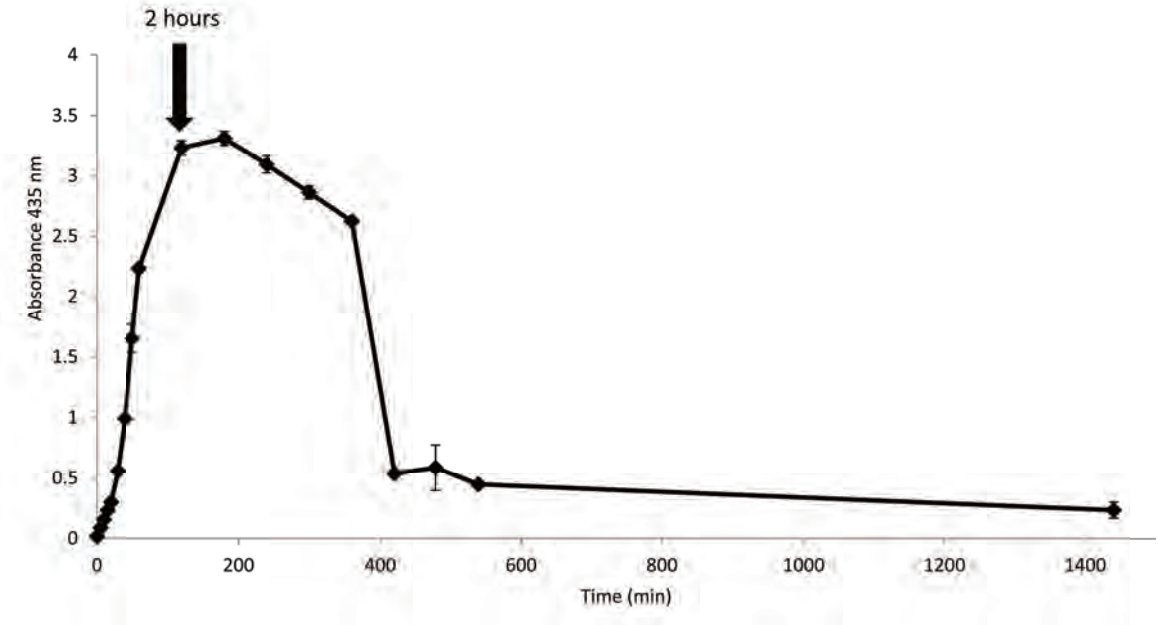

Figure 11.3: The effect of time on glyphosate complex formation over a 24 h period at room temperature. Values are presented as mean values ± SD (n= 3)

Jobs method of continuous variation

The Jobs method of continuous variation (Figure 11.4) was used to evaluate the stoichiometric ratio between glyphosate (in its dithiocarbamic acid state) and copper. Calculated values for molar absorptivity (ε) and stability constant (K_f) are shown in Table 11.1.

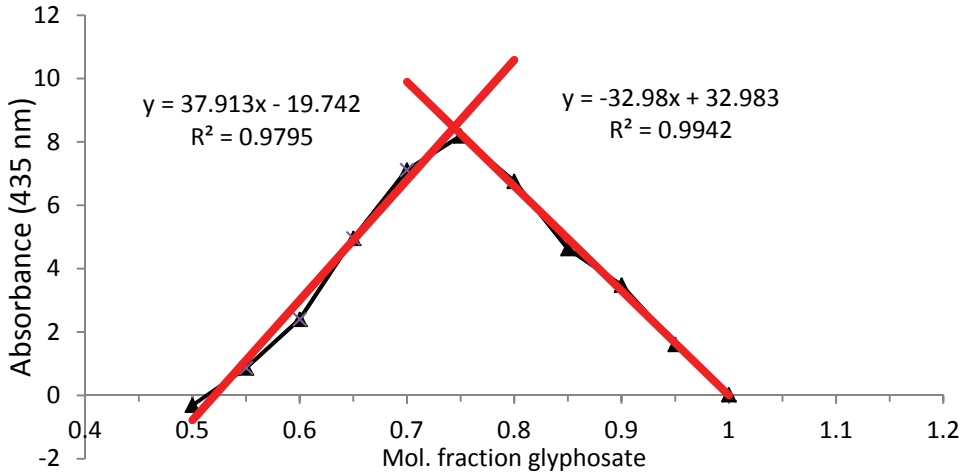

Figure 11.4: A Jobs plot used for the determination of stoichiometric ratios (experimental and theoretical) between glyphosate and copper. The data presented indicates mol fraction values of glyphosate from 0.5. Although this experiment was conducted from a mol. fraction of 0.5. Values are presented as mean values ± SD (n=3).

Results from Figure 11.4 indicate an experimental mole ratio of 0.75, therefore a glyphosate: copper complex ratio of 3:4. The calculated theoretical mole ratio was 0.74, which validates results observed experimentally. The results observed were not in agreement with those reported by Jan and co-workers (Jan *et al*., 2009) who observed an experimental mole ratio of 1:2 (copper: glyphosate).

Results in Table 11.1 indicate a higher molar absorptivity and lower stability constant when compared to literature (Jan *et al*., 2009).

Table 11.1: Molar absorptivity (ε) and stability constant (Kf) values calculated for the glyphosate detection system

Parameter	**Experimental data**	**(Jan *et al*., 2009)**
ε ($mol^{-1}.cm^{-1}$)	1.05×10^4	1.86×10^3
K_f	8.07×10^4	1.06×10^5

Glyphosate standard curve

The lower (0-90 µg/mL) and higher (400-1000 µg/mL) range standard curves produced for the glyphosate detection system are shown in Figure 11.5.

No detectable glyphosate complex formation was observed at lower range glyphosate concentrations (Figure 11.5) as noted by a poor correlation coefficient (R^2) of 0.0099. The higher range standard curve (Figure 11.5) indicated better linearity (R^2 = 0.968) with an increase in absorbance with an increase in glyphosate concentration. The higher range standard curve was used to determine the LOD, LOQ, RSD, intercept and slope. The calculated results are shown in Table 11.2.

Table 11.2: The calculated optical parameters of the glyphosate detection method

Parameter	**Experimental data**	**(Jan *et al*., 2009)**
LOD (µg/mL)	126.46	1.10
LOQ (µg/mL)	421.56	3.70
RSD (%)	7.60	2.37
Intercept	-1.89	0.01
Slope	0.005	0.003

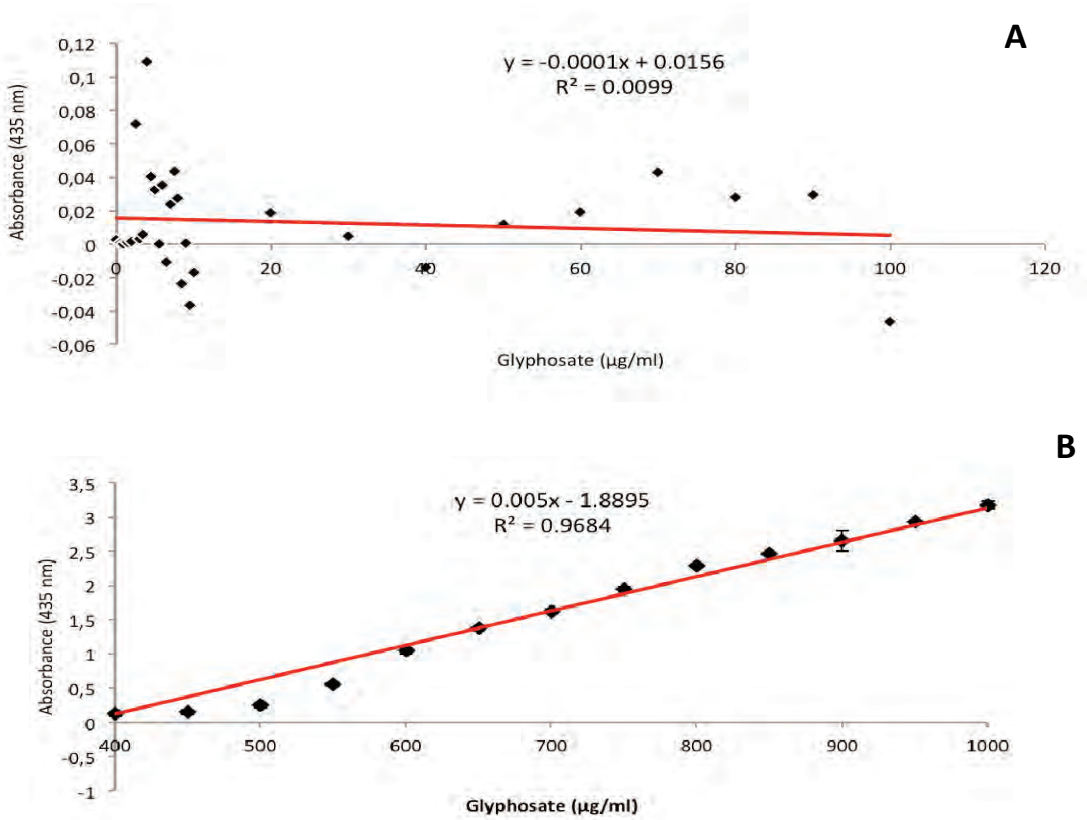

Figure 11.5: Standard curves for the glyphosate detection system. A: lower range (0-90 µg/mL) and B: higher range (400-1000 µg/mL). The standard curves presented were prepared by testing increasing concentrations of glyphosate. Values are presented as mean values

Parameters reported in literature show a more sensitive, precise detection system when compared to results calculated for the current study. The LOD (126.46 µg/mL) and LOQ (421.56 µg/mL) values were considerably higher than those observed by (Jan *et al*., 2009). Low LOD and LOQ values are favourable, considering that glyphosate exists in water in low concentrations. This loss in sensitivity could be attributed to scaling down this detection system. Future experiments involved attempting to improve the sensitivity of this system using micellar media.

Glyphosate detection system specificity

The specificity of the glyphosate detection system was assessed by testing the system on the glyphosate structural analogues, glycine and AMPA (its primary metabolite). The results are shown in Figure 11.6. Results in Figure 11.6a and b indicate that the structural analogues of glyphosate were not detected by the detection method. This is advantageous as experiments carried out on environmental water samples will not be confounded by the presence of either one of these compounds.

Sensitization of the glyphosate system (micellar media)

Figure 11.7 shows the effects of different surfactants (CTAB, SDS, Triton X and Tween 20) on the detection of glyphosate (750 µg/mL).

Results observed in Figure 11.7 show an increase in absorbance in 0.005% SDS micellar media as compared to the control reaction (glyphosate in dH_2O alone). It cannot be conclusively stated that the observed effect was occurring, because the curve for the control reaction produced an unusual trend. The control reaction was expected to remain fairly constant in its absorbance values; therefore this experiment was repeated (Figure 11.8A). Results obtained for CTAB (Figure 11.7) indicated an increase in absorbance at a CTAB concentration of 0.01%, but the standard error found for this result was fairly high; therefore this experiment was also repeated (Figure 11.8B). No improvement in absorbance values was observed with micellar media containing Tween 20 (Figure 11.7) and Triton X (Figure 11.7).

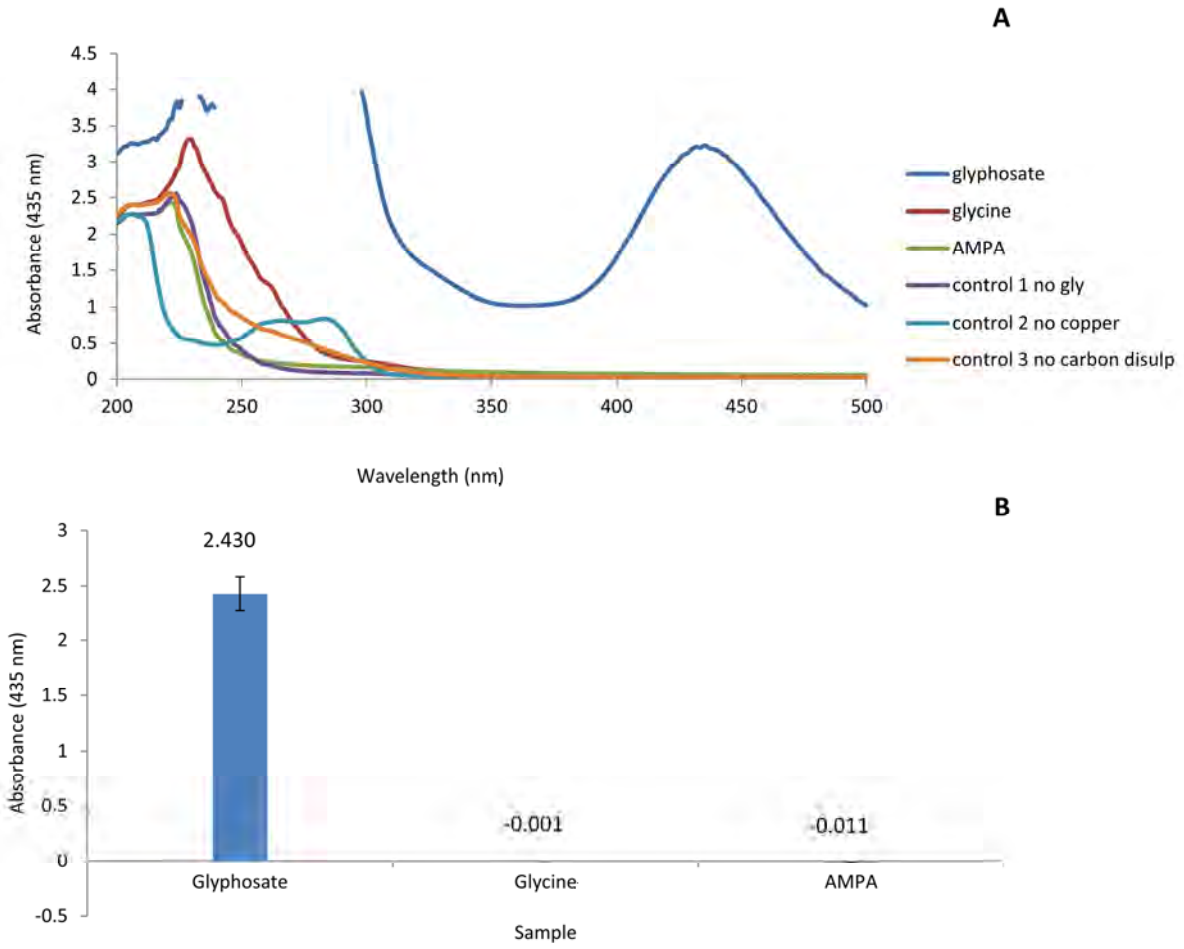

Figure 11.6: The detection of glyphosate structural analogues, glycine and AMPA. A: Spectral scan (200 - 500 nm), B: Spectrophotometric analysis (435 nm). Data points represent mean values ± SD (n= 3)

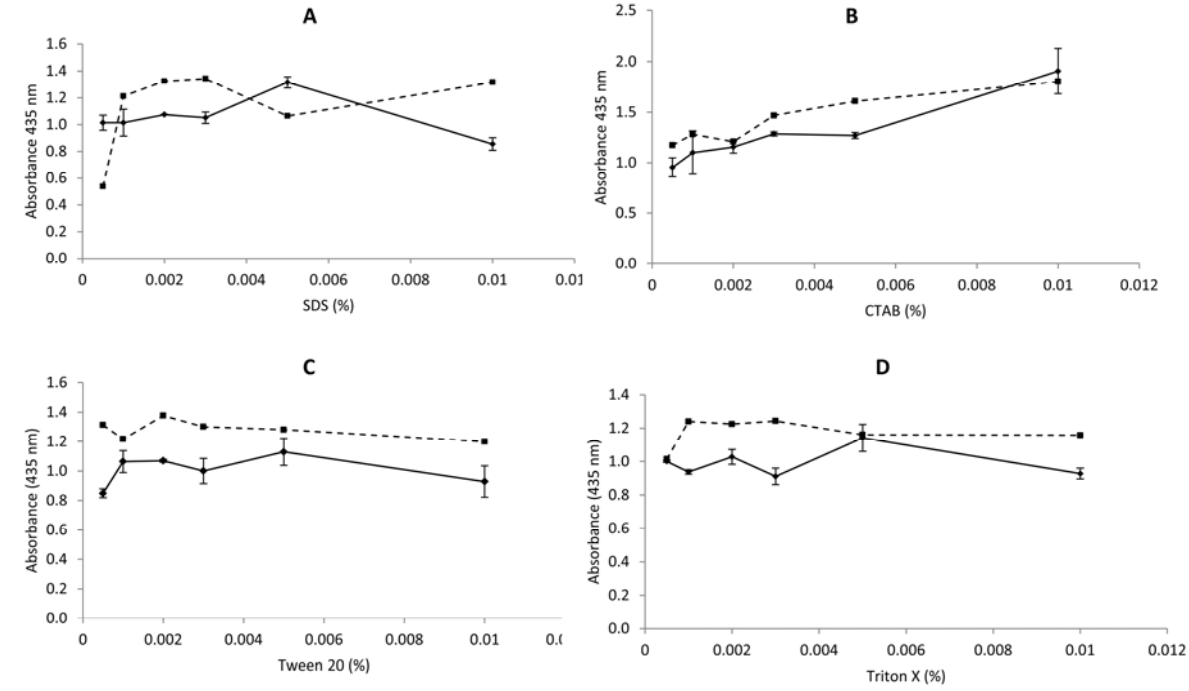

Figure 11.7: The effect of varying concentrations (0.0005-0.01%) of different micellar media (solid line) on glyphosate complex formation. A: SDS, B: CTAB, C: Tween 20, D: Triton X. A control reaction (dotted line) with glyphosate prepared in dH_2O only. Data points represent mean values ± SD (n=3)

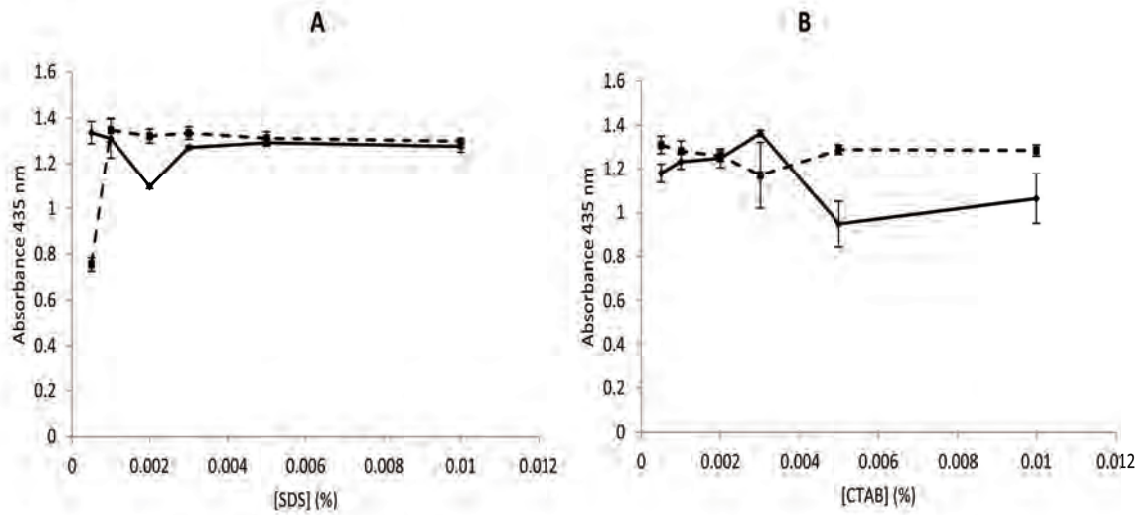

Figure 11.8: The effect of varying concentrations (0.0005-0.01%) of different micellar media (solid line) on glyphosate complex formation. A: SDS, B: CTAB. A control reaction (dotted line) with glyphosate prepared in dH_2O only. Data points represent mean values ± SD (n=3).

Results observed in Figure 11.8 show the repeat experiments conducted for the surfactants SDS and CTAB. The data obtained was not reproducible to the previous experiments conducted, using these two types of surfactants (Figure 11.7) and accurate conclusions could not be drawn with respect to the effect the surfactants had on the glyphosate assay sensitivity. Future experiments will employ the use of the cloud point extraction method (also known as micelle mediated extraction) as a preconcentration step before analysis, to allow the quantification of glyphosate at low concentrations. The principle of this method is based on the phase separation characteristics exhibited in aqueous solutions of certain surfactant micelles, when heated to a specific temperature (cloud point temperature) (Pongpiachan, 2009).The two layers formed are known as the aqueous and the surfactant rich phase (the surfactant phase is used for the concentration of the chosen analyte), containing a surfactant concentration close to its critical micellar concentration (CMC) (Carabias-Martinez *et al*., 2000). The CMC is the concentration of surfactant above which the surfactant begins to form micelles (Ruckstein and Nagarajan, 1975). This CMC is highly variable and susceptible to many factors including the concentration and structure of counter ions in solution (Yu *et al*., 2011). Overall this technique is advantageous because it does not require the use of harmful solvents, allows for ease of preparation and produces more precise and accurate results when compared to older extraction techniques e.g. solid-phase extraction (Tabrizi, 2006).

3-(4, 5-Dimethylthiazol-2-yl)-2, 5-Diphenyltetrazolium bromide (MTT) assay (cell viability)

The MTT assay was used to determine the effect of pure glyphosate (99.5%) and its formulations (Roundup and Wipeout) on cell viability (Figure 11.9) in whole blood samples (n=5). A concentration range of 0.1-500 µg/mL was chosen to include the compliance limits for drinking water in Europe (0.1 µg/mL) and the USA (0.7 µg/mL). Equivalent concentrations of pure glyphosate were also prepared to allow for comparison with the glyphosate formulations. The use of formulations is important in the success of glyphosate as a non-selective weed killer, as glyphosate alone does not display herbicidal activity (Duke and Powles, 2008). Once combined with salts e.g. sodium or isopropylamine, and other adjuvants e.g. propylene glycol or petroleum distillate, this herbicidal action is activated, the compound is stabilized and its foliar penetration is enhanced (Duke and Powles, 2008). Different glyphosate formulations vary in the types of surfactants/salts used and thus these formulations vary in their chemical properties (Battaglin *et al*., 2005). This is an important fact to consider when assessing and establishing the toxicity effects of these herbicides.

Results obtained for pure glyphosate (Figure 11.9A) and Wipeout (Figure 11.9C) indicated initial cytotoxic effects from a concentration of 10 µg/mL (44.27% and 20.81% reduced cell viability respectively). The maximum cytotoxic effect was observed at a pure glyphosate concentration of 50 µg/mL (54.75% reduced cell viability) and a Wipeout concentration of 500 µg/mL (56.69% reduced cell viability). The Roundup formulation (Figure 11.9B) showed the least cytotoxic effect when compared to Wipeout and pure glyphosate, with the maximum cytotoxic effect being demonstrated at a concentration of 10 µg/mL (27.80% reduced cell viability). Although the results of this study showed that pure glyphosate and the two

formulations tested were cytotoxic at concentrations above the compliance limits previously mentioned, there are other reports that contest this result. (Benachour *et al*., 2007) compared the cytotoxic effect of glyphosate and its most popular branded formulation, Roundup on human embryonic kidney (293) and placental (JEG3) cell lines. This study concluded that Roundup was toxic at concentrations lower than the concentrations recommended for agricultural use (0.29-0.59 µg/mL). A study conducted by (Richard *et al*., 2005) using Roundup and glyphosate on placental cells, reported similar findings. (Gui *et al*., 2012) reported a 10 - 25% reduction in cell viability (PC12 cells) after a 24 h exposure period to 0.56 µg/mL of glyphosate.

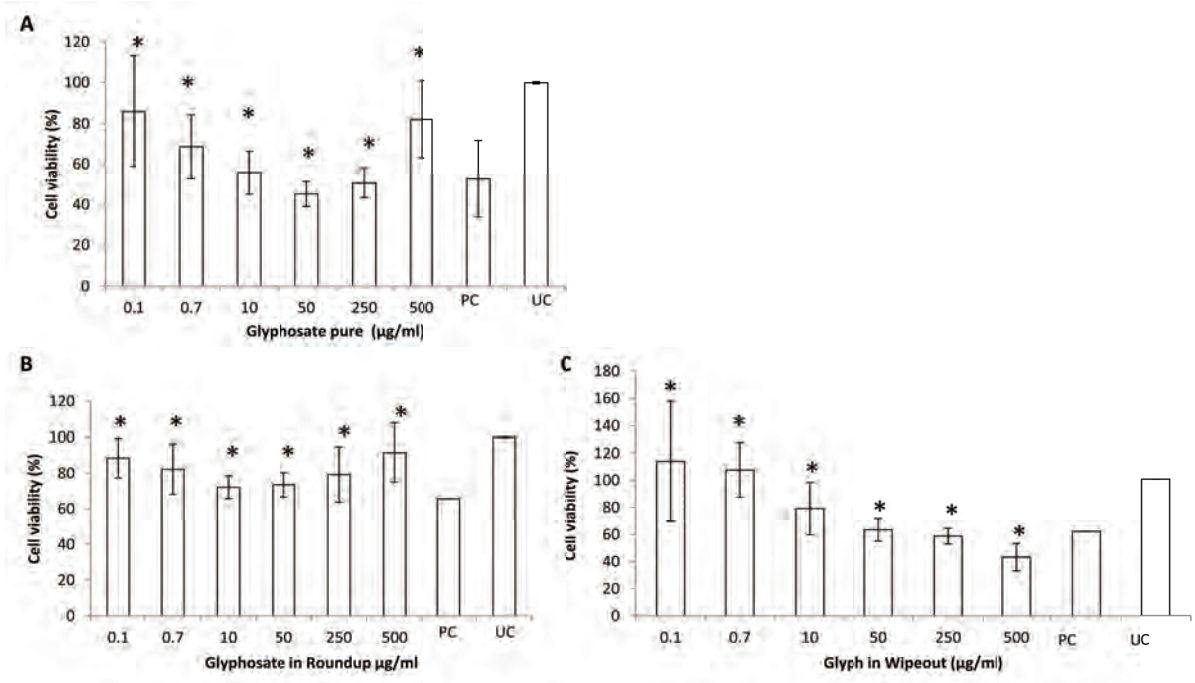

*Figure 11.9: The effects of Roundup (B), Wipeout (C) and equivalent concentrations of pure (99.5%) glyphosate (A) on whole blood cell viability were evaluated using the MTT assay. Results are indicated as a percentage (%) in comparison to the untreated control (UC). Whole blood samples were exposed to increasing concentrations (µg/mL) of Roundup, Wipeout and equivalent concentrations of pure glyphosate for 18 h and incubated with MTT reagent for 30 min. Error bars indicate ± SEM (n=5). 5 µg/mL of LPS was used as a positive control (PC).*P≤0.05 relative to UC.*

Several studies have shown that pure glyphosate has a lower cytotoxicity when compared to the different formulations containing this active ingredient (Gasnier *et al*., 2009, Mann and Bidwell, 1999). This supports the theory that the additional adjuvants that make up commercial formulations play a significant role in the toxicity attributed to these herbicides. This statement is further strengthened by the data observed for pure glyphosate and Wipeout, but observations in this study have also shown that Roundup is less cytotoxic than pure glyphosate. Lethal concentration 50 (LC50) values calculated for pure glyphosate, Wipeout and Roundup were 12589, 347 and 1×10^{69} µg/mL respectively. Pure glyphosate and Roundup showed an increase in cell viability at concentrations of 250 and 500 µg/mL. This trend confounded LC50 results with curves generated by probit analysis (please refer to procedure 12) resulting in correlation coefficients of 0.175 and 0.0036 respectively. This is not an uncommon result as not all dose-response curves produce Gaussian sigmoids, therefore this may imply that this regression model (probit) is not suited to the data-set being assessed. Future work will investigate the use of other analysis tools e.g. logit, which are used when a normal distribution is not observed. Studies (dose dependent response) indicate a decrease in cell viability with increasing glyphosate/ glyphosate-herbicide formulation concentrations (Benachour *et al*., 2007, Gasnier *et al*., 2009, Gui *et al*., 2012 , Koller *et al*., 2012). Interference in the MTT assay could account for the trend observed, thereby producing an overestimation of cell viability or underestimation of the cytotoxic effect caused by these compounds. Several compounds including cellular enzymes and components found in cell media are known to cause the reduction of tetrazolium salts, thereby, causing inaccuracies in the results obtained (Funk *et al*., 2007).

Whole blood contains many different cell types e.g. lymphocytes, erythrocytes and granulocytes, which reduce the sensitivity of this assay, simply because a measured response not only reflects the T-cells but

also all other blood components, present (Min *et al*., 2010). Most studies investigating the cytotoxicity of glyphosate and its formulations employ the use of cell lines, which have proven to be more sensitive.

Cytokine production

Cytokines are an important group of small polypeptides which function in modulating growth, survival and differentiation in living organisms (Smith *et al*., 2012). Cytokines are upregulated in response to injury, infection or disease states (Smith *et al*., 2012, Watkins *et al*., 1995). Tumour necrosis factor α (TNFα), IL-1β and IL-6 have extremely crucial functions in the pathology of inflammation (Watkin *et al*., 2007)

The effect of pure glyphosate and Roundup on the release of TNFα, IL-1β and IL-6 are shown in Fig.11.10 (results for Wipeout are not shown as ELISA results for the positive and untreated control were not obtained, will have to be repeated).

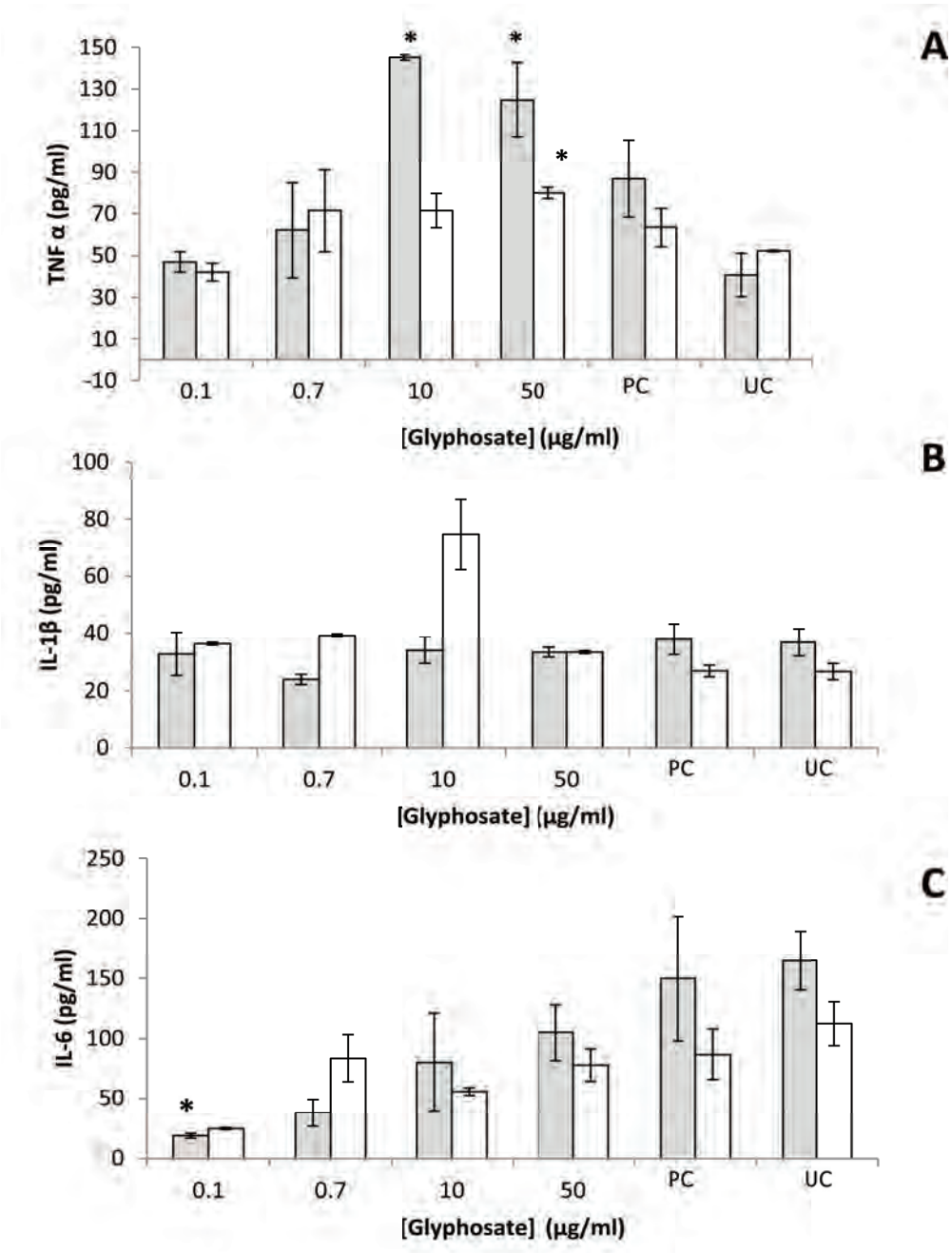

*Figure 11.10: The effect of different concentrations of pure glyphosate (white) and Roundup (grey) on cytokine production and release in human whole blood (n= 3). A: TNFα; B: IL-1β and C: IL-6. Error bars indicate ± SEM (n=3). Five µg/mL of LPS was used a positive control (PC).*P≤0.05 relative to the UC (untreated control).*

Results shown for Roundup indicate a significant (P≤0.05) dose-dependent induction of TNFα (1.51 fold) when compared to the untreated control (Fig.11.10A). Pure glyphosate (Fig.11.10A) also showed an induction of TNFα to a lesser extent than that observed for the Roundup formulation. Roundup did not stimulate significant secretion of IL-1β (Fig.11.10B). Results observed for IL-1β (Fig.11.10B) show that LPS did not significantly induce IL-1β, this contradicts what has been found in literature with studies by (Pugin *et al*., 1995) concluding the capacity of LPS to induce IL-1β in human blood at picomolar concentrations. The lack of alteration in IL-1β could possibly be explained by the presence of an inhibitory compound, but further investigation will have to be carried out to validate this statement. Pure glyphosate caused an initial increased secretion of IL-1β (2.81 fold) up to 10 µg/mL, which was followed by suppression at a concentration of 50 µg/ml (Figure 11.10B). This result suggests that pure glyphosate could display biphasic action, whereby initial stimulation is observed followed by suppression (Coppack, 2001). The action by glyphosate on IL-1β has not been documented in literature.

Pure glyphosate and Roundup showed inhibition of IL-6 production when compared to the untreated control. To date this effect has not been reported in literature.

Although data presenting the effect of glyphosate and glyphosate-based formulations on proinflammatory cytokines is severely limited, the results observed suggest that glyphosate does modulate the release of pro-inflammatory marker IL-1β, IL-6 and TNFα and Roundup modulates the release of TNFα and IL-6.

11.4 Conclusions

This system was successfully scaled-down to a total assay volume of 1 mL. The incubation time for this reaction was found to be optimal after 2 h with a sharp decrease in absorbance readings after a 3 h incubation period. This detection system showed specificity for glyphosate, when tested on its structural analogues, namely, glycine and aminomethylphosphonic acid (AMPA, a primary metabolite of glyphosate).

The cytotoxicity (MTT assay) study in human whole blood indicated a maximum cytotoxic effect at pure glyphosate and Wipeout concentrations of 50 µg/mL and 500 µg/mL respectively. Roundup showed the least cytotoxic effect overall. In the pro-inflammatory response studies pure glyphosate was shown to modulate the release on TNFα, IL-6, and IL-1β and Roundup was shown to modulate the production of TNFα and IL-6.

Scaling down, optimizing and characterizing (optical characteristics) the glyphosate assay is important in improving and understanding the fundamentals of this system before future development focuses on a nanofibre immobilized glyphosate detection system. The development of this detection system is further validated by reporting the possible cytotoxic and pro-inflammatory effects of this herbicide in humans.

11.5 Recommendations

Future work will involve the improvement of the glyphosate detection system sensitivity (Cloud point extraction) and immobilization of copper onto nanofibres (Nylon-6/chitosan) for glyphosate detection. The cytotoxic effect and pro-inflammatory response of glyphosate and its formulations will also be investigated in white blood cells and the TERT-HDLEC cell line. The genotoxic effect of glyphosate and its formulations will also be assessed in the Jurkat cell line using the comet assay.

12 ACETYLCHOLINESTERASE IMMOBILISED ELECTROSPUN NANOFIBRES FOR THE DETECTION OF ORGANOPHOSPHORUS AND CARBAMATE-BASED PESTICIDES

12.1 Introduction

The objective of the study was to immobilise acetylcholine esterase onto electrospun Nylon 6/ chitosan nanofibres for potential utilisation for detection of pesticides.

Due to its pivotal role in the cholinergic nervous system, acetylcholinesterase (AChE) has been the subject of many studies. In ecotoxicology, AChE is widely used as a biomarker of effect to evaluate the health of the aquatic environment. Biomarkers provide biological responses that are useful tools informing about pollutant exposure and their possible toxic effects in living organisms (Durieux *et al*., 2010). OPs and CPs are extremely potent inhibitors of AChE, found in cholinergic neurons. When AChE is blocked, AChE accumulates at the cholinergic receptor sites thereby causing the excessive stimulation of the receptor ultimately leading to death. Long term exposure to low levels of OPs and CPs can lead to persistent and addictive inhibition of AChE resulting in delayed neuropathy (Williams *et al*., 1997). Rapid, sensitive, selective and reliable determination of OPs and CPs is therefore necessary in order to take immediate necessary action. Current analytical techniques such as gas chromatography (GC) and liquid chromatography (LC) coupled to sensitive detectors are reliable, but cannot be carried out in the field. In addition, these techniques are time consuming, expensive and have to be performed by highly trained technicians.

In order to address these problems, biosensors based on inhibition of the cholinesterases AChE and BChE have been developed (Singh *et al*., 1999). Both AChE and BChE have been immobilised on different supports for constructing cholinesterase biosensors, used for detecting inhibitors (Amine *et al*., 2006, Singh *et al*., 1999). However, the majority of OP and CP biosensors to date have used AChE as the recognition component. The presence of these pesticides blocks AChE activity leading to decreased device response. In an AChE-based sensor, the signal is inversely proportional to pesticide concentration. The determination of pesticides has become increasingly important in recent years because of the widespread use of these compounds, which is due to their large range of biological activity and a relatively low persistence. The development of an efficient biosensor requires the immobilisation of adequate amount of recognition elements (enzyme) while maintaining its biological activity. Storage stability, or shelf life, refers to an enzyme's ability to maintain its catalytic abilities in the period between manufacture and eventual use. Operational stability describes the persistence of enzyme activity during a process, i.e. under conditions of use. Both storage and operational stabilities affect the usefulness of enzyme-based products.

12.2 Experimental section

Materials and reagents

Nylon 6, acetic acid, formic acid, chitosan, gluteraldehyde, sodium phosphate, ATChL substrate, 5,5-dithiobis-(2-nitrobenzoic acid), carbofuran. Analysis was carried out using the following instrumentation: Powerwave$_X$ Bio-Tek Instruments, INC (KC Junior), Scanning Electron Microscope (SEM) operating at an accelerated voltage of 20 kV after a gold sputter coating.

Electrospinning of nanofibres from nylon 6 and chitosan

Initially, Nylon 6 was dissolved in Acetic acid (AA)/ Formic acid (FA) (50:50, v/v) at a concentration of 16 wt%. Chitosan was then added to the dissolved nylon 6 at a concentration of 3 wt% with respect to nylon 6 concentration. A homogenous nylon 6 and chitosan blend was then used for electrospinning. Electrospinning was performed at room temperature. The polymer blend was placed in a 5 mL syringe with a metal needle of 0.6 mm in diameter. A power supply was used to provide a high voltage, 25 kV to the syringe needle tip and with a tip-to-collector distance of 15 cm and a solution flow rate of 1 mL/h a metal collector.

Enzyme immobilization

The electrospun Nylon 6/chitosan nanofibres were immersed in 5% glutaraldehyde (GA) solution for 2 h at 4°C followed by rinsing with distilled water (see Figure 12.1). The membranes were then immersed in 0.5 mg/mL solution of AChE in 0.1 M sodium phosphate buffer solution (pH 7.0) for 30 h at 4°C. Non-selectively

bound protein was removed by washing with 0.1 M sodium phosphate buffer (pH 7.0). The amount of bound protein was determined by Bradford's assay (Bradford, 1976).

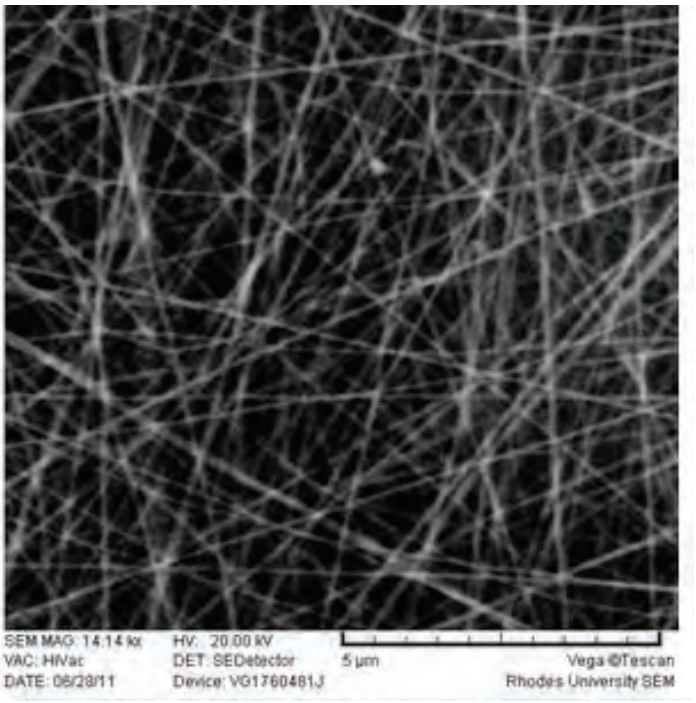

Figure 12.1: Scanning Electron micrograph of electrospun nylon-6/chitosan nanofibres

Enzyme assays

The activity of the free and immobilized AChE was determined according to the micro-Ellman method (Ellman *et al*., 1961) using ATChI as substrate and 5, 5-dithiobis- (2-nitrobenzoic acid) as a chromogen. For the immobilised enzyme assay, soluble enzyme was substituted by 2 × 1 cm² enzyme loaded electrospun nanofibres. Each mixture reaction (1 mL) in microcentrifuges was vortexed for 15 s and the reaction stopped after the appropriate time by placing on ice. The enzyme reaction product interacted with DTNB and the absorbance by the yellow solution was followed spectrophotometrically at 412 nm every 30 s. One unit of enzymatic activity was defined as the amount of enzyme that catalyses 1 µmol of substrate to product per minute. To evaluate effect of temperature and pH, AChE activity was measured in the range of 4 – 40°C and the pH range of 4 – 9.0. The activities of the free and immobilized AChE, after storage in phosphate buffer solution at 4°C were determined at 7 day intervals over a period of 49 days. Reusability of bound AChE was examined by conducting the activity measurement of the bound AChE at 15 min time intervals. After each activity measurement, the bound AChE was washed several times with 0.1 M sodium phosphate pH 7.0.

Acetylcholinesterase (AChE) inhibition studies

The inhibitory effects of a CP, carbofuran on the activity of the free and immobilised AChE was determined through the measure of the reduction of the activity towards a fixed concentration of ATChI and in the presence of different concentrations of the pesticides. Stock solutions of 1-10 µg/L carbofuran were prepared by dissolving in an ethanol medium. The reaction mixture, consisting of 15 µL (free enzyme) or 1 cm² immobilised AChE, sodium phosphate buffer and 30 µl DTNB was pre-incubated within defined carbofuran concentrations ranging from 0.1 µg/L to 10 µg/L for 15 min at 25 °C before initiating the enzymatic reaction with 15 µL ATChI to give a total volume of 300 µL. The effect of pre-incubation time was also determined. Enzyme inhibition was determined according to the following equation:

$$\text{Inhibition efficiency (\%)} = (A0 - Ai)/A0 * 100 \quad (14)$$

Where A*0* represents the AChE activity in the absence of the inhibitor, A*i* the enzyme activity after exposure to the inhibitor

Reusability of immobilised AChE

Reusability of bound AChE was examined by re-using the same functionalised nanofibres to conduct the activity measurement of the bound AChE at 15 min time intervals. After each reaction, the nanofibres on which AChE was immobilised were washed several times with double distilled water (ddH_2O) to remove any residual substrate. The washed membranes were then reintroduced into a fresh reaction medium and enzyme activity determined under optimum conditions. The percentage of specific activity retained relative to the specific activity after one use was calculated.

Storage stability

The activities of the free and immobilised AChE, after storage in 0.1 M sodium phosphate buffer of appropriate pH at 4°C were determined at 7 day intervals over a period of 49 days.

12.3 Results and Discussion

Glutaraldehyde (GA) has found widespread use for enzyme immobilisation. It reacts rapidly with amine groups at around neutral pH (Okuda *et al*., 1991) generating thermally and chemically stable crosslinks. Glutaraldehyde (GA) can react with several functional groups of proteins, such as amine, thiol, phenol, and imidazole because the most reactive amino acid side-chains are nucleophiles (Habeeb and Hiramoto, 1968). The crosslinking of proteins to a support material to generally implies the ε-amino group of lysine residues (Avrameas and Ternynck, 1969). This is highly advantageous because most proteins contain many lysine residues, usually located on the protein surface due to their polarity. Furthermore, lysine residues are generally not involved in the catalytic site, which allows moderate crosslinking to preserve protein conformation and thus biological activity (Avrameas, 1969). However, enzyme immobilization via covalent binding often results in enzyme conformation which reduces its flexibility and may cause reduction in enzyme mobility to induce fit to a substrate (Hopwood *et al*., 1970) that may lead to a reduction of AChE activities.

The effect of GA concentration on the amount of AChE immobilised onto the nanofibres was determined for GA concentrations ranging from 0% to 25%. The amount of enzyme immobilised was determined via the Bradford's assay and the results shown in Figure 12.2.

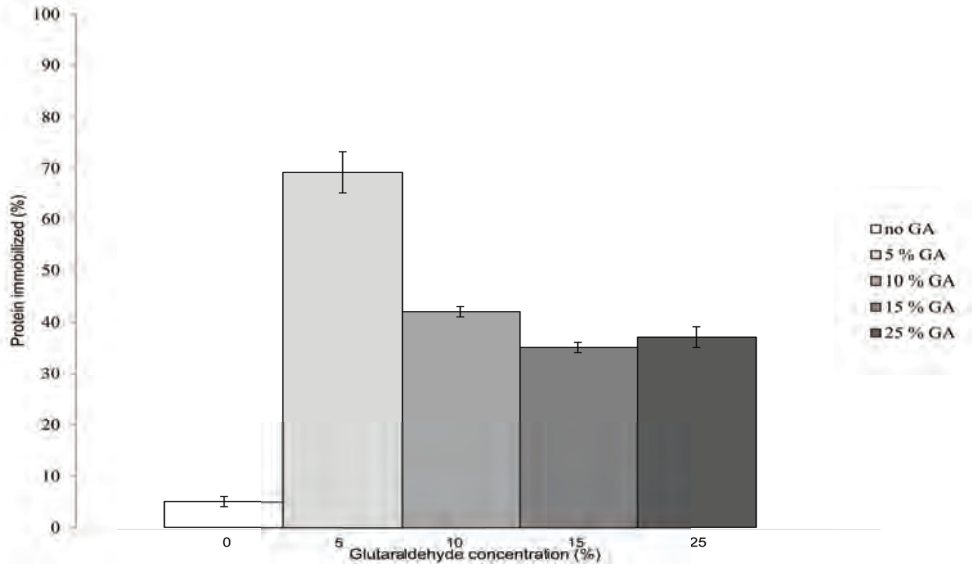

Figure 12.2: Effect of crosslinker concentration (GA) on the protein immobilisation. 0.5 mg/mL AChE, GA pre-activated nanofibres ±SD, (n=3)

In the absence of GA, less that 10% AChE was immobilised on to the nanofibre surfaces. When the nanofibres were treated with 5% GA, about 70% AChE was immobilised onto the nanofibres. GA concentrations between 10 and 25% resulted in lower amounts of protein being immobilised relative to 5% GA. The optimum cross-linker concentration chosen for future studies was 5% glutaraldehyde (0.334 mg/cm^2 of AChE was immobilized onto the nanofibres).

The effect of pH on the activity of the free and immobilised enzyme was studied at pH 4.0 and 9.0 (Fig.12.3).

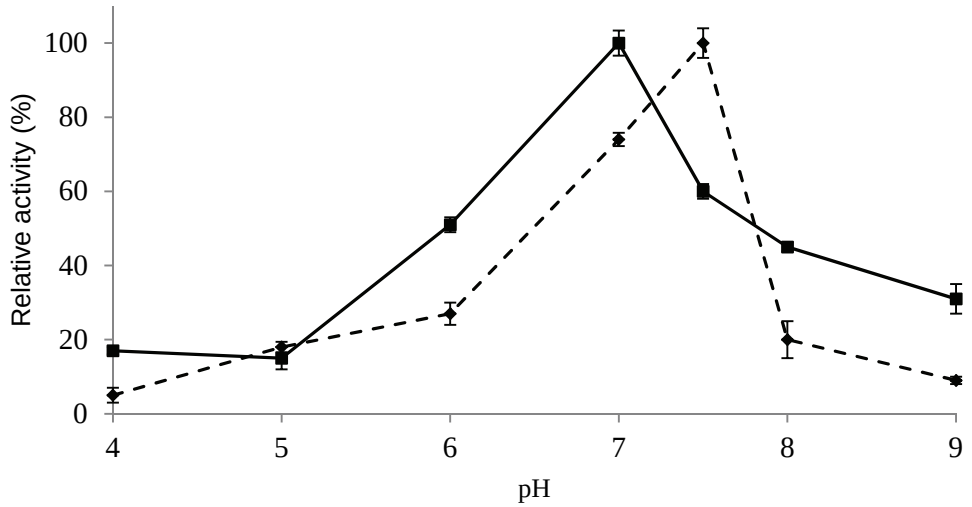

Figure 12.3: Effect of pH on the activity of free (dotted line) and immobilized (solid line) AChE. The reactions were carried out at room temperature in 0.1M potassium acetate buffer (pH 4.0 and pH 5.0) and 0.1M phosphate buffer pH ranging from 6.0 to 9.0. ±SD, (n= 3)

As shown in Fig.12.3, the optimum pH for free AChE is 7.5. The pH optimum for free AChE has been documented in literature, with studies indicating a buffer dependent pH optimum range between pH 7.5-9.0 (Monsan, 1978). The optimum pH for immobilized AChE (Fig.12.3) was observed at pH 7.0. According to (Stoilovo *et al*., 2010), the pH of an immobilized enzyme is dependent on the modification of the support. Since ionic charges influence the enzyme activity profile, binding enzymes to polyelectrolyte supports, such as chitosan, often shift the pH optimum (Valliant *et al*., 2000). (Sahin *et al*., 2005) reported similar findings to this study for AChE immobilized in Ca-alginate and alginate/carrageenan beads. Although some studies support the data observed for immobilized AChE, other studies have reported different pH optima. The optimum pH for immobilized AChE can vary depending on several factors including, methods of immobilization, the buffer system and the type of polymer used to immobilize the enzyme (Marinov *et al*., 2009).

The effect of temperature on the relative activity of the free and immobilised AChE was studied in the temperature range 4 – 40°C (Figure 12.4).

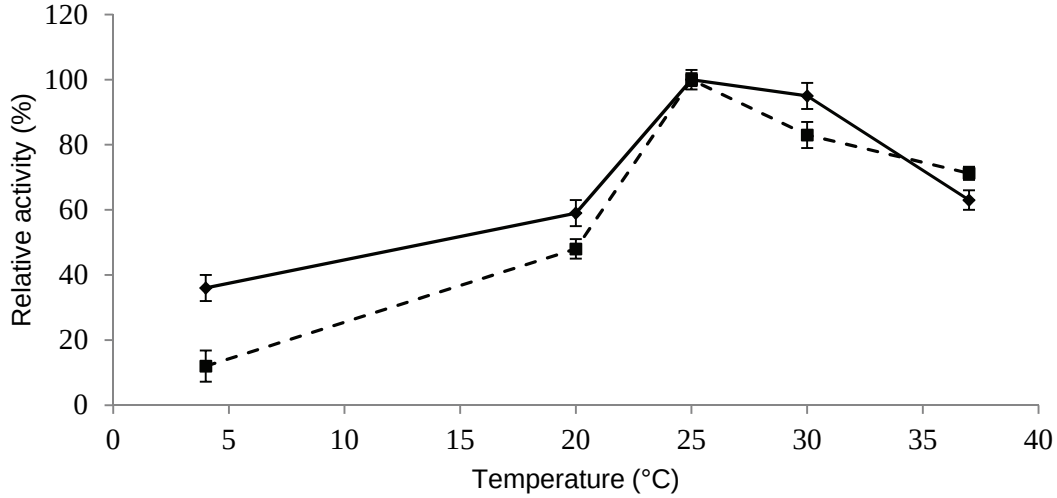

Figure 12.4: Effect of temperature on activity of acetylcholinesterase immobilized on nylon-6/chitosan electrospun nanofibres. Free AChE (dotted line); Immobilized AChE (solid line). ±SD, (n=3)

Both the immobilised and soluble AChE an optimum temperature was 25°C. Different results have been obtained for AChE immobilised on other supports including electrospun nanofibrous material (Stoilovo *et al*., 2010) were immobilised enzyme had a higher optimum temperature (30°C). However it can be noted that at

30°C, immobilised AChE had above 90% relative activity which was considerably higher than that observed for soluble AChE. This indicated that the immobilised AChE had improved thermal tolerance and resisted denaturation due to the rise in temperature. The improvement in thermal tolerance observed, was due to immobilization and cross-linking providing a rigid backbone for AChE molecules, thus decreasing the effect of higher temperatures on the enzyme structure and the catalytic activity of AChE (Kilinc *et al*., 2002).

Immobilised AChE showed significantly higher thermal stability compared to the free enzyme (Figure 12.5). After incubation at 60°C for 2 h, immobilised AChE retained ~49% of its initial activity whilst free AChE lost >90% of its activity after 1 h incubation.

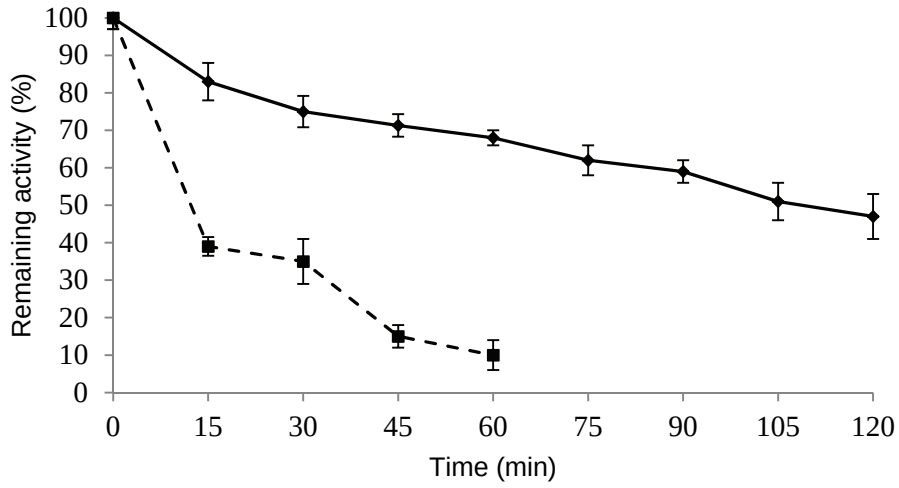

Figure 12.5: Thermal stability of free (dotted line) and immobilised (solid line) electric eel AChE after pre-incubation at 60°C over time. All other reaction conditions were kept at optimum levels, ± SD (n=3).

The effect of repeated use on the activity of the immobilised AChE is shown in Figure 12.6. After 8 reusing cycles, the relative activity of the immobilised AChE decreased to about 35% of its initial activity. These results were similar to those reported by (Stoilovo *et al*., 2010), where AChE immobilised on nanofibres electrospun from polyacrylonitrile and subsequently modified by high molecular weight chitosan showed about 40% residual activity after 10 reuse cycles.

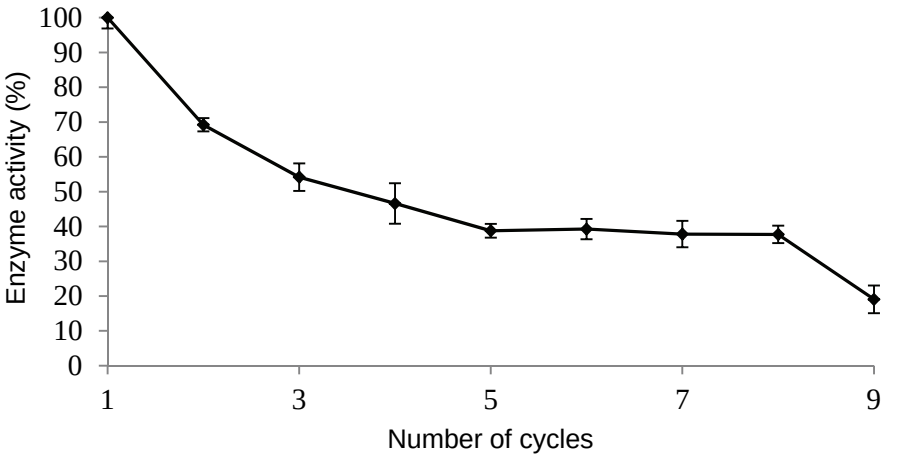

Figure 12.6: The influence of the number of reuse on the activity of immobilised AChE with repeated cycles. All cycles were carried out at room temperature (± 22 °C). Reusability of bound AChE was examined by conducting activity assays at time intervals of 15 min. ± SD (n=3).

Storage stability is of great importance in industrial application of immobilised enzymes. For industrial applications, the enhanced storage stability and reusability of the immobilised enzymes is of great importance because as it effectively reduces costs.

The activity of the free AChE decreased rapidly in the first 7 days (35%) and had lost most of its activity (>90%) on day 21 (Figure 12.7). In contrast, the activity of immobilised AChE for the first 7 days was >80% and after 49 days, the enzyme still had 50% activity.

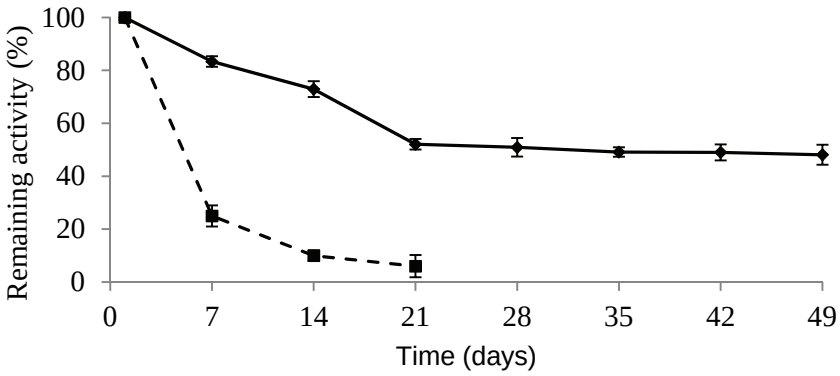

Figure 12.7: Storage stability of immobilized and free AChE: Both immobilized (solid line) and free enzyme (dotted line) were store in 0.1M phosphate buffer (pH 7.0 and pH 7.5 respectively) at 4°C and enzyme activity tested at 7 day intervals. ± SD (n=3).

In order to demonstrate the usefulness of the immobilised acetylcholinesterase in the analysis of pesticides, its response to different concentrations of a CP (carbofuran) was determined Figure 12.8.

Effect of carbofuran on AChE activity

Fixed concentrations of carbofuran displayed an inhibitory effect on the activity of AChE in both the free and immobilized state (Fig.12.8). This result suggests that immobilizing AChE onto a solid matrix did not have any effect with respect to the susceptibility of this enzyme to this inhibitor. This observation has been well documented in literature with other studies reporting similar results (Fukuto, 1990).Carbofuran (CP) displays very low solubility in water and is therefore often prepared in a solvent. Solvents have also been shown to decrease enzyme activity (Ebrahimi *et al*., 2010). The degree of quantified inhibition is highly dependent on the type of pesticide being assessed as well as the organic solvent being used.

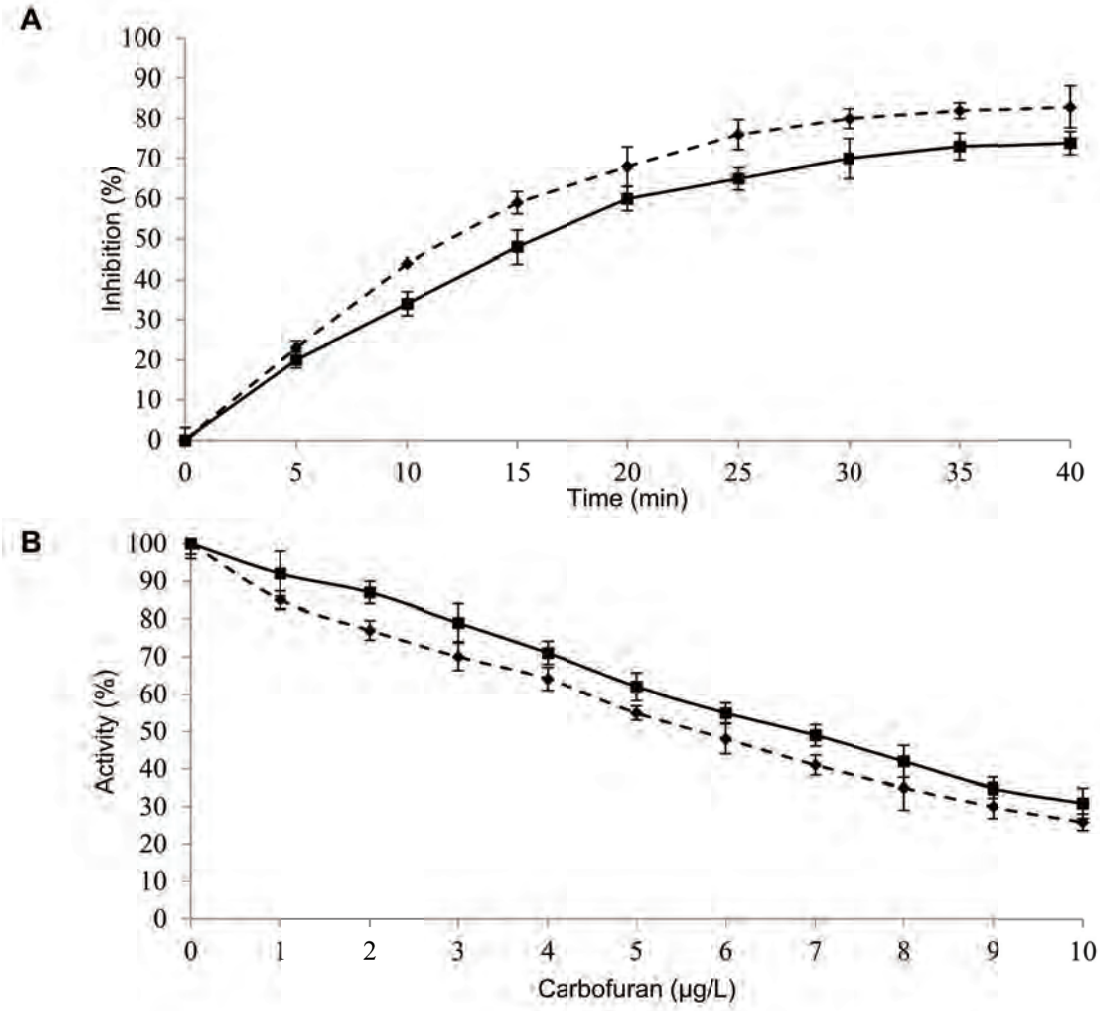

Figure 12.8: Effect of carbofuran on the activity of AChE (a) effect of incubation time at a fixed concentration (1 µg/L) of carbofuran (b) the effect of different concentrations of the CP on AChE activity, ± SD (n=3). Free AChE (dotted line) Immobilized AChE (solid line).

12.4 Conclusions

Nanofibrous nylon 6/chitosan membranes tailored for AChE immobilizations were fabricated via electrospinning. The AChE was covalently bound to the nanofibrous membrane after it was crosslinked with glutaraldehyde. In this study, the effect of exposing free and immobilised AChE to carbofuran (CP) was determined. The present study successfully demonstrated that the immobilisation of AChE resulted in an improvement in the enzyme's storage stability. Moreover, the enzyme could be reused for nine consecutive recycles with retention of activity. The improvement storage stability, reusability and inhibition effect by carbofuran (for the free and immobilized AChE states) indicates the possibility of using AChE as a biosensor for the detection of carbofuran.

12.5 Recommendations

In general, the objectives of this study were met; AChE was successfully immobilised on nanofibres electrospun from a blend of nylon 6 and chitosan. The method for the preparation of the support matrix was cost effective and, most importantly, did not involve the use of cytotoxic agents. Although the enzyme lost its activity, it showed remarkable reusability and storage stability providing a promising tool for the rapid detection of AChE inhibitors. The most challenging aspects, however, are: (i) improving the selectivity of AChE for pesticide detection (ii) improving reusability and (iii) reducing loss of enzyme activity during immobilisation.

13 REFERENCES

ABRAHAM, M. 2006. Today's seawater is tomorrow's drinking water: UCLA engineers develop revolutionary nanotech water desalination membrane. *UCLA Newsroom*.

ABU-YOUSSEF, M. A. M., DEY, R., GOHAR, Y., MASSOUD, A. A. A., ÖHRSTRÖM, L. & LANGER, V. 2007. Synthesis and Structure of Silver Complexes with Nicotinate-Type Ligands Having Antibacterial Activities against Clinically Isolated Antibiotic Resistant Pathogens. *Inorganic Chemistry,* 46**,** 5893-5903.

AHN, D. J. & KIM, J.-M. 2008. Fluorogenic Polydiacetylene Supramolecules: Immobilization, Micropatterning, and Application to Label-Free Chemosensors. *Acc. Chem. Res.,* 41**,** 805-816.

AL-RAJAB, A. J. & SCHIAVON, M. 2010. Degradation of 14C-glyphosate and aminomethylphosphonic acid (AMPA) in three agricultural soils. *Journal of Environmental Sciences* 22**,** 1374-1380.

ALI, M. M. M., MOHAMED, Z. K., KLENA, J. D., AHMED, S. F., MOUSSA, T. A. A. & GHENGHESH, K. S. 2012. Molecular characterization of diarrheagenic Escherichia coli from Libya. *American Journal of Tropical Medicine and Hygiene,* 86**,** 866-871.

ALULA, M. T., MOHAMED, A.-M. I. & BEKHIT, A. A. 2010. Simultaneous spectrophotometric determination of iron (II) and copper (II) in tablets by chemometric methods. *Thai J. Pharm. Sci.,* 34**,** 93-106.

AMINE, A., MOHAMMADI, H., BOURAIS, I. & PALLESCHI, G. 2006. Enzyme inhibition-based biosensors for food safety and environmental monitoring. *Biosensors and Bioelectronics* 21**,** 1405-1425.

AMOROS, I., ALONSO, J. L., ROMAGUERA, S. & CARRASCO, J. M. 2007. Assessment of toxicity of a glyphosate-based formulation using bacterial systems in lake water. *Chemosphere* 67**,** 2221-2228.

ANADON, A., MARTINEZ-LARRANAGA, M. R., MARTINEZ, M. A., CASTELLANO, V. J., MARTINEZ, M., MARTIN, M. T., NOZAL, M. J. & BERNAL, J. L. 2009. Toxicokinetics of glyphosate and its metabolite aminomethyl phosphonic acid in rats. *Toxicological Letters* 190**,** 91-95.

ANTOLINI, M., BOZZOLI, A., GHIRON, C., KENNEDY, G., ROSSI, T. & URSINI, A. 1999. Analogues of 4,5-bis(3,5-dichlorophenyl)-2-trifluoromethyl-1H-imidazole as potential antibacterial agents. *Bioorganic & Medicinal Chemistry Letters,* 9**,** 1023-1028.

ARMIENTA, M. A. & SEGOVIA, N. 2008. Arsenic and fluoride in the groundwater of Mexico. *Environ. Geochem. Health,* 30**,** 345-353.

ASLAN, K., LAKOWICZ, J. R. & GEDDES, C. D. 2004. Nanogold-plasmon-resonance-based glucose sensing. *Anal. Biochem.,* 330**,** 145-155.

ASTM 2010. Standard test method for determining the antimicrobial activity of immobilized antimicrobial agents under dynamic contact conditions: ASTM E2149-10.

AVRAMEAS, S. 1969. Coupling of enzymes to proteins with glutaraldehyde. Use of the conjugates for the detection of antigens and antibodies. *Immunochemistry,* 6**,** 43-52.

AVRAMEAS, S. & TERNYNCK, T. 1969. The cross-linking of proteins with glutaraldehyde and its use for the preparation of immunoadsorbents. *Immunochemistry* 6**,** 53-66.

BALAJI, T., EL-SAFTY, S. A., MATSUNAGA, H., HANAOKA, T. & MIZUKAMI, F. 2006. Optical sensors based on nanostructured cage materials for the detection of toxic metal ions. *Angew. Chem., Int. Ed.,* 45**,** 7202-7208.

BAMFIELD, P. 2001. *Chromic Phenomena: Technological Applications of Colour Chemistry*, Royal Society of Chemistry.

BATTAGLIN, W. A., KOLPIN, D. W., SCRIBNER, E. A., KUIVILA, K. M. & M.W., S. 2005. Glyphosate, other herbicides, and transformation products in midwestern streams, 2002. *Journal of American Water Resources Association* 41**,** 323-332.

BENACHOUR, N., SIPAHUTAR, H., MOSLEMI, S., GASNIER, C., TRAVERT, C. & SERALINI, G. E. 2007. Time and dose-dependent effects of Roundup on human embryonic and placental cells. *Archives of Environmental Contamination and Toxicology* 53**,** 126-133.

BENAMU, M. A., SCHNEIDER, M. I. & SANCHEZ, N. E. 2010. Effects of the herbicide glyphosate on biological attributes of Alpaida veniliae (Araneae, Araneidae), in laboratory. *Chemosphere,* 78**,** 871-876.

BERG, M., LUZI, S., TRANG, P. T. K., VIET, P. H., GIGER, W. & STUEBEN, D. 2006. Arsenic Removal from Groundwater by Household Sand Filters: Comparative Field Study, Model Calculations, and Health Benefits. *Environ. Sci. Technol.,* 40**,** 5567-5573.

BEURET, C. J., ZIRULNIK, F. & GIMENEZ, M. S. 2005. Effect of the herbicide glyphosate on liver peroxidation in pregnant rats and their fetuses. *Reproductive Toxicology* 19**,** 501-504.

BEZERRA, M. A., DOS, S. W. N. L., LEMOS, V. A., KORN, M. D. G. A. & FERREIRA, S. L. C. 2007. On-line system for preconcentration and determination of metals in vegetables by Inductively Coupled Plasma Optical Emission Spectrometry. *J. Hazard. Mater.,* 148**,** 334-339.

BIERI, M. & BUERGI, T. 2005. Adsorption Kinetics, Orientation, and Self-Assembling of N-Acetyl-L-cysteine on Gold: A Combined ATR-IR, PM-IRRAS, and QCM Study. *J. Phys. Chem. B,* 109**,** 22476-22485.

BOSQUE-SENDRA, J. M., ALMANSA-LOPEZ, E., GARCIA-CAMPANA, A. M. & CUADROS- RODRIGUEZ, L. 2003. Data analysis in the determination of stoichiometries and stability constants of complexes. *Analytical Sciences* 19**,** 1431-1439.

BOTHWELL, T. H. 1979. *Iron Metabolism in Man*, Blackwell Scientific.

BRITZ-MCKIBBIN, P., ICHIHASHI, T., TSUBOTA, K., CHEN, D. D. Y. & TERABE, S. 2003. Complementary on-line preconcentration strategies for steroids by capillary electrophoresis. *Journal of Chromatography A,* 1013**,** 65-76.

BROOK, T. E. & NARAYANASWAMY, R. 1998. Polymeric films in optical gas sensors. *Sens. Actuators, B,* B51**,** 77-83.

BROWN, S. 2006. Water, water everywhere. *ScienceNOW Daily News*.

BUSARANON, K., SUNTORNSUK, W. & SUNTORNSUK, L. 2006. Comparison of UV spectrophotometric method and high performance liquid chromatography for the analysis of flunarizine and its application for the dissolution test. *J. Pharm. Biomed. Anal.,* 41**,** 158-164.

CANER, H., YILMAZ, E. & YILMAZ, O. 2007. Synthesis, characterization and antibacterial activity of poly(N-vinylimidazole) grafted chitosan. *Carbohydr. Polym.,* 69**,** 318-325.

CARABIAS-MARTINEZ, R., RODRIGUEZ-GONZALO, E., MORENO-CORDERO, B., PEREZ-PAVON, J., GARCIA-PINTO, C. & FERNANDEZ LAESPADA, E. 2000. Review: Surfacant cloud point extraction and preconcentration of organic compounds prior to chromatography and capillary electrophoresis. *Journal of Chromatography A* 902**,** 251-265.

CARNEIRO, J. M. T., DIAS, A. C. B., ZAGATTO, E. A. G. & HONORATO, R. S. 2002. Spectrophotometric catalytic determination of Fe(III) in estuarine waters using a flow-batch system. *Anal. Chim. Acta,* 455**,** 327-333.

CARR, H. S., WLODKOWSKI, T. J. & ROSENKRANZ, H. S. 1973. Silver sulfadiazine: in vitro antibacterial activity. *Antimicrobial Agents and Chemotherapy,* 4**,** 585-587.

CARRAWAY, E. R., DEMAS, J. N. & DEGRAFF, B. A. 1991. Photophysics and oxygen quenching of transition-metal complexes on fumed silica. *Langmuir,* 7**,** 2991-8.

CARTIGNY, B., AZAROUAL, N., IMBENOTTE, M., MATHIEU, D., VERMEERSCH, G., GOULLE, J. P. & LHERMITTE, M. 2004. Determination of gyphosate in biological fluids by 1H and 31P NMR spectroscopy. *Forensic Science International* 143**,** 141-145.

CHAN, Y. C., CHANG, S. C., HSUAN, S. L., CHIEN, M. S., LEE, W. C., KANG, J. J., WANG, S. C. & LIAO, J. W. 2007. Cardiovascular effects of herbicides and formulated adjuvants on isolated rat aorta and heart. *Toxicology in Vitro,* 21**,** 595-603.

CHEN, J. & TEO, K. C. 2001. Determination of cobalt and nickel in water samples by flame atomic absorption spectrometry after cloud point extraction. *Anal. Chim. Acta,* 434**,** 325-330.

CHENG, T., XU, Y., ZHANG, S., ZHU, W., QIAN, X. & DUAN, L. 2008. A Highly Sensitive and Selective OFF-ON Fluorescent Sensor for Cadmium in Aqueous Solution and Living Cell. *J. Am. Chem. Soc.,* 130**,** 16160-16161.

CHIGOME, S., DARKO, G. & TORTO, N. 2011. Electrospun nanofibers as sorbent material for solid phase extraction. *Analyst (Cambridge, U. K.),* 136**,** 2879-2889.

CHIGOME, S. & TORTO, N. 2011. A review of opportunities for electrospun nanofibers in analytical chemistry. *Anal. Chim. Acta,* 706**,** 25-36.

CHIGOME, S. & TORTO, N. 2012. Electrospun nanofiber-based solid-phase extraction. *TrAC, Trends Anal. Chem.,* 38**,** 21-31.

CHIMENTAO, R. J., COTA, I., DAFINOV, A., MEDINA, F., SUEIRAS, J. E., DE, L. F. J. L. G., FIERRO, J. L. G., CESTEROS, Y. & SALAGRE, P. 2006. Synthesis of silver-gold alloy nanoparticles by a phase-transfer system. *J. Mater. Res.,* 21**,** 105-111.

CHMIELEWSKA, E., TYLUS, W. & MORVOVA, M. 2006. Supplementary research of clinoptilolite-rich tuff composites after adsorption trials using the XPS technique. *Cent. Eur. J. Chem.,* 4**,** 1-12.

CHOWDHURY, S., BHETHANABOTLA, V. R. & SEN, R. 2009. Silver-copper alloy nanoparticles for metal enhanced luminescence. *Appl. Phys. Lett.,* 95**,** 131115/1-131115/3.

CHUNG, M. G., KIM, H. W., KIM, B. R., KIM, Y. B. & RHEE, Y. H. 2012. Biocompatibility and antimicrobial activity of poly(3-hydroxyoctanoate) grafted with vinylimidazole. *Int. J. Biol. Macromol.,* 50**,** 310-316.

CONGIU, C., COCCO, M. T. & ONNIS, V. 2008. Design, synthesis, and in vitro antitumor activity of new 1,4-diarylimidazole-2-ones and their 2-thione analogues. *Bioorganic & Medicinal Chemistry Letters,* 18**,** 989-993.

COOLEY, J. F. 1902. *Apparatus for electrically dispersing fluids*.

COPPACK, S. W. 2001. Pro-inflammatory cytokines and adipose tissue. *Proceedings of the Nutrition Society* 60**,** 349-356.

CORBETT, J. V. 1995. Accidental poisoning with iron supplements. *MCN Am J Matern Child Nurs,* 20**,** 234.

CORBIERRE, M. K., CAMERON, N. S., SUTTON, M., MOCHRIE, S. G. J., LURIO, L. B., RUHM, A. & LENNOX, R. B. 2001. Polymer-Stabilized Gold Nanoparticles and Their Incorporation into Polymer Matrices. *J. Am. Chem. Soc.,* 123**,** 10411-10412.

COSTA, M., DAVIDSON, T. L., CHEN, H., KE, Q., ZHANG, P., YAN, Y., HUANG, C. & KLUZ, T. 2005. Nickel carcinogenesis: Epigenetics and hypoxia signaling. *Mutat. Res., Fundam. Mol. Mech. Mutagen.,* 592**,** 79-88.

COTTON, S. A. 1976. The biochemistry of iron. *Educ. Chem.,* 13**,** 180-3.

COUTINHO, F. B. C., COUTINHO, L. F. M., MAZO, L. H., NIXDORF, S. L., CAMARA, C. A. P. & LANCAS, F. M. 2007. Direct determination of glyphosate using hydrophilic interaction chromatography with coulometric detection at copper microelectrode. *Analytica Chimica Acta* 592**,** 30-35.

CRANE, L., ANASTASSIADOU, M., HAGE, S. E., STIGLIANI, J. L., BAZIARD-MOUYSSET, G., PAYARD, M., LEGER, J. M., BIZOT-ESPIARD, J.-G., KTORZA, A., CAIGNARD, D.-H. & RENARD, P. 2006. Design and synthesis of novel imidazoline derivatives with potent antihyperglycemic activity in a rat model of type 2 diabetes. *Bioorganic & Medicinal Chemistry,* 14**,** 7419-7433.

DA, S. L. & MASOTTI, A. 2010. Chitin and chitosan as multipurpose natural polymers for groundwater arsenic removal and As2O3 delivery in tumor therapy. *Mar. Drugs,* 8**,** 1518-1525.

DALVIE, M. A., AFRICA, A. & LONDON, L. 2009. Change in the quantity and acute toxicity of pesticides sold in South African crop sectors 1994-1999. *Environmental International,* 35**,** 683-687.

DAVIES, R. L. & ETRIS, S. F. 1997. The development and functions of silver in water purification and disease control. *Catalysis Today,* 36**,** 107-114.

DEMAS, J. N., DEGRAFF, B. A. & XU, W. 1995. Modeling of Luminescence Quenching-Based Sensors: Comparison of Multisite and Nonlinear Gas Solubility Models. *Anal. Chem.,* 67**,** 1377-80.

DENKHAUS, E. & SALNIKOW, K. 2002. Nickel essentiality, toxicity, and carcinogenicity. *Crit Rev Oncol Hematol,* 42**,** 35-56.

DENYER, S. P. 1995. Mechanisms of action of antibacterial biocides. *International Biodeterioration & Biodegradation,* 36**,** 227-245.

DESAI, K., KIT, K., LI, J., MICHAEL, D. P., ZIVANOVIC, S. & MEYER, H. 2009. Nanofibrous chitosan non-wovens for filtration applications. *Polymer,* 50**,** 3661-3669.

DEUK, L. Y., LEE, K.-H., KIM, B.-Y. & CHO, N.-I. 2010. Silver nanoparticles dispersed in electrospun polyacrylonitrile nanofibers via chemical reduction. *Journal of Sol-Gel Science and Technology,* 54**,** 63-68.

DI, M. G., LANZA, M. & CAMPAGNA, S. 1995. Luminescent RuII-polypyridine complexes in poly-2-hydroxyethylmethacrylate matrixes as oxygen sensors. *Adv. Mater. (Weinheim, Ger.),* 7**,** 468-71.

DINI, F., MARTINELLI, E., PAOLESSE, R., FILIPPINI, D., D'AMICO, A., LUNDSTROEM, I. & DI, N. C. 2011. Polymer matrices effects on the sensitivity and the selectivity of optical chemical sensors. *Sens. Actuators, B,* B154**,** 220-225.

DIXIT, S. & HERING, J. G. 2003. Comparison of Arsenic(V) and Arsenic(III) Sorption onto Iron Oxide Minerals: Implications for Arsenic Mobility. *Environ. Sci. Technol.,* 37**,** 4182-4189.

DODANI, S. C., HE, Q. & CHANG, C. J. 2009. A Turn-On Fluorescent Sensor for Detecting Nickel in Living Cells. *J. Am. Chem. Soc.,* 131**,** 18020-18021.

DOSHI, J. & RENEKER, D. H. 1995. Electrospinning process and applications of electrospun fibers. *J. Electrost.,* 35**,** 151.

DRIEHAUS, W., SEITH, R. & JEKEL, M. 1995. Oxidation of arsenate(III) with manganese oxides in water treatment. *Water Res.,* 29**,** 297-305.

DUKE, S. O. & POWLES, S. B. 2008. Mini-review glyphosate: a once in a century herbicide. *Pest Management* 63**,** 319-325.

DURIEUX, E., FARVER, T., FITZGERALD, P., EDER, K. & OSTRACH, D. 2010. Natural factors to consider when using acetylcholinesterase activity as neurotoxicity biomarker in young-of-year striped bass (Morone saxatilis). *Fish Physiology and Biochemistry* 37**,** 21-29.

DUTTA, A., MAHAPATRA, S. S. & DATTA, J. 2011. High performance PtPdAu nano-catalyst for ethanol oxidation in alkaline media for fuel cell applications. *Int. J. Hydrogen Energy,* 36**,** 14898-14906.
EBLIN, K. E., BOWEN, M. E., CROMEY, D. W., BREDFELDT, T. G., MASH, E. A., LAU, S. S. & GANDOLFI, A. J. 2006. Arsenite and monomethylarsonous acid generate oxidative stress response in human bladder cell culture. *Toxicol. Appl. Pharmacol.,* 217**,** 7-14.
EBRAHIMI, M., PLACIDO, L., ENGEL, L., SHAMSASHAGI, K. & CZERMAK, P. 2010. A novel ceramic membrane reactor system for the continuous enzymatic synthesis of oligosaccharides. *Desalination,* 250**,** 1105-1108.
ELCI, L., SOYLAK, M. & OZCAN, B. 2003. Coprecipitation of Cu(II), Ni(II), Fe(III), Cd(II), Pb(II), and Co(II) in wastewater, sediment, and metallic zinc samples with HMDTC-HMA for flame atomic absorption spectrometric determination. *Anal. Lett.,* 36**,** 987-999.
ELLIS, J. T., SCHULMAN, I. & SMITH, C. H. 1954. Generalized siderosis with fibrosis of liver and pancreas in Cooley's (Mediterranean) anemia; with observations on the pathogenesis of the siderosis and fibrosis. *Am J Pathol,* 30**,** 287-309.
ELLMAN, G., COURTNEY, K., ANDRES, V. & FEATHERSTONE, R. 1961. A new and rapid colorimetric determination of acetylcholinesterase activity. *Biochemical Pharmacology,* 7**,** 88-95.
ENDO, K., NAKAGAWA, M., SAKANAKURA, H., INOUE, Y., MASAHIRO, I. & SUGIHARA, G. 2012. Study on hydrogen sulfide gas production potential test for ground improvement by recycled gypsum and lime. *Zairyo,* 61**,** 31-36.
FAN, L.-J. & JONES, W. E., JR. 2006. A Highly Selective and Sensitive Inorganic/Organic Hybrid Polymer Fluorescence "Turn-on" Chemosensory System for Iron Cations. *J. Am. Chem. Soc.,* 128**,** 6784-6785.
FANG, X., MA, H., XIAO, S., SHEN, M., GUO, R., CAO, X. & SHI, X. 2011. Facile immobilization of gold nanoparticles into electrospun polyethyleneimine/polyvinyl alcohol nanofibers for catalytic applications. *J. Mater. Chem.,* 21**,** 4493-4501.
FARRUGGIA, G., IOTTI, S., PRODI, L., MONTALTI, M., ZACCHERONI, N., SAVAGE, P. B., TRAPANI, V., SALE, P. & WOLF, F. I. 2006. 8-Hydroxyquinoline Derivatives as Fluorescent Sensors for Magnesium in Living Cells. *J. Am. Chem. Soc.,* 128**,** 344-350.
FAY MIKE, A. H., INGERMAN LISA, SWARTS STEVEN. G 2005. Agency for Toxic Substances and Disease Registry (ATSDR). *In:* DEPARTMENT OF PUBLIC HEALTH AND HUMAN SERVICES, P. H. S. (ed.). Atlanta, GA.
FDFA. 2006. *Federal Department of Foreign Affairs Presence Switzerland* [Online]. Available: http://www.swissworld.org/en/switzerland/swiss_specials/green_technology/nanotechnology/.
FORMHALS, A. 1934. Process and apparatus for preparing artificial threads. US Patent.
FORMOSINHO, S. J. 1976. Quenching of excited aromatic molecules by paramagnetic species. *Mol. Photochem.,* 7**,** 13-39.
FRENOT, A. & CHRONAKIS, I. S. 2003. Polymer nanofibers assembled by electrospinning. *Curr. Opin. Colloid Interface Sci.,* 8**,** 64.
FUKUTO, T. 1990. Mechanism of action of organophosphorous and carbamate insecticides. *Environmental Health Perspectives* 87**,** 245-254.
FUNK, D., SCHRENK, H. H. & FREI, E. 2007. Serum albumin leads to false positive results in the XTT and the MTT assay. *Biotechniques,* 43**,** 178-182.
GAO, L., WANG, J. Q., HUANG, L., FAN, X. X., ZHU, J. H., WANG, Y. & ZOU, Z. G. 2007. Novel Inorganic-Organic Hybrid Fluorescence Chemosensor Derived from SBA-15 for Copper Cation. *Inorg. Chem. (Washington, DC, U. S.),* 46**,** 10287-10293.
GAO, L., WANG, Y., WANG, J., HUANG, L., SHI, L., FAN, X., ZOU, Z., YU, T., ZHU, M. & LI, Z. 2006. A Novel ZnII-Sensitive Fluorescent Chemosensor Assembled within Aminopropyl-Functionalized Mesoporous SBA-15. *Inorg. Chem.,* 45**,** 6844-6850.
GARCIA, S. F., NAVAS, D. A. & LASERNA, J. J. 1983. Kinetic fluorimetric determination of inorganic species by bromate oxidation of chelating agent and complexation with metal ions. *Anal. Chem.,* 55**,** 253-6.
GASNIER, C., DUMONT, C., BENACHOUR, N., CLAIR, E., CHAGNON, M. C. & G.E., S. 2009. Glyphosate-based herbicides are toxic and endocrine disruptors in human cell lines. *Toxicology,* 262**,** 184-191.
GAVRILENKO, N. A. & SARANCHINA, N. V. 2009. Analytical properties of 1-(2-pyridylazo)-2-naphthol immobilized on a polymethacrylate matrix. *J. Anal. Chem.,* 64**,** 226-230.
GEHIN, A., GUILLAUME, Y. C., MILLET, J., GUYON, C. & L., N. 2005. Vitamins C and E reverse effect of herbicide-induced toxicity on human epidermal cells HaCaT: a biochemometric approach. *International Journal of Pharmaceutics* 288**,** 219-226.

GERBER, T. I. A., HOSTEN, E., MAYER, P. & TSHENTU, Z. R. 2006. Synthesis and characterization of rhenium(III) and (V) pyridylimidazole complexes. *J. Coord. Chem.,* 59**,** 243-253.
GHOLIVAND, M. B., GERAVANDI, B. & PARVIN, M. H. 2011. Anodic Stripping Voltammetric Determination of Iron(II) at a Carbon Paste Electrode Modified with Dithiodianiline (DTDA) and Gold Nanoparticles (GNP). *Electroanalysis,* 23**,** 1345-1351.
GHOSH, S. K. & PAL, T. 2007. Interparticle Coupling Effect on the Surface Plasmon Resonance of Gold Nanoparticles: From Theory to Applications. *Chem. Rev. (Washington, DC, U. S.),* 107**,** 4797-4862.
GOKER, H., ERTAN, R., AKGUN, H. & YULUG, N. 1991. Synthesis and antifungal activity of some new benzimidazole derivatives. *Archiv der Pharmazie,* 324**,** 283-286.
GOODMAN, J. E., PRUEITT, R. L., DODGE, D. G. & THAKALI, S. 2009. Carcinogenicity assessment of water-soluble nickel compounds. *Crit. Rev. Toxicol.,* 39**,** 365-417.
GREINER, A. & WENDORFF, J. H. 2007. Electrospinning: a fascinating method for the preparation of ultrathin fibers. *Angew. Chem., Int. Ed.,* 46**,** 5670.
GUETLICH, P. & GOODWIN, H. A. 2004. Spin crossover - an overall perspective. *Top. Curr. Chem.,* 233**,** 1-47.
GUGGENBICHLER, J. P., BÖSWALD, M., LUGAUER, S. & KRALL, T. 1999. A new technology of microdispersed silver in polyurethane induces antimicrobial activity in central venous catheters. *Infection,* 27**,** S16-S23.
GUI, Y. X., FAN, X. N., WANG, H. M., WANG, G. & CHEN, S. D. 2012 Glyphosate induced cell death through apoptotic and autophagic mechanisms. *Neurotoxicology and Teratology* 34**,** 344-349
GUPTA, A. S. & BARHATE, V. D. 2012. Development of extractive spectrophotometric determination of iron (II) with [N-(O-hydroxy benzylidene) pyridine-2-amine]. *Int. J. Curr. Pharm. Res.,* 4**,** 32-35.
HABEEB, A. & HIRAMOTO, R. 1968. Reaction of proteins with glutaricaldehyde. *Arch. Biochem. Biophys* 126**,** 16-26.
HAGIWARA, H., KAWANO, A., FUJINAMI, T., MATSUMOTO, N., SUNATSUKI, Y., KOJIMA, M. & MIYAMAE, H. 2011. Conformational effect of a spin crossover iron(II) complex: Bis[N-(2-methylimidazol-4-yl)methylidene-2-aminoethyl]propanediamineiron(II) perchlorate. *Inorg. Chim. Acta,* 367**,** 141-150.
HANSARD, S. P. & LANDING, W. M. 2009. Determination of iron(II) in acidified seawater samples by luminol chemiluminescence. *Limnol. Oceanogr.: Methods,* 7**,** 222-234.
HANSELMAN, G., WILKIE 2003. Manure-Borne Estrogens as Potential Environmental Contaminants: A Review. *ENVIRONMENTAL SCIENCE & TECHNOLOGY,* 37 (24)**,** 5171-8.
HE, C., ZHU, W., XU, Y., CHEN, T. & QIAN, X. 2009. Trace mercury(II) detection and separation in serum and water samples using a reusable bifunctional fluorescent sensor. *Anal. Chim. Acta,* 651**,** 227-233.
HE, X., LIU, H., LI, Y., WANG, S., LI, Y., WANG, N., XIAO, J., XU, X. & ZHU, D. 2005. Gold nanoparticle-based fluorometric and colorimetric sensing of copper(II) ions. *Adv. Mater. (Weinheim, Ger.),* 17**,** 2811-2815.
HERING, J. G., CHEN, P.-Y., WILKIE, J. A. & ELIMELECH, M. 1997. Arsenic removal from drinking water during coagulation. *J. Environ. Eng. (N. Y.),* 123**,** 800-807.
HOEBEN, F. J. M., JONKHEIJM, P., MEIJER, E. W. & SCHENNING, A. P. H. J. 2005. About Supramolecular Assemblies of π-Conjugated Systems. *Chem. Rev. (Washington, DC, U. S.),* 105**,** 1491-1546.
HOECKER, H. 2002. Plasma treatment of textile fibers. *Pure Appl. Chem.,* 74**,** 423-427.
HOFFBRAND, A. V. & HERBERT, V. 1999. Nutritional anemias. *Semin. Hematol.,* 36**,** 13-23.
HOPWOOD, D., CALLEN, C. & MCCABE, M. 1970. The reactions between glutaraldehyde and various proteins. An investigation of their kinetics. *Histochem.,* 2**,** 137-150.
HUANG, X.-J., CHEN, P.-C., HUANG, F., OU, Y., CHEN, M.-R. & XU, Z.-K. 2011. Immobilization of Candida rugosa lipase on electrospun cellulose nanofiber membrane. *J. Mol. Catal. B: Enzym.,* 70**,** 95-100.
INSTITUTE, M. 2006. Overview and comparison of conventional water treatment technologies and nano-based technologies.
IRVING H. M. N. H, H. F., T. S. WEST 1981. IUPAC Compendium of Analytical Nomenclature, Definitive Rules. Oxford: Pergamon Press: .
JAIN, L., EL-SAYED , EL-SAYED 2006. Calculated Absorption and Scattering Properties of Gold Nanoparticles of Different Size, Shape, and Composition: Applications in Biological Imaging and Biomedicine. *J. Phys. Chem. B,* 110 (14)**,** 7238–7248.

JAIN, P. K., HUANG, X., EL-SAYED, I. H. & EL-SAYED, M. A. 2007. Review of some interesting surface plasmon resonance-enhanced properties of noble metal nanoparticles and their applications to biosystems. *Plasmonics,* 2**,** 107-118.

JAN, M. R., SHAH, J., MUHAMMAD, M. & ARA, B. 2009. Glyphosate herbicide residue determination in samples of environmental importance using spectrophotometric method. *Journal of Hazardous Materials* 169**,** 742-745.

JANKOWSKI, K., YAO, J., KASIURA, K., JACKOWSKA, A. & SIERADZKA, A. 2005. Multielement determination of heavy metals in water samples by continuous powder introduction microwave-induced plasma atomic emission spectrometry after preconcentration on activated carbon. *Spectrochim. Acta, Part B,* 60B**,** 369-375.

JANS, H. & HUO, Q. 2012. Gold nanoparticle-enabled biological and chemical detection and analysis. *Chemical Society Reviews,* 41**,** 2849-2866.

JIRSAK, O., SANETRNIK, F., LUKAS, D., KOTEK, V., MARTINOVA, L. & CHALOUPEK, J. 2004. *Process and apparatus for producing nanofibers from polymer solution by electrostatic spinning*. Copyright (C) 2011 American Chemical Society (ACS). All Rights Reserved.

JONES, M. M. & VAUGHN, W. K. 1978. HSAB theory and acute metal ion toxicity and detoxification processes. *J. Inorg. Nucl. Chem.,* 40**,** 2081-8.

JONES, M. R., OSBERG, K. D., MACFARLAN, R. J., LANGILLE, M. R. & MIRKIN, C. A. 2011. Templated Techniques for the Synthesis and Assembly of Plasmonic Nanostructures. *Chem. Rev.* , 111 (6)**,** 3736–3827

KARATEPE, A. U., SOYLAK, M. & ELCI, L. 2003. Separation/preconcentration of copper, lead, and iron in natural water samples on chromosorb-105 resin prior to flame atomic absorption spectrometric determinations. *Anal. Lett.,* 36**,** 797-812.

KASPRZAK, K. S., BAL, W. & KARACZYN, A. A. 2003. The role of chromatin damage in nickel-induced carcinogenesis. A review of recent developments. *J. Environ. Monit.,* 5**,** 183-187.

KASRILS, R. 2003. Parliamentary Media Briefing. Minister of Water Affairs and Forestry.

KATTA, P., ALESSANDRO, M., RAMSIER, R. D. & CHASE, G. G. 2004. Continuous electrospinning of aligned polymer nanofibers onto a wire drum collector. *Nano Letters,* 4**,** 2215-2218.

KAZACHENKO, A. S., LEGLER, A. V., PER'YANOVA, O. V. & VSTAVSKAYA, Y. A. 2000. Synthesis and antimicrobial activity of silver complexes with histidine and tryptophan. *Pharmaceutical Chemistry Journal,* 34**,** 257-258.

KEMLO, J. A. & SHEPHERD, T. M. 1977. Quenching of excited singlet states by metal ions. *Chem. Phys. Lett.,* 47**,** 158-62.

KHABNADIDEH, S., REZAEI, Z., KHALAFI-NEZHAD, A., BAHRINAJAFI, R., MOHAMADI, R. & FARROKHROZ, A. A. 2003. Synthesis of N-Alkylated derivatives of imidazole as antibacterial agents. *Bioorganic & Medicinal Chemistry Letters,* 13**,** 2863-2865.

KHAN, N., SONI, L., GUPTA, A., WAKODE, S., WAGH, R. & KASKHEDIKAR, S. 2006. QSAR analysis of N-alkyl imidazole analogues as antibacterial agents. *Indian Journal of Pharmaceutical Sciences,* 68**,** 341-346.

KILINC, A., ONAL, S. & TELEFONCU, A. 2002. Stabilization of papain by modification with phenylalanine content. *Turkish Journal of Chemistry* 26**,** 311-316.

KIRICHENKO, V. F., Y. BUDYKA, A. 2007. *Electrospinning of Micro and Nanofibers: Fundamentals in Separation and Filtration Processes*.

KIRIYAMA, T. & KURODA, R. 1988. Anion-exchange enrichment and spectrophotometric determination of traces of gallium in natural waters. *Fresenius' Z. Anal. Chem.,* 332**,** 338-40.

KLASEN, H. J. 2000. Historical review of the use of silver in the treatment of burns. I. Early uses. *Burns,* 26**,** 117-130.

KLEDZIK, K., ORLOWSKA, M., PATRALSKA, D., GWIAZDA, M., JEZIERSKA, J., PIKUS, S., OSTASZEWSKI, R. & KLONKOWSKI, A. M. 2007. Cu(II) recognition materials: Fluorophores grafted on mesoporous silica supports. *Appl. Surf. Sci.,* 254**,** 441-451.

KLEYI, P., WALMSLEY, R. S., GUNDHLA, I. Z., WALMSLEY, T. A., JAUKA, T. I., DAMES, J., WALKER, R. B., TORTO, N. & TSHENTU, Z. R. 2012. Syntheses, protonation constants and antimicrobial activity of 2-substituted N-alkylimidazole derivatives. *S. Afr. J. Chem.,* 65**,** 231-238.

KLIMANT, I. & WOLFBEIS, O. S. 1995. Oxygen-Sensitive Luminescent Materials Based on Silicone-Soluble Ruthenium Diimine Complexes. *Anal. Chem.,* 67**,** 3160-6.

KLUEH, U., WAGNER, V., KELLY, S., JOHNSON, A. & BRYERS, J. D. 2000. Efficacy of silver-coated fabric to prevent bacterial colonization and subsequent device-based biofilm formation. *Journal of Biomedical Materials Research,* 53**,** 621-631.

KOH, Y. K., CHIU, T. Y., BOOBIS, A., CARTMELL, E., SCRIMSHAW, M. D. & LESTER, J. N. 2008 Treatment and removal strategies for estrogens from wastewater. *Environ Technol.,* 29(3)**,** 245-67.

KOKKINOS, C., ECONOMOU, A., RAPTIS, I. & SPELIOTIS, T. 2008. Disposable mercury-free cell-on-a-chip devices with integrated microfabricated electrodes for the determination of trace nickel(II) by adsorptive stripping voltammetry. *Anal. Chim. Acta,* 622**,** 111-118.

KOLLER, V. J., FURHACKER, M., NERSESYAN, A., MISIK, M., EISENBAUER, M. & KNASMUELLER, S. 2012 Cytotoxic and DNA-damaging properties of glyphosate and Roundup in human-derived buccal epithelial cells. *Archives of Toxicology*.

KOLUSHEVA, S., SHAHAL, T. & JELINEK, R. 2000. Cation-Selective Color Sensors Composed of Ionophore-Phospholipid-Polydiacetylene Mixed Vesicles. *J. Am. Chem. Soc.,* 122**,** 776-780.

KOOLS, S. A. E., VAN ROOVERT, M., VAN GESTEL, C. A. M. & N.M, V. S. 2005. Glyphosate degradation as a soil health indicator for heavy metal polluted soils. *Soil Biology & Biochemistry* 37**,** 1303-1307.

KOWALEWSKI, T. A., BŁOŃSKI, S. & BARRAL, S. 2005. Experiments and modelling of electrospinning process. *Bulletin of the Polish Academy of Sciences: Technical Sciences,* 53**,** 385-394.

KREIBIG, U. & VOLLMER, M. 1995. *Optical Properties of Metal Clusters. (Springer Series in Materials Science 25)*, Springer.

KRIEGEL, C., ARRECHI, A., KIT, K., MCCLEMENTS, D. J. & WEISS, J. 2008. Fabrication, Functionalization, and Application of Electrospun Biopolymer Nanofibers. *Critical Reviews in Food Science and Nutrition,* 48**,** 775-797.

KRUSE, L. I., KAISER, C., DEWOLF, W. E., FINKELSTEIN, J. A., FRAZEE, J. S., HILBERT, E. L., ROSS, S. T., FLAIM, K. E. & SAWYER, J. L. 1990. Some benzyl-substituted imidazoles, triazoles, tetrazoles, pyridinethiones, and structural relatives as multisubstrate inhibitors of dopamine β-hydroxylase. 4. Structure-activity relationships at the copper binding site. *Journal of Medicinal Chemistry,* 33**,** 781-789.

KUENSTL, L., GRIESEL, S., PRANGE, A. & GOESSLER, W. 2009. Arsenic speciation in bodily fluids of harbor seals (Phoca vitulina) and harbor porpoises (Phocoena phocoena). *Environ. Chem.,* 6**,** 319-327.

LAKOWICZ, J. R. 1983. *Principles of Fluorescence Spectroscopy*, Plenum Press.

LANSDOWN, A. B. 2002. Silver. I: Its antibacterial properties and mechanism of action. *Journal of wound care,* 11**,** 125-130.

LEE, C. H. L., SHIH, C. P., HSU, K. H., HUNG, D. Z. & LIN, C. C. 2008a. The early prognostic factots of glyphosate-surfactant intoxication. *American Journal of Emergency Medicine* 26**,** 275-281.

LEE, S.-H., KUMAR, J. & TRIPATHY, S. K. 2000. Thin Film Optical Sensors Employing Polyelectrolyte Assembly. *Langmuir,* 16**,** 10482-10489.

LEE, S. J., BAE, D. R., HAN, W. S., LEE, S. S. & JUNG, J. H. 2008b. Different morphological organic-inorganic hybrid nanomaterials as fluorescent chemosensors and adsorbents for CuII ions. *Eur. J. Inorg. Chem.***,** 1559-1564.

LEYDEN, D. E., PATTERSON, T. A. & ALBERTS, J. J. 1975. Preconcentration and x-ray fluorescence determination of copper, nickel, and zinc in sea water. *Anal. Chem.,* 47**,** 733-5.

LI, L. & HSIEH, Y.-L. 2005. Ultra-fine polyelectrolyte fibers from electrospinning of poly(acrylic acid). *Polymer,* 46**,** 5133-5139.

LI, L. N., LI, N. B. & LUO, H. Q. 2006. A new chemiluminescence method for the determination of nickel ion. *Spectrochim. Acta, Part A,* 64A**,** 391-396.

LI, Q., ZHAO, X., JIANG, K. & LIU, G. 2007. Study of spectrophotometric method for determination of trace copper after the separation and enrichment with solid phase extractant-microcrystalline phenolphthalein. *Chin. Sci. Bull.,* 52**,** 65-70.

LI, S., TAO, S., WANG, F., HONG, J. & WEI, X. 2010a. Chemiluminescence reactions of luminol system catalyzed by nanoparticles of a gold/silver alloy. *Microchim. Acta,* 169**,** 73-78.

LI, W. R., XIE, X. B., SHI, Q. S., ZENG, H. Y., OU-YANG, Y. S. & CHEN, Y. B. 2010b. Antibacterial activity and mechanism of silver nanoparticles on Escherichia coli. *Applied Microbiology and Biotechnology,* 85**,** 1115-1122.

LIEU, P. T., HEISKALA, M., PETERSON, P. A. & YANG, Y. 2001. The roles of iron in health and disease. *Mol. Aspects Med.,* 22**,** 1-87.

LIN, T. F. & WU, J. K. 2001. Adsorption of Arsenite and Arsenate within Activated Alumina Grains: Equilibrium and Kinetics. *Water Res.,* 35**,** 2049-2057.
LOBNIK, A., OEHME, I., MURKOVIC, I. & WOLFBEIS, O. S. 1998. pH optical sensors based on sol-gels. Chemical doping versus covalent immobilization. *Anal. Chim. Acta,* 367**,** 159-165.
LOK, C. N., HO, C. M., CHEN, R., HE, Q. Y., YU, W. Y., SUN, H., TAM, P. K. H., CHIU, J. F. & CHE, C. M. 2007. Silver nanoparticles: Partial oxidation and antibacterial activities. *Journal of Biological Inorganic Chemistry,* 12**,** 527-534.
MA, S., HILL, J. O. & HENG, S. 1992. A thermal analysis study of the influence of exchangeable cations on the pyrolysis of Victorian brown coal. *Thermochim. Acta,* 197**,** 79-89.
MA, Z., MASAYA, K. & RAMAKRISHNA, S. 2006. Immobilization of Cibacron blue F3GA on electrospun polysulphone ultra-fine fiber surfaces towards developing an affinity membrane for albumin adsorption. *Journal of Membrane Science,* 282**,** 237-244.
MAHMOUD, W. H. 2001. Iron ion-selective electrodes for direct potentiometry and potentiotitrimetry in pharmaceuticals. *Anal. Chim. Acta,* 436**,** 199-206.
MANN, R. M. & BIDWELL, J. R. 1999. The toxicity of glyphosate and several glyphosate formulations to four species of southwestern Australian frogs. *Archives of Environmental Contamination and Toxicology* 36**,** 193-199.
MARINOV, I., GABROVSKA, K., VELICHKOVA, J. & GODJEVARGOVA, T. 2009. Immobilisation of acetylcholinesterase on nanostructure polyacrylonitrile membrane. *International Journal of Biological Molecules* 44**,** 338-345.
MARTIN, J. H. & FITZWATER, S. E. 1988. Iron deficiency limits phytoplankton growth in the north-east Pacific subarctic. *Nature (London),* 331**,** 341-3.
MARTIN, J. H., GORDON, R. M. & FITZWATER, S. E. 1990. Iron in Antarctic waters. *Nature (London),* 345**,** 156-8.
MAYER, A. B. R. 2001. Colloidal metal nanoparticles dispersed in amphiphilic polymers. *Polymers for Advanced Technologies* 12**,** 96-106.
MCCANN, M., COYLE, B., BRIODY, J., BASS, F., O'GORMAN, N., DEVEREUX, M., KAVANAGH, K. & MCKEE, V. 2003. Synthesis and antimicrobial activity of (Z)-3-(1H-imidazol-1-yl)-2-phenylpropenenitrile and its metal complexes: X-ray crystal structures of the Zn(II) and Ag(I) complexes. *Polyhedron,* 22**,** 1595-1601.
MCDONAGH, C., MACCRAITH, B. D. & MCEVOY, A. K. 1998. Tailoring of Sol-Gel Films for Optical Sensing of Oxygen in Gas and Aqueous Phase. *Anal. Chem.,* 70**,** 45-50.
MELAIYE, A., SUN, Z., HINDI, K., MILSTED, A., ELY, D., RENEKER, D. H., TESSIER, C. A. & YOUNGS, W. J. 2005. Silver(I)−Imidazole Cyclophane gem-Diol Complexes Encapsulated by Electrospun Tecophilic Nanofibers: Formation of Nanosilver Particles and Antimicrobial Activity. *Journal of the American Chemical Society,* 127**,** 2285-2291.
MENG, X., KORFIATIS, G. P., JING, C. & CHRISTODOULATOS, C. 2001. Redox transformations of arsenic and iron in water treatment sludge during aging and TCLP extraction. *Environ Sci Technol,* 35**,** 3476-81.
MILLS, A., LEPRE, A., THEOBALD, B. R. C., SLADE, E. & MURRER, B. A. 1997. Use of Luminescent Gold Compounds in the Design of Thin-Film Oxygen Sensors. *Anal. Chem.,* 69**,** 2842-2847.
MIN, J. L., BARRETT, A., WATTS, T., PETTERSSON, F. H., LOCKSTONE, H. E., LINDGREN, C. M., TAYLOR, J. M., ALLEN, M., ZONDERVAN, K. T. & MCCARTHY, M. I. 2010. Variability of gene expression profiles in human blood and lymphoblastoid cell lines. *BMC Genomics* 11**,** 1-14.
MOHAN, D. & PITTMAN, C. U. 2007. Arsenic removal from water/wastewater using adsorbents. A critical review. *J. Hazard. Mater.,* 142**,** 1-53.
MOHR, G. J. & WOLFBEIS, O. S. 1994. Optical sensors for a wide pH range based on azo dyes immobilized on a novel support. *Anal. Chim. Acta,* 292**,** 41-8.
MONSAN, P. 1978. Influence of the conditions of trypsin immobilisation onto Spherosil on coupling efficiency. *European Journal of Applied Microbiology and Biotechnology,* 5**,** 1-11.
MONTGOMERY, M. A. & ELIMELECH, M. 2007. Water and Sanitation in Developing Countries: Including Health in the Equation. *Environ. Sci. Technol.,* 41**,** 16-24.
MORI, M., UYAMA, Y. & IKADA, Y. 1994. Surface modification of polyethylene fiber by graft polymerization. *J. Polym. Sci., Part A: Polym. Chem.,* 32**,** 1683-90.
MORTATTI, J., KRUG, F. J., PESSENDA, L. C. R., ZAGATTO, E. A. G. & JOERGENSEN, S. S. 1982. Determination of iron in natural waters and plant material with 1,10-phenanthroline by flow injection analysis. *Analyst (London),* 107**,** 659-63.

MORTON, W. J. 1902. *Method of dispersing fluids*.
MULROONEY, S. B. & HAUSINGER, R. P. 2003. Nickel uptake and utilization by microorganisms. *FEMS Microbiol. Rev.,* 27**,** 239-261.
MULVANEY, P. 1996. Surface Plasmon Spectroscopy of Nanosized Metal Particles. *Langmuir,* 12**,** 788-800.
MUÑOZ-BONILLA, A. & FERNÁNDEZ-GARCÍA, M. 2012. Polymeric materials with antimicrobial activity. *Progress in Polymer Science (Oxford),* 37**,** 281-339.
NAM, Y. S., YOON, J. J., LEE, J. G. & PARK, T. G. 1999. Adhesion behaviors of hepatocytes cultured onto biodegradable polymer surface modified by alkali hydrolysis process. *J. Biomater. Sci., Polym. Ed.,* 10**,** 1145-1158.
NANOSTATICS. 2007. *Company Bronchure* [Online]. Available: www.nanostatics.com.
NANOWERK 2007. Nanotechnology pesticide filter debuts in India.
NAZEERUDDIN, M. K., DI, C. D., HUMPHRY-BAKER, R. & GRATZEL, M. 2006. Highly selective and reversible optical, colorimetric, and electrochemical detection of mercury(II) by amphiphilic ruthenium complexes anchored onto mesoporous oxide films. *Adv. Funct. Mater.,* 16**,** 189-194.
NEMATI KHARAT, A., BAKHODA, A., FOROUTANNEJAD, S. & FOROUTANNEJAD, C. 2011. Molecular Structure and Antimicrobial Activity of a Luminescent Dinuclear Silver(I) Complex of Phenyl-bis(2-pyridyl)phosphine. *Zeitschrift fur Anorganische und Allgemeine Chemie,* 637**,** 2260-2264.
NEMEC, A. A., LEIKAUF, G. D., PITT, B. R., WASSERLOOS, K. J. & BARCHOWSKY, A. 2009. Nickel mobilizes intracellular zinc to induce metallothionein in human airway epithelial cells. *Am. J. Respir. Cell Mol. Biol.,* 41**,** 69-75.
NOMIYA, K., TSUDA, K., SUDOH, T. & ODA, M. 1997. Ag(I)-N bond-containing compound showing wide spectra in effective antimicrobial activities: Polymeric silver(I) imidazolate. *Journal of Inorganic Biochemistry,* 68**,** 39-44.
OBERHAUSEN, K. J., RICHARDSON, J. F., BUCHANAN, R. M. & PIERCE, W. 1989. Synthesis, structure and properties of a N3 tridentate bis-imidazolyl ligand with copper(II). *Polyhedron,* 8**,** 659-668.
OFOMAJA, E. A., UNUABONAH, I. E. & OLADOJA, N. A. 2005. Removal of lead from aqueous solution by palm kernel fibre. *S. Afr. J. Chem.,* 58**,** 127-130.
OGAWA, K., GUO, F. & SCHANZE, K. S. 2009. Phosphorescence quenching of a platinum acetylide polymer by transition metal ions. *J. Photochem. Photobiol., A,* 207**,** 79-85.
OISHI, M. 2010. Removal of dissolved estrogen in sewage effluents by β-cyclodextrin polymer. *Sci Total Environ. ,* 409**,** 112-5.
OKUDA, K., URABE, I., YAMADA, Y., OKADA, H. & PAPAVASSILIOU, G. 1991. Reaction of glutaraldehyde with amino and thiol compounds. . *Journal of Fermentation and Bioengineering* 71**,** 100-105.
PAGNANELLI, F., PAPINI, M. P., TORO, L., TRIFONI, M. & VEGLIO, F. 2000. Biosorption of Metal Ions on Arthrobacter sp.: Biomass Characterization and Biosorption Modeling. *Environ. Sci. Technol.,* 34**,** 2773-2778.
PAPAVASSILIOU, G. C. 1976. Surface plasmons in small gold-silver alloy particles. *J. Phys. F,* 6**,** L103-L105.
PEARSON, R. G. 1963. Hard and soft acids and bases. *J. Am. Chem. Soc.,* 85**,** 3533-9.
PENG, X., DU, J., FAN, J., WANG, J., WU, Y., ZHAO, J., SUN, S. & XU, T. 2007. A Selective Fluorescent Sensor for Imaging Cd2+ in Living Cells. *J. Am. Chem. Soc.,* 129**,** 1500-1501.
PETRIK, S. & MALY, M. 2010. Production nozzle-less electrospinning nanofiber technology. *Mater. Res. Soc. Symp. Proc.,* 1240E**,** No pp. given, Paper #: 1240-WW03-07.
PITARCH, A., DÍEZ-OREJAS, R., MOLERO, G., PARDO, M., SÁNCHEZ, M., GIL, C. & NOMBELA, C. 2001. Analysis of the serologic response to systemic Candida albicans infection in a murine model. *Proteomics,* 1**,** 550-559.
POKROVSKI, G. S., KARA, S. & ROUX, J. 2002. Stability and solubility of arsenopyrite, FeAsS, in crustal fluids. *Geochim. Cosmochim. Acta,* 66**,** 2361-2378.
POLETTA, G. L., LARRIERA, A., KLEINSORGE, E. & MUDRY, M. D. 2009. Genotoxicity of the herbicide formulation roundup (glyphosate) in broad-snouted caiman (Caiman latirostris) evidenced by the comet assay and the micronucleas test. *Mutation Research* 672**,** 95-102.
PONGPIACHAN, S. 2009. Application of cloud point extraction for the determination of pyrene in natural water. *Southeast Asian J Trop Med Public Health* 40**,** 392-400.
PRABHAKARAN, D., NANJO, H. & MATSUNAGA, H. 2007. Naked eye sensor on polyvinyl chloride platform of chromo-ionophore molecular assemblies: A smart way for the colorimetric sensing of toxic metal ions. *Anal. Chim. Acta,* 601**,** 108-117.

PUGIN, L., ULEVITCH, R. J. & TOBIAS, P. S. 1995. Tumor necrosis factor-alpha and interleukin-1 beta mediate human endothelial cell activation in blood at low endotoxin concentrations. *Journal of Inflammatory* 45**,** 49-55.

QI, X., JUN, E. J., XU, L., KIM, S.-J., HONG, J. S. J., YOON, Y. J. & YOON, J. 2006. New BODIPY Derivatives as OFF-ON Fluorescent Chemosensor and Fluorescent Chemodosimeter for Cu2+: Cooperative Selectivity Enhancement toward Cu2+. *J. Org. Chem.,* 71**,** 2881-2884.

QIN, W., ZHANG, Z. J. & WANG, F. C. 1998. Chemiluminescence flow system for the determination of Fe(II) and Fe(III) in water. *Fresenius' J. Anal. Chem.,* 360**,** 130-132.

QUAFF, A. R. & ASHHAR, M. M. 2005. Removal of arsenic(III) by activated tea waste and activated charcoal: a comparative study. *J. Indian Water Works Assoc.,* 37**,** 63-69.

RADHESHKUMAR, C. & MÜNSTEDT, H. 2006. Antimicrobial polymers from polypropylene/silver composites—Ag+ release measured by anode stripping voltammetry. *Reactive and Functional Polymers,* 66**,** 780-788.

RAI, M., YADAV, A. & GADE, A. 2009. Silver nanoparticles as a new generation of antimicrobials. *Biotechnology Advances,* 27**,** 76-83.

RAJENDRAPRASAD, N. & BASAVAIAH, K. 2010. Highly sensitive spectrophotometric determination of olanzapine using cerium(IV) and iron(II) complexes of 1,10-phenanthroline and 2,2'-bipyridyl. *J. Anal. Chem.,* 65**,** 482-488.

RAMAKRISHNA, S., FUJIHARA, K., TEO, W.-E., YONG, T., MA, Z. & RAMASESHAN, R. 2006. Electrospun nanofibers: solving global issues. *Mater. Today (Oxford, U. K.),* 9**,** 40.

RAYLEIGH 1882. XX. On the equilibrium of liquid conducting masses charged with electricity. *Philosophical Magazine Series 5,* 14**,** 184-186.

REICHERT, A., NAGY, J. O., SPEVAK, W. & CHARYCH, D. 1995. Polydiacetylene Liposomes Functionalized with Sialic Acid Bind and Colorimetrically Detect Influenza Virus. *J. Am. Chem. Soc.,* 117**,** 829-30.

REN, F., MENG, J., WU, Y., HONG, L., XIA, Q. & LUO, J. 2009. Determination of arsenic speciation in environmental samples by flow injection hydride generation atomic absorption spectrometry. *Yejin Fenxi,* 29**,** 19-23.

RENEKER, D. H. & CHUN, I. 1996. Nanometer diameter fibers of polymer, produced by electrospinning. *Nanotechnology,* 7**,** 216-223.

RENEKER, D. H., YARIN, A. L., FONG, H. & KOOMBHONGSE, S. 2000. Bending instability of electrically charged liquid jets of polymer solutions in electrospinning. *J. Appl. Phys.,* 87**,** 4531-4547.

RESSALAN, S. & IYER, C. S. P. 2004. Review of spectrofluorimetric methods for the determination of copper, nickel and zinc. *Rev. Anal. Chem.,* 23**,** 159-232.

REYNOLDS, A. J., HAINES, A. H. & RUSSELL, D. A. 2006. Gold Glyconanoparticles for Mimics and Measurement of Metal Ion-Mediated Carbohydrate-Carbohydrate Interactions. *Langmuir,* 22**,** 1156-1163.

RICHARD, S., MOSLEMI, S., SIPAHUTAR, H., BENACHOUR, N. & G.E., S. 2005. Differential effects of glyphosate and Roundup on human placental cells and aromatase. *Environmental Health Perspectives* 113**,** 716-720.

RILEY, J. P. & CHESTER, R. 1971. *Introduction of Marine Chemistry*, Academic.

ROE, A. M. 1963. The thermal condensation of imidazoles with carbonyl compounds. *Journal of the Chemical Society (Resumed)***,** 2189-2194.

ROSI, N. L. & MIRKIN, C. A. 2005. Nanostructures in Biodiagnostics. *Chem. Rev. (Washington, DC, U. S.),* 105**,** 1547-1562.

ROSTOM, S. A. F., ASHOUR, H. M. A., RAZIK, H. A. A. E., FATTAH, A. E. F. H. A. E. & EL-DIN, N. N. 2009. Azole antimicrobial pharmacophore-based tetrazoles: Synthesis and biological evaluation as potential antimicrobial and anticonvulsant agents. *Bioorganic & Medicinal Chemistry,* 17**,** 2410-2422.

ROWAN, R., TALLON, T., SHEAHAN, A. M., CURRAN, R., MCCANN, M., KAVANAGH, K., DEVEREUX, M. & MCKEE, V. 2006. 'Silver bullets' in antimicrobial chemotherapy: Synthesis, characterisation and biological screening of some new Ag(I)-containing imidazole complexes. *Polyhedron,* 25**,** 1771-1778.

RUAN, B., TIAN, Y., ZHOU, H., WU, J., LIU, Z., ZHU, C., YANG, J. & ZHU, H. 2009. Synthesis, crystal structure and in vitro antibacterial activity of two novel silver(I) complexes. *Journal of Organometallic Chemistry,* 694**,** 2883-2887.

RUCKSTEIN, E. & NAGARAJAN, R. 1975. Critical micelle concentration. Transition point for micellar size distribution *Journal of Physical chemistry,* 79**,** 2622-2626.

RUEDAS-RAMA, M. J. & HALL, E. A. H. 2008. Azamacrocycle Activated Quantum Dot for Zinc Ion Detection. *Anal. Chem. (Washington, DC, U. S.),* 80**,** 8260-8268.
RURACK, K. 2001. Flipping the light switch 'ON' - the design of sensor molecules that show cation-induced fluorescence enhancement with heavy and transition metal ions. *Spectrochim. Acta, Part A,* 57A**,** 2161-2195.
SABAA, M. W., MOHAMED, N. A., MOHAMED, R. R., KHALIL, N. M. & ABD, E. L. S. M. 2010. Synthesis, characterization and antimicrobial activity of poly (N-vinyl imidazole) grafted carboxymethyl chitosan. *Carbohydr. Polym.,* 79**,** 998-1005.
SAFAVI, A., ABDOLLAHI, H. & HORMOZI, N. M. R. 2002. Simultaneous kinetic determination of Fe(III) and Fe(II) by H-point standard addition method. *Talanta,* 56**,** 699-704.
SAHIN, F., DEMIRAL, G. & TUMTURK, H. 2005. A novel matrix for the immobilisation of acetylcholinesterase. *International Journal of Biological Macromolecules* 37**,** 148-153.
SALAME, P., ZEMAN, A. & MULHAUSER, F. 2011. IAEA activities on application of nuclear techniques in development and characterization of materials for hydrogen economy. *Adv. Mater. Res. (Durnten-Zurich, Switz.),* 324**,** 461-464.
SALINS, L. L. E., GOLDSMITH, E. S., ENSOR, C. M. & DAUNERT, S. 2002. A fluorescence-based sensing system for the environmental monitoring of nickel using the nickel binding protein from Escherichia coli. *Anal. Bioanal. Chem.,* 372**,** 174-180.
SAMANT, B. S. & SUKHTHANKAR, M. G. 2011. Compounds containing 2-substituted imidazole ring for treatment against human African trypanosomiasis. *Bioorganic & Medicinal Chemistry Letters,* 21**,** 1015-1018.
SAMSUDIN, S. A., HASSAN, A., MOKHTAR, M. & S., J. S. M. 2006. Chemical Resistance Evaluation of Polystyrene/Polypropylene Blends: Effect of Blend Compositions and SEBS Content. *Malaysian Polymer Journal (MPJ),* 1**,** 11-24.
SAQUING, C. D., MANASCO, J. L. & KHAN, S. A. 2009. Electrospun Nanoparticle–Nanofiber Composites via a One-Step Synthesis. *Small* 5**,** 944 - 951.
SARKAR, K., DHARA, K., NANDI, M., ROY, P., BHAUMIK, A. & BANERJEE, P. 2009. Selective zinc(II)-ion fluorescence sensing by a functionalized mesoporous material covalently grafted with a fluorescent chromophore and consequent biological applications. *Adv. Funct. Mater.,* 19**,** 223-234.
SAYO, K., DEKI, S. & HAYASHI, S. 1999. A novel method of preparing nano-sized gold and palladium particles dispersed in composites that uses the thermal relaxation technique. *The European Physical Journal D - Atomic, Molecular, Optical and Plasma Physics,* 9**,** 429-432.
SCHWARZENBACH, G. & SCHELLENBERG, M. 1965. Complex chemistry of the methylmercury cation. *Helv. Chim. Acta,* 48**,** 28-46.
SCOTT, A. & O'REILLY, A. Catalytic metal ion fixation onto activated carbon surface through microbial biosorption. 1991. Miner. Met. Mater. Soc., 263-73.
SENGONUL, M., RUZICKA, J., ATTYGALLE, A. B. & LIBERA, M. 2007. Surface modification of protein nanocontainers and their self-directing character in polymer blends. *Polymer,* 48**,** 3632-3640.
SHARMA, S., GANGAL, S. & RAUF, A. 2009. Convenient one-pot synthesis of novel 2-substituted benzimidazoles, tetrahydrobenzimidazoles and imidazoles and evaluation of their in vitro antibacterial and antifungal activities. *European Journal of Medicinal Chemistry,* 44**,** 1751-1757.
SHEEHAN, D. J., HITCHCOCK, C. A. & SIBLEY, C. M. 1999. Current and emerging azole antifungal agents. *Clinical Microbiology Reviews,* 12**,** 40-79.
SHIN, S. & JANG, J. 2007. Thiol containing polymer encapsulated magnetic nanoparticles as reusable and efficiently separable adsorbent for heavy metal ions. *Chem. Commun. (Cambridge, U. K.)***,** 4230-4232.
SHIOWATANA, J., BENYATIANB, K. & SIRIPINYANOND, A. 2000. Determination of Cd, Co, Hg, and Ni in seawater after enrichment on activated carbon by slurry sampling electrothermal AAS. *At. Spectrosc.,* 21**,** 179-186.
SIGEL, A., SIGEL, H., SIGEL, R. K. O. & EDITORS 2007. *Nickel and it's Surprising Impact in Nature. [In: Met. Ions Life Sci., 2007; 2]*, John Wiley & Sons Ltd.
SILL, T. J. & VON, R. H. A. 2008. Electrospinning: Applications in drug delivery and tissue engineering. *Biomaterials,* 29**,** 1989-2006.
SILVESTRY-RODRIGUEZ, N., SICAIROS-RUELAS, E. E., GERBA, C. P. & BRIGHT, K. R. 2007. Silver as a disinfectant.
SINGH, A., FLOUNDERS, A., VOLPONI, J., ASHLEY, C., WALLY, K. & SHOENIGER, J. 1999. Development of sensors for direct detection of organophosphates. Part I: Immobilisation

characterisation and stabilisation of acetylcholinesterase and organophosphate hydrolase on silica supports. *Biosensors and Bioelectronics* 14**,** 703-713.
SINGH, T. S. & PANT, K. K. 2004. Equilibrium, kinetics and thermodynamic studies for adsorption of As(III) on activated alumina. *Sep. Purif. Technol.,* 36**,** 139-147.
SMEDLEY, P. L. & KINNIBURGH, D. G. 2002. A review of the source, behaviour and distribution of arsenic in natural waters. *Appl. Geochem.,* 17**,** 517-568.
SMIT, E., BUTTNER, U. & SANDERSON, R. D. 2005. Continuous yarns from electrospun fibers. *Polymer,* 46**,** 2419-2423.
SMITH, J. A., DAS, A., RAY, S. K. & N.L., B. 2012. Review: role of pro-inflammatory cytokines released from microglia in neurodegenerative diseases. *Brain Research Bulletin* 87**,** 10-20.
SMITH, W. F. 2003. *Foundation of Materials Science Engineering, 3rd Edition*, McGraw-Hill.
STAFILOV, T. 2000. Determination of trace elements in minerals by electrothermal atomic absorption spectrometry. *Spectrochim. Acta, Part B,* 55B**,** 893-906.
STOILOVA, O., MANOLOVA, N., GABROVSKA, K., MARINOV, I., GODJEVARGOVA, T., MITA, D. G. & RASHKOV, I. 2010. Electrospun Polyacrylonitrile Nanofibrous Membranes Tailored for Acetylcholinesterase Immobilization. *Journal of Bioactive and Compatible Polymers,* 25**,** 40-57.
STOILOVO, O., MANOLOVA, N., GABROVSKA, K., MARINOV, I., GODJEVARGOVA, T., MITA, D. & RASHKOV, I. 2010. Electrospun polyacrylonitrilenanofibrous membranes tailored for acetylcholinesterase immobilization. *J. Bioact. Compat,* 25**,** 40-57.
STOZHKO, N. Y., MOROSANOVA, E. I., KOLYADINA, L. I. & FOMINA, S. V. 2005. Determination of iron(II) and iron(III) in wine by inverse voltammetry. *Zavod. Lab., Diagn. Mater.,* 71**,** 14-18.
SUN, Y., ZENG, X. & BAI, L. 2011. Adsorption of arsenate from aqueous solution by Mg/Al layered double oxide. *Huanjing Kexue Xuebao,* 31**,** 1377-1385.
SUNDARAY, B., SUBRAMANIAN, V., NATARAJAN, T. S., XIANG, R.-Z., CHANG, C.-C. & FANN, W.-S. 2004. Electrospinning of continuous aligned polymer fibers. *Appl. Phys. Lett.,* 84**,** 1222-1224.
TABRIZI, A. B. 2006. A cloud point extraction-spectrofluorimetric method for determination of thiamine in urine. *Bull. Korean. Chem. Soc,* 27**,** 1604-1608.
TAKARA, E. A., PASINI-CABELLO, S. D., CERUTTI, S., GASQUEZ, J. A. & MARTINEZ, L. D. 2005. On-line preconcentration/determination of copper in parenteral solutions using activated carbon by inductively coupled plasma optical emission spectrometry. *J. Pharm. Biomed. Anal.,* 39**,** 735-739.
TAN, K. & OBENDORF, S. K. 2007. Fabrication and evaluation of electrospun nanofibrous antimicrobial nylon 6 membranes. *Journal of Membrane Science,* 305**,** 287-298.
TAVALLALI, H. & NIKE, E. 2011. A simple and selective sensor for determination of iron(II) in drug samples based on paptode. *Asian J. Biochem. Pharm. Res.,* 1**,** 91-97.
TAYLOR, G. 1964. Disintegration of Water Drops in an Electric Field. *Proceedings of the Royal Society of London. Series A, Mathematical and Physical Sciences,* 280**,** 383-397.
TAYLOR, G. 1969. Electrically Driven Jets. *Proceedings of the Royal Society of London. A. Mathematical and Physical Sciences,* 313**,** 453-475.
TAYLOR, S. R. & MCLENNAN, S. M. 1985. *The Continental Crust. Its Composition and Evolution*, Blackwell Scientific.
TEO, W. E. & RAMAKRISHNA, S. 2006. A review on electrospinning design and nanofibre assemblies. *Nanotechnology,* 17**,** R89-R106.
THOMAS, G. 2007. Medicinal Chemistry: An introduction. *John Wiley & Sons, Ltd*.
TODA, K., OHBA, T., TAKAKI, M., KARTHIKEYAN, S., HIRATA, S. & DASGUPTA, P. K. 2005. Speciation-capable field instrument for the measurement of arsenite and arsenate in water. *Anal Chem,* 77**,** 4765-73.
TOLAYMAT, T. M., EL, B. A. M., GENAIDY, A., SCHECKEL, K. G., LUXTON, T. P. & SUIDAN, M. 2010. An evidence-based environmental perspective of manufactured silver nanoparticle in syntheses and applications: A systematic review and critical appraisal of peer-reviewed scientific papers. *Sci. Total Environ.,* 408**,** 999-1006.
TONELLO, P. S., ROSA, A. H., ABREU, C. H. & MENEGARIO, A. A. 2007. Use of diffusive gradients in thin films and tangential flow ultrafiltration for fractionation of Al(III) and Cu(II) in organic-rich river waters. *Anal. Chim. Acta,* 598**,** 162-168.
TOPTEC. 2011. *Company Bronchure* [Online]. Available: www.toptec.co.kr.
TORIGOE, K., NAKAJIMA, Y. & ESUMI, K. 1993. Preparation and characterization of colloidal silver-platinum alloys. *J. Phys. Chem.,* 97**,** 8304-9.

UNEP/GRID-ARENDAL. 2008. *UNITED NATIONS ENVIRONMENTAL PROGRAMME* [Online]. Available:http://www.grida.no/graphicslib/detail/areas-of-physical-and-economic-water-scarcity_1570.

VALLIANT, F., MILLAN, A., MILLAN, P., DORNIER, M., DECLOUX, M. & REYNES, M. 2000. Co-immobilized pectinlyase and endocellulase on chitin and nylon supports. *Process Biochemistry* 35**,** 989-996.

VAN, H. D. L. & ZUKOSKI, C. F. 1998. Formation Mechanisms and Aggregation Behavior of Borohydride Reduced Silver Particles. *Langmuir,* 14**,** 7034-7046.

VARNES, A. W., DODSON, R. B. & WEHRY, E. L. 1972. Interactions of transition-metal ions with photoexcited states of flavines. Fluorescence quenching studies. *J. Amer. Chem. Soc.,* 94**,** 946-50.

VOSBURGH, W. C. & COOPER, G. R. 1941. Complex ions. I. The identification of complex ions in solution by spectrophotometric measurements. *J. Am. Chem. Soc.,* 63**,** 437-42.

WAN, L.-S., WU, J. & XU, Z.-K. 2006. Porphyrinated Nanofibers via Copolymerization and Electrospinning. *Macromolecular Rapid Communications,* 27**,** 1533-1538.

WANG, M. 2009. Gold nanoparticle probes. *Coordination Chemistry Reviews* 253**,** 1607–1618.

WANG, X., CHEN, TANG 2011. Simultaneous determination of three naturally occurring estrogens in environmental waters by high-performance liquid chromatography. *Journal of Separation Science,* 34**,** 2371-5.

WANG, X., DREW, C., LEE, S.-H., SENECAL, K. J., KUMAR, J. & SAMUELSON, L. A. 2002. Electrospun Nanofibrous Membranes for Highly Sensitive Optical Sensors. *Nano Lett.,* 2**,** 1273-1275.

WANG, Y., LI, Y., SUN, G., ZHANG, G., LIU, H., DU, J., YANG, S., BAI, J. & YANG, Q. 2007. Fabrication of Au/PVP nanofiber composites by electrospinning. *J. Appl. Polym. Sci.,* 105**,** 3618-3622.

WANG, Y., QIAN, G., XIAO, Z., WANG, H., LONG, L., WANG, H., LI, Z. & LIU, X. 2010. Synthesis and characterisation of anthracene-based fluorophore and its interactions with selected metal ions. *Inorg. Chim. Acta,* 363**,** 2325-2332.

WANG, Z., WAN, L., LIU, Z., HUANG, X. & XU, Z. 2009. Enzyme immobilization on electrospun polymer nanofibers: An overview. *Journal of Molecular Catalysis B: Enzymatic,* 56**,** 189-195.

WATKIN, R. W., HARPER, L. V., VERNALLIS, A. B., LANG, S., LAMBERT, P. A., RANASINGHE, A. M. & ELLIOTT, T. S. J. 2007. Pro-inflammatory cytokines IL-&, TNFα, IL-1β, procalcitonin, lipopolysaccharide binding protein and c-reactive protein in infective endocarditis. *Journal of Infection* 5**,** 220-225.

WATKINS, L. R., MAIER, S. F. & GOEHLER, L. E. 1995. Review article: immune activation: the role of pro-inflammatory cytokines in inflammation, illness responses and pathological pain states. *Pain* 63**,** 289-302.

WHITE, T. C., MARR, K. A. & BOWDEN, R. A. 1998. Clinical, cellular, and molecular factors that contribute to antifungal drug resistance. *Clinical Microbiology Reviews,* 11**,** 382-402.

WILLIAMS, F., CHARLTON, C., DEBLAQUIERE, G., MUTCH, E., KELLY, S. & BLAIN, P. 1997. The effects of multiple low dose of organophosphate on target enzymes in brain and diaphragm in the mouse. *Human & Experimental Toxicology* 16**,** 67-71.

WOOLLEY, D. W. 1944. Some biological effects produced by benzimidazole and their reversal by purines. *Journal of Biological Chemistry,* 152**,** 225-232.

WU, Y. & CLARK, R. L. 2008. Electrohydrodynamic atomization: a versatile process for preparing materials for biomedical applications. *J Biomater Sci Polym Ed,* 19**,** 573-601.

XAVIER, M. P., GARCIA-FRESNADILLO, D., MORENO-BONDI, M. C. & ORELLANA, G. 1998. Oxygen Sensing in Nonaqueous Media Using Porous Glass with Covalently Bound Luminescent Ru(II) Complexes. *Anal. Chem.,* 70**,** 5184-5189.

XU, J., CHE, P. & MA, Y. 1996a. More sensitive way to determine iron using an iron(II)-1,10-phenanthroline complex and capillary electrophoresis. *J Chromatogr A,* 749**,** 287-94.

XU, W., KNEAS, K. A., DEMAS, J. N. & DEGRAFF, B. A. 1996b. Oxygen Sensors Based on Luminescence Quenching of Metal Complexes: Osmium Complexes Suitable for Laser Diode Excitation. *Anal. Chem.,* 68**,** 2605-2609.

YAO, J., DOU, W., QIN, W. & LIU, W. 2009. A new coumarin-based chemosensor for Fe3+ in water. *Inorg. Chem. Commun.,* 12**,** 116-118.

YAVUZ, C. T., MAYO, J. T., YU, W. W., PRAKASH, A., FALKNER, J. C., YEAN, S., CONG, L., SHIPLEY, H. J., KAN, A., TOMSON, M., NATELSON, D. & COLVIN, V. L. 2006. Low-Field Magnetic Separation of Monodisperse Fe3O4 Nanocrystals. *Science,* 314**,** 964-967.

YOE, J. H. & JONES, A. L. 1944. Colorimetric detn. of Fe with disodium 1,2-dihydroxybenzene-3,5-disulfonate. *Ind. Eng. Chem., Anal. Ed.,* 16**,** 111-15.
YOO, H. S., KIM, T. G. & PARK, T. G. 2009. Surface-functionalized electrospun nanofibers for tissue engineering and drug delivery. *Advanced Drug Delivery Reviews,* 61**,** 1033-1042.
YOON, B., LEE, S. & KIM, J.-M. 2009. Recent conceptual and technological advances in polydiacetylene-based supramolecular chemosensors. *Chem. Soc. Rev.,* 38**,** 1958-1968.
YOON, J., CHAE, S. K. & KIM, J.-M. 2007. Colorimetric sensors for volatile organic compounds (VOCs) based on conjugated polymer-embedded electrospun fibers. *J. Am. Chem. Soc.,* 129**,** 3038-3039.
YU, D., HUANG, F. & XU, H. 2011. Determination of critical concentration by synchronous fluorescence spectrometry. *The Royal Society of Chemistry* 1-19.
ZAMANI, M., MORSHED, M., VARSHOSAZ, J. & JANNESARI, M. 2010. Controlled release of metronidazole benzoate from poly ε-caprolactone electrospun nanofibers for periodontal diseases. *Eur. J. Pharm. Biopharm.,* 75**,** 179-185.
ZELENY, J. 1914. The Electrical Discharge from Liquid Points, and a Hydrostatic Method of Measuring the Electric Intensity at Their Surfaces. *Physical Review,* 3**,** 69-91.
ZENDELOVSKA, D., PAVLOVSKA, G., CUNDEVA, K. & STAFILOV, T. 2001. Electrothermal atomic absorption spectrometric determination of cobalt, copper, lead and nickel traces in aragonite following flotation and extraction separation. *Talanta,* 54**,** 139-146.
ZENG, Z. & JEWSBURY, R. A. 2000. Fluorometric determination of iron using 5-(4-methoxyphenylazo)-8-(4-toluenesulfonamido)quinoline. *Analyst (Cambridge, U. K.),* 125**,** 1661-1665.
ZHANG, A.-S. & ENNS, C. A. 2009. Iron homeostasis: Recently identified proteins provide insight into novel control mechanisms. *J. Biol. Chem.,* 284**,** 711-715.
ZHANG, S., LI, X.-Y. & CHEN, J. P. 2009. Preparation and evaluation of a magnetite-doped activated carbon fiber for enhanced arsenic removal. *Carbon,* 48**,** 60-67.
ZHANG, Y., LI, B. & XU, C. 2010. Visual detection of ascorbic acid via alkyne-azide click reaction using gold nanoparticles as a colorimetric probe. *Analyst,* 135**,** 1579-1584.
ZHANG, Z. & SEITZ, W. R. 1984. A fluorescence sensor for quantifying pH in the range from 6.5 to 8.5. *Anal. Chim. Acta,* 160**,** 47-55.
ZHANG, Z., ZHANG, Y., MA, W., RUSSELL, R., SHAKHSHER, Z. M., GRANT, C. L., SEITZ, W. R. & SUNDBERG, D. C. 1989. Poly(vinyl alcohol) as a substrate for indicator immobilization for fiber-optic chemical sensors. *Anal. Chem.,* 61**,** 202-5.
ZHAO, W., ALI, M. M., AGUIRRE, S. D., BROOK, M. A. & LI, Y. 2008a. Paper-Based Bioassays Using Gold Nanoparticle Colorimetric Probes. *Anal. Chem. (Washington, DC, U. S.),* 80**,** 8431-8437.
ZHAO, W., BROOK, M. A. & LI, Y. 2008b. Design of gold nanoparticle-based colorimetric biosensing assays. *ChemBioChem,* 9**,** 2363-2371.
ZHOU, F.-L., GONG, R.-H. & PORAT, I. 2009. Mass production of nanofibre assemblies by electrostatic spinning. *Polymer International,* 58**,** 331-342.
ZHU, G., ZHU, Z. & QIU, L. 2002. A fluorometric method for the determination of iron(II) with fluorescein isothiocyanate and iodine. *Anal. Sci.,* 18**,** 1059-1061.
ZHU, X. W., LIU, S. S., GE, H. L. & LIU, Y. 2009. Comparison between the short-term and long-term toxicity of six triazine herbicides on photobacteria Q67. *Water Research* 43**,** 1731-1739.
ZIABARI, M., MOTTAGHITALAB, V. & HAGHI, A. K. Structural characteristics evaluation of electrospun nonwoven webs. 2009. Nova Science Publishers, Inc., 35-58.

14 APPENDIX. TECHNOLOGY TRANSFER

Patent applications

1. Dezzline A. Ondigo, Zenixole Tshentu, Nelson Torto, An indicator for the Detection of Ni^{2+} ,*South African Provisional Patent Application number 2012/08972*
2. Dezzline A. Ondigo, Zenixole Tshentu, Nelson Torto, An indicator for the Detection of Fe^{2+}, *South African Provisional Patent Application number 2012/08973*
3. Bellah O. Pule, Slyvestre Degni, Nelson Torto, An indicator for the detection of 17β-Estradiol, *South African Provisional Patent Application number 2012/08971*

Published articles

1. Sheriff Adewuyi, Dezzline A. Ondigo, Ruphino Zugle, Zenixole Tshentu, Tebello Nyokong and Nelson Torto, A highly selective and sensitive pyridylazo-2-naphthol-poly(acrylic acid) functionalized electrospun nanofiber fluorescence ‘‘turn-off’’ chemosensory system for Ni^{2+},Anal. Methods, 4 (2012) 1729.
2. Syntheses, characterization and antimicrobial activity of silver(I) complexes containing 2-hydroxymethyl-N-alkylimidazole ligands, Phumelele Kleyi, Ryan S. Walmsley, Manuel A. Fernandes, Nelson Torto, Zenixole R. Tshentu, Polyhedron 41 (2012) 25-29.
3. Syntheses, protonation constants and antimicrobial activity of 2-substituted N-alkylimidazole derivatives, Phumelele Kleyi, Ryan S. Walmsley, Isaac Z. Gundhla, Tara A. Walmsley, Tembisa I. Jauka, Joanna Dames, Rod B. Walker, Nelson Torto, Zenixole R. Tshentu, S. Afr. J. Chem, 65 (2012) 231-238.

Articles under review

1. Low Ah Kee N., Tshentu Z., Chigome S., Walmsley R., Kleyi P., Torto N., Pletschke B.I. and Frost C.L. (2012) Evaluation of an effective test system for investigating a pro-inflammatory response in water samples collected from the Swartkops River, Eastern Cape, South Africa. Water SA. “Under review to Water SA”
2. Bridget Adekemi Moronkola, Sherrif Adewuyi, Kehinde Nurudeen Awokoya, Dezzline Ondigo, Phumelele Kleyi, Samuel Chigome, Zenixole Tshentu, and Nelson Torto, 2-Amino-4,6-dihydroxylpyrimidine functionalized polyvinylmethylketone nanofibers for selective uptake of arsenate from wastewater “Under review to Journal of Hazardous Materials”

Articles in preparation

1. Bellah O. Pule, Slyvestre Degni, Nelson Torto, Electrospun fiber Colorimetric probe based on Au NPs for 17β-estradiol associated with dairy farming effluent “In preparation for submission to Analytical Methods”
2. Dezzline A. Ondigo and Nelson Torto, Electrospun Based Nanoprobes for Optical Diagnostics of Toxic Metal Ions “In preparation for submission to Trends in Analytical Chemistry”
3. Dezzline A. Ondigo, Zenixole Tshentu, Nelson Torto, Colorimetric Probe for Detection of Ni^{2+} ions in Water Based on Silver-Copper Alloy Nanoparticles Hosted in Electrospun Nanofibers “In preparation for submission to Analytical Chemistry”
4. Dezzline A. Ondigo, Zenixole Tshentu, Nelson Torto, Electrospun Nanofiber Based Colorimetric Probe for Rapid Detection of Fe^{2+} Ions in Aqueous Media “In preparation for submission to Analytical Chemistry”
5. Tendai Mafuma, Susan van Dyk, Samuel Chigome, Nelson Torto, Brett Plestchke, Immobilisation and characterisation of acetylcholinesterase on nanofibers electrospun from a nylon 6 and chitosan blend and its potential use for carbofuran and demeton-S-methyl sulfone detection “*In preparation for submission to Enzyme and Microbial Technology”*
6. Evaluation of the antimicrobial activity of electrospun nylon 6 nanofibers incorporated with 2-substituted *N*-alkylimidazole derivatives for the bacterial treatment of water, Phumelele Kleyi, Zenixole R. Tshentu and Nelson Torto, “In *preparation for submission to Polymer.”*.

Conferences

1. 4^{th} SEANAC International Conference, Joaquim Chissano International Conference Centre, Maputo, 7-12 July 2012, Dezzline A. Ondingo, Zenixole R. Tshentu and Nelson Torto, “Development of Diagnostic Probes for Detection of Toxic Metal Ions in Water”
2. 4^{th} SEANAC International Conference, Joaquim Chissano International Conference Centre, Maputo, 7-12 July 2012, Bellah O. Pule, Slyvestre Degni and Nelson Torto, “Development of Electrospun fiber Colorimetric Probe for Endocrine Disruptors”

3. 4th SEANAC International Conference, Joaquim Chissano International Conference Centre, Maputo, 7-12 July 2012, Bridget A. Moronkola and Nelson Torto, “2-amino 4,6 dihydroxylpyrididine- functionalized polyvinylmetylketone for the selective uptake of arsenic from wastewater”
4. 4th SEANAC International Conference, Joaquim Chissano International Conference Centre, Maputo, 7-12 July 2012, Phumelele Kleyi, Zenixole R. Tshentu and Nelson Torto, “Electrospun nylon 6 nanofibers doped with 2-substituted *N*-alkylimidazole derivatives for the inhibition of the growth of pathogens in drinking water”
5. 18th Eastern Cape South African Society for Biochemistry and Molecular Biology (EC SASBMB) Conference. Grahamstown, 18 November 2011, Tendai S. Mafuma, S Chigome, Brett Pletschke and Nelson Torto, “Immobilization of Electric Eel Acetylcholinesterase on Nanofibers Electrospun from a Nylon-6 and Chitosan Blend”